

Machinability Evaluation of Ti-48Al-2Nb-0.7Cr-0.3Si in Finishing Operations by Milling

Santiago David Castellanos Villa

Thesis submitted to the Faculty of Engineering of the University of Porto-FEUP

in partial fulfillment of the requirement for the degree of

Doctor in Mechanical Engineering

Supervisors

Prof. Dr. Fernando Jorge Lino Alves

Prof. Dr. Rui Jorge de Lemos Neto

Faculdade de Engenharia da Universidade do Porto (FEUP)

Departamento de Engenharia Mecânica (DEMec)

Programa Doutoral em Engenharia Mecânica (PRODEM)

PORTO 2019

Para:

Mi Esposa Ana Claudia

Mi Hijo Guilherme

Mis Padres Victor Manuel, Maria del Carmen

Jorge Estuardo, Rosario y Piedad

ABSTRACT

Over the last 30 years, key industries such as the military, aeronautics and automotive have shown a growing interest in the use of advanced titanium-based alloys, such as titanium aluminides (TiAl), which are used in the manufacture of high-performance components that operate in aggressive environments at temperatures of up to 800°C.

These parts are typically manufactured by near-net shape forming processes and completed with machining operations. However, the machining of this type of alloy is a major challenge, due to the low levels of surface integrity and the rapid wear of cutting tools, which are induced by the low ductility and high tendency to surface hardening of these alloys. As a result of this low machinability, the use of TiAl is still limited.

In order to meet this objective, a specific experimental design was proposed to define the effects of the cutting tool and the cutting parameters on the machinability criteria evaluated. Thus, it was possible to determine the most appropriate operational parameters for the studied configuration.

The initial experimental phase was performed in a group of six inserts with three types of insert materials and two different cutting-edge geometries (Sharp edge and T-Land edge), under a range of previously tested nominal cutting parameters. Based on this initial study, a second experimental phase was performed with a larger cutting parameter range, but only with the insert that presented the best performance in the first phase of the study.

From these experiments, the empirical relationships between tool performance (in terms of cutting forces) and surface integrity (surface roughness and hardness, hardened surface layer and lamellar deformation) were analyzed.

The results obtained detected cutting speed as the most influential parameter, followed by chip thickness and depth of cut. In highlight, it was observed that the surface roughness was improved by increasing the cutting speed. The hardened surface layer was mainly affected by the cutting speed and cutting depth, although the latter was more favorable as it deepened.

From the point of view of the cutting inserts, it was possible to obtain surfaces with good quality levels. The T-Land edge geometry proved to be the most advantageous in terms of surface quality, while the tool material with lower cobalt content and smaller grains showed lower cutting forces, which suggests greater durability. Inserts with higher cobalt content also show good performance, but with lower cutting parameter ranges.

The machinability of this Ti-48Al-2Nb-0.7Cr-0.3Si alloy was evaluated in terms of chip formation mechanism using a high-speed camcorder and the measurement of cutting forces in a conventional turning operation. During this analysis it was observed that the low ductility of this alloy motivates the formation of small discontinuous and fractured chips, however, the increase in the cutting speed allowed to form longer chips, as a consequence of the likely increase in temperature in the cutting zone, which slightly reduces the cutting forces.

In general terms, this study presents relevant information that contributes to the consolidation of knowledge about the machinability of this gamma titanium aluminide alloy and proposes an experimental methodology that allows the coupling of new types of inserts and deeper knowledge about TiAl alloys.

RESUMO

Nos últimos 30 anos, indústrias-chave como a militar, aeronáutica e automóvel têm demonstrando um crescente interesse no uso de ligas especiais de titânio, tais como os aluminetos de titânio (TiAl), os quais são utilizados na fabricação de componentes de elevado desempenho que operam em ambientes agressivos a temperaturas até 800°C.

Estas peças são tipicamente fabricadas por processos de conformação *near-net shape* e completadas com operações de maquinagem. No entanto, a maquinagem deste tipo de liga é um grande desafio devido aos baixos níveis de integridade superficial e rápido desgaste que das ferramentas de corte, os quais são induzidos pela baixa ductilidade e elevada tendência ao encruamento superficial que apresentam estas ligas. Como resultado desta baixa maquinabilidade o uso destas ligas é ainda limitado.

Para cumprir este objetivo foi proposto um plano experimental próprio para definir os efeitos da ferramenta de corte e dos parâmetros de corte sobre os critérios de maquinabilidade avaliados. Isto permitiu determinar os parâmetros operacionais mais adequados para a configuração estudada.

A fase experimental inicial foi realizada num grupo de seis pastilhas com três tipos de substratos e duas geometrias de aresta de corte diferentes (*Sharp edge* e *T-Land edge*), sob uma gama de parâmetros nominais de corte previamente testados. Com base neste estudo inicial, foi realizada uma segunda fase experimental com um gama de parâmetros de corte maior, mas só com a pastilha que apresentou o melhor desempenho na primeira fase do estudo.

Tendo em conta estas experiências, foram analisadas as relações empíricas entre o desempenho da ferramenta (em termos de forças de corte) e a integridade superficial (rugosidade e dureza superficial, camada superficial endurecida e deformação lamelar).

Os resultados obtidos detetaram como o parâmetro mais influente a velocidade de corte, seguido pela espessura da avara e a profundidade de corte. Constatou-se ainda que a rugosidade da superfície foi melhorada pelo aumento da velocidade de corte. A camada de superfície endurecida foi afetada principalmente pela velocidade de corte e pela

profundidade de corte, embora esta última tenha-se revelado mais favorável, à medida que se aprofundava.

Do ponto de vista das pastilhas de corte, foi possível obter superfícies com bons níveis de qualidade. A geometria da aresta *T-Land* provou ser a mais vantajosa em termos de qualidade superficial, enquanto que o material da ferramenta com menor teor de cobalto e grãos mais pequenos apresentou forças de corte menores, o que sugere uma maior durabilidade da ferramenta. As pastilhas com substratos com maior quantidade de cobalto apresentaram também bons desempenhos, mas com gamas de parâmetros de corte mais restritos.

A maquinabilidade desta liga Ti-48Al-2Nb-0.7Cr-0.3Si foi avaliada em termos do mecanismo de formação da apanha através de uma câmara de vídeo de alta velocidade, e medição das forças de corte numa operação de torneamento convencional. Na análise dos resultados observou-se que a baixa ductilidade desta liga motiva a formação de pequenas apanhas descontínuas e fraturadas, não obstante, o aumento da velocidade de corte, permitiu formar apanhas mais longas, como consequência do provável aumento da temperatura na zona de corte, o que diminuiu ligeiramente as forças de corte.

Em termos gerais este trabalho apresenta informação relevante que contribui para a consolidação do conhecimento acerca da maquinabilidade desta liga de alumineto de titânio gama e propõe uma metodologia experimental que permite acoplar novos tipos de pastilhas e contribuir para um conhecimento mais profundo acerca das ligas de TiAl.

ACKNOWLEDGEMENTS

First of all, I would like to express my deepest and most sincere gratitude to my mentor Prof. Dr. Jorge Lino Alves for his invaluable and sincere friendship. His guidance, motivation, supervision and confidence throughout my doctoral studies have allowed me to enhance my technical knowledge and generate a greater understanding of the present research topic. For Prof. Dr. Rui Lemos Neto, my co-author, as his extensive knowledge of materials and manufacturing technologies, as well as his advice were a valuable guide in the development of this work.

I would also like to sincerely thank the support, professionalism and recommendations provided by Dr. André Cavaleiro and Prof. Dr. Abílio Pinho de Jesus, which allowed me to perfect my knowledge of materials and machining processes.

In addition, I express my sincere thanks to Dr. Marta Saraiva (Sandvik, Sweden) for providing several of the inserts used in the experimental work and to Mr. José Manuel Diego (Sandvik, Spain) for all the discussion on cutting and machining which has been very valuable and well used.

A special thank you to Prof. Dra. Ana Reis, head of the Unidade de Tecnologias Avanzadas de Fabrico of the INEGI, for giving me the wonderful opportunity to be part of UTAF and provide me with the necessary infrastructure and inputs, without which the execution of the experimental work would not have been possible.

I would also like to express special thanks to José Francisco Teixeira for his sincere friendship and constant collaboration throughout these years of research. I also take this opportunity to express my gratitude to Andreia Durães, Armanda Marquez Teixeira, Carlos Rocha, Isaac Ferreira, José Silva, Rui Soares, Ricardo Paiva, Sertorio Lares and Tiago Fraga da Silva for their precious friendship and valuable help during these years of research work at the INEGI.

In the same way, I have to express my gratitude to José Costa for his collaboration and teachings in CNC machining, to Miguel Vigário de Figueiredo and Rui Martins da Silva for the support and flexibility to carry out the mechanical tests, to Carlos Pinto Moreira de Sá (CEMUP) for his professionalism and help in the analysis of the images, to Ramiro

Acknowledgements

Martins (ISEP) for the studies of superficial integrity, to the Prof. Dr. Mário Vaz and Eng. Nuno Viriato Ramos (LOME) for the realization of the high speed filming, to Eng. Leonardo Santana for his help in the statistical analysis and my special thanks to Pedro Falcão Alves, André Silva Alves and Domingos Pereira Carvalho of the FEUP machining laboratories team for their cooperation and service.

For the interest and words of encouragement, I would also like to thank Prof. Dr. António Torres Marques, Prof. Dra. Teresa Duarte, Eng. Bártolo Paiva and Eng. Pedro Mimoso Ferreira.

To the University of the Armed Forces - ESPE of Ecuador, thank you for the financial support without which it would not have been possible to carry out my doctoral studies abroad.

Last but not least, I would also like to express my special thanks to my invaluable friends María José, Armando, Fernanda, Joaquim and Liliana as well as my brother-in-law and good friend João Paulo, who directly or indirectly, with their valuable advice and constant encouragement, helped me in various stages of this work and during my life in Portugal.

TABLE OF CONTENTS

Abstract	i
Resumo	iii
Acknowledgements	v
Table of Contents	vii
List of Figures	xi
List of Tables	xix
List of Symbols	xxi
List of Abbreviations	xxiii
Chapter 1 : Introduction.....	1
1.1. Background	3
1.2. Research Motivation	4
1.3. Research Questions.....	7
1.4. Research Objectives.....	8
1.5. Thesis Outline	9
Chapter 2 : Literature Review	11
2.1. General Remarks	13
2.1.1. Applications.....	13
2.1.2. Properties of titanium aluminides alloys	14
2.1.3. Microstructure of titanium aluminides alloys	16
2.1.3.1. Alpha-2 (α_2 -Ti ₃ Al) microstructure	17
2.1.3.2. Gamma (γ -TiAl) microstructure.....	18
2.1.3.3. Two-phase (α_2/γ) microstructure	18
2.1.3.3.1. Near Gamma Microstructure	19
2.1.3.3.2. Duplex Microstructure	19
2.1.3.3.3. Nearly Lamellar Microstructure.....	19
2.1.3.3.4. Fully Lamellar Microstructure	19
2.1.4. Summary	20

Table of Contents

2.2. Machinability.....	22
2.2.1. Thermal conductivity effect in machinability	24
2.2.2. Chemical affinity effect in machinability	25
2.2.3. Ductility effect in machinability	25
2.2.4. Hardness and Strength effect in machinability.....	26
2.2.5. Work Hardening effect in machinability.....	28
2.2.6. Summary.....	29
2.3. Surface Integrity	30
2.3.1. Roughness.....	31
2.3.2. Surface Cracking Phenomenon	33
2.3.3. Lamellar Deformation	36
2.3.3.1. Subsurface Hardening	37
2.3.3.2. Residual stresses	41
2.3.4. Summary.....	44
2.4. Machining parameters	45
2.4.1. Cutting Tools Performance with Titanium Aluminides	46
2.4.1.1. Cemented Carbide Tools	47
2.4.1.2. Cubic Boron Nitride and Polycrystalline Diamond.....	54
2.4.2. Cutting Forces and Chip Formation.....	57
2.4.3. Summary.....	62
Chapter 3 : Experimental Design.....	63
3.1. Experimental Approach.....	65
3.2. Assessment criteria	66
3.2.1. Material properties	66
3.2.2. Surface Integrity.....	67
3.2.3. Cutting Forces.....	68
3.2.4. Chip Formation	68
3.3. Factors and levels.....	69
3.3.1. Workpiece material factors	70

3.3.2. Cutting tools factors.....	72
3.3.3. Cutting parameters.....	78
3.4. Statistical Design.....	80
3.5. Experimental Procedure.....	83
3.5.1. Workpiece material characterization.....	85
3.5.2. Surface integrity	87
3.5.2.1. Surface texture	87
3.5.2.2. Surface Properties Analysis	88
3.5.3. Cutting Forces	90
3.5.4. Chip Formation.....	91
3.6. Discussion.....	93
Chapter 4 : Results and Discussions.....	95
4.1. Material Characterization.....	97
4.1.1. Metallographic analysis.....	99
4.1.2. Mechanical Tests	101
4.1.3. Summary	102
4.2. Cutting Forces	104
4.2.1. Effect of tool characteristics on cutting forces	105
4.2.2. Effect of cutting parameters on cutting forces.....	106
4.3. Assessment of surface integrity.....	109
4.3.1. Surface Roughness and surface topography	109
4.3.1.1. Effect of tool characteristics on surface finish	110
4.3.1.2. Effect of cutting parameters on surface finish.....	111
4.3.1.3. Surface topography.....	114
4.3.2. Hardened surface layer.....	118
4.3.2.1. Surface hardness.....	119
4.3.2.1.1. Effect of tool characteristics on surface hardness	119
4.3.2.1.2. Effect of cutting parameters on surface finish	120
4.3.2.2. Microhardness Profile.....	122

Table of Contents

4.3.2.2.1. Effect of tool characteristics on microhardness profile	122
4.3.2.2.2. Effect of cutting parameters on microhardness profile	124
4.3.3. Lamellar deformation	127
4.4. Chip Formation	130
4.4.1. Results from high-speed recording	131
4.4.1.1. Effect of tool characteristics on chip formation	133
4.4.1.2. Effect of cutting parameters on chip formation	134
4.4.2. Cutting forces	134
Chapter 5 : Conclusions and future work	137
5.1. General Conclusions	139
5.2. Answer to the Research Questions	143
5.3. Major Contributions	152
5.4. Future Work	153
5.5. Publications	154
References	155
Appendices	169

LIST OF FIGURES

Figure 1.	(a) Milled specimen of Ti-48Al-2Nb-0.7Cr-0.3 Si, and (b) cutting tool used to perform the preliminary tests.....	7
Figure 2.	Aerospace application of TiAl; (a) cast and additive manufacturing low pressure turbine (LPT) blade of Ti-48Al-2Nb-2Cr (at%) by GENx [8, 18], (b) casted high pressure compressor (HPC) blade of Ti-45Al-8Nb-0.5 (B,C) (at%) by Thyssen, GfE, Leistritz for Rolls Royce [29, 30].....	13
Figure 3.	General application of titanium aluminides; (a) complex machined structural panel in γ -TiAl [41], (b) turbocharger wheel in Ti-48Al-2Nb-0.7Cr-0.3Si (at%) produced via additive manufacturing by electron beam melting technology (EBM) [42], (c) casted turbocharger wheel produced in γ -TiAl [43], (d) high pressure compressor casing of military engine manufactured by powder metallurgy in γ -TiAl, (e) forged connecting rod (conrod) produced in γ -TiAl [44], and (f) exhaust valves produced by near-net shape technology (NNS) in γ -TiAl [41].	14
Figure 4.	Comparison of high-temperature properties for TiAl and some selected alloys; (a) specific modulus versus temperature, and (b) specific strength versus Larson–Miller parameter for creep rupture [27].	15
Figure 5.	Comparison of high-temperature properties for TiAl and selected alloys; specific strength versus temperature (adapted from [27]).	15
Figure 6.	Binary equilibrium phase diagram of Ti-Al alloys [22] and microstructures of TiAl phases; (a) hexagonal α 2-Ti3Al, and (b) tetragonal γ -TiAl [2].	17
Figure 7.	Microstructures of Ti-48Al; (a) near gamma, (b) duplex, (c) nearly-lamellar and (d) fully lamellar [6].	20
Figure 8.	Images of adherent workpiece material on the tool cutting edge, after 40 min of milling (adapted from [108]).	25
Figure 9.	Yield stress of the Ti-36.5 at% Al alloy (α 2/ γ microstructure) as a function of the angle between the lamellar boundaries and load axis (adapted from [49]).	26
Figure 10.	Variation of specific yield strength as a function of the temperature for TiAl-based alloys and Nickel superalloys (adapted from [35]).	27
Figure 11.	Microhardness profile of Ti-45Al-2Mn-2Nb +0.8 vol% TiB2 (adapted from [67]).	28
Figure 12.	Key factors that define the surface integrity of machined parts (adapted from [65]).	30
Figure 13.	Effect of tool failure on surface integrity in γ titanium aluminides [124].	31

Figure 14.	Cutting environment influence on surface roughness Ra and Rt in turning operations of a Ti-45Al-2Nb-2Mn-0.8B alloy (adapted from [80]).	32
Figure 15.	Influence of geometry parameters of the tool on surface finishing Ra and Rt, in milling Ti-45Al-2Nb-2Mn + 0.8 vol% TiB2 XD alloy (adapted from [98]).	33
Figure 16.	Fractography of; (a) turning sample in Ti-45Al-2Nb-2Mn - 0.8 vol% TiB2 (adapted from Mantle et al. [71]), and (b) milling sample in Ti - 48Al -2Nb -0,7Cr -0,3Si.	34
Figure 17.	Rotating bending fatigue life testing at 3000 rpm of turned and polished titanium aluminide (Ti-45Al-2Nb-2Mn- 0.8%TiB2 at% samples (adapted from [71]).	35
Figure 18.	Stress – number of cycles curves for turned ECM and EDT specimens of Ti-45Al-2Mn-2Nb+0.8 vol% TiB2 XD at% (adapted from [70]).	36
Figure 19.	Plastic lamellar deformation of; (a) milling surface in Ti -48Al -2Nb - 0,7Cr -0,3Si, and (b) turning surface in Ti-45Al- 8Nb-0.2C-0.2B [125].	37
Figure 20.	Microhardness depth profile of a titanium aluminide Ti-45Al-2Nb-2Mn-0.8% TiB2 (adapted from [69]).	38
Figure 21.	Microhardness depth profile of Ti-45Al-8Nb-0.2C (adapted from [127]).	38
Figure 22.	Microhardness depth profile on Ti-48Al-2Mn-2Nb for different tool wear (adapted from [142]).	39
Figure 23.	Microhardness depth profile of Ti-48Al-2Mn-2Nb under different cutting speeds (adapted from [142]).	39
Figure 24.	Microhardness depth profile for HSM for two different cutting speeds (adapted from [68]).	40
Figure 25.	Microhardness depth profile between two lubricoolant strategies (adapted from [80]).	40
Figure 26.	Residual stress models [117].	41
Figure 27.	Schematic indicative of the current capabilities of the multiple methods by Withers [145].	42
Figure 28.	Residual stress measurement at the surface of a Ti-48Al-2Mn-2Nb (at%) + 2TiB (wt%) obtained by electro-discharge, ground and polished (adapted from [96]).	42
Figure 29.	Residual stress showed in grinding operations at different speeds (adapted from [146]).	43
Figure 30.	Residual stress profiles of shot peening (SP), turning (T), grinding (G) on Ti-45Al-5Nb-0.2B-0.2C (adapted from [87]).	43
Figure 31.	Main effect plot – mean for residual stress in Ti 48-2-2-08 [69].	44

Figure 32.	Common surface integrity defects on the titanium aluminides machined surfaces (author images).	46
Figure 33.	Correlation between binder content and WC grain size with main properties of cemented carbides [152].	48
Figure 34.	Cutting tool life on; (a) turning, and (b) milling of TiAl with and without TiB ₂ content (adapted from [59]).	49
Figure 35.	Images of tool rake face with wear by; (a) microcracks, and (b) built-up edge [81].	49
Figure 36.	Specific cutting pressure (K_c) with cutting speed and feed rate for fine grain (MG) (<1 μm) and coarse grain (CG) (1-2 μm) carbide inserts in milling Ti-45Al-2Nb-2Mn+0.8TiB ₂ [24].	50
Figure 37.	Flank wear of fine grain (MG) (<1 μm) and coarse grain (CG) (1-2 μm) carbide inserts in milling of Ti-45Al-2Nb-2Mn+0.8TiB ₂ [24].	50
Figure 38.	Tool wear observation for coated and uncoated ISO K10-grade carbide tools, by Priarone et al. [124].	51
Figure 39.	Tool wear after turning Ti-45Al-2Mn-2Nb-0.8 B for 10 seconds under different cooling conditions (adapted from [80]).	52
Figure 40.	Flank wear after 10 seconds of cutting in turning Ti-45Al-2Nb-2Mn-0.8B alloy (adapted from [80]).	52
Figure 41.	Tool wear curves for turning, when using cutting inserts with nose radius of: (a) 8 mm (RCMT 0803), and (b) 12 mm (RCMT 1204) [82].	53
Figure 42.	Flank wear curves for cutting tools with rake angle of 4° and 12° with and without finishing treatment, when milling Ti-48Al-2Cr-2Nb [108].	53
Figure 43.	Tool wear of CBN and coated tungsten carbide tools (CC) in boring Ti-46Al-0.5Mo-0.8Cu-0.2Si (adapted from [44]).	54
Figure 44.	Workpiece (a) surface, (b) subsurface, and (c) chip after turning Ti-46.8Al-1Mo-0.2Si at $V_c=300\text{m/min}$ [148].	55
Figure 45.	Tool wear observations for 50% CBN, 92% CBN and PCD cutting insert after turning Ti-43.5Al-4Nb-1Mo-0.1B [14].	55
Figure 46.	Tool life curves of CBN and PCD tools when turning Ti-43.5Al-4Nb-1Mo-0.1B (adapted from [124]).	56
Figure 47.	Tool life curves for cryogenic-assisted turning of Ti-43.5Al-4Nb-1Mo-0.1B with PCD tool [124].	56
Figure 48.	Comparison of milling forces for Ti-6Al-2Zr-1Mo-1V and Ti-48Al-2Mn-2Nb at $V_c=120\text{ m/min}$, $f_z=0.08\text{ mm/tooth}$, $a_p=5\text{ mm}$, $a_e=0.5\text{ mm}$ (adapted from [142]).	57
Figure 49.	Cutting parameters effect on the cutting forces when turning Ti-48Al-2Mn-2Nb (adapted from [125]).	58

List of Figures

Figure 50.	Cutting forces variation for milling Ti-47Al-2Nb-2Mn +0.8 TiB2 with cutting speed and feed (adapted from [24]).	58
Figure 51.	Cutting force along the time in turning with a different nose radius (adapted from [163]).	59
Figure 52.	Milling forces curves under different tool wear for Ti-48Al-2Mn-2Nb [142].	59
Figure 53.	Cutting forces components at different lubricoolant supply pressure [80].	60
Figure 54.	The ratio of cutting forces to tool/chip contact area at different lubricoolant pressure, and break-outs on the tool cutting edge (adapted from [80]).	60
Figure 55.	Cutting force at different workpiece temperatures in Ti-45Al-5NB-0,2B-0,2C (TNBV5) alloy (adapted from [73]).	61
Figure 56.	Specific cutting force as a function of the workpiece temperature of the TNBV5 alloy (adapted from [73]).	61
Figure 57.	Phases of the proposed experimental plan.	65
Figure 58.	The most commonly used criteria for assessing machinability [64, 66].	66
Figure 59.	Cast cylindrical ingots of Ti-48Al-2Nb-0.7 Cr-0.3Si obtained via VAR.	71
Figure 60.	Micrograph of Ti-48Al-2Nb-0.7Cr-0.3Si after; (a) abrasive wet cutting process, and (b) EDWM process.	72
Figure 61.	Round insert face milling cutter.	73
Figure 62.	Cutting insert and edge geometries.	74
Figure 63.	Cutting insert material S10, (a) SEM micrograph in BSED mode, and (b) EDS analysis.	75
Figure 64.	Cutting insert material S25, (a) SEM micrograph in BSED mode, and (b) EDS analysis.	76
Figure 65.	Cutting insert material S30, (a) SEM micrograph in BSED mode, and (b) EDS analysis.	76
Figure 66.	Effective diameter in cut for round cutter insert, and calculation formula [178].	78
Figure 67.	Chip thinning effect on round inserts [178].	79
Figure 68.	Chart of work stages.	81
Figure 69.	(a) DECKEL-MAHO DMU 60 eVo linear machining centre used for milling tests, (b) Renishaw touch probe device for workpiece measurement, (c) BLUM laser measuring system, and (d) high-pressure internal lubrication system.	84

Figure 70.	Samples of Ti-48Al-2Nb-0.7Cr-0.3Si; (a) before, and (b) after milling operation.	85
Figure 71.	Wire EDM Machine MITSUBISHI DWC 90SZ.	85
Figure 72.	(a) STRUERS Planopol-3 automatic grinder polishing machine, (b) Olympus PMG 3 optical microscope.	86
Figure 73.	Tensile test specimen geometry; (a) dimension, and (b) cut samples.	86
Figure 74.	(a) MTS 810 material testing system, (b) MTS 634.25F-24 mechanical extensometer, and (c) Microhardness tester MATSUZAWA MXT70	87
Figure 75.	(a) HOMMELWERKE LV-50 surface measurer system, (b) BRUKER NPLEX 3D digital microscope, and (c) Layout of the workpiece surface sections where roughness was determined.	88
Figure 76.	The layout of the workpiece surface sections where hardness was determined.	88
Figure 77.	(a) Layout of the workpiece sections used for the surface metallurgy analysis, and (b) dimensions of cutted sample mounted on epoxy hot resin.	89
Figure 78.	Microhardness measuring template and example of surface roughness depth profile.	89
Figure 79.	Lamellar deformation measuring template.	90
Figure 80.	Experimental set-up for cutting force measurement in milling operations.	90
Figure 81.	Dynamometer set-up for cutting force measurement in milling operations.	91
Figure 82.	(a) Conventional lathe machine FFI, and (b) experimental setup for analyses of the chip formation.	92
Figure 83.	Experimental set-up for; (a) high-speed recording of chip formation, and (b) cutting force measurement.	92
Figure 84.	Chemical composition of raw material (wt%).	98
Figure 85.	Casting defects in ingots of Ti-48Al-2Nb-0.7Cr-0.3Si; a) scar, b) flow marks, and c) shrinkage cavity.	98
Figure 86.	(a) SEM image of a pore, and (b) optical microscope image of the cross-section in the central region of the Ti-48Al-2Nb-0.7Cr-0.3Si ingot.	99
Figure 87.	(a) Transversal, and (b) longitudinal samples of the Ti-48Al-2Nb-0.7Cr-0.3Si ingot.	99
Figure 88.	Microstructure of the Ti-48Al-2Nb-0.7Cr-0.3Si.	100
Figure 89.	Micrograph of Ti-48Al-2Nb-0.7Cr-0.3Si showing γ -TiAl and α_2 -Ti ₃ Al phases segregated at lamellar colonies.	100
Figure 90.	Morphological contrast of Ti-48Al-2Nb-0.7Cr-0.3Si microstructure; (a) optical microscope image, (b) segmented regions image of α_2	

	(white) and γ (black) phases, and (c) phase map distribution of α_2 (red) and γ (green) phases in eutectoid lamellar colonies.....	101
Figure 91.	Tensile strength of Ti-48Al-2Nb-0.7Cr-0.3Si.....	101
Figure 92.	Ductility of Ti-48Al-2Nb-0.7Cr-0.3Si.....	102
Figure 93.	Radial hardness profile distribution across ingot.	102
Figure 94.	(a) Cutting forces profile when machining with a S10-XL insert at $V_c=70$ m/min, $a_p=0.5$ mm and $hex=0.04$ mm, and (b) Layout of the workpiece sections where surface integrity was determined.	104
Figure 95.	Resultant machining force FR by; a) material, b) edge insert geometry, and c) cutting insert.....	106
Figure 96.	Tool wear of; (a) S30-XM, and (b) S30-XL inserts after milling Ti-48Al-2Nb-0.7Cr-0.3Si at $V_c=70$ m/min, $a_p=0.5$ mm and $hex=0.04$ mm (Trial 4).	106
Figure 97.	Effect of cutting speed (V_c) on resultant machining force (FR).	107
Figure 98.	Effect of; (a) depth of cut (a_p), and (b) chip thickness (hex) in resultant machining force (Fr).	107
Figure 99.	Main effect plot – means for resultant machining force FR (N).	108
Figure 100.	Arithmetical mean roughness R_a by; a) tool material, b) edge insert geometry, and c) cutting insert.....	111
Figure 101.	Effect of cutting speed (V_c) in arithmetical mean roughness R_a	112
Figure 102.	Effect of depth of cut (a_p) in arithmetical mean roughness R_a	112
Figure 103.	Effect of chip thickness (hex) in arithmetical mean roughness R_a	113
Figure 104.	Main effect plot – means for arithmetical mean roughness R_a (μm) for S10-XL inserts.	114
Figure 105.	Machined surfaces with S10-XL at $V_c = 110$ m/min, $a_p = 0.5$ mm, $hex = 0.04$ mm; (a) defect-free area, and (b) region with defects.....	115
Figure 106.	Machined surfaces with S10-XL inserts at; (a) $V_c= 70$ m/min, $a_p= 0.3$ mm and $hex=0.03$ mm, (b) $V_c= 70$ m/min, $a_p= 0.5$ mm and $hex= 0.04$ mm, (c) $V_c= 45$ m/min, $a_p= 0.3$ mm and $hex= 0.04$ mm, and (d) $V_c= 45$ m/min, $a_p= 0.5$ mm and $hex= 0.03$ mm.	116
Figure 107.	Topographies of the machined surfaces; (a) Cutting insert S30-XM: $V_c = 45$ m/min, $a_p = 0.5$ mm and $hex = 0.03$ mm, and (b) Cutting insert S30-XM: $V_c = 70$ m/min, $a_p=0.5$ mm and $hex = 0.04$ mm.....	117
Figure 108.	Surface defects on machined surface of different samples; (a) S10-XL at $V_c= 110$ m/min, $a_p=0.5$, $hex=0.04$, (b) S25-XM at $V_c=70$ m/min, $a_p=0.3$, $hex 0.03$, (c) and (d) S30-XL at $V_c=70$ m/min, $a_p=0.3$, $hex 0.03$	118
Figure 109.	Average surface hardness by; (a) cutting tool materials, (b) edge insert geometry, and (c) cutting insert.	119

Figure 110. Effect of cutting speed (V_c) on the average surface hardness.	120
Figure 111. Effect of axial depth of cut (ap) on the average surface hardness.	120
Figure 112. Effect of chip thickness (a_p) in the average of the Surface hardness.	121
Figure 113. Main Effects Plot – means for surface roughness ($HV_{0.025}$).	121
Figure 114. Hardness profile as a function of the depth below the machined surface.	122
Figure 115. Hardness profiles for S25-XL insert.	123
Figure 116. Difference between surface hardness and peak hardness sorted by; (a) material type, (b) edge insert geometry, and (c) cutting insert.	124
Figure 117. Effect of; (a) cutting speed (V_c), (b) axial depth of cut (ap), and (c) chip thickness (hex), in the average values of the difference between surface hardness and peak hardness (Δ Hardness).	125
Figure 118. Effect of; (a) cutting speed (V_c), (b) axial depth of cut (ap), and (c) chip thickness (hex) in the average hardened layer depth.	125
Figure 119. Effect of cutting speed (V_c) in the peak hardness value and surface hardness.	126
Figure 120. Effect of the axial depth of cut (ap) in the peak hardness value and surface hardness.	126
Figure 121. Impact of the chip thickness (hex) in the peak hardness value and surface hardness.	127
Figure 122. Deformed lamellar layer in accordance with; (a) lamellar orientation, and (b) γ -phase content.	128
Figure 123. Average of the depth of the deformed layer vs. surface hardness by; (a) material, and (b) edge insert geometry.	128
Figure 124. Effect of; (a) cutting speed (V_c), (b) axial depth of cut (ap), and (c) chip thickness (hex) in the depth of the deformed layer (DDL).	129
Figure 125. Effect of; (a) cutting speed (V_c), (b) axial depth of cut (a_p), and (c) chip thickness (a_p) in the depth of the deformed layer (DDL) for S10-XL insert.	129
Figure 126. Frames from video sequences during chip formation in the trial 1 for: (a) S10-XL and (b) S25-XM inserts.	131
Figure 127. SEM images of; (a) chip obtained with S25-XM at $V_c=38$ m/min, $ap=0.3$ and $f=0.14$ mm/rev, and (b) magnification of the upper side of the chip.	132
Figure 128. Optical microscopy image of the cross-section of a Ti-48Al-2Nb- 0.7Cr-0.3Si chip obtained when cutting with S25-XM at: (a) $V_c=38$ m/min, $ap=0.3$ mm, and $f=0.14$ mm/rev, and (b) $V_c=53$ m/min, $ap=$ 0.5 mm. and $f=0.14$ mm/rev.	132

Figure 129. Optical microscopy images of chips obtained from experimental trials.133

Figure 130. Sliding surface of chips cut with S10-XL inserts in experiments; (a) 1, and (b) 2.134

Figure 131. Cutting forces profiles for S10-XL insert at: (a) $V_c=38$ m/min, $ap= 0.3$ mm, (b) $V_c=38$ m/min, $ap= 0.5$ mm, (c) $V_c=53$ m/min, $ap= 0.3$ mm, and (d) $V_c=38$ m/min, $ap= 0.3$ mm.135

Figure 132. Cutting forces profiles for S25-XM insert at $V_c = 53$ m/min, (a) $ap= 0.3$ mm, and (b) $ap=.0.5$ mm.....136

Figure 133. Radar graph: (a) surfaces roughness, and (b) surface microhardness and peak value of microhardness profile.....147

Figure 134. Main effects plot-means for; (a) resultant machining forces F_r , (b) surface roughness R_a , and (c) Surface hardness.150

Figure 135. Effect of cutting speed, chip thickness and axial depth of cut with an S25-XM cutting insert on the; (a) Cutting force F_r , (b) Surface roughness R_a , and (c) Surface hardness.151

Figure 136. Effect of cutting speed, chip thickness and axial depth of cut with a S25-XM cutting insert on the; (a) Cutting force F_r , (b) Surface roughness R_a , and (c) Surface hardness.152

LIST OF TABLES

Table 1.	Properties of TiAl alloys, Ti-based alloys, and Ni-based superalloys [47–49].....	16
Table 2.	Summary of the most used α_2/γ TiAl and their attributes.	21
Table 3.	Effect of alloying elements in TiAl.	21
Table 4.	Factors affecting machinability [64–66].	22
Table 5.	Commonly used criteria for assessing the machinability of TiAl.....	23
Table 6.	Influence of TiAl properties on their machinability.	29
Table 7.	Factors and level analyzed in the program of the exploratory experiment.....	70
Table 8.	Milling cutter specifications.....	73
Table 9.	Cutting parameters used in the exploratory test.....	74
Table 10.	Cutting insert specifications (Tool geometry and material).	77
Table 11.	Factors and selected levels in exploratory tests for cutting tools.....	77
Table 12.	Factors and levels selected in exploratory tests for cutting parameters.	80
Table 13.	L4 orthogonal array used in the first phase of the experimental work.....	82
Table 14.	L16 orthogonal array for the first phase of the experimental work.....	82
Table 15.	Experimental array for the chip formation.	91
Table 16.	Mechanical properties of Ti-48Al-2Nb-0.7Cr-0.3Si.	103
Table 17.	ANOVA table for resultant force <i>FR</i>	109
Table 18.	Surface Roughness in the machining of γ -TiAl.....	110
Table 19.	ANOVA table for the arithmetic means roughness <i>Ra</i>	114
Table 20.	ANOVA table for the arithmetic means surface hardness.....	122
Table 21.	Experimental array used in the experimental work for the chip formation.....	130
Table 22.	Procedure for Assessing Machinability.....	145
Table 23.	Percentage contribution ratio (PCR) of cutting parameters in evaluation criteria.....	149

LIST OF SYMBOLS

a_e	Radial cut or engagement
a_p	Axial depth of cut
at%	Atomic percentage
D_{cap}	Effective cutting diameter
f_z	Feed rate per tooth
F_a	Axial force
F_r	Radial force
F_R	Resultant machining Force
F_t	Tangential force
F_x	Force in X direction
F_y	Force in Y direction
F_z	Force in Z direction
h_{ex}	Chip thickness
iC	Insert diameter
PCR%	Percentage contribution ratio
R_a	Arithmetical mean surface roughness
R_t	Maximum height of the profile
R_z	Roughness height
V_B	Average flank wear
V_c	Cutting speed
vol%	Volume percentage
W_v	Workpiece speed
wt%	Weight percentage
γ -TiAl	Gamma titanium aluminides

LIST OF ABBREVIATIONS

ANOVA	Analysis of variance
ASTM	American Society for Testing and Materials
BDTT	Brittle to ductile transition temperature
BUE	Built-up edge
CBN	Cubic boron nitride
CVD	Chemical vapor deposition
DOC	Depth of cut
DOE	Design of experiments
ECM	Electro-chemical machining
EDM	Electrical discharge machining
EDS	Energy dispersive spectroscopy
EDT	Electro-discharge texturing
EDWM	Electrical discharge wire machining
HK	Knoop hardness
HSM	High-speed machining
HT	High temperature
HV	Vickers hardness
ISO	International Standards Organization
K _c	Specific cutting force
LAM	Laser-assisted machining
LPT	Low-pressure turbine
MQL	Minimum quantity lubrication
MRR	Material removal rate
PCBN	Polycrystalline cubic boron nitride
PCD	Polycrystalline diamond

List of Abbreviations

PHV	Peak hardness value
PVD	Physical vapor deposition
RT	Room temperature
SEM	Scanning electron microscopy
SI	Surface integrity
SS	Sum of squares
TiAl	Titanium aluminides
UAC	Ultrasound-assisted machining
VAR	Vacuum arc melting
WC	Cemented tungsten carbide
XRD	X-Ray diffraction

Chapter 1 : Introduction

In the development of new materials, understand its benefits and disadvantages regarding the processing and manufacturing is extremely important for successful entry into new markets and applications. Due to the increasing use of titanium aluminides in aeronautical components, the scientific community and mainly the aerospace industry, intends to encourage and stimulate their use.

In this chapter, a brief introduction of the importance and manufacture of titanium aluminides is presented, especially for the aeronautical industry. Then, the motivation and the objectives are exposed, to finally describe the design and the organization of the thesis.

1.1. Background

Since the beginning of its industrialization in the 50s [1], titanium alloys have allowed the development of new technologies in industries such as military, aerospace, automotive and nuclear. This is due to the advantages offered by its physical, chemical and mechanical properties in terms of design and performance.

In the same way, these technological advances have promoted the development of new titanium alloys, among which the titanium aluminides (TiAl), which stand out for their performance in components subjected to high temperatures (turbocharger turbine wheel, turbine blades, etc.).

Titanium aluminides are ordered intermetallic materials, composed of titanium with a high percentage of aluminum (22-56 at%) and other alloying elements (niobium, chromium, silicon, boron among others), [2], which are mainly known for their low density, high specific strength and excellent resistance to corrosion and creep.

In the 90s, the first technical applications of these materials were carried out by the American Air Force to reduce the weight of propulsion engines in military aircraft (F22 - Abductor) [3–5]. At the end of two decades of research, as of 2011, GE Aviation was the first company to successfully implement an alloy of TiAl (Ti-48Al-2Cr-2Nb) in the blades of the low-pressure turbines (LPT) of its aero-engines GEnx™ [2, 6–8]. Likewise, as of 2016, companies such as the CFM International and Pratt & Whitney have integrated other alloys of TiAl (Ti 43.5Al-4Nb-1Mo-0.1B) in their families of commercial windmills (LEAP and PW100G) [9–12].

Currently, all these engines are used successfully in a wide range of commercial aircraft such as the Boeing 787, Boeing 747, Boeing 737, Airbus A320neo and COMAC C919 among others [7, 10, 13].

In addition to aeronautical applications, titanium aluminides have also been the subject of research in the automotive industry, where they were initially implemented in Formula 1 competition cars, and then used in commercial engine components (turbines and exhaust valves) as is the case of Ferrari, Mitsubishi Motors Inc. and Daimler AG [8, 14].

Due to the marked interest within the aeronautical and automotive industries to develop more efficient mechanical devices with lower operating costs and more environmentally

friendly, several regional and European research projects have been developed with the objective of promoting the implementation of these alloys to industrial level (e.g. MMTech, DATACAST, TIALCHARGER, LIVALVES) [15–17].

Although these projects have improved the production processes of these alloys, nevertheless, the degree of industrialization of titanium aluminides is still low, mainly due to the technological challenges involved in the use of advanced manufacturing processes to obtain components with excellent mechanical properties.

Generally, TiAl parts are manufactured using advanced technologies such as VAR skull melting, precision casting, powder metallurgy or additive manufacturing [11, 18–20]. Regardless of the use of these technologies, the need for machining as a final stage of manufacturing to meet the functional characteristics of the components remains indispensable.

To achieve greater acceptance at an industrial level, it is crucial that machining technologies ensure reliable and economic processes.

Concerning these processes, most of the researches have been conducted mainly by two work teams; European Commission coordinates the first one in collaboration with several universities, where the University of Aachen, the Politecnico di Torino and the University of the Basque Country (Spain) stand out, which are characterized by the publication of their projects and results. On the other hand, Rolls Royce, in collaboration with the University of Birmingham and the British government, leads the second research group. The focus of these studies is oriented towards the study of the machinability of these alloys.

Despite the continuous activity of these groups, knowledge about the behavior of titanium aluminides in the machining process is still scarce compared to other alloys with similar characteristics, which is why it is essential to study in depth the problems that involves the machinability of titanium aluminides in order to improve manufacturing conditions and encourage their use.

1.2. Research Motivation

After conducting a study on additive manufacturing and milling of complex surfaces in Ti-6Al-4V [21], it was noted that for the manufacturing of high performance mechanical

components, the aerospace industry has turned its attention to the use of new Ti alloys with unique mechanical characteristics such as titanium aluminides.

The use of titanium aluminides as an alternative to nickel superalloys in the production of mechanical components in the aeronautical and automotive industry has increased in recent years. However, its acceptance has been limited mainly by the difficulty of manufacturing parts with acceptable surface quality.

Since these alloys were created, understanding and studying their potential benefits and drawbacks about processing, manufacturing and design technologies has been one of the main interests of the industrial and scientific community in its improvement.

Within these studies, the knowledge of the state and surface characteristics of the mechanical components have proved to be very important, especially when it comes to machined parts, due to the impact that the surface changes produced by the cutting process (mechanical, metallurgical and chemical) have in the performance, longevity and reliability of the pieces.

Although the chemical composition and physical properties of these alloys have been widely studied, the machinability of titanium aluminides could not be substantially improved. Therefore, these alloys are still considered within the group of materials with limited machinability, even becoming inferior to conventional titanium alloys and nickel superalloys.

Considering that titanium aluminides are intermetallic materials, it is inappropriate to associate their cutting mechanism with that of metallic materials. This is due to characteristics such as its ionic bonds that induce transgranular fracture mechanisms [22], its face centered tetragonal microstructure that is naturally fragile (ductility ~ 2%) [2] and its high stiffness over a range of elevated temperatures, as a result of the large amount of energy required by Ti-Al atomic bonds for its diffusion.

As can be inferred, the mechanical, chemical and physical properties of titanium aluminides cause difficulties for machining parts with consistent quality levels, which restricts their end use. The main challenge in machining these materials lies mainly in the integrity of the obtained surfaces, regardless of the cutting tool types or machining processes used.

Regarding productivity, this characteristic translates into severe wear and premature damage to the cutting tool, causing frequent tool changes and resulting in high production costs. Also, the deterioration of the tool cutting-edge increases the probability of inducing surface damage.

Each of these difficulties must be overcome by studying the appropriate combination of cutting parameters, tool geometry, tool material, and machining strategies.

Several research studies have been carried out on the machinability of titanium aluminides from the beginning of their use. These studies cover processes such as turning, milling, boring, drilling, grinding, electrical discharge machining, electrochemical machining, and ultrasonic milling.

Published studies have provided essential knowledge on the mechanisms of surface cutting and integrity in TiAl. Generally, these studies comprise a series of experimental tests that present numerical, analytical and statistical results, the influence of the cutting parameters, cutting tool geometry and material, among others. A considerable number of these results have contributed substantially to the scientific findings on the machining of titanium aluminides. However, due to confidentiality protocols much of this information has not been reported or its content has limited information

Despite this, the literature on the machinability of TiAl shows that most of the studies have been carried out in turning operations and only a few papers have considered the study of milling. Probably, this is due to the complexity in the analysis of the cutting mechanism associated with the milling operations.

Due to this preliminary work and the growing interest in studying the machinability of TiAl alloys, an opportunity was identified to contribute to the study of machinability in the milling processes of these alloys.

The motivation of this work is to contribute to the understanding of the machinability of titanium aluminides, by performing a complete experimental study which analyses the effects that milling operations cause on the surface integrity of a gamma titanium aluminide (Ti-48Al-2Nb-0.7Cr-0.3 Si).

1.3. Research Questions

After further study in TiAl machining, it was found that the research about the milling of complex surfaces are conducted mostly with solid spherical end-mills, with only a few studies on the use of toroidal geometry cutting tools [23, 24]. Considering this background, an opportunity was identified to test the use of this geometry of tools in the milling of a TiAl alloy (Ti-48Al-2Nb-0.7Cr-0.3 Si).

Consequently, several exploratory tests were carried out in the milling of convex surfaces (Figure 1) with interchangeable inserts toroidal milling cutters (round inserts) using cutting tools, parameters and cutting conditions used in other scientific works for different types of alloys.

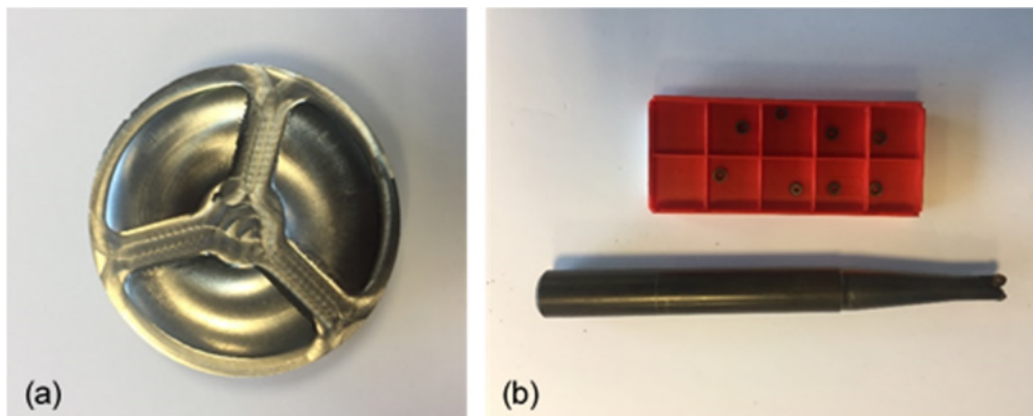


Figure 1. (a) Milled specimen of Ti-48Al-2Nb-0.7Cr-0.3 Si, and (b) cutting tool used to perform the preliminary tests.

The first results showed that these tools produce surfaces with reasonable surface finishes ($R_a \approx 0,25 \mu\text{m}$). However, for the manufacture of this model, the consumption of cutting inserts was high due to the extremely rapid wear (lifetime < 2 min).

Although the preliminary tests were performed on convex surfaces, the present experimental work was carried out on obtaining flat surfaces, since this operation allows a better evaluation and analysis of the results.

In addition, the correct selection of cutting parameters, geometry and material of the tool was revealed as a key challenge mainly due to the limited published scientific and technical information about the machinability of these materials.

Consequently, from this first experimental test, several doubts and questions were raised regarding the definition of the machinability of this alloy, the cutting tools and range of

cutting parameters used, among others. These uncertainties were summarized in three main questions, which are presented below:

- What is the procedure that must be followed to evaluate the machinability of a TiAl alloy for milling with toroidal cutting tools of round interchangeable inserts?
- What type of round cutting inserts are best suited for finishing operations when milling a Ti-48Al-2Nb-0.7Cr-0.3Si alloy?
- What range of cutting parameters should be used in finishing operations when milling a Ti-48Al-2Nb-0,7Cr-0,3Si alloy with interchangeable round insert tools?

The formulation of these questions allowed structuring the general objective and the specific objectives of this study.

1.4. Research Objectives

The main objective of this research is to evaluate the machinability of the gamma titanium aluminide Ti-48Al-2Nb-0.7Cr-0.3Si in the milling of flat surfaces with interchangeable round insert tools. The present study focuses mainly on the analysis of the effects caused by the cutting parameters, tool material and geometry of the cutting-edge insert, on the surface integrity of the machined parts.

In order to achieve the main aim, it is necessary to set specific objectives that are described below:

Analyze the published studies regarding the machinability of titanium aluminides, with attention to the effect induced by cutting tools, cutting parameters and machining conditions on the surface quality and subsurface integrity of the pieces, in order to publish a bibliographic review that allows identifying the main problems that are exhibited in the machining of these alloys.

Design an experimental methodology in order to evaluate the machinability of these alloys in milling operations with round inserts. The purpose of this objective is to define the set of evaluation criteria and operational parameters to be used in the present study.

Perform a series of experiments, using several round cutting inserts with different cutting-edge geometries and insert materials, under a set of defined cutting parameters and

machining conditions. The purpose of these experiments is to assess the machinability of the TiAl alloy by the proposed experimental methodology.

Analysis of the impact of cutting parameters and tool characteristics on the integrity of machined surfaces and identify the most influential factors in the milling with round cutting inserts of the alloy under study.

Define a range of useful cutting parameters for the toroidal cutting tools with interchangeable round inserts, to establish a reference point in the machining of this alloy.

1.5. Thesis Outline

The thesis is organized in five chapters, which are described below:

Chapter I offers a brief introduction about titanium aluminides, as well as the current situation of research in the machining of this material. In addition, this chapter indicates the reasons that motivated the present study, the main unknowns' factors that allowed establishing the objectives of the research and the structure of the thesis.

Chapter II presents a detailed bibliographic review on the machining of titanium aluminides, with a particular emphasis on the integrity of machined surfaces, cutting tools and cutting conditions. In the initial part of this section, the properties and metallographic structure of these alloys are also analyzed from the perspective of machinability. This chapter is focused on fulfilling the first specific objective of the thesis.

Chapter III details the proposed experimental program for the evaluation of machinability; this section includes the selection of the evaluation criteria, the factors, and levels to be analyzed, the design of the experiment (DOE) and the procedures for samples preparation, machine configuration tools, equipment, and analysis techniques.

Chapter IV presents and discusses the results obtained in the experimental phase, dealing with aspects such as the characterization of the alloy, the study of the formation and morphology of the chip, the effect of the inserts characteristics and the cutting parameters in the cutting forces and surface integrity.

Finally, chapter V analyzes the obtained results and answers the questions raised at the beginning of this work, refers the contributions and achievements of this research, and raises possible areas for future research.

Chapter 2 : Literature Review

The purpose of this chapter is to describe the current state of the published literature on the machinability of titanium aluminides from the perspective of surface quality and integrity. Some background information concerning the characteristics and classification of these alloys is presented at the beginning of this chapter. An overview of these materials properties' effects, cutting parameters, and tool characteristics on machined surfaces is provided below. The importance of this chapter lies in the understanding of the main problems presented in the machining of these alloys.

Finally, it should be noted that, because of the limited information available about TiAl machining, some of the experimental works have been analyzed from different approaches.

2.1. General Remarks

Titanium-based alloys are commonly used in industries such as aerospace, automotive, chemical and nuclear, mainly due to their remarkable specific strength and corrosion resistance [25, 26]. Due to these attributes, new alloys with unique characteristics have been developed. Among these new materials, it is possible to highlight titanium aluminides that are optimized for high temperatures applications.

2.1.1. Applications

Titanium aluminides (TiAl) are intermetallic compounds of ordered phases, which are composed of titanium, a high percentage of aluminum (22-56 at%), and other alloying elements in smaller proportions (10 at%) that act essentially as phase stabilizers. These alloys are characterized by ionic and metallic bonds with ordered microstructure that provide a unique combination of both metallic and ceramic characteristics.

TiAl main field of application is the aeronautical industry. They are even considered a potential substitute for Ni-based superalloys [27, 28]. Nowadays, they have an important presence in aircraft engine manufacturers, being used in blades for low-pressure turbines (Pratt & Whitney PW1100, GENx-1B, and LEAP-1A engines), and in high-pressure compressors (Pratt & Whitney PW1100G-JM turbo engines) [4, 8, 10] (Figure 2).

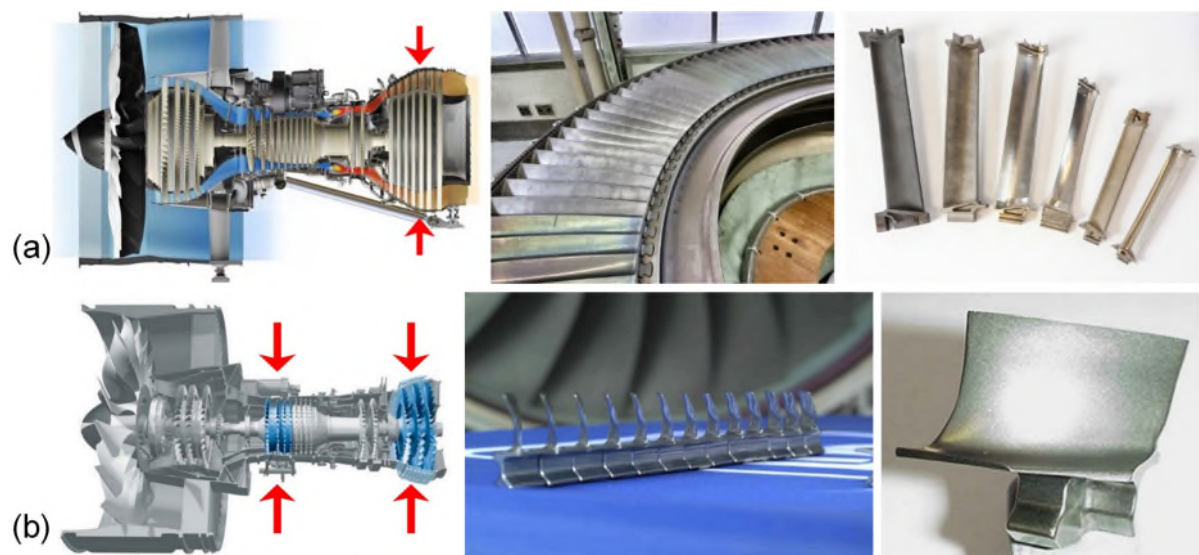


Figure 2. Aerospace application of TiAl; (a) cast and additive manufacturing low pressure turbine (LPT) blade of Ti-48Al-2Nb-2Cr (at%) by GENx [8, 18], (b) casted high pressure compressor (HPC) blade of Ti-45Al-8Nb-0.5 (B,C) (at%) by Thyssen, GfE, Leistriz for Rolls Royce [29, 30].

Other TiAl fields of application is the automotive industry which manufactures components for commercial or competition engines (turbocharger wheels, connecting rods and exhaust valves) [17, 31–33], the military industry, using it in rocket fins [2, 3, 34–39], while in the aerospace sector they have used for the fabrication of honeycomb panels and lattice panel cores [10, 40]. Figure 3 shows various components manufactured in titanium aluminides.

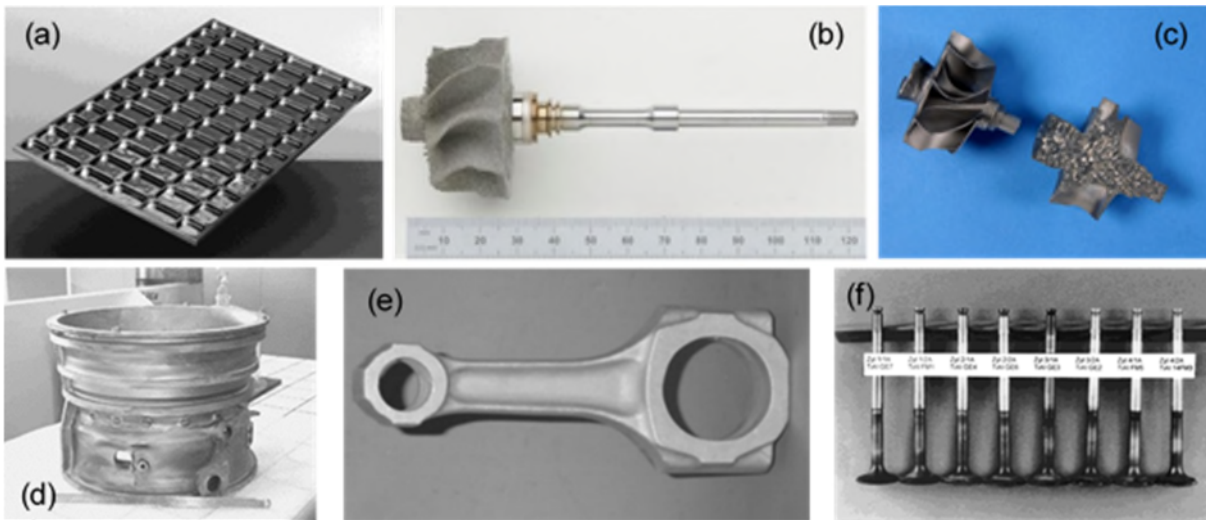


Figure 3. General application of titanium aluminides; (a) complex machined structural panel in γ -TiAl [41], (b) turbocharger wheel in Ti-48Al-2Nb-0.7Cr-0.3Si (at%) produced via additive manufacturing by electron beam melting technology (EBM) [42], (c) casted turbocharger wheel produced in γ -TiAl [43], (d) high pressure compressor casing of military engine manufactured by powder metallurgy in γ -TiAl, (e) forged connecting rod (conrod) produced in γ -TiAl [44], and (f) exhaust valves produced by near-net shape technology (NNS) in γ -TiAl [41].

As it can be noted, TiAl are mostly used in high demand applications. However, the difficulty of manufacturing parts and the complexity of their processing entail higher costs and limit their scope of use [28, 45].

2.1.2. Properties of titanium aluminides alloys

TiAl exhibit an interesting combination of physical, chemical and mechanical properties, due to their intermetallic nature. The main factor determining the mechanical properties of these alloys at both ambient and elevated temperatures is the concentration of aluminum. The most noticeable properties are their low density ($3.7\text{--}4.7\text{g/cm}^3$), which is even lower than other conventional Ti-based alloys, and also their ability to retain some of their characteristics at high temperatures, such as:

Specific stiffness (Figure 4.a) and resistance to creep (Figure 4.b) at temperatures between 700 to 900°C (~970 to 1170°K) [10, 28].

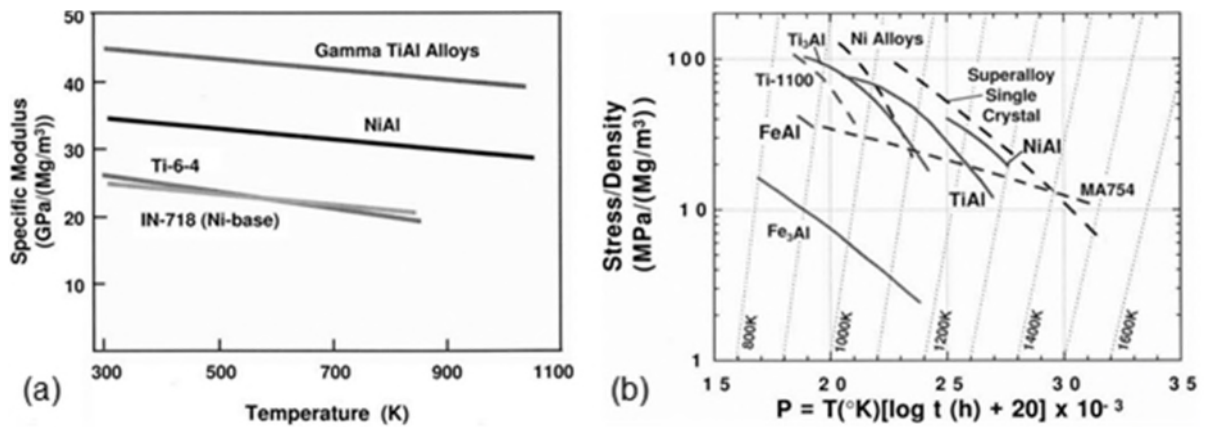


Figure 4. Comparison of high-temperature properties for TiAl and some selected alloys; (a) specific modulus versus temperature, and (b) specific strength versus Larson–Miller parameter for creep rupture [27].

Excellent specific strength (Figure 5); Young modulus $E=175\text{GPa}$ at 20°C and 150GPa at 700°C [10, 28].

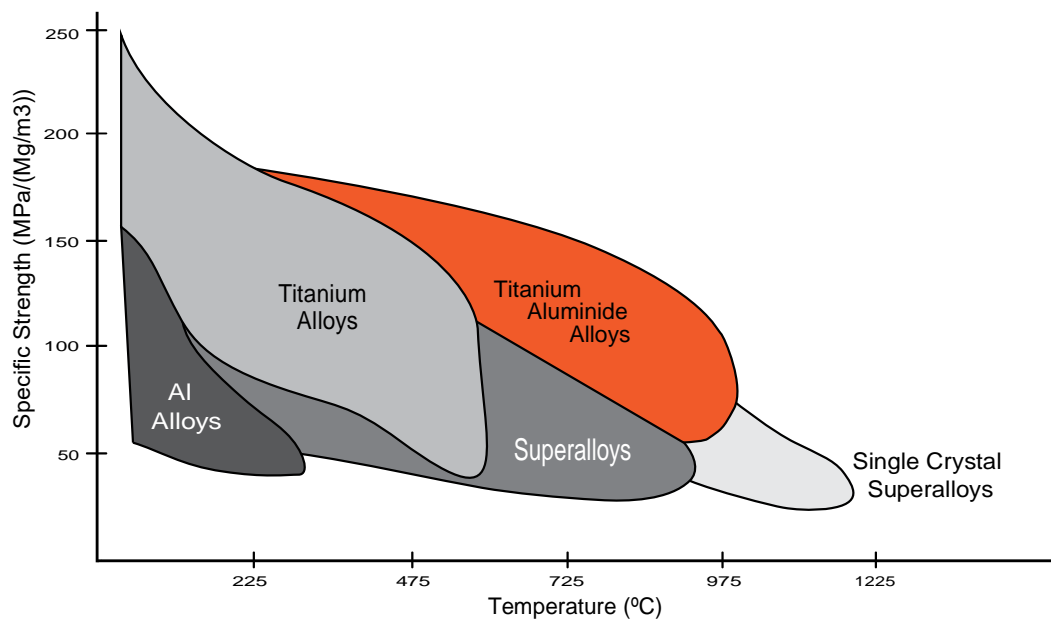


Figure 5. Comparison of high-temperature properties for TiAl and selected alloys; specific strength versus temperature (adapted from [27]).

Resistance to oxidation and corrosion, because titanium aluminides tend to form TiO_2 at high temperatures, rather than the more protective Al_2O_3 that characterizes the most oxidation-resistant superalloys, This fact restricts its working temperature to 600-760°C [46].

Table 1 presents different data and compares the properties of TiAl with other materials.

Table 1. Properties of TiAl alloys, Ti-based alloys, and Ni-based superalloys [47–49].

Property	Unit	TiAl-based alloys		Ti-based alloys	Ni-based superalloys
		α_2 -Ti ₃ Al	γ -TiAl		
Density	g/cm ³	4.1-4.7	3.7 – 3.9	4.54	8.3
Young Modulus RT	GPa	100-145	160 – 176	96-117	206
Yield Strength	MPa	700-990	400-650	380-1150	1000
Tensile Strength	MPa	800-1140	450 – 800	480-1200	1200
Fracture Toughness at RT	MPa \sqrt{m}	13-30	12-35	12-50	30-100
Ductility at RT	%	2-10	1-4	10-25	3-25
Ductility at HT	%/°C	10-20/660	10-60/870	12-50	20-80/870
Creep limit	°C	730	750-900	600	800-1090
Oxidation limit	°C	700	750-900	600	1090
Hardness	HV10	285	285-350	360±30	320-390
Melting Point	°C	1460	1600	1600	1400
Thermal conductivity	(W/m K)	22	22	7.3	11.3

Bearing in mind the specific properties of titanium aluminides (hardness, yield and tensile strength), it could be concluded that to machine this type of alloys, similar considerations to those of conventional titanium alloys are required, although properties such as the low ductility and the limit toughness at RT temperature make this material more challenging to machine since these attributes cause cracked surfaces.

Similarly, the low thermal conductivity and low Young's modulus are undesirable in terms of machinability, as they reduce the heat dissipation in the cutting zone, increase vibrations during machining, accelerate cutting tool wear, among others [26, 29].

From the perspective of product design and development, the physical properties of these alloys are obviously of great interest, while for processing and manufacturing it poses serious challenges.

2.1.3. Microstructure of titanium aluminides alloys

The ordered intermetallic titanium aluminide alloys are formed by the strong affinity between titanium and aluminum. These alloys constitute a unique titanium-based alloy,

exhibiting a microstructure with a long-range molecular arrangement at both ambient and high temperatures, up to $\sim 1000^\circ\text{C}$ [22, 48].

The characteristics of these materials are directly related to the concentration of aluminum and their microstructure, meaning that their properties depend on the type of bonds between atoms, ions, and molecules, as well as how they are ordered [3, 50].

To understand their properties, it is necessary to identify the microstructure [49, 51]. The binary titanium-aluminum phase diagram of Figure 6 shows the three solid phases, where the shaded area of the graph identifies the titanium aluminides of most significant commercial interest.

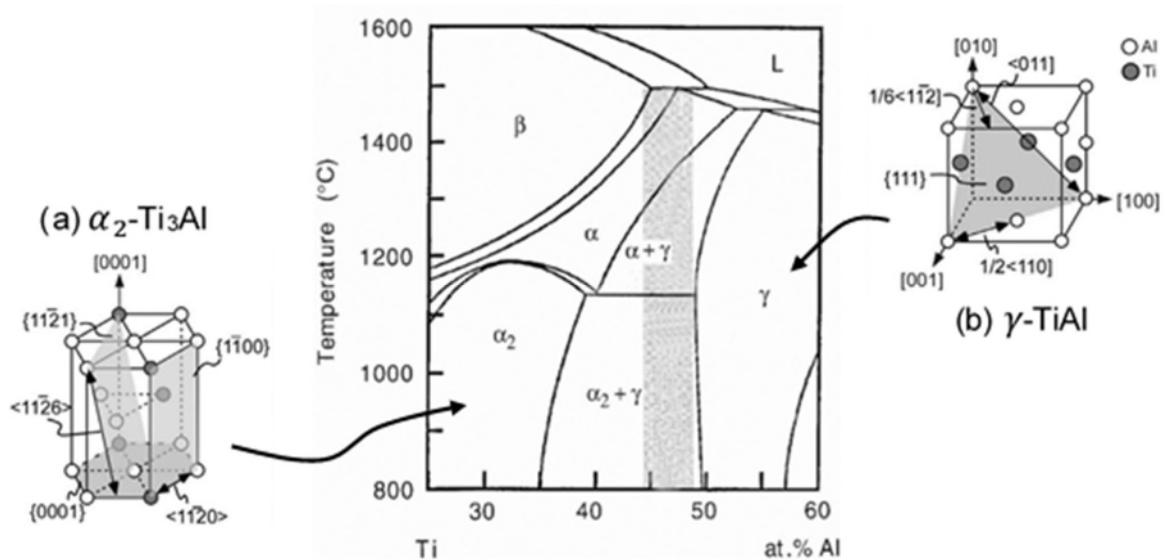


Figure 6. Binary equilibrium phase diagram of Ti-Al alloys [22] and microstructures of TiAl phases; (a) hexagonal α_2 -Ti₃Al, and (b) tetragonal γ -TiAl [2].

In terms of microstructure, TiAl can be classified into three categories: alpha-2 (α_2 -Ti₃Al), gamma (γ -TiAl), and alpha-2/gamma (α_2/γ) phases, which are discussed below [48, 52, 53].

2.1.3.1. Alpha-2 (α_2 -Ti₃Al) microstructure

In a composition range from 22-35 at% of Al, there is the stability zone of the α_2 phase, which is maintained in an orderly state, at a temperature of up to 1180°C and more specifically for 32 at% of Al. These alloys are characterized by an hexagonal microstructure (Figure 6.a), with high specific strength up to 800°C , higher density (4.3 g/cm^3), lower elastic modulus (145 GPa) and better ductility (2-10%) than γ alloys [54].

In the development of these alloys, the addition of alloying elements, such as niobium, seek to enhance the ductility at room temperature. The most studied α_2 alloys present a typical composition of 23 to 25 at% Al, 11-18 at% Nb, 3 at% V and approximately 1 at% Mo [48, 54, 55].

2.1.3.2. Gamma (γ -TiAl) microstructure

The gamma phase (γ -TiAl) has 49-58 at% aluminum. For 52 at% Al this phase remains ordered until the melting temperature of $\sim 1440^\circ\text{C}$ and is characterized by equiaxial grains with an average size of $50\ \mu\text{m}$ [55].

This phase exhibits a tetragonal face-centered microstructure, which stands out for demonstrating an intrinsically fragile behavior, because of the limited mobility of the dislocations. Its ductility varies with grain size with elongation below 1-4%. The addition of V, Mn or Cr help enhance its ductility but only in α_2/γ microstructures [56].

Gamma microstructure shows higher elastic modulus (175 GPa) and lower density ($3.9\ \text{g/cm}^3$) than conventional titanium alloys and α_2 alloys, though it retains its mechanical strength at higher temperatures [2, 50, 52]. According to several authors [9, 22, 35, 39, 47, 57], this material is one of the most attractive alternative to engineering applications.

Typically, these alloys contain between 48 and 54 at% of Al and 1-10 at% of elements such as V, Cr, Mn, Nb, Ta, W, or Mo [2, 46].

2.1.3.3. Two-phase (α_2/γ) microstructure

TiAl with 35-49 at% Al are located in a duplex phase zone characterized by an α_2/γ microstructure. This microstructure consists of two types of constituents, the first in a single γ phase and the others with colonies of eutectoid a lamellar structure of alternating α_2 and γ plates, which are formed as a result of the transformation of the alpha structure (α) during cooling to room temperature. The eutectoid colonies typically measure between 10 and $35\ \mu\text{m}$ in diameter and the lamellar plates have a thickness between $0.1\ \mu\text{m}$ and $1\ \mu\text{m}$. In the case of structures with $\sim 48\%$ of Al, after being thermally treated, they can form complete lamellar structures with colonies up to $1000\ \mu\text{m}$ in diameter [22, 28, 49].

Typically, the γ phase is the most frequent and α_2 is the complementary phase. The α_2/γ microstructure has a better balance of mechanical properties than single-phase alloys, mainly demonstrating higher resistance to high temperatures, better ductility and toughness [54, 55].

Duplex phase TiAl are divided into four classes, namely near-gamma, duplex, near-lamellar and fully lamellar. These microstructures are obtained by heat treatment at specific temperatures (from 1200°C to 1450°C).

2.1.3.3.1. Near Gamma Microstructure

The near gamma microstructure (Figure 7.a) is obtained after heat treatment at 1250°C in the $\alpha_2 + \gamma$ phase region. These alloys present zones of γ coarse grains mixed with elongated regions of equiaxed γ grains with dispersed α_2 particles. The average granulometry of these microstructures ranges from 30 μm to 50 μm [2, 47].

2.1.3.3.2. Duplex Microstructure

The duplex microstructure (Figure 7.b) is obtained by heat treatment in the phase field $\alpha + \gamma$ at temperatures around 1320°C. These microstructures are characterized by lamellar fine eutectoid colonies together with equiaxed γ grains with an average grain size of 10 μm . This fine grain size gives the material a high ductility and resistance, but a lower resistance to creep and fatigue [6, 14].

2.1.3.3.3. Nearly Lamellar Microstructure

The nearly-lamellar microstructure (Figure 7.c) is obtained at an intermediate temperature (~1360 °C) between fully lamellar and duplex temperatures. This microstructure shows coarse eutectoid lamellar colonies with fine equiaxed γ grains in the range of 150 μm to 200 μm [2, 47].

2.1.3.3.4. Fully Lamellar Microstructure

The fully lamellar microstructure is formed above the transus line (1400 °C), in the α phase region (Figure 7.d). This microstructure is characterized by a completely lamellar morphology of alternate plates of $\alpha_2 + \gamma$ phases with a colony size between 200 μm and

1000 μm . Coarse colonies size provides excellent creep and fatigue resistance, but with abnormal low ductility and strength [1, 9, 58].

The mechanical properties of two-phase titanium aluminides are strongly dependent on the proportion and morphology of each phase. However, the addition of a third component promotes new phases that improve their mechanical properties.

In general, in two-phase alloys, small additions of Cr, V or Mn improve ductility. B is a grain refining agent, while Nb, Mo, and Ta contribute to enhance the toughness of these alloys, although they increase their density [9, 50]. Figure 7 shows the four categories of microstructures of dual phase titanium aluminides.

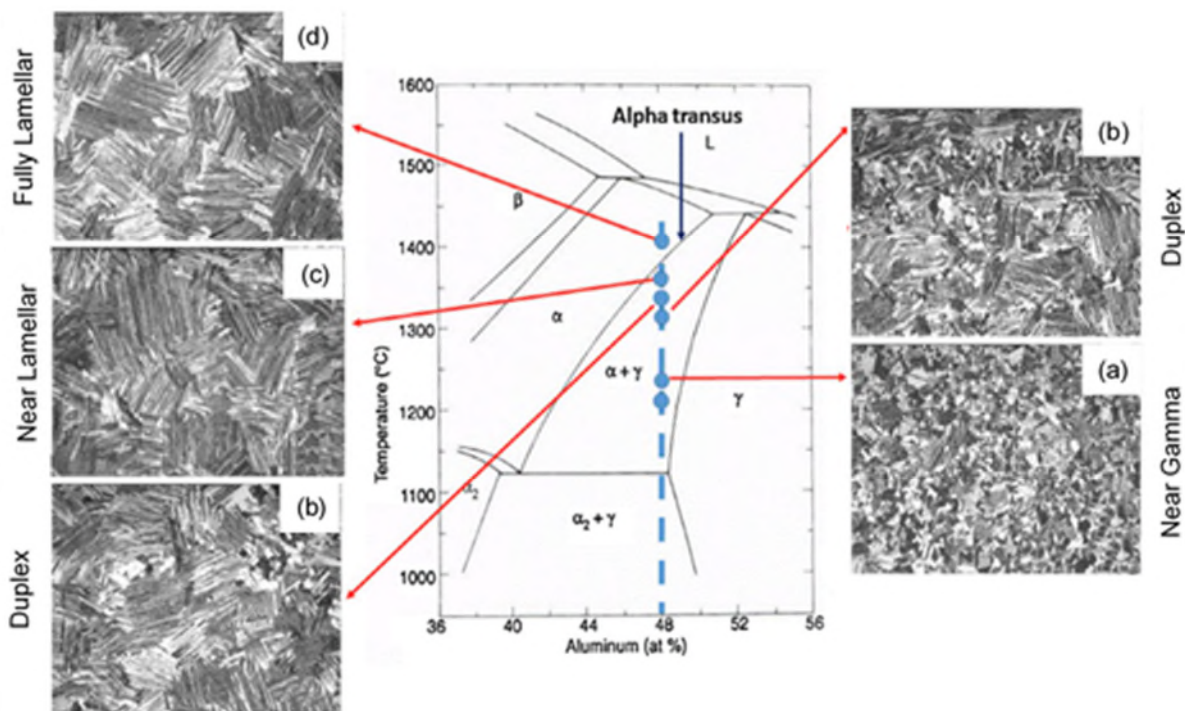


Figure 7. Microstructures of Ti-48Al; (a) near gamma, (b) duplex, (c) nearly-lamellar and (d) fully lamellar [6].

2.1.4. Summary

Titanium aluminides are important materials for both the aerospace and automotive industries due to properties such as lower density, higher stiffness, and higher temperature resistance, when compared to conventional titanium-based alloys. These materials are used primarily in components that require high strength, fracture toughness and resistance to fatigue, creep and corrosion.

These alloys have two types of microstructure at room temperature: the first one is the α_2 (Ti_3Al) which occurs when the Al content is between 22-35 at%, while the second one is the γ -TiAl which exists in a 49-56 at% Al content. Alloys in the 35-50 at% Al range exhibit a combined structure α_2/γ .

In terms of properties, γ -TiAl are considered the most suitable for applications at high temperatures (1450°C). However, their high fragility has not allowed their commercial use. Consequently, the most studied and used alloys are α_2/γ with a percentage of ~48 at% Al (Table 2), which possess superior ductility and good mechanical properties, although they reduce the application temperature below 760 °C due to their poor toughness (12 MPa $\sqrt{\text{m}}$).

Table 2. Summary of the most used α_2/γ TiAl and their attributes.

Alloy	Attributes	Ref.
Ti-48Al-2Nb-2Cr	Ductility, fracture, toughness	[33, 54, 59]
Ti-45Al-2Nb-2Mn-0.8 vol% TiB ₂	Tensile and fatigue strength, fluidity	[35, 41]
Ti-47Al-2Nb-2Mn-0.8 vol% TiB ₂	Elevated temperature strength, fluidity	[35, 41]
Ti-47Al-2Nb-1Mn-0.5W-0.5Mo-0.2Si	Creep resistance	[60]
Ti-47Al-2W-0.5Si	Creep and oxidation resistance	[60]
Ti-48Al-2Nb-0.7Cr-0.3Si	Ductility	[32, 61–63]

In general, small additions of different elements can to improve their mechanical properties and oxidation resistance. Table 3 shows the effect of these alloying elements.




Table 3. Effect of alloying elements in TiAl.

Alloying Element	Effect
Cr, Mn, Zr	Improve ductility
Cr, Zr, W, Si, C, B, O	Improve tensile strength
W, Ta, Mo, Si, C	Improve creep resistance
Nb, W, ta, Si	Improve oxidation resistance
B	Grain size control

2.2. Machinability

Machinability can be defined as the response measurement of a material to cutting through a machining process, or also as the set of knowledge and methodologies acquired in the machining of a given material. This understanding can be considered as an exclusive property of the material, but a large number of other factors involved in machining (Table 4) connects this property to the machining process under a specific set of conditions [64].

Table 4. Factors affecting machinability [64–66].

		
Material Characteristics	Cutting Tool	Machining Parameters
Mechanical properties Chemical properties Physical properties Microstructure Processing Heat treatment	Material properties Grain size Coating Geometry Edge Surface Finish Tool holder/cutter Teeth number	Machining process Cutting parameters Tool tilt and lead angle Toolpath and CAM Workpiece clamping Cutting environment Machine Rigidity Vibration

Information about machinability commonly consists of machining parameters such as cutting speeds, feeds, cutting depths, energy consumption, machining techniques, tool geometries, among others. The constant development of advanced materials such as TiAl, as well as new cutting tools and machine tools, requires machinability studies to be continuously updated through original research, as is the case of this thesis.

The study of machinability is a task that encompasses a large number of criteria, tests, and methodologies that allow to evaluate the effect of the factors involved in the machining of workpieces, cutting tools and production costs, whether the object of evaluation is the workpiece material or the cutting tool. The main methods used to analyze this property are described in Table 5.

Table 5. Commonly used criteria for assessing the machinability of TiAl.

Assessing Criteria	Description	Ref.
Surface integrity and surface finishing	<p>This criterion is mainly focused on analyzing in detail the effect that the machining parameters cause at the surface of the machined parts and determining the optimum machining conditions.</p> <p>In the case of TiAl, this procedure is focused on the analysis of work hardening, residual stresses, roughness and surface defects.</p>	[23, 67–71]
Chip formation	<p>The study of the chip formation provides a better understanding of the behavior of material during the machining process. The purpose of this technique is to determine the characteristics of the cutting process according to the type of chip.</p> <p>For TiAl this methodology has been less studied, mainly due to the tiny needle-shaped chip type, which makes this method of analysis more challenging.</p>	[72–74]
Cutting forces and power consumption	<p>The measurement of cutting forces makes it possible to monitor the behavior of the material during the machining process and relate these data to surface quality, damage and tool life. This methodology requires less material, and machining time than the other criteria. However, it demands more controlled experimental conditions.</p> <p>For TiAl, the study of cutting forces is frequently used, namely for the comparative analysis of different tool types and their characteristics, as well as the machining environments and the selection of the optimum range of cutting parameters.</p>	[59, 67, 75–80]
Tool wear and lifetime	<p>This criterion is one of the most commonly used methods for evaluating machinability, which analyzes the behavior of the material through the type of wear of the cutting tool.</p> <p>In the case of the TiAl, wear criteria of 100-300 μm from the cutting edge are normally used as the end of tool life parameter.</p>	[23, 65, 76, 81, 82]
Cutting temperature	<p>This type of analysis is mainly used to compare the machinability of a material under different cutting conditions and to detect temperature variation mostly caused by wear of the cutting tool.</p> <p>For TiAl this type of analysis is used typically as a complementary method for studies of tool life and wear.</p>	[83–86]
Mechanical Properties	<p>This kind of analysis seeks to identify and classify several materials into groups with similar mechanical properties, to determine a set of cutting parameters and ideal cutting conditions for each group.</p> <p>TiAl have different studies where they are mainly classified by the type of the microstructure; however, the special characteristics of the different phases, demand for each case a specific study.</p>	[9, 75, 82, 87, 88]

Several publications about machinability of titanium aluminides [89–95] report that this area of knowledge is still developing, in contrast to Ti-based alloys. Published studies

focus principally on processes such as turning, grinding, drilling, milling and electrical discharge machining (EDM) [27, 69, 75, 96–101].

Several authors [35, 64, 102–107] agree that TiAl is significantly more difficult to process than Ni-based superalloys, describing it as a material with extremely low machinability. This peculiarity is due to its mechanical, physical and chemical properties. The most frequent problems that are reported are the nucleation of microcracks, tendency to surface hardening, reduced useful tool life, among others.

The following is a more detailed explanation of these properties' effects on the machinability of titanium aluminides.

2.2.1. Thermal conductivity effect in machinability

The thermal conductivity of the workpiece material plays an essential role in its machinability. For cutting temperature, an excellent ability to quickly dissipate the heat generated by the machining process through the material is in general advantageous.

The inherent low thermal conductivity of Ti-based alloys makes their machining more complicated than the majority of other materials [90]. In case of TiAl, the thermal conductivity is ~ 22 W/mK [2], which is higher than that of conventional titanium alloys and nickel superalloys (~ 7.3 W/mK and ~ 11.3 W/mK respectively), but its effects are not less significant.

During machining, small and fine chips are usually produced. These chips of reduced contact area and fast-flow, combined with low thermal conductivity, resulting in very high cutting temperatures concentrated near the cutting edge of the tool. As a result, the cutting tools suffer increased wear, inducing adverse effects on the workpiece surface integrity.

Similarly, low thermal conductivity accompanied by high strength at high temperatures, lead to limitations for the determination of suitable ranges of machining parameters, as well as for tool selection, especially in continuous cutting operations, such as turning and drilling [48, 99].

In addition to these problems, the combination of these two properties leads to additional difficulties such as higher cutting forces, energy consumption, and vibrations.

2.2.2. Chemical affinity effect in machinability

Titanium is distinguished by its high affinity to various chemical elements. Due to this characteristic, all cutting tool materials tend to react chemically with Ti alloys, especially at cutting temperatures over 500°C [90].

In general, the high reactivity causes chips to weld at the tip and cutting edge of the tools (BUE), resulting in increased wear, catastrophic failures, and severe edge chipping. Also, the combination of this affinity with high thermal stresses induces wear by dissolution-diffusion of the tool, growing with the temperature of the cutting zone [25, 26].

Several studies demonstrate the existence of a high chemical affinity and a strong adhesive bond between TiAl and the cutting tools. This phenomenon was detected in most of the tested tools and it occurs mainly on the face of the rake (Figure 9), demonstrating that this effect is exhibited regardless of the type of material or coating.

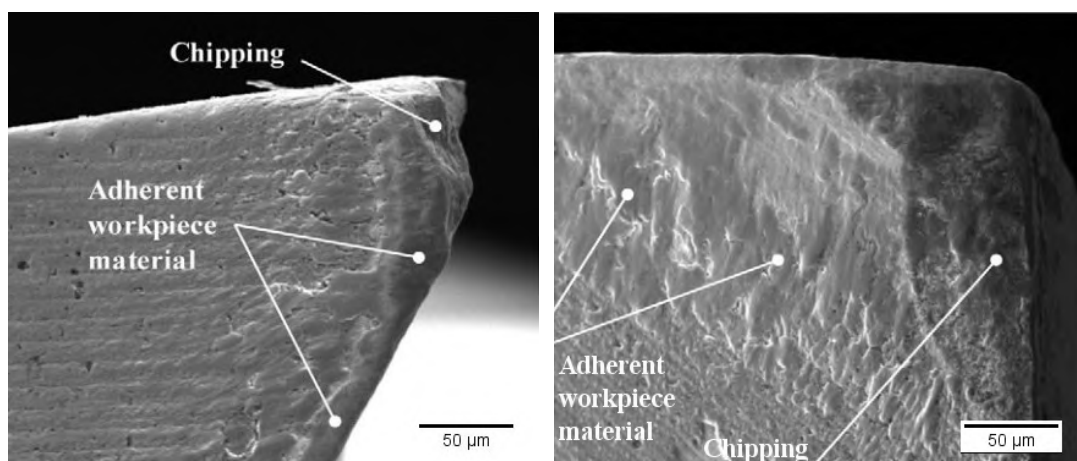


Figure 8. Images of adherent workpiece material on the tool cutting edge, after 40 min of milling (adapted from [108]).

On the other hand, the reactivity of these materials, in addition to the cutting tool damage, also causes seizure and chipping on machined surfaces [46, 109].

2.2.3. Ductility effect in machinability

Low ductility is generally beneficial in terms of machinability, because it promotes chip breaking, reduces cutting edge wear, and extends the tool life. Unfortunately, due to their intermetallic nature, titanium aluminides have extremely low ductility at room temperature (between 1 and 4%), which makes them excessively brittle [90, 102].

As mentioned above, the most used and studied TiAl are those with a α_2/γ structure. George et al.[49], studied the ductility of these alloys, and found that the yield stress of the lamellar structure is highly dependent on the angle between the lamellar boundaries and the load axis (Figure 9), due to the difference of the yield stress between the α_2 and γ lamellar. They identify as the main reason for the low ductility, the fragility of the lamellar boundaries at perpendicular tensile loads.

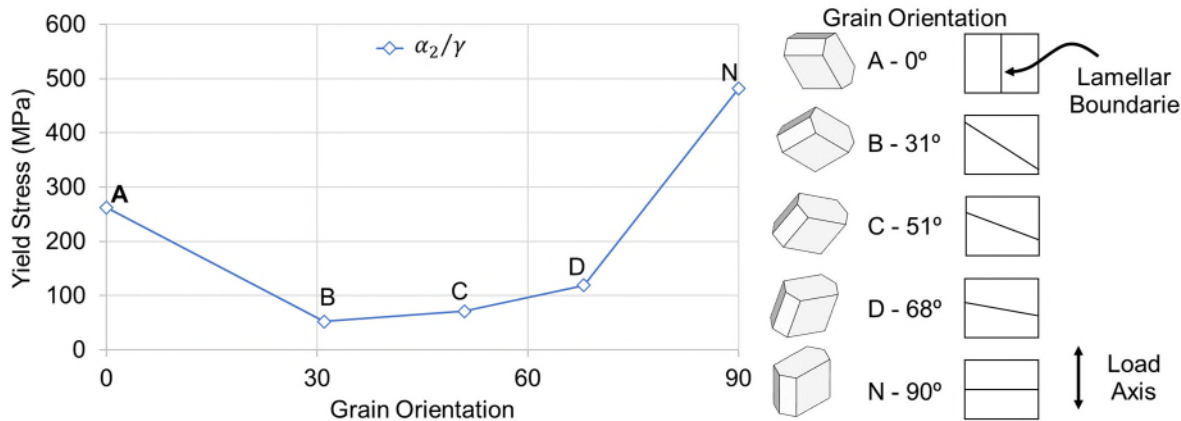


Figure 9. Yield stress of the Ti-36.5 at% Al alloy (α_2/γ microstructure) as a function of the angle between the lamellar boundaries and load axis (adapted from [49]).

This brittleness behavior affects the surface quality because, in the cutting process of brittle materials, the chip formation is more similar to a fracture process, which promotes severe manufacturing faults on the surfaces. The primary defects observed are grain detachment, smearing, residual stresses, and cracks nucleation or propagation. In addition to these drawbacks, the low ductility also promotes abrasive wear on cutting tools [110].

Typically, the ductility of materials rises with temperature, however, in TiAl, this variation only begins in a temperature range of brittle to ductile transition temperature (BDTT) of 600 to 800°C [49].

As already mentioned, brittleness is one of the main challenges to overcome in machining titanium aluminides, and this is one of the main problems that limit their large-scale industrial implementation [89, 97].

2.2.4. Hardness and Strength effect in machinability

Materials with high mechanical strength and hardness are considered difficult to machine because of the influence of these properties on accuracy, surface integrity, fatigue

strength, roughness, etc. The evaluation of these properties effect is determined by measuring the cutting forces and temperature at the workpiece/tool interface.

The combination of high cutting forces and high temperatures in the cutting area promotes rapid tool wear and cutting-edge deformation, which increases tool consumption and manufacturing costs [5, 67].

In order to eliminate or reduce the adverse effects of these properties on the workpiece and extend the service life of the cutting tool, suitable cutting parameter ranges are generally determined, coupled with lubricoolant strategies [2, 5].

The hardness (320 ± 35 HV10) and mechanical strength (400 - 990 MPa) of titanium aluminides are similar or even lower than nickel-based alloys (355 ± 35 HV10 and 1000 MPa) or conventional titanium alloys (360 ± 30 HV10 and 800-1100 MPa). However, the ability to keep these properties at high temperatures ($\sim 700^\circ\text{C}$) without substantial changes is a serious drawback to their machinability (Figure 10) [2, 22].

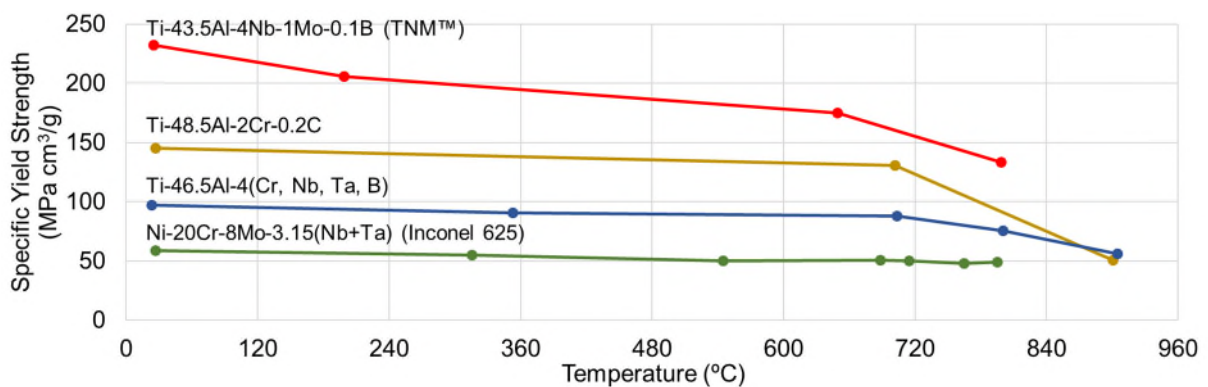


Figure 10. Variation of specific yield strength as a function of the temperature for TiAl-based alloys and Nickel superalloys (adapted from [35]).

Comparing to standard titanium alloys, TiAl machining generates higher cutting forces. In this field, several works were published, mainly by Mantle, Aspinwall and their collaborators [69, 79, 111, 112], showing that the components of the cutting forces (tangential, radial and feed) can be between 130 % to 200 % higher than for the Ti-6Al-4V alloy. In the same way, the temperature at the tool/workpiece interface can be up to 100°C higher. These results reveal the greater difficulty of the TiAl cutting process.

2.2.5. Work Hardening effect in machinability

Work hardening is the increase in the hardness of a surface layer caused by plastic deformation. A substantial increase in the surface hardness and thickness of this layer causes residual stresses, affects the surface integrity of the part and compromises the performance of the components.

In machining, this phenomenon affects the surface integrity of the parts and the tool life. This fact is due to the accelerated wear of the tool cutting edge, caused by the increase in the cutting load of the hardened layers. Additionally, surface hardening affects the energy required for the metal cutting process [113].

Mantle et al. [71] report that in TiAl machining, the increase in hardness indicates a high susceptibility to strain hardening, which further reduces the already poor surface ductility of the material, decreasing fatigue life. In addition, they report that surface hardness values can be up to double the nominal hardness and that cutting parameters are not significantly influential in this phenomenon.

The temperature at the cutting interface of the material affects the surface hardening, mainly at a depth of the layer. The use of high-pressure lubrication systems has been shown to cause an increase of up to 10% in the maximum hardness, due to the cooling effect that reduces the temperature and, thus, the ductility of the workpiece in the cutting area [67] (Figure 11).

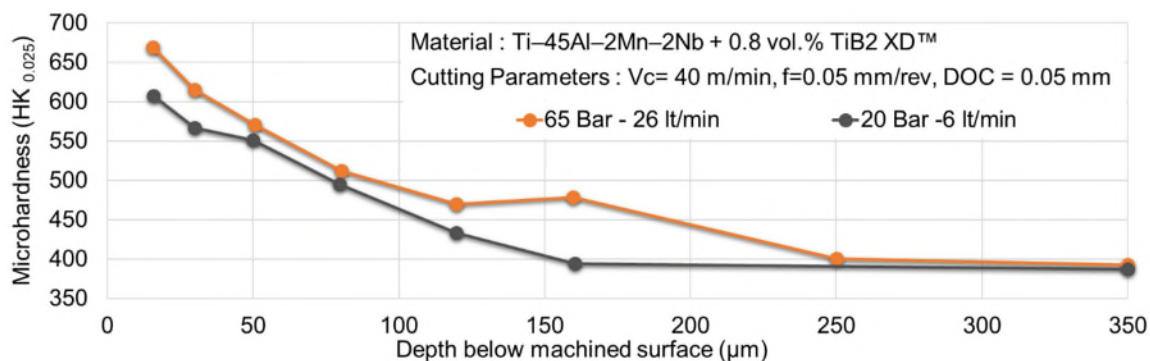


Figure 11. Microhardness profile of Ti-45Al-2Mn-2Nb +0.8 vol% TiB2 (adapted from [67]).

In general, the work hardening effect in the machinability of titanium aluminides is one of the most studied topics of these alloys.

2.2.6. Summary

In conclusion, from the perspective of the TiAl characteristics, the excellent properties that optimize their technical performance are also the leading cause of their poor machinability. These properties promote high cutting temperatures and high cutting forces, which substantially accelerates the tool deterioration, the damage to surface integrity and low machining efficiency.

Titanium aluminides raise important challenges to the study of their machinability, mainly due to the need to mitigate the effect of their properties and optimize machining conditions. Table 6 summarizes the impact of the main features affecting the machinability of TiAl.

Table 6. Influence of TiAl properties on their machinability.

Property	Description	Ref.
Thermal Conductivity	The low thermal conductivity causes the heat produced at the cutting interface to dissipate through the cutting tool, leading to accelerated wear of the cutting edge.	[5, 82, 114]
Chemical reactivity and Inclusions	The high reactivity and chemical affinity of titanium with the base material of the cutting tools as well as with its coatings, lead to the adhesion of particles in the cutting edge of the tool, forming an unstable edge that deteriorates the machined surfaces, which consequently causes typical defects such as smearing, tears, and surface cracking. This behavior is more evident in titanium aluminides containing boron (TiB ₂).	[69, 84, 109]
Ductility	In terms of surface integrity, the low ductility of titanium aluminides (1-4 at%) is a serious disadvantage, because it mainly promotes crack initiation and lamellar deformation, which influences surface integrity as well as fatigue strength of machined components.	[97, 114, 115]
Hardness and strength	The intrinsic capacity to keep hardness and strength at temperatures between 700 °C and 800 °C, makes the formation of chips more difficult, which generates an increase in cutting forces and accelerates the wear of cutting tools.	[56, 81, 84]
Work Hardening	Titanium aluminides show a great tendency to work hardening, due to its low capacity to deform plastically because of its ordered microstructures and ionic bonds. This behavior affects the quality of the parts in terms of roughness and surface integrity, as well as the service life of the tools.	[56, 71, 116]

2.3. Surface Integrity

Surface integrity (Figure 12) is the topographic, mechanical, chemical and metallurgical condition of a surface obtained by a manufacturing process. It can be characterized by external properties such as roughness, waviness, shape defects, texture, among others, as well as by its subsurface condition (hardness layer, residual stresses, plastic deformation, cracks, fragility, etc.) [117].

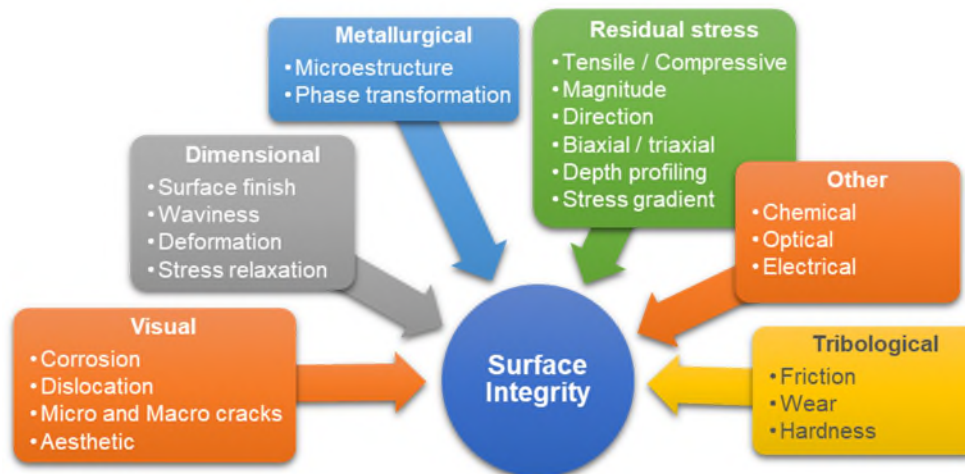


Figure 12. Key factors that define the surface integrity of machined parts (adapted from [65]).

For machining, the surface integrity is influenced by aspects such as mechanical properties of the workpiece material, characteristics of the cutting tools (material, geometry, type, etc.), type of machining process (turning, milling, grinding, EDM, etc.), operational conditions (clamping systems, cutting environment, cutting fluid, trajectories, etc.) and machining parameters (cutting speed, feed, cutting depth, etc.) [118–120].

Regarding the machining of titanium aluminides, several studies [69, 80, 108, 114, 121] focus on establishing the effect of cutting parameters (cutting speed, feed and cutting depth), and operational conditions on the quality of the surfaces obtained. These researches usually include the analysis of characteristics such as roughness, surface cracks, plastic deformation, surface hardening, residual stresses, fatigue resistance, among others. However, there is still a lack of information in the analysis of these correlations, which allows the establishment of certain machining parameters to improve the integrity of machined surfaces.

2.3.1. Roughness

In terms of machinability, roughness is the main characteristic that defines the quality of machined parts. In addition, this attribute provides the first indication of the external surface integrity of the pieces. In general, roughness is mainly affected by the integrity of the cutting edge of the tool (Figure 13) and by the cutting parameters of the process, of which cutting speed and feed rate have been shown to be the most influential [122, 123].

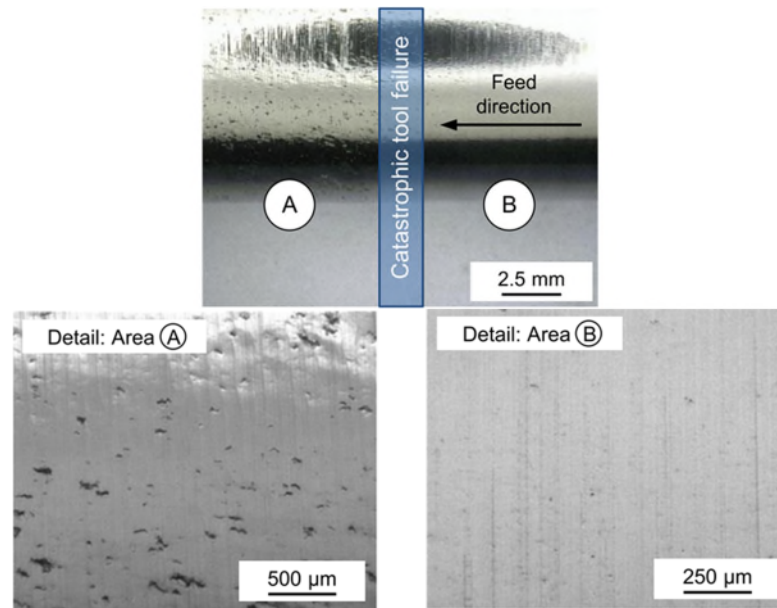


Figure 13. Effect of tool failure on surface integrity in γ titanium aluminides [124].

Machining processes such as turning or milling may produce surface roughness (R_a) values up to $0.2 \mu\text{m}$ [68]. Several studies [59, 67, 68, 124, 125] have reported that changes in cutting speeds, feed rates and depth of cut can be very useful in improving surface roughness. The authors usually recommend selecting slow feeds and high cutting speeds.

Beranoagirre and López de Lacalle [126] found that in milling operations, surface roughness improved from $0.42 \mu\text{m}$ to $0.37 \mu\text{m}$, when the cutting speed increased from 60 to 70 m/min. Likewise, Kollahdouz et al. [68], identified a similar trend in milling with high cutting speeds (HSM) and observed that the R_a decreased from 0.36 to $0.15 \mu\text{m}$ when the cutting speed varied from 300 to 600 m/min. However, other authors [127] report that for cutting speeds of 340 m/s, the roughness was higher than for a speed range of 160 to 250 m/min ($0.8 \mu\text{m}$ and $0.3 \mu\text{m}$ respectively). This effect can be explained by the rapid tool wear at high cutting speeds. This effect may vary depending on the influence of the lubricoolant strategy.

The optimization techniques of the cutting environment such as minimum quantity lubrication (MQL), high-pressure coolant or cryogenic cooling, are mainly focused on reducing the impact of temperature on the cutting edge, in search of prolonging the useful life of the tool and improving the roughness of surfaces.

Several authors [68, 76, 84, 123, 128–131] have conducted their studies on the machinability of titanium aluminides in dry conditions, due to the need to avoid the influence of the lubricant on the results. However, this condition is the least favorable for machining this material.

Experimental results indicate that cryogenic cooling systems and minimum quantity lubrication conditions improve surface roughness (Figure 14) and tool flank wear [80]. Furthermore, the use of high-pressure systems with excessively high flow rates increase the risk of tool cutting edge breakage, resulting in increased surface roughness.

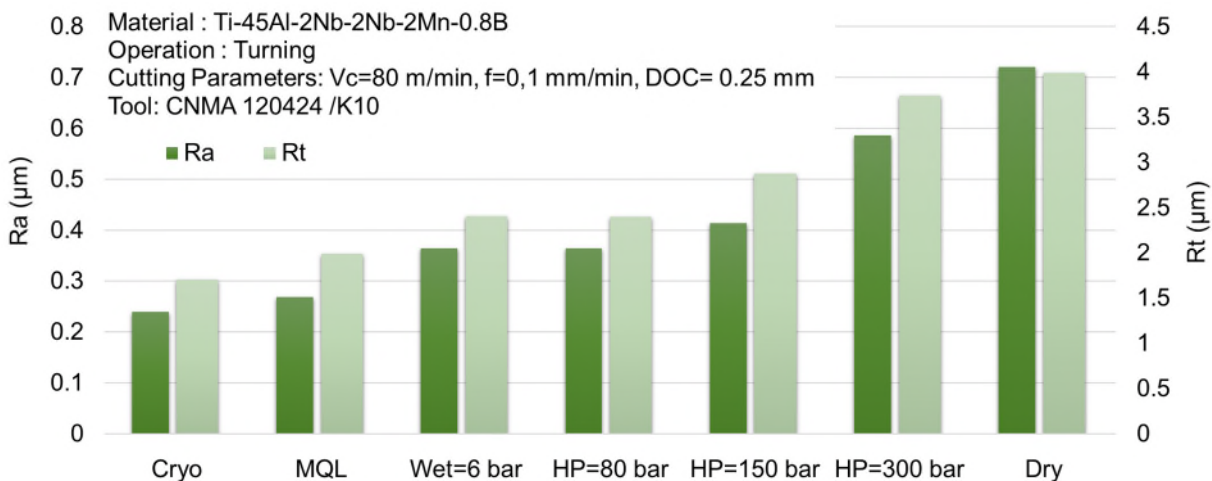


Figure 14. Cutting environment influence on surface roughness Ra and Rt in turning operations of a Ti-45Al-2Nb-2Mn-0.8B alloy (adapted from [80]).

Similarly, the surface roughness is also affected by the characteristics of the tool, such as geometry, cutting angles, tip radius, material, and coating, among others. Priarone et al. [108], reported that the use of a tool with a radial angle of 4°, an edge radius of ~10 µm, and an additional finishing of the cutting edge, improve the surface roughness (Figure 15). In addition, this research concludes that a larger edge radius results in a better finishing of the machined surface, and the reduction of the radial rake angle reduces tool wear.

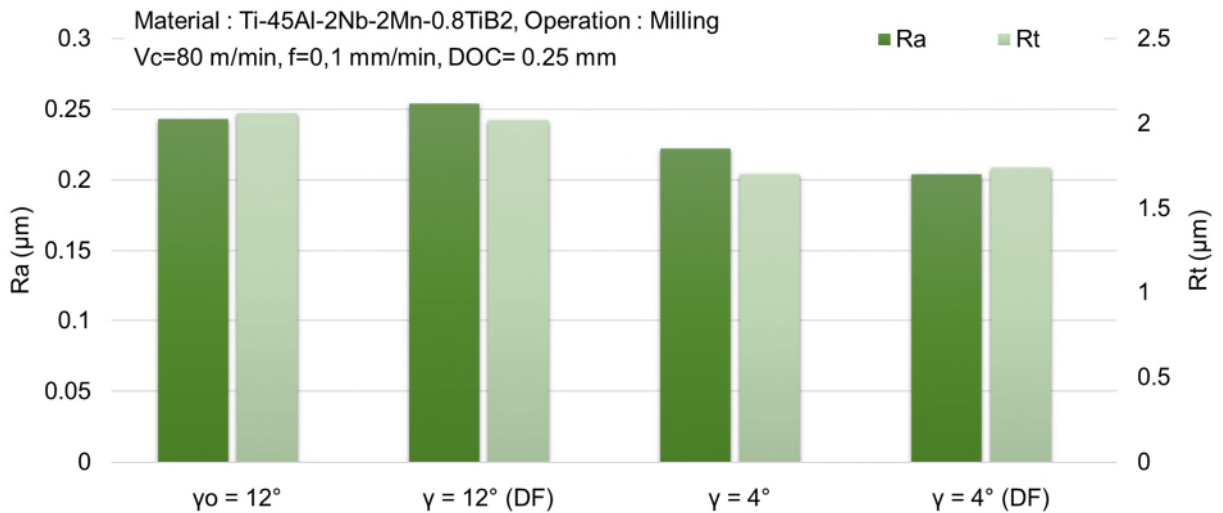


Figure 15. Influence of geometry parameters of the tool on surface finishing Ra and Rt, in milling Ti-45Al-2Nb-2Mn + 0.8 vol% TiB2 XD alloy (adapted from [98]).

In general, most researchers report surface roughness values (Ra, Rt, and Rz) suitable for aeronautical applications (Ra equal to or less than $0.4 \mu\text{m}$ [97]).

2.3.2. Surface Cracking Phenomenon

Surface cracking is analyzed in several studies on the machinability of titanium aluminides [59, 67, 69–71, 130]. This problem is influenced by factors such as microstructure (type and size of grains), mechanical properties (ductility, hardness, mechanical strength), machining process (grinding, milling, turning, drilling, etc.) and cutting conditions (parameters, environment, tools, etc.) [132, 133].

Low ductility is reported as the main characteristic of the material causing this problem [71]. In the case of α_2/γ alloys, the beginning of surface cracking is detected at the γ - γ lamellae interface. Figure 16 shows cracks in turned and milled TiAl specimens, where cracks occur due to interlamellar plate failure within the lamellae colonies, oriented at a favorable angle to the applied load [49].

The appearance of these surface failures is proportional to the cutting time, tool wear and machining parameters. Sharman et al. [67], identified that the cutting environment does not affect the level of cracking, while the depth of cut has a significant influence (67%) on the density and size of surface cracks (crack length $150 \mu\text{m}$ and $50 \mu\text{m}$ for cutting depths of 0.1 mm and 0.05 mm, respectively).

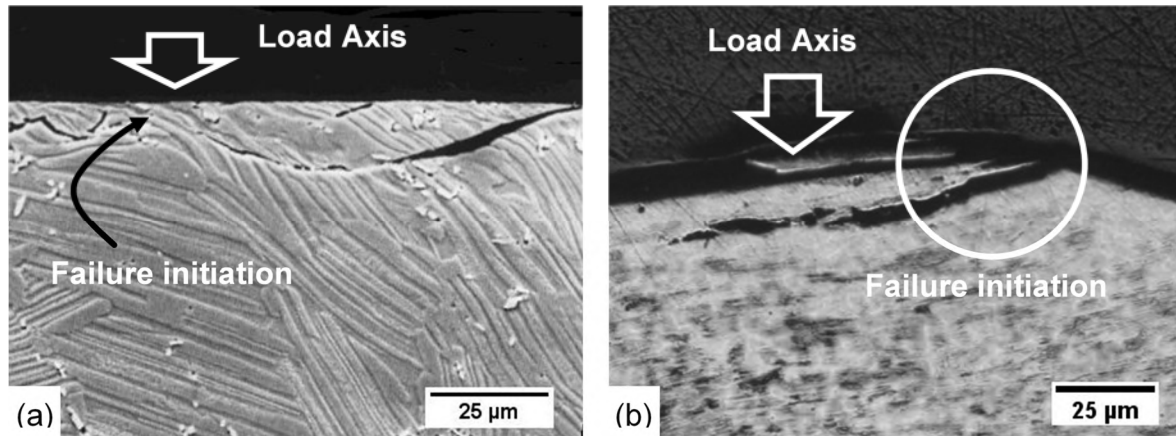


Figure 16. Fractography of; (a) turning sample in Ti-45Al-2Nb-2Mn - 0.8 vol% TiB₂ (adapted from Mantle et al. [71]), and (b) milling sample in Ti -48Al -2Nb -0,7Cr -0,3Si.

Generally, to avoid the nucleation of surface cracks in machining, it is recommended to use high cutting speeds to raise the temperatures in the tool-workpiece interface, thus increasing the ductility of the material and reducing the possibility of cracks initiation and propagation. To obtain this effect for TiAl, it should be taken into account that the chip formation temperature must exceed the brittle to ductile transition temperature (BDTT) of 600°C to 700°C [88]. Because of this characteristic, the application of this approach becomes more difficult for these materials.

Several authors [69, 127] studied the temperature in the cutting zone during machining. The results show that in milling, the temperature at the tool/piece interface can be around 420°C, which is not enough to optimize the BDTT and produce defect-free surfaces.

Uhlmann et al. [73] showed that after machining a part preheated to 300 °C, the number and size of cracks on the surface were significantly smaller than machining at room temperature. This work revealed the presence of small cracks in the surfaces up to a preheating temperature of 700°C. Defect-free surfaces were only obtained if the workpiece temperature rises to 800 °C or higher.

The use of technologies such as laser-assisted hybrid processes could probably improve BDTT, thus the integrity of machined surfaces. However, only a few studies on laser-assisted process have been published so far for titanium-based alloys [134–136] and even more limited research on titanium aluminides [97].

From the perspective of cutting tools, several studies have been conducted on the nucleation and propagation of cracks on machined surfaces using coated, and uncoated

cemented tungsten carbide (WC) tools [59, 76, 84, 108, 121, 130]. These studies display that surfaces produced with WC tools have a greater tendency to surface cracking, compared to other tool types, such as polycrystalline cubic boron nitride (PCBN), polycrystalline diamond (PCD) and cubic boron nitride (CBN) [97].

In this context, Priarone et al. [124] investigated this behavior in turning operations with PCD and CBN tools and noted that the better ability of CBN tools to retain the sharpness of the cutting edge, decreases the number of cracks compared to WC tools [67]. This phenomenon demonstrates the strong dependence between surface integrity and tool wear.

On the other hand, the main problem for the use of cracked surfaces in critical applications is their sensitivity to fatigue failure [137]. Evaluation studies on the growth of fatigue cracks in titanium aluminides [2, 114, 115] reveal that they are affected by microstructural defects caused by manufacturing processes. It is also concluded that, to promote the initiation of fatigue cracking in lamellar microstructures, it is necessary to exceed the fatigue limit, which in the case of these alloys is close to the tensile strength (approximately 85%).

Regarding fatigue life, it was found that surfaces produced in turning operations with R_a between 0.46-1.04 μm , had a longer average fatigue life than those obtained by polishing (R_a of 0.12 μm) [71], even those machined with worm tools (Figure 17).

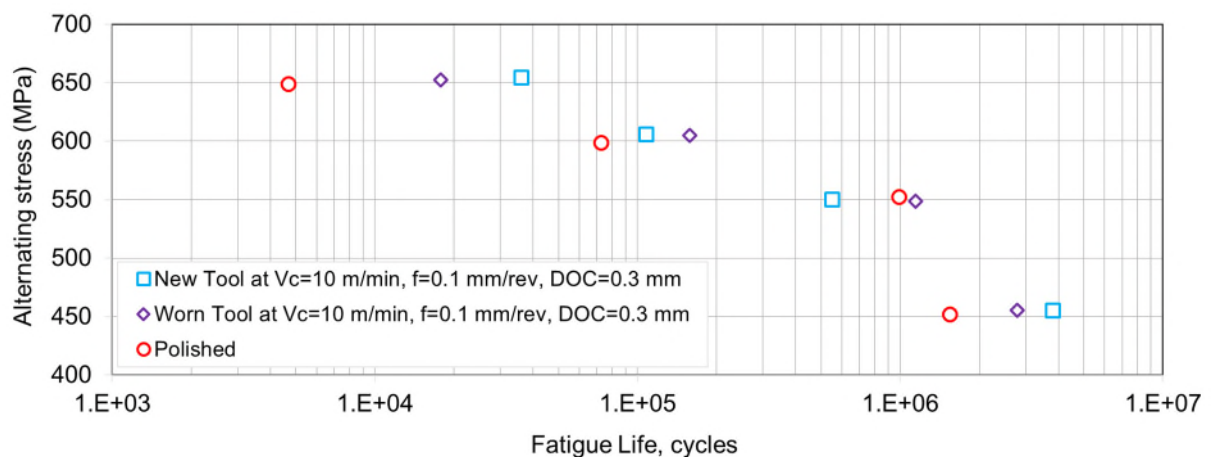


Figure 17. Rotating bending fatigue life testing at 3000 rpm of turned and polished titanium aluminide (Ti-45Al-2Nb-2Mn-0.8%TiB2 at% samples (adapted from [71])).

Sharman et al. [70], reported that the turned surfaces showed higher fatigue strength than surfaces obtained by electrochemical machining (ECM) and electro-discharge texturing (EDT) (Figure 18). This higher resistance occurs due to residual compressive stresses

caused by lamellar deformation in the subsurface layer of the turned parts. Also, it was reported that cracks up to 5 μm deep in the turned surfaces do not affect fatigue strength, thanks to the effect of residual compressive stresses.

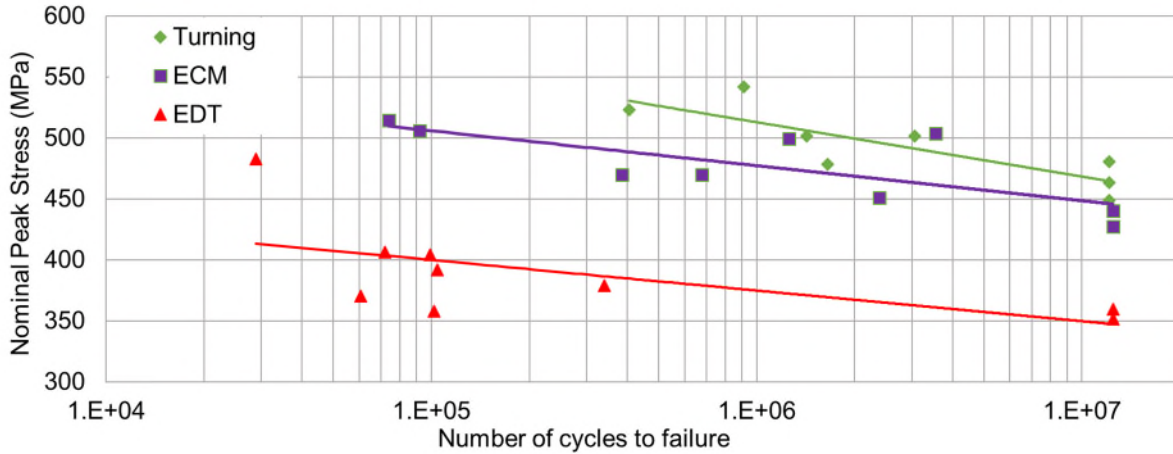


Figure 18. Stress – number of cycles curves for turned ECM and EDT specimens of Ti-45Al-2Mn-2Nb+0.8 vol% TiB2 XD at% (adapted from [70]).

In conclusion, surface cracking is usually a constant problem in machining processes that can hardly be eliminated, although it can be compensated to a certain extent by the presence of residual compressive stresses.

2.3.3. Lamellar Deformation

The final surface and geometry of a part is a result of a sequence of paths, such as roughing, semi-finishing and finishing. These operations cause surface and subsurface changes in the workpieces and can make the next steps more challenging to perform.

From the perspective of internal surface integrity, it is important to understand that the primary subsurface defects in titanium aluminides are hardening and residual stresses, mainly caused by lamellar deformation from machining operations. This behavior is caused by their low ductility and ability to keep the mechanical strength at high temperature [117, 138, 139].

Because lamellar deformation is not considered a subsurface defect by itself, the studies developed on titanium aluminides [69, 71, 114, 130] focus on two aspects. The first is the analysis of subsurface hardening and residual stresses as a function of the magnitude of the deformation, and the second is the determination of the effect of machining parameters on the characteristics of the deformation.

Figure 19 shows an example of lamellar deformation in two different titanium aluminide alloys.

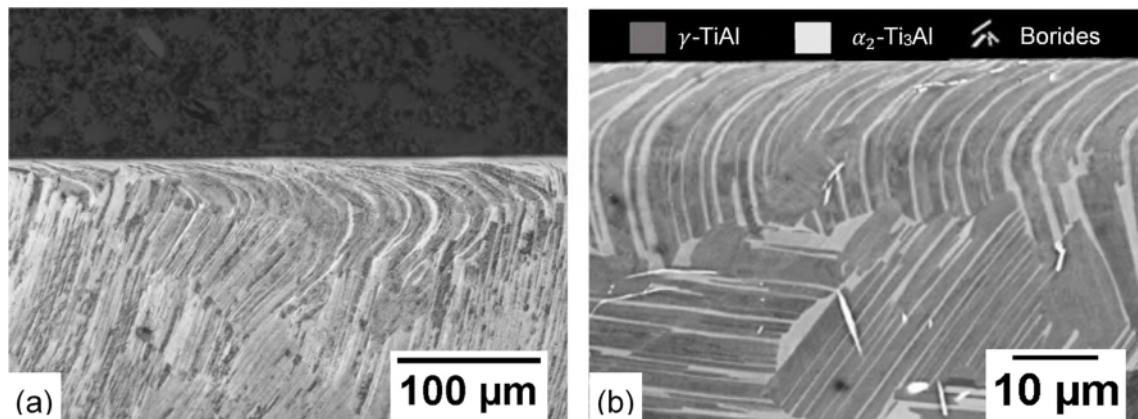


Figure 19. Plastic lamellar deformation of; (a) milling surface in Ti-48Al-2Nb-0.7Cr-0.3Si, and (b) turning surface in Ti-45Al-8Nb-0.2C-0.2B [125].

In general, the impact of cutting parameters on lamellar deformation can be evaluated by studying the thickness of the deformed microstructure [109, 127]. In this regard, Mantle et al. [69, 71] observed that the deformation could be between 20 and 30 μm deep in machined surfaces. However, it has been noted that the depth of the deformed microstructure can decrease using additional techniques such as laser-assisted machining (LAM), ultrasound-assisted machining (UAC) or cryogenic cooling strategies. It has been observed that UAC reduces the deformed layer from 39 μm to 17 μm [97, 140], while cryogenic refrigeration decreases the depth of subsurface changes from 30 μm to 10 μm [80]. Relatively to defects induced by lamellar deformation, a detailed explanation is presented below.

2.3.3.1. Subsurface Hardening

In TiAl, the hardening of the sub-surface is usually higher than that of the surface. This behavior is strongly influenced by its low deformation capacity [2, 98, 116, 141].

Hardened layers of up to 300 μm thickness have been reported with maximum hardness values of up to ~ 950 HV at 30 μm from the surface, and surface hardness of around ~ 600 HV (~ 350 HV for bulk material) [69]. Figure 20 shows an example of this type of microhardness profile within a layer depth of about 250-300 μm and a peak value of 680 HV.

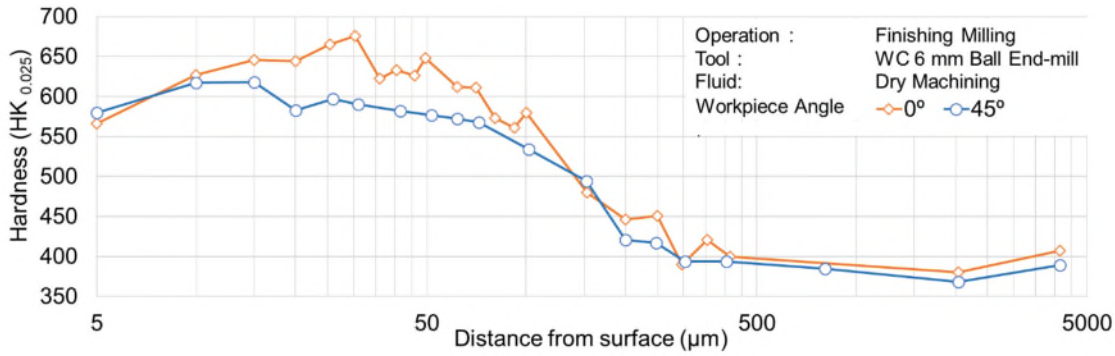


Figure 20. Microhardness depth profile of a titanium aluminide Ti-45Al-2Nb-2Mn-0.8% TiB2 (adapted from [69]).

As a result of subsurface hardening, the service life of the cutting tools is strongly affected. In order to diminish this effect, Sharman et al. [67] studied the impact of conventional and high-pressure refrigerant flow systems (20 and 65 bar, respectively), and reported hardness layers confined to depths of 200-250 μm, as well as maximum hardness of about 560-630 HV at 15 μm from the surface and a lesser impact of the conventional system.

In general, it is concluded that the lower temperature in the cutting zone induced by the action of a flood cooling system reduces the BDTT, and therefore increases the tendency to hardening. However, low temperatures at the tool/material interface also contribute to maintaining the cutting edge of the tool and consequently to reduce surface and subsurface defects.

The effect of tool wear on subsurface hardening is also the subject of research by several authors [24, 69, 81, 127, 142]. The results show that cutting tools with 300 μm of flank wear (VB) tend to increase the hardness of the subsurface up to 15% in the workpieces. Figure 21 shows the influence of the worn tool on surface hardening with a difference of ~90 HV at maximum microhardness.

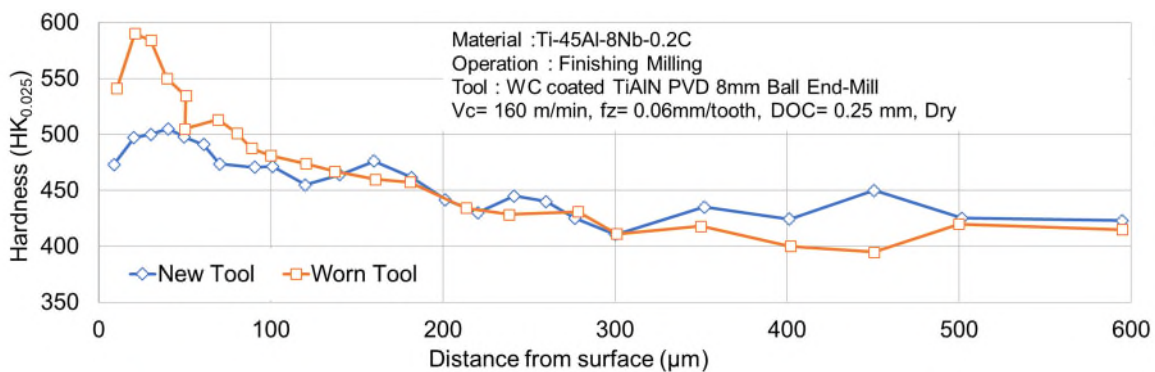


Figure 21. Microhardness depth profile of Ti-45Al-8Nb-0.2C (adapted from [127]).

Ge et al. [142], with new and worn WC tools, showed that surface hardness increased from 380 HV, in bulk material, to 575 HV and 600 HV, using cutting tools with a flank wear of 0.120 and 0.210 μm respectively, demonstrating the effect of tool wear on the hardening tendency (Figure 22).

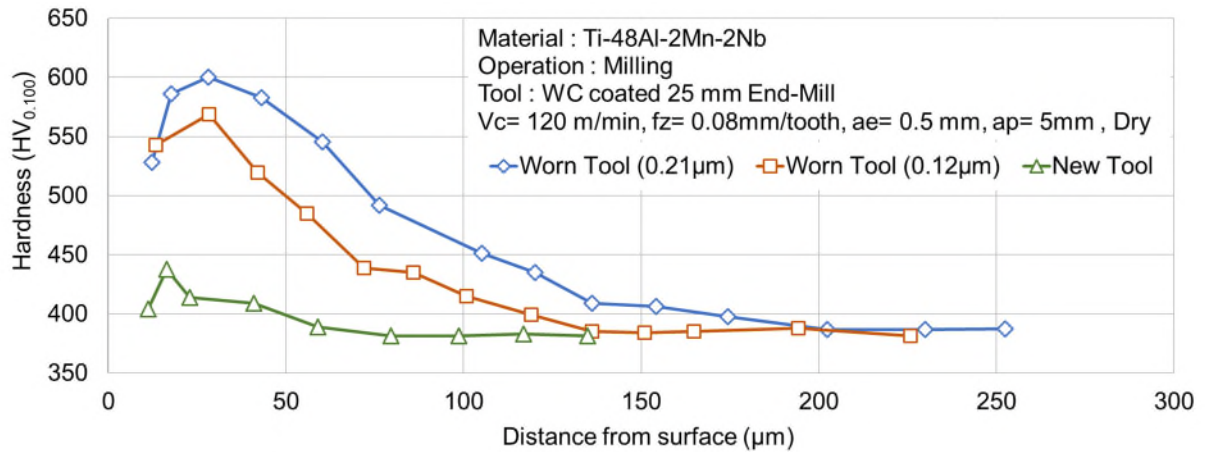


Figure 22. Microhardness depth profile on Ti-48Al-2Mn-2Nb for different tool wear (adapted from [142]).

Additionally, this research analyzed the impact of the cutting speed (60, 120, 240 m/min) on the layer hardness, and observed that the subsurface hardening decreased with the cutting speed, mainly from 60 m/min to 120 m/min (Figure 23).

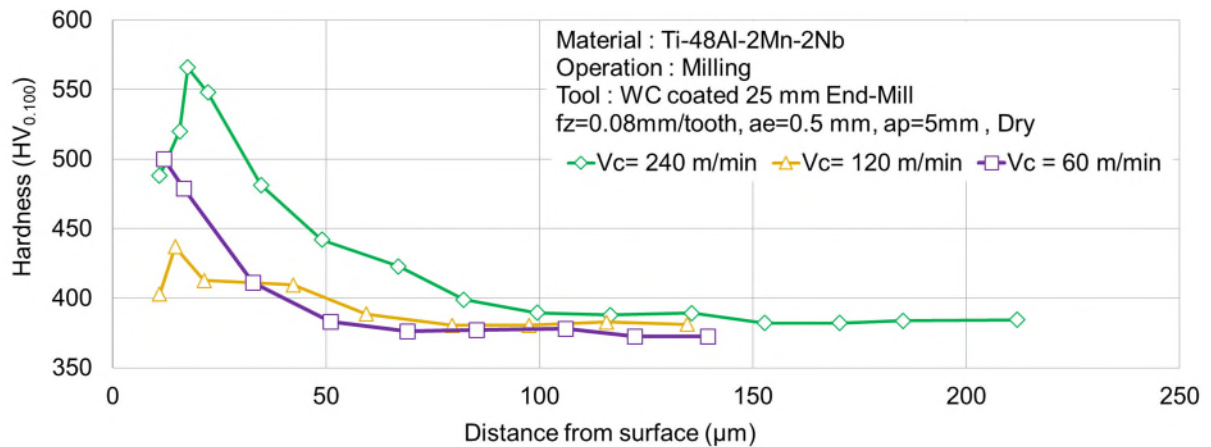


Figure 23. Microhardness depth profile of Ti-48Al-2Mn-2Nb under different cutting speeds (adapted from [142]).

Studies [68] on the performance of TiAl alloy under high-speed machining (HSM) conditions note that subsurface hardness increased from 320 HV (bulk material) to 950 HV and 840 HV for cutting speeds of 300 m/min and 600 m/min respectively (Figure 24). This result confirms that increasing cutting speed has a positive impact on the hardening trend.

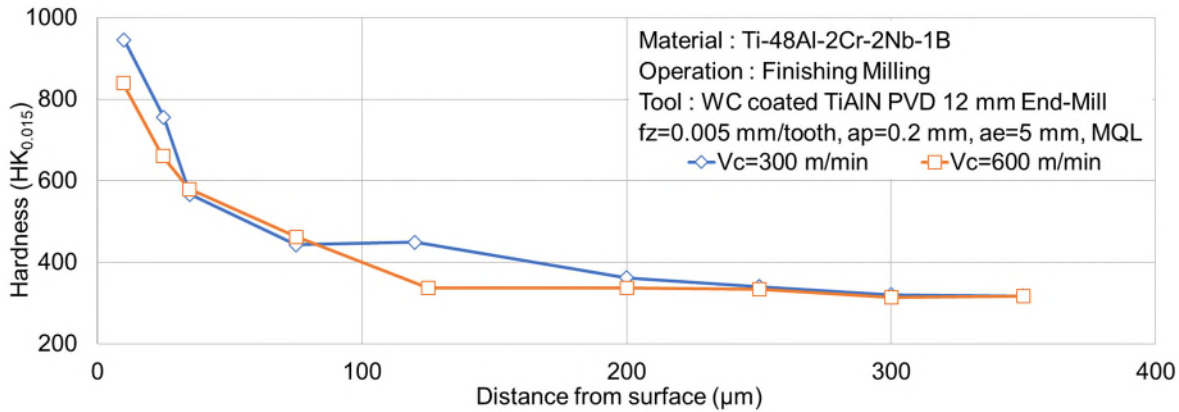


Figure 24. Microhardness depth profile for HSM for two different cutting speeds (adapted from [68]).

Different researchers (3, 44, 53, 75, 76, 88, 89) have studied the effect of various cooling conditions, such as dry machining, minimum quantity lubrication, conventional flood cooling, high-pressure lubricant supply, and cryogenic cooling systems. All of them have reported hardened layers and subsurface microstructural changes for all lubrication conditions.

Klocke et al. [80] studied the influence of lubrication strategies on surface integrity and concluded that cryogenic cooling with liquid nitrogen might be seen as a promising strategy in the future to reduce microstructural changes in the subsurface layer and decrease the wear of cutting tools.

Figure 25 presents a comparison of the depth profile of microhardness between conventional and cryogenic lubrication, showing a considerable reduction in the depth of the hardened layer (around 60%). In addition, cryogenic cooling appears as the most important condition, unlike conventional conditions and MQL, which do not indicate great benefits in terms of reducing tool wear.

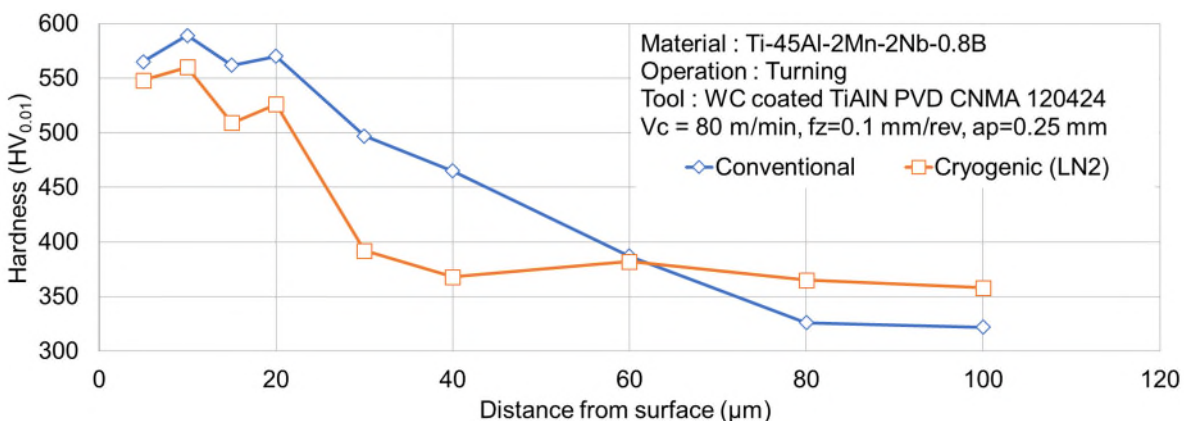


Figure 25. Microhardness depth profile between two lubricoolant strategies (adapted from [80]).

All studies on titanium aluminides machining show that the cutting processes create a certain level of hardening on the surface, where the main factor responsible for this effect is the tool wear. Based on the results analyzed, it is possible to conclude that no hardened layers greater than 300 μm are evident and that the maximum values are commonly found at a depth of $\sim 20 \mu\text{m}$.

The same way, it can be observed that the thermal softening effect in the cutting area does not directly contribute to the reduction of hardness growth. Therefore, the impact of coolant conditions on surface hardening is mainly focused on preserving the cutting edge of the tool to reduce lamellar deformation, and consequently work hardening.

2.3.3.2. Residual stresses

During the cutting process, the surfaces are under mechanical and thermal loads, which cease to act after the material is cut. However, part of this energy is retained on the surface of the workpiece, giving rise to residual stresses (Figure 26). These stresses on machined surfaces can be considered a dangerous or favorable condition, depending on the type of application. Nevertheless, they commonly cause the formation or propagation of cracks and fatigue failures [121, 143].

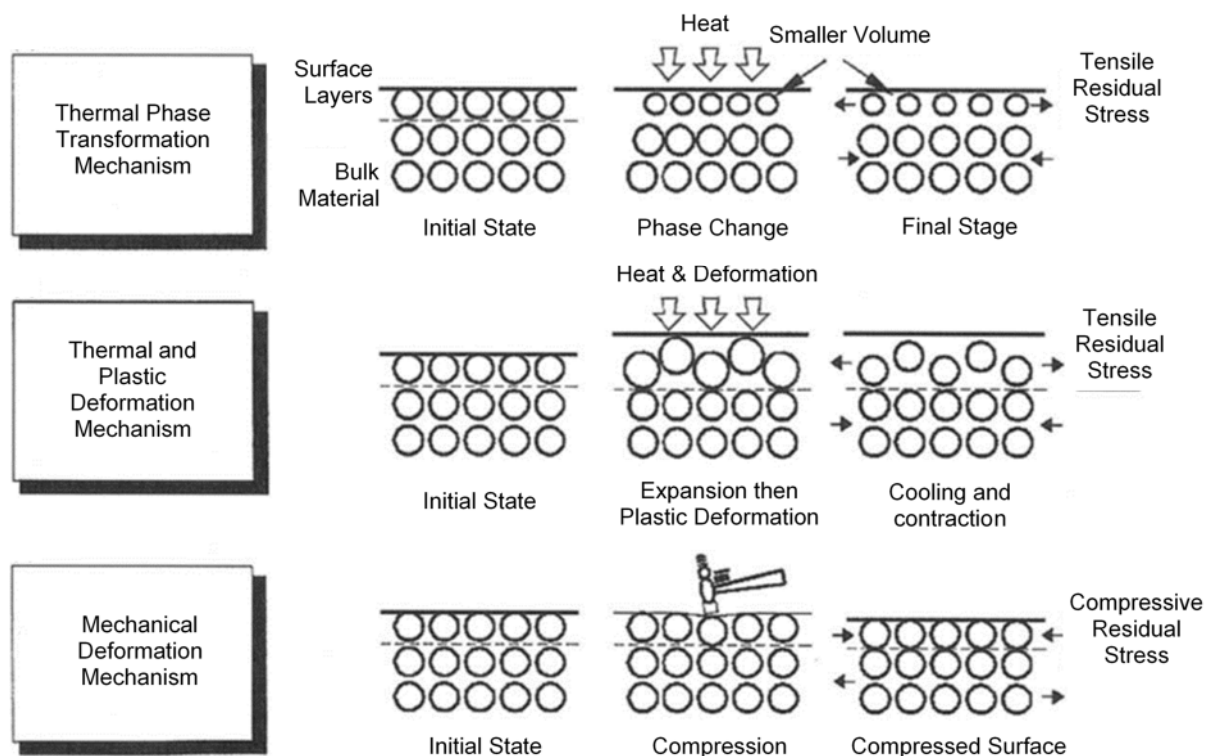


Figure 26. Residual stress models [117].

In general, the evaluation of residual stresses on machined surfaces is a complicated task. Usually the verification of their existence, type and depth are determined by various specialized measurement techniques (Figure 27) [118, 144, 145].

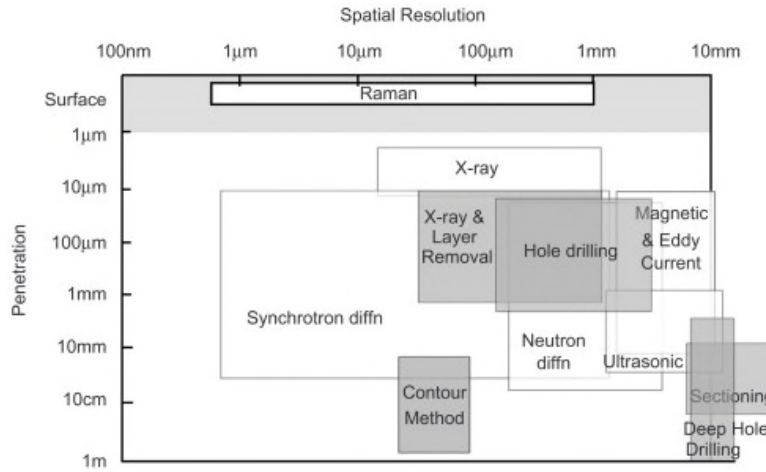


Figure 27. Schematic indicative of the current capabilities of the multiple methods by Withers [145].

Hood et al. [130] corroborated that the use of the X-ray diffraction technique presents several difficulties due to the overlapping reflections caused by the microstructure of the material, and therefore recommend the use of the blind hole drilling technique.

Residual stresses can be of two kinds: tensile or compressive. The kind of stress that affects a surface depends, largely, on the machining process. TiAl tend to present mainly compressive stresses. However, electro-discharge machining (EDM) process causes tensile residual stresses, due to the great thermal contraction of the liquid surface and rapid solidification, inducing plastic deformations and biaxial tensile stresses [96]. Similarly, the polished surfaces show residual tensile stresses, but significantly higher than in EDM (Figure 28).

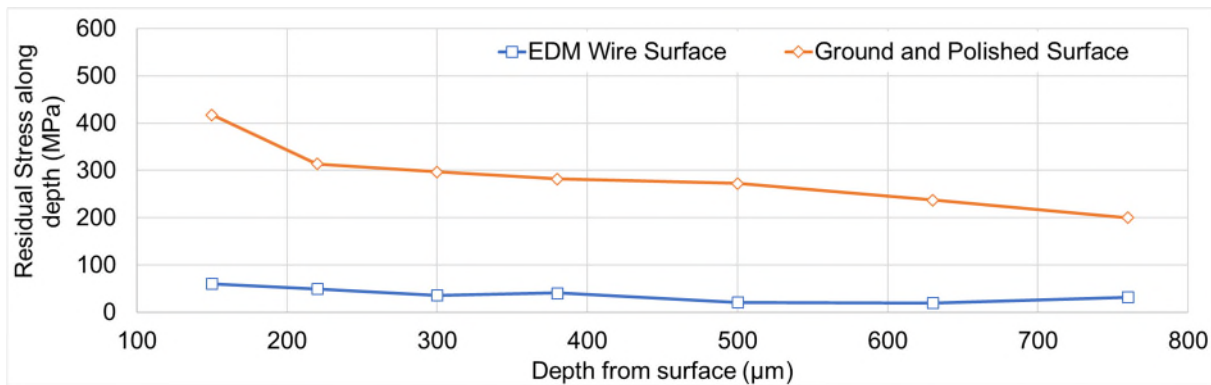


Figure 28. Residual stress measurement at the surface of a Ti-48Al-2Mn-2Nb (at%) + 2TiB (wt%) obtained by electro-discharge, ground and polished (adapted from [96]).

In the case of tensile stresses, Klocke et al. [123] studied this phenomenon for grinding and concluded that the increase in workpiece speed (V_w) changes these tensile stresses to compressive. They consider this parameter as the most influential for grinding (Figure 29).

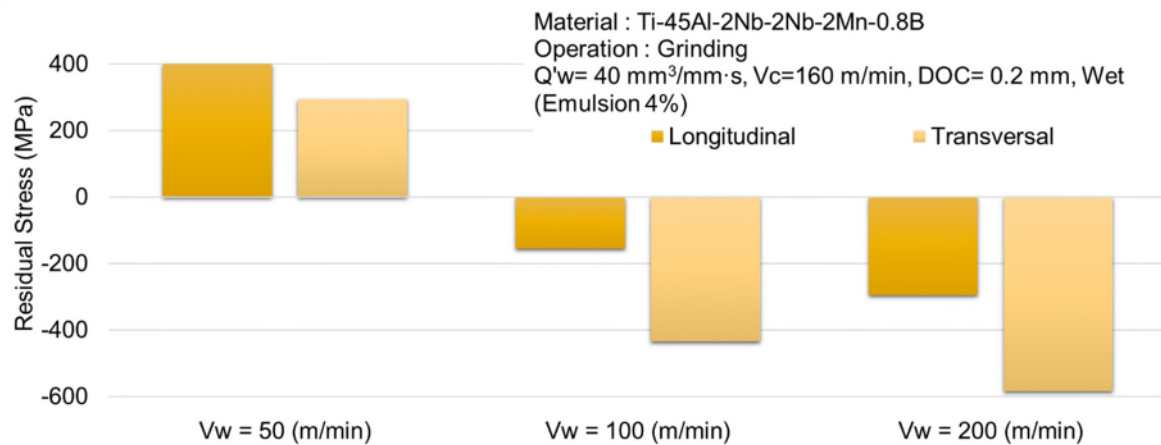


Figure 29. Residual stress showed in grinding operations at different speeds (adapted from [146]).

On the other hand, residual compressive stresses on the surface are considered advantageous because they tend to inhibit the initiation and propagation of cracks in the compressive area. A study [87] in turning, grinding and shot-blasting of TiAl indicates that all these processes induce compressive stresses (Figure 30), and as a result, the machined surfaces showed higher fatigue strength.

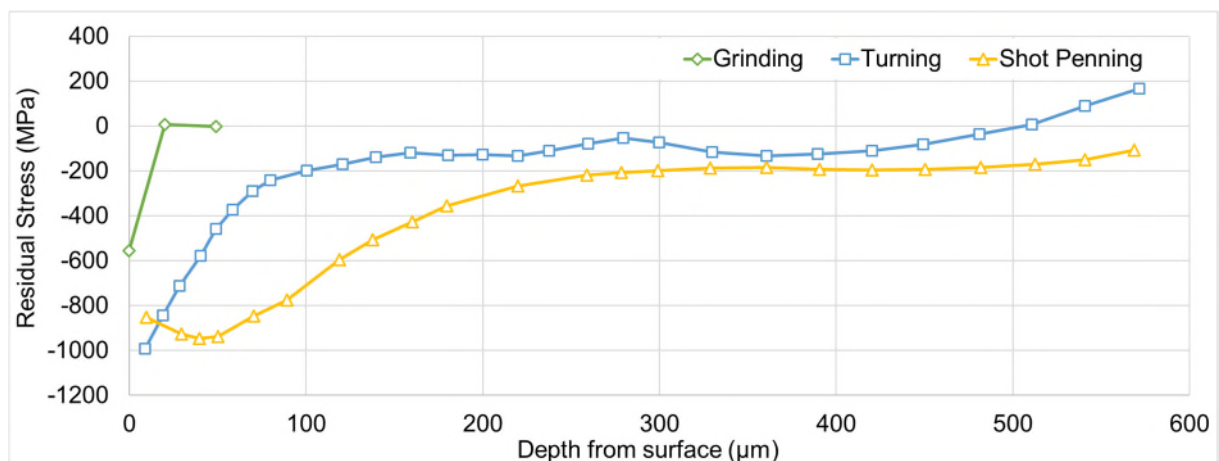


Figure 30. Residual stress profiles of shot peening (SP), turning (T), grinding (G) on Ti-45Al-5Nb-0.2B-0.2C (adapted from [87]).

Most publications about residual stresses are focused on the analysis of fatigue life of machined components [70, 71, 114, 121], and only a few papers study the effect of machining conditions (cutting parameters, environment, tool geometry, among others) on

residual stresses. In general, when machining titanium aluminides, the increased feed rate, tool wear, milling direction, and tool orientation angle can contribute considerably to residual compressive stresses. Figure 31 shows the effect of some machining conditions on residual stress.

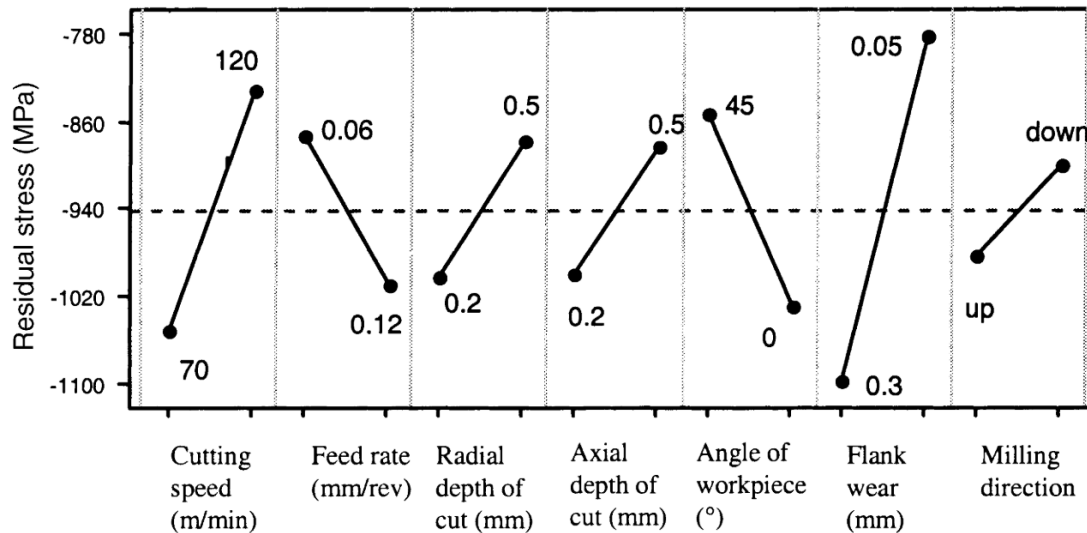


Figure 31. Main effect plot – mean for residual stress in Ti 48-2-2-08 [69].

From the perspective of cutting tools, the impact of geometry, material, coating and cutting-edge wear on residual stresses has been studied by Priarone and his collaborators [81, 108, 124, 127]. These studies concluded that excessive tool wear causes residual compressive stresses that alter the fatigue strength of the workpieces, due to the more significant plastic deformation caused by the growth of the tool/material contact area [67].

In general, all authors agree that machining titanium aluminide alloys cause residual compressive stresses and that these stresses end up to be beneficial as they retard the growth of fissures during fatigue cycles [129].

2.3.4. Summary

Titanium aluminides raise significant challenges to machining processes, mainly due to the need to avoid the presence of surface defects, such as surface drags, cavities, cracking, subsurface hardness, among others. In general, the surface integrity in TiAl machining is mainly affected by the inadequate selection of cutting parameters and rapid tool wear.

In the case of topographic properties, the achievement of mean roughness (R_a) with values below $0.4 \mu\text{m}$ is not a drawback in this type of alloys. However, the presence of cracks, tears, and other defects affects the quality of the surfaces and are the biggest challenge to

overcome. The use of cooling systems is an essential topic in this area, due to its significant impact on the quality of machined surfaces. For these alloys, it has been determined that working in dry conditions and with cooling systems with pressures higher than 150 bar is the least favorable.

From the perspective of subsurface integrity, the main problem is the formation of a hardened layer, which reaches depths of up to 250 μm , with hardness values up to three times the base material. The major problem with this trend is the effect it has on tool service life due to increased loads on the cutting edge.

On the other hand, machining causes residual compressive stresses in the subsurface layer of the workpiece. This condition is considered advantageous mainly for restricting the propagation of surface cracks, and consequently increasing the fatigue strength.

Appendix A-1 contains a summary of the various research studies that investigate the surface integrity of these alloys.

2.4. Machining parameters

As mentioned above, machining of titanium aluminide alloys is considered a challenge, due to the unusual pattern of response to the cutting process that affects the surface integrity of the workpieces. The main drawbacks affecting these alloys are feed marks, smearing, tearing surface, surface cavities, and lay patterns, among others (Figure 32).

These surface integrity defects of machined parts are closely related to machining parameters such as cutting speed, feed rate, cutting depth, tool geometry, tilt angle and tip radius, among others. When defining these parameters, an initial step is tool selection, which includes the choice of material and geometry, followed by determination of cutting speed, feed rate and cutting depth [27, 54, 57, 106, 122, 124]. Establishing the right combination of machining parameters in order to reduce their impact on surface integrity is usually a complicated task [23, 44, 75, 87, 97, 132].

Nowadays, several authors [9, 75, 124, 126, 147, 148] agree that the study of these parameters in the machining of titanium aluminides is vital for the development of their industrial application.

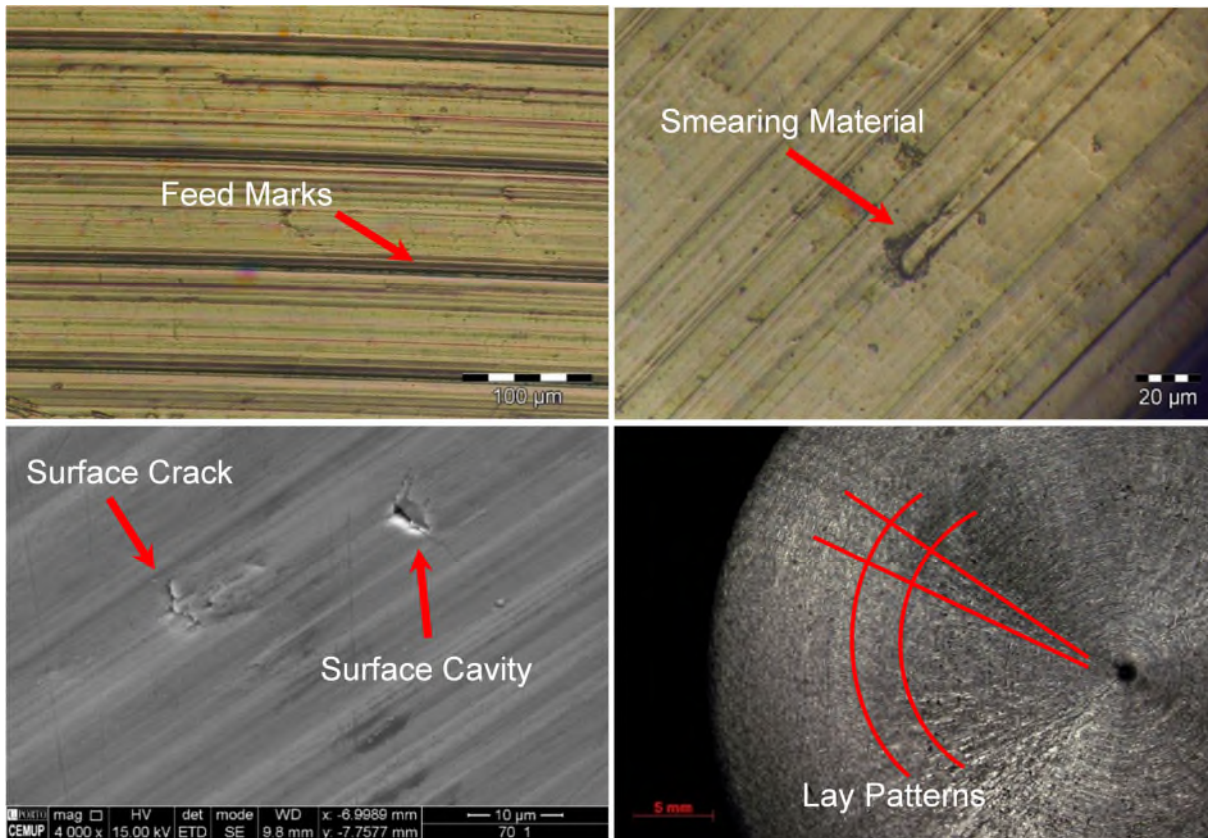


Figure 32. Common surface integrity defects on the titanium aluminides machined surfaces (author images).

2.4.1. Cutting Tools Performance with Titanium Aluminides

In machining, cutting tools are submitted to thermal and mechanical loads. For titanium aluminides, these loads are significantly higher, leading to rapid wear of the cutting edge. For this reason, the cutting tools must have a balance of characteristics that combines thermal resistance, mechanical strength, toughness, and hardness.

The machinability of titanium aluminides has been studied through the use of various types of cutting tool materials with high hardness, such as cemented tungsten carbide (WC), cubic boron nitride (CBN) and polycrystalline diamond (PCD) [98].

From these materials, tungsten carbide tools (WC) are the primary choice in research works. These tools can use single or multiple coating layers of aluminum oxide (Al_2O_3), aluminum–chromium–nitride (AlCrN), titanium nitride (TiN), titanium carbide (TiC), titanium carbo-nitride (TiCN) or titanium aluminum nitride (TiAlN), to improve their performance.

Due to their abrasion resistance, polycrystalline diamond tools and cubic boron nitride (CBN) have been shown to perform significantly better in TiAl machining than tungsten carbide but only in continuous cutting process (turning, drilling, etc.) [5, 99, 124, 149, 150], because in milling operations these materials have been shown have several disadvantages due to the discontinuous cutting process [44, 107, 131].

Most research studies on machining of TiAl use commercial cutting geometries developed for standard titanium alloys. However, it has been shown that these geometries are less effective from the perspective of tool life, surface integrity and productivity. There are few published studies [108, 130] with cutting geometries designed for titanium aluminides.

From the perspective of cutting parameters, the use of high-speed machining (HSM) is usually recommended as a viable way to produce components with adequate surface integrity. The term HSM is used to designate a range of high cutting speeds (above 600 m/min in the case of nickel superalloys) [69, 151], but it has been shown that cutting speed rates above 150 m/min are not suitable for titanium aluminides [44].

Therefore, the expression HSM for TiAl is used to describe machining at cutting speeds between 100 to 130 m/min. However, the use of these parameters reports limited cutting times [68, 142].

2.4.1.1. Cemented Carbide Tools

Cemented carbide tools are the most widely used industrially. This material is characterized by high fatigue strength, high compressive strength, high stiffness and hardness. These tools are manufactured by compacting and sintering hard carbide particles, mainly tungsten carbides (WC) bonded with a metallic cobalt (Co) binder. The carbide grain size and binder content determine the relative balance of hardness and toughness (Figure 33).

Cemented carbide tools are classified into six grades P, M, K, N, S and H, according to the workpiece material ISO classification (DIN ISO 513). Each grade is divided into groups designated by a numbering system that representing its position on a scale of hardness, toughness and suitability of the grade for application ranges, i.e. K01 is a wear

resistance grade suitable for light finishing operations, while K40 is a tough grade suitable for roughing machining process [64, 66, 139].

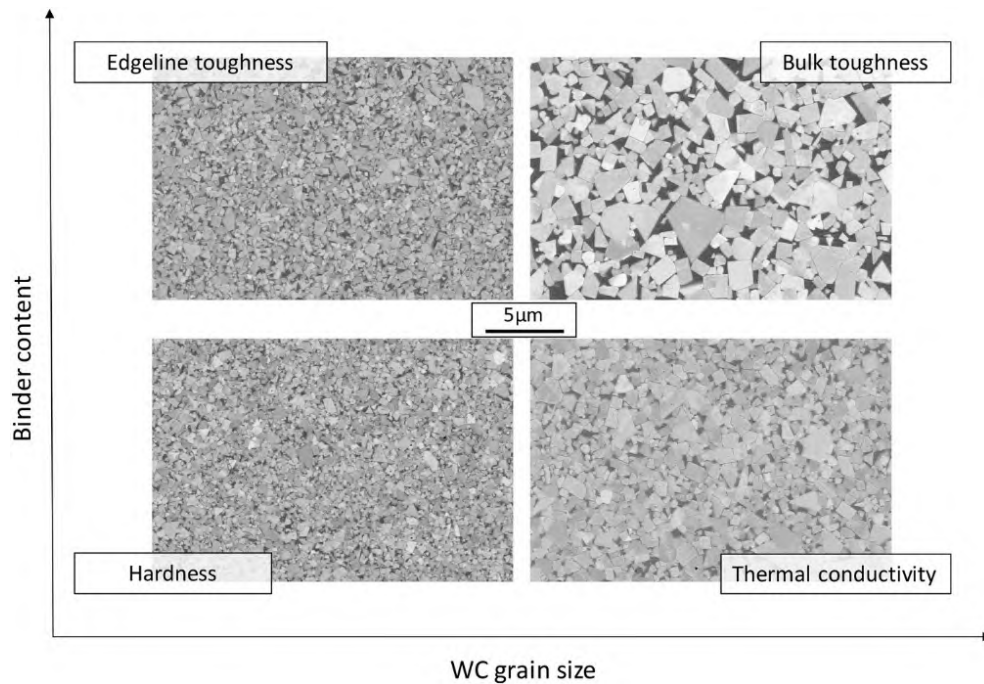


Figure 33. Correlation between binder content and WC grain size with main properties of cemented carbides [152].

The P grades are suitable for machining different grades of steel or long chip material, this grade are rated from 01 to 50, while M grades is recommended for stainless steel and heat resistance alloys, K grades are used for short chipping materials such as cast iron, these both grades are index from 01 to 40, N grades are suitable for non-ferrous metal and alloys, S are for heat-resistance superalloys and titanium-based alloys, and H grade are for hard and hardened materials, these grades are rated from 01 to 30 [153]. It is also important to note that the quality of carbide can vary significantly from manufacturer to manufacturer, as classification systems do not rigorously describe the criteria for classifying carbide grades.

In the study of cemented tungsten carbide (WC) tools, one of the leading research objectives is the analysis of the flank wear mechanism. For titanium aluminides, several authors [59, 67, 107, 124] agree that the mechanism of wear presented at these tools are: abrasion, material adhesion, and cracking on the cutting edges.

The primary damage mechanism presented by WC tools is abrasive wear. This impairment is more evident in alloys with higher boride contents (TiB_2). Experimental studies [59] in turning and milling operations showed that abrasion wear caused by TiB_2 reduces the tool life by up to 10 times (Figure 34), and promotes cracks initiation on the surface.

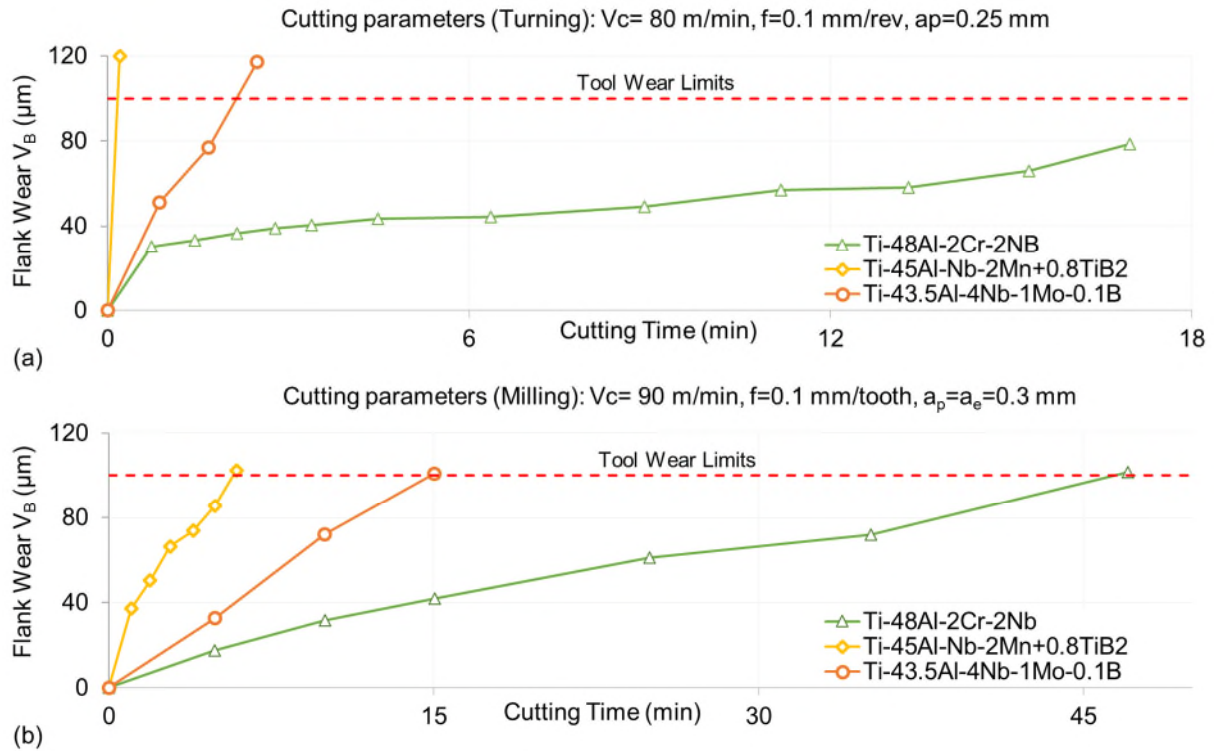


Figure 34. Cutting tool life on; (a) turning, and (b) milling of TiAl with and without TiB₂ content (adapted from [59]).

Another wear mechanism commonly reported is material adhesion at the cutting edge (BUE) [24] (Figure 35.a). This phenomenon increases the cutting radius of the tool, causing the temperature increase at the tool/workpiece interface, leading to deformation of its cutting edge and cracking the rake face (Figure 35.b).

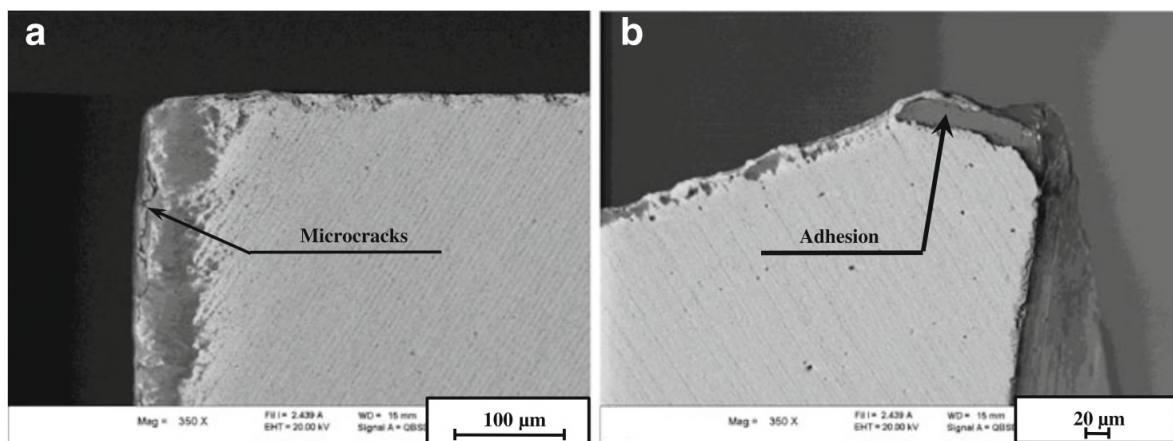


Figure 35. Images of tool rake face with wear by; (a) microcracks, and (b) built-up edge [81].

Cracking of the rake face on WC tools can also be produced by a cutting-edge fatigue wear mechanism. This mode of fatigue wear is lower on fine-grained carbide tools (< 1 μm) due to their higher cobalt content, which increases fracture resistance by $\sim 64\%$ compared to coarse-grained tools ($1\text{--}2$ μm) [24].

Various studies [24, 44, 98, 154, 155] agree that when TiAl is machined with WC tools with small grain size ($\sim 1 \mu\text{m}$), specific cutting pressure and wear resistance at lower cutting speeds is improved, compared to coarser grain inserts, as shown in Figure 36 and Figure 37.

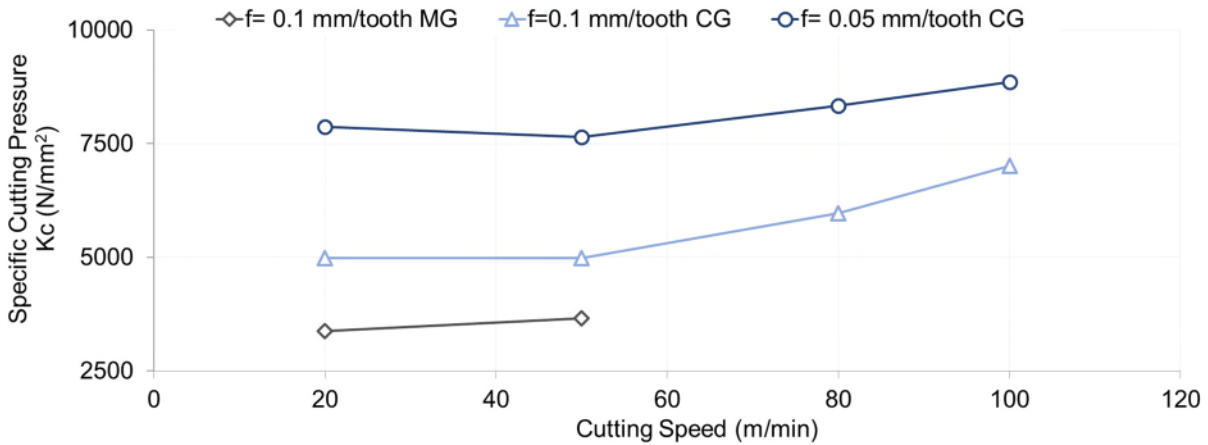


Figure 36. Specific cutting pressure (K_c) with cutting speed and feed rate for fine grain (MG) ($<1 \mu\text{m}$) and coarse grain (CG) ($1-2 \mu\text{m}$) carbide inserts in milling Ti-45Al-2Nb-2Mn+0.8TiB2 [24].

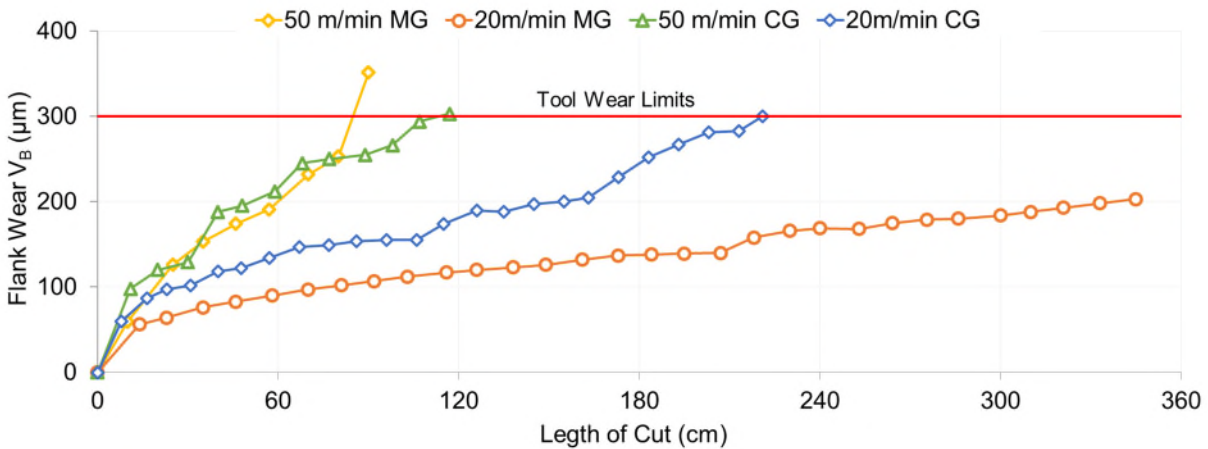


Figure 37. Flank wear of fine grain (MG) ($<1 \mu\text{m}$) and coarse grain (CG) ($1-2 \mu\text{m}$) carbide inserts in milling of Ti-45Al-2Nb-2Mn+0.8TiB2 [24].

On the other hand, comparative studies on the performance of coated WC tools show that coatings do not provide significant advantages to the tool in the machining of titanium aluminides. In fact several works [24, 71, 98] verified that uncoated WC tools with a higher straight grade, fine grain and approximately 6 wt% Co performed better than coated WC for turning and drilling operations.

Priarone et al. [124] showed that coated tools have a shorter service life than uncoated tools, presenting mainly abrasion damage on the flank side (Figure 38).

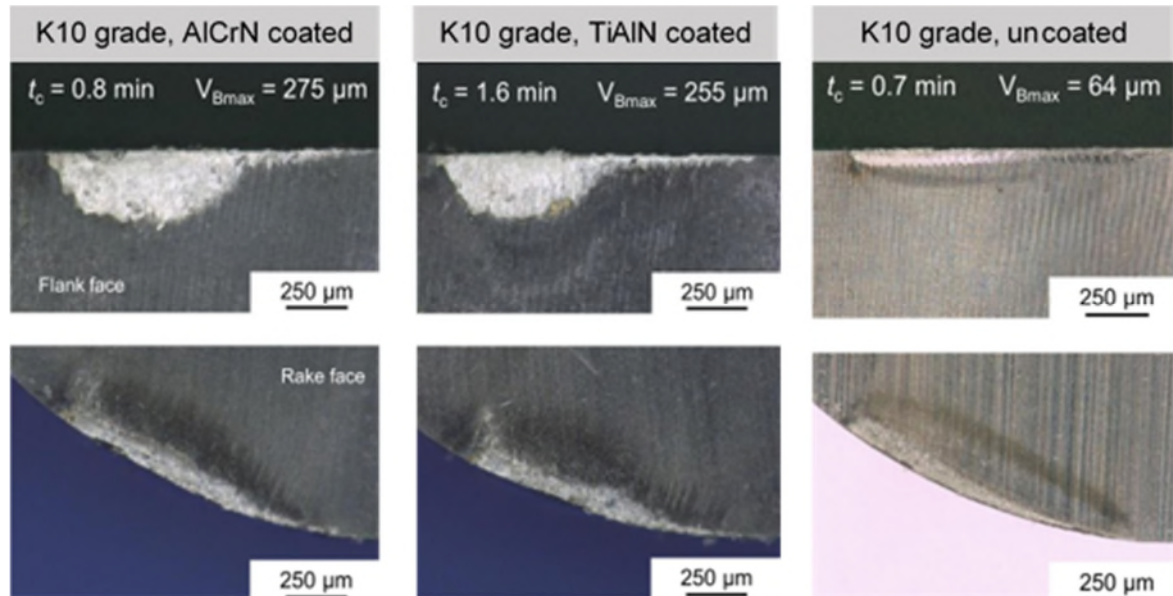


Figure 38. Tool wear observation for coated and uncoated ISO K10-grade carbide tools, by Priarone et al. [124].

However, AlSiTiN and CrAlSiN coatings have been shown to improve cutting time by up to three times compared to uncoated tools [108].

From a perspective of cutting parameters, when machining TiAl with coated or uncoated WC tools, removal rates up to 10 times lower than conventional Ti alloys are usually recommended to reach similar tool lives [156].

On this subject, the first investigations about machining TiAl [98] recommend cutting speeds of 12-18 m/min, feed rates of 0.065 to 0.11 mm/rev and cutting depths of 1.5-3 for turning, and cutting speeds of 17-20 m/min, feed rates of 0.01-0.04 mm per tooth and depths of 1 to 5 mm for milling. Nevertheless, more recent research [68, 82, 124, 126, 157] on machining with uncoated carbide tools has shown that the productivity limit of WC tools can reach cutting speeds around 70 m/min. High-speed machining (cutting speed \sim 120 m/min) cannot be used with this type of tool due to the accelerated wear of the cutting edge [158].

Experimental studies [81] using uncoated carbide tools at cutting speeds of 35, 50, and 71 m/min in milling, showed that in the range of 35 to 50 m/min, tool life decreases rapidly from 70 min to 15 min, but after 50 m/min the tool life pattern changes and becomes almost constant. In addition, concerning cutting conditions, it was also concluded that tool life is extended up to 6 times with the use of minimum quantity lubrication (MQL) and 24 times with wet lubrication.

Klocke et al. [80] evaluated the impact of minimum quantity lubrication (air/vegetable oil mixture at 5.5 bar), conventional wet (6% mineral oil at 6 bar), high pressure (6% oil with jet nozzle at 80, 150 and 300 bar) and cryogenic (liquid nitrogen with jet nozzle at 2 bar) conditions on the performance of uncoated WC cutting inserts in turning. They showed that in terms of tool wear, the cryogenic condition is the most efficient cutting environment (Figure 39).

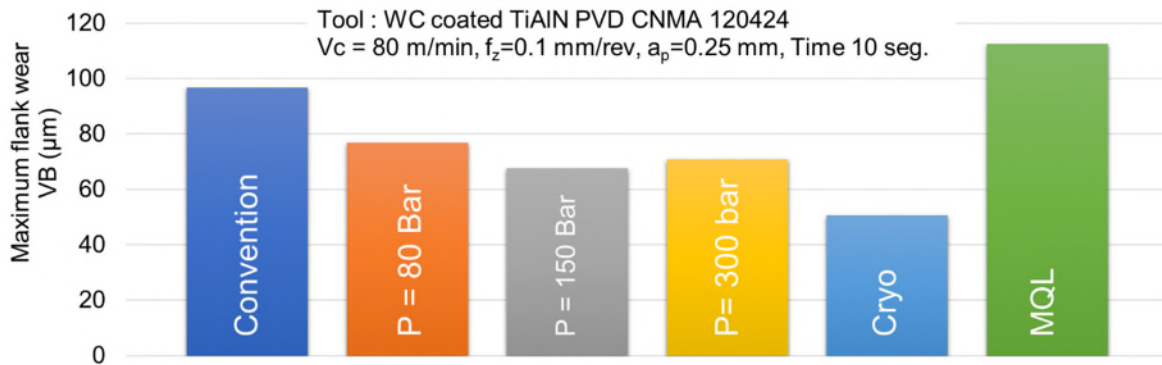


Figure 39. Tool wear after turning Ti-45Al-2Mn-2Nb-0.8 B for 10 seconds under different cooling conditions (adapted from [80]).

Figure 40 shows the tool cutting flank wear observed under different cutting environment conditions. Additionally, this study showed that the nose radius significantly affects tool performance.

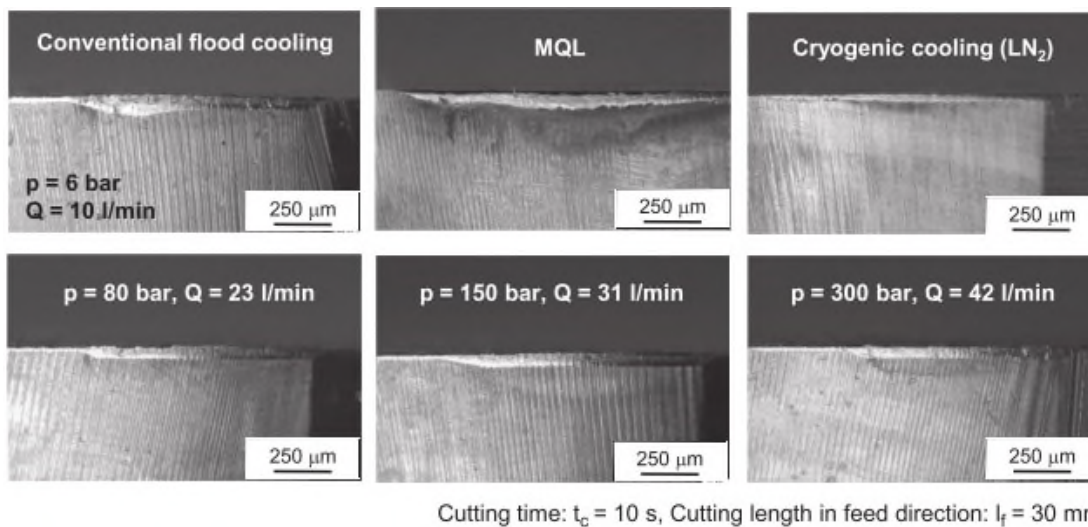


Figure 40. Flank wear after 10 seconds of cutting in turning Ti-45Al-2Nb-2Mn-0.8B alloy (adapted from [80]).

The nose radius has a high impact on the cutting process, due to its influence on the size of the contact zone between the tool and the workpiece, the cutting forces and the wear mechanism. A reduced radius shows more significant wear, and consequently shorter

cutting edge life [159]. Experimental studies carried out with round inserts [82] show cutting times of 25 and 40 min for nose radii of 4 and 6 mm, respectively.

These results indicate that for machining titanium aluminides, a larger nose radius increases the cutting time. However, it is observed that the round inserts (higher nose radius) demonstrate great sensitivity to cutting parameters because they present a low performance at cutting speeds higher than 25 m/min (Figure 41).

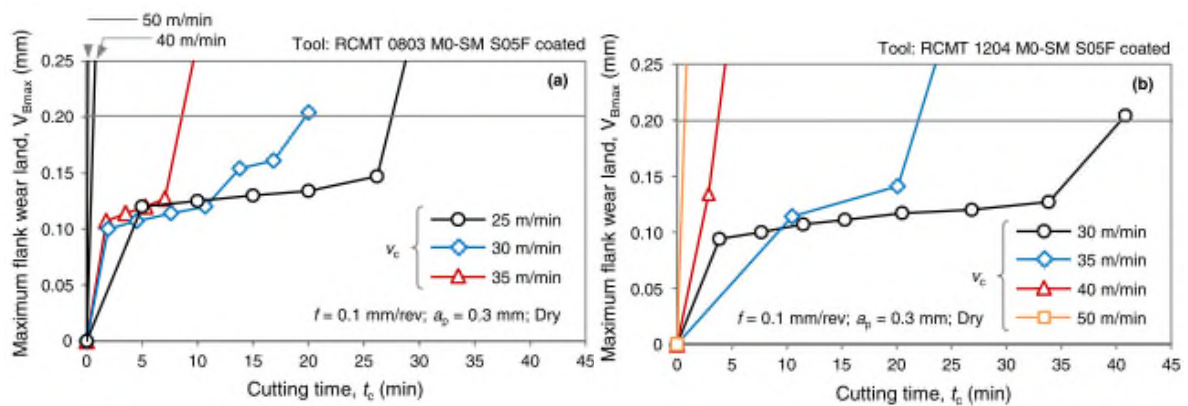


Figure 41. Tool wear curves for turning, when using cutting inserts with nose radius of: (a) 8 mm (RCMT 0803), and (b) 12 mm (RCMT 1204) [82].

Other cutting tools features such as rake angle and cutting-edge treatment show a considerable effect on tool performance [108]. A reduction of the rake angle from 12° to 4° , combined with a cutting-edge finishing treatment, reveals a positive impact in terms of tool life, increasing cutting time by 98% (Figure 42).

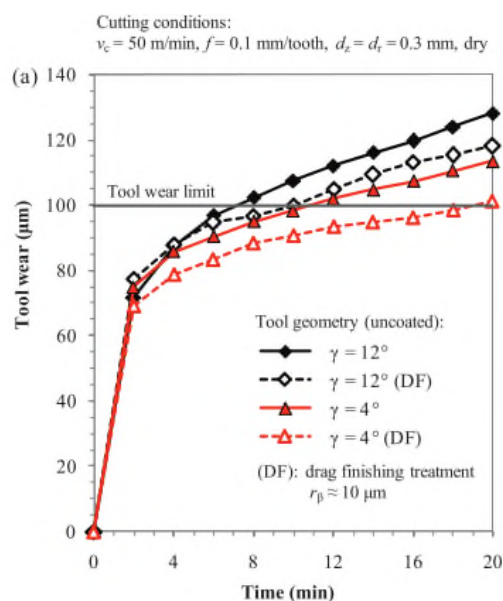


Figure 42. Flank wear curves for cutting tools with rake angle of 4° and 12° with and without finishing treatment, when milling Ti-48Al-2Cr-2Nb [108].

In summary, ISO K10, K20, and K30 cemented carbide tools, coated or uncoated, with fine grain and lower cobalt content, reduced cutting angle, larger nose radius and improved cutting-edge surface finish, have proven to provide better performance in machining TiAl. Furthermore, coatings materials such as TiAlN, Al₂O₃ or TiCN do not report important advantage over non-coated tungsten carbide tools. Cutting speeds of 35 to 70 m/min and use of cooling methods are recommended for machining these alloys with WC tools.

2.4.1.2. Cubic Boron Nitride and Polycrystalline Diamond

Cubic boron nitride (CBN) and polycrystalline diamond (PCD) tools are commonly referred to as high performance cutting tools, due to their high hardness (Knoop hardness number ~30 and ~50 GPa, respectively), thermal conductivity (~100 and ~560 W/m-K respectively) [65], wear resistance and high performance in machining difficult-to-cut materials such as titanium or nickel-based alloys [91, 103, 106].

In the machining of titanium aluminides, CBN tools show mainly wear mechanisms of diffusion, craters, flank wear and BUE on the cutting edge [147, 160]. Unfortunately, there is limited information about the service life or cutting time of these tools. Some studies in boring operations [44] have shown that CBN presents greater flank wear and shorter cutting length than cemented carbide tools (Figure 43). This difference is attributed to the binder content and larger grain size of the CBN particles.

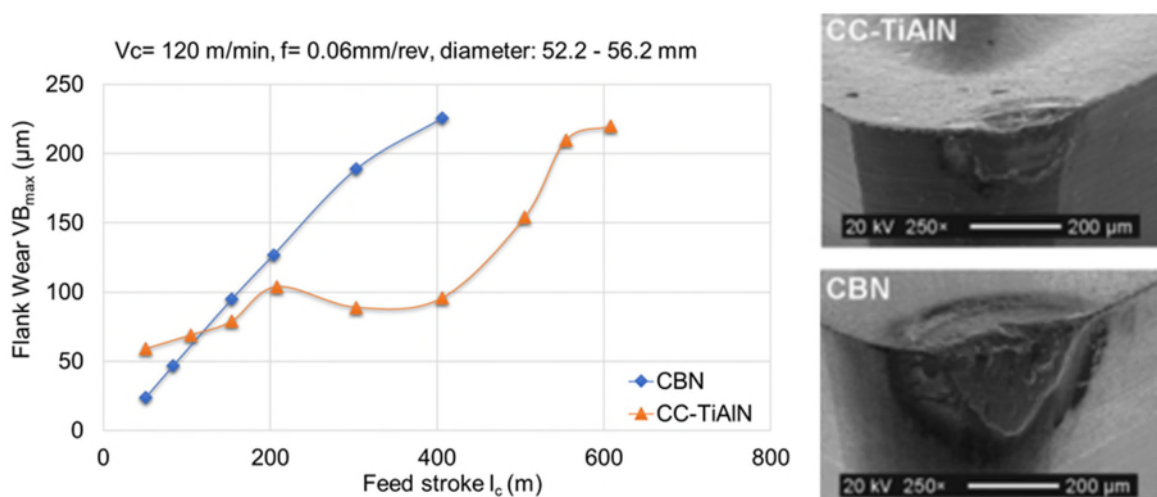


Figure 43. Tool wear of CBN and coated tungsten carbide tools (CC) in boring Ti-46Al-0.5Mo-0.8Cu-0.2Si (adapted from [44]).

CBN tools demonstrated a low machining performance at cutting speeds (V_c) between 20 and 40 m/min. Zhang et al. [107] indicate that at this V_c range, the cutting edge tends to

have notch failures and rapid wear. However, when the cutting speed increases to 140 m/min, the notch wear disappears, although flank wear is still present.

From the perspective of surface integrity, favorable results have been obtained with cutting speed of 300 m/min, using cutting tools with 80% CBN concentrations and 20% TiC/WC (DeBeers DBC 80) [148]. Practically crack-free surfaces and chips with very smooth undersides are observed (Figure 44) due to the thermal effect of the high cutting speed at the tool/chip interface.

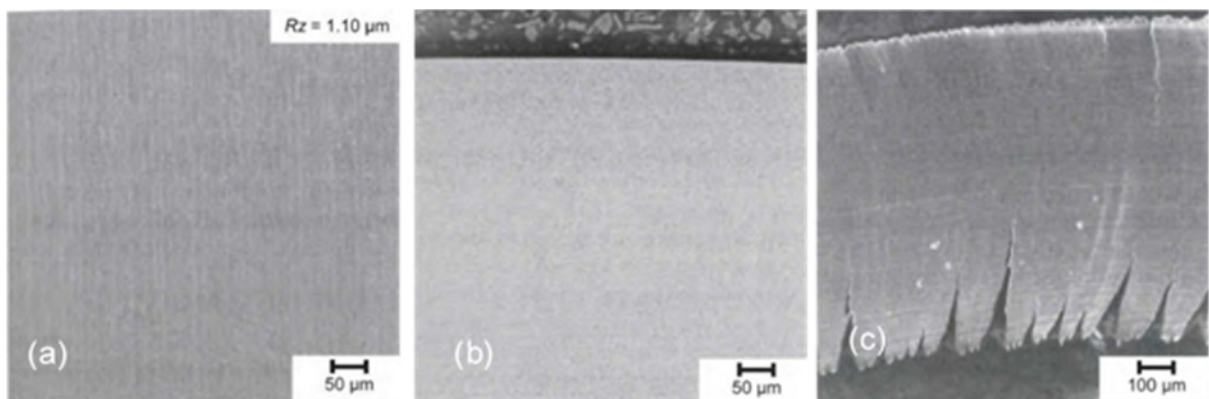


Figure 44. Workpiece (a) surface, (b) subsurface, and (c) chip after turning Ti-46.8Al-1Mo-0.2Si at $V_c=300\text{m/min}$ [148].

On the other hand, Priarone et al. [124], analyzed the wear of CBN and PCD tools in turning operations and detected that PCD tools show less flank wear (V_B) than tools with 50% CBN content. However, tools with 92% CBN content show lower V_B than PCD tools (Figure 45).

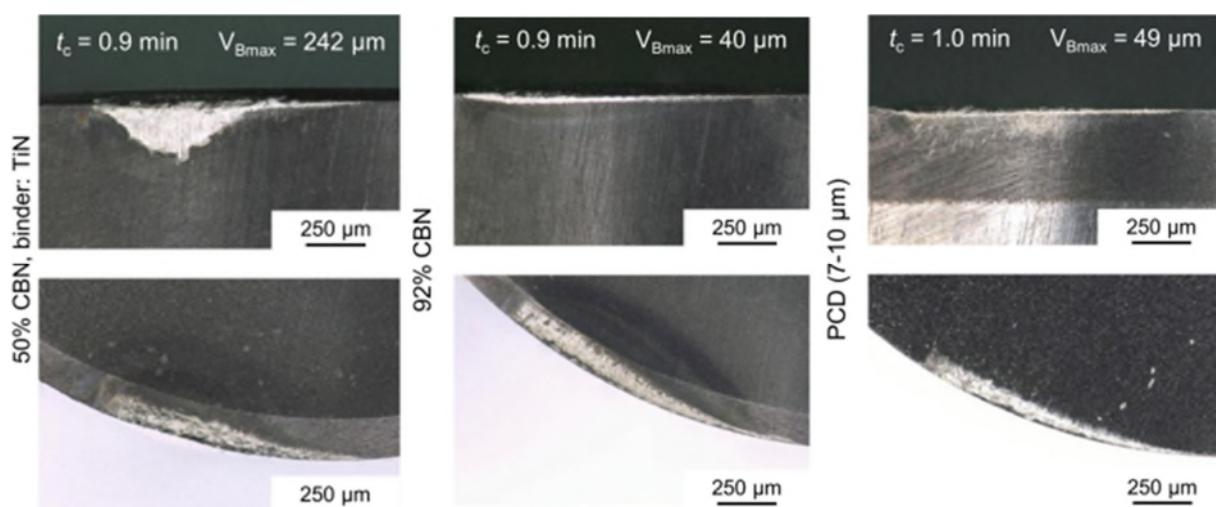


Figure 45. Tool wear observations for 50% CBN, 92% CBN and PCD cutting insert after turning Ti-43.5Al-4Nb-1Mo-0.1B [14].

Service time of CBN and PCD tools show a slight difference in the first minutes of cutting, but as the cutting time increases, this difference is more significant, becoming up to 8 times higher (Figure 46). It was noticed that for PCD tool, the grain size of the particles does not represent an influential factor for their resistance to damage.

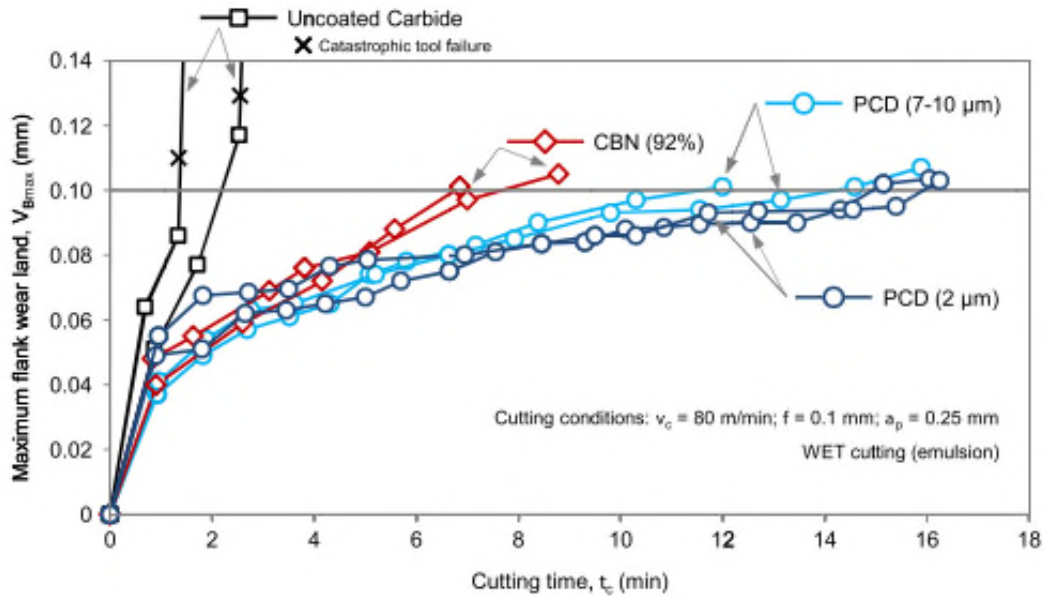


Figure 46. Tool life curves of CBN and PCD tools when turning Ti-43.5Al-4Nb-1Mo-0.1B (adapted from [124]).

For increase the service life of PCD tools, cryogenic cutting conditions provides significant benefits. This improvement is caused by the reduction of the thermal load on the cutting edge, which consequently reduces tool wear. Liquid nitrogen can promote cutting times of up to 30 minutes in continuous turning processes (Figure 47).

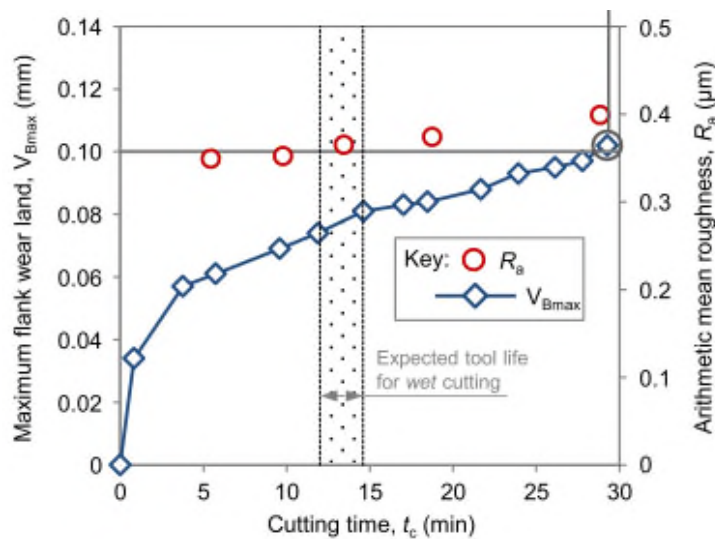


Figure 47. Tool life curves for cryogenic-assisted turning of Ti-43.5Al-4Nb-1Mo-0.1B with PCD tool [124].

Some publications [107, 124, 131, 148] report a slight advantage of cubic boron nitride tools over WC tools, in terms of workpiece surface integrity and process productivity. In addition, the use of polycrystalline diamonds can be considered more promising for the machining of TiAl. However, process parameters and surface integrity of the workpiece, among other aspects, remain largely unexplored.

2.4.2. Cutting Forces and Chip Formation

The machinability of materials is studied in multiple ways. Nevertheless, the analysis of the cutting forces seems to better reflect the behavior of the working material during the machining process, with lesser consumption of resources and time.

The tangential (F_t), radial (F_r) and axial (F_a) force components are essential physical parameters present in all machining processes. They can vary depending on factors such as: cutting parameters (cutting speed, feed rate and cutting depth), workpiece material properties (physical, mechanical and chemical properties), cutting tool characteristics (geometry, material, etc.) and cutting environment [122, 161, 162].

When machining titanium aluminides, it is known that the cutting forces are considerably higher than in other titanium-based alloys such as Ti-6Al-4V ($F_a = +200\%$, $F_r = +200\%$ and $F_t = +130\%$) [67] or Ti-6Al-2Zr-1Mo-1V ($F_a = +200\%$, $F_r = 190\%$ and $F_t = 180\%$) (Figure 48) [142].

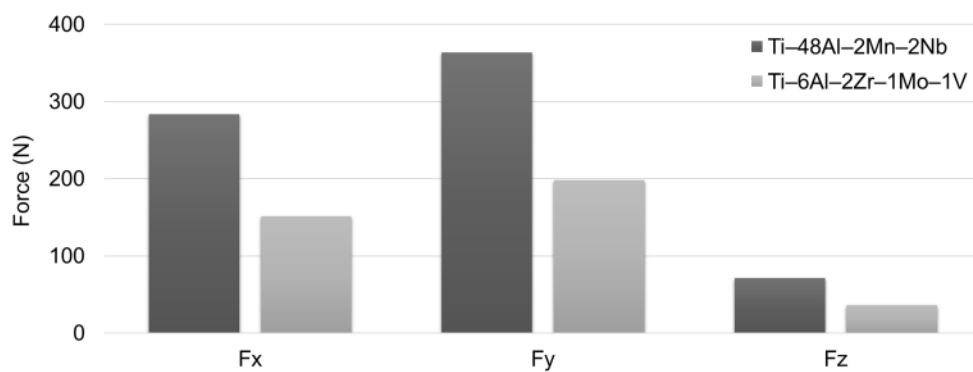


Figure 48. Comparison of milling forces for Ti-6Al-2Zr-1Mo-1V and Ti-48Al-2Mn-2Nb at $V_c=120$ m/min, $f_z=0.08$ mm/tooth, $a_p=5$ mm, $a_e=0.5$ mm) (adapted from [142]).

From the perspective of cutting parameters, these alloys are more susceptible to variation in cutting depth and feed rate (Figure 49). Results presented by Sharman et al. [67] identified the cutting depth as the most influential parameter in cutting forces, with a contribution ratio of 67.6%.

Increase in feed rate raises the machining force, but on a smaller scale [44]. Changes in cutting speed can mean a slight (30 to 50 m/min) or large (50 to 70 m/min) variation in the progress of the cutting forces.

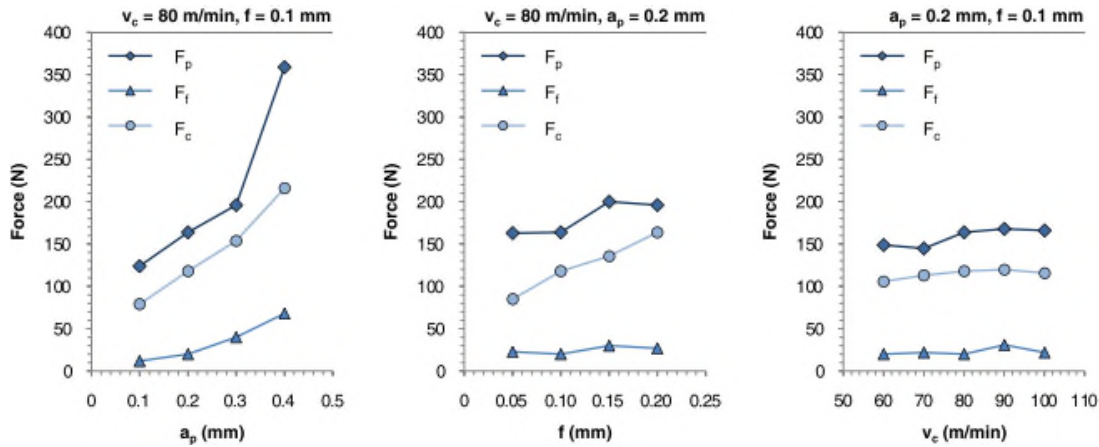


Figure 49. Cutting parameters effect on the cutting forces when turning Ti-48Al-2Mn-2Nb (adapted from [125]).

Several studies [24, 44, 67] have identified that the effect of the cutting speed in the range of 20 to 50 m/min has a minimal impact on the resulting cutting force. However, this effect becomes more significant with an increase in cutting speed above 50 m/min (Figure 50).

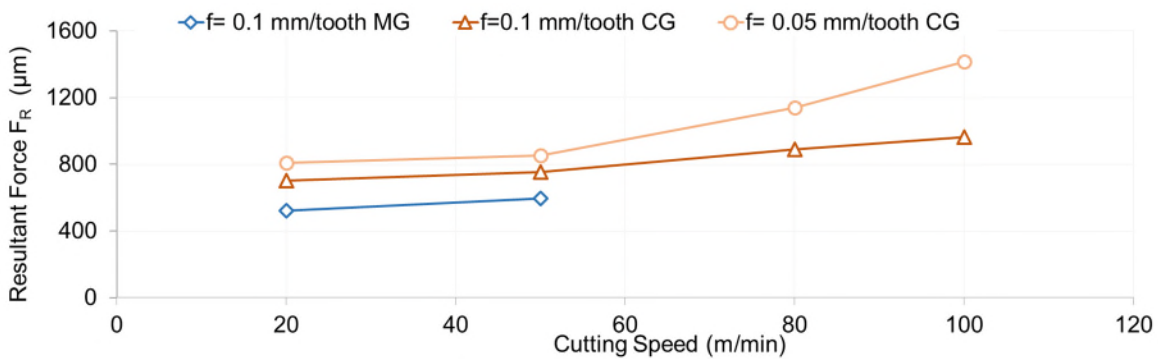


Figure 50. Cutting forces variation for milling Ti-47Al-2Nb-2Mn + 0.8 TiB2 with cutting speed and feed (adapted from [24]).

This increase is explained by the surface work hardening, which leads to a higher mechanical load on the tool/part interface. This behavior is confirmed through the chip formation, where an increase in hardness from 296 HV (bulk material) to 460HV and 670HV (in formed chips) is observed after machining at $V_c=20\text{m/min}$ and 50 m/min , respectively [24].

Nevertheless, Ge et al. [142] shows that the cutting forces do not change significantly in a range of 50 to 240 m/min, concluding that the variation influenced by the cutting speed is given in function of the cutting tools features (material, geometry, size, among others).

Besides wear, the geometry of the tool also influences the behavior of the cutting force. The nose radius has a characteristic impact on the tool wear mechanism and cutting forces. Machining with smaller nose radii presents lower cutting forces [159]. Yao et al. [163], has found an increase of ~ 70 N in the components of the cutting forces with nose radii of 0.8 and 1.2 mm (Figure 51).

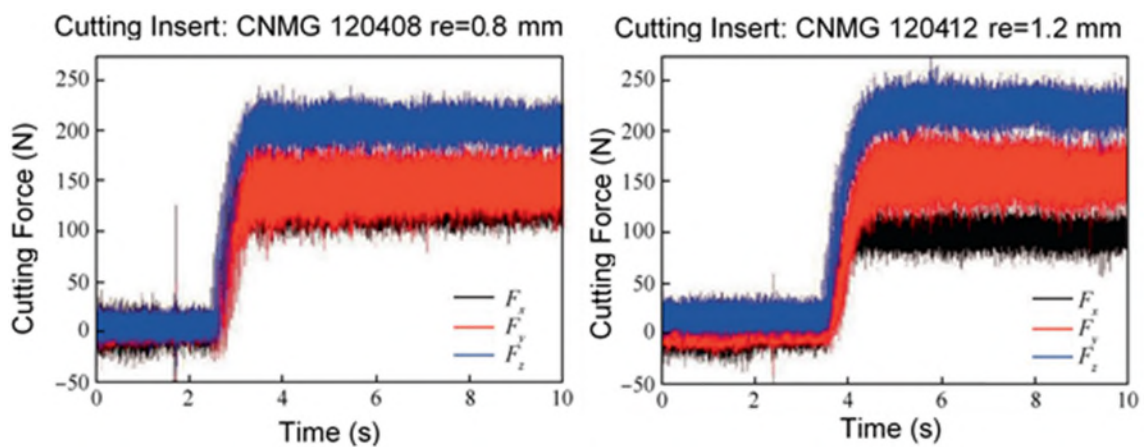


Figure 51. Cutting force along the time in turning with a different nose radius (adapted from [163]).

Significant variations in cutting forces have been reported as an effect of tool wear, stating that flank wear (V_B) of $200 \mu\text{m}$ can increase cutting forces by up to 260% (Figure 52). This effect has been reduced by using high-pressure cooling conditions.

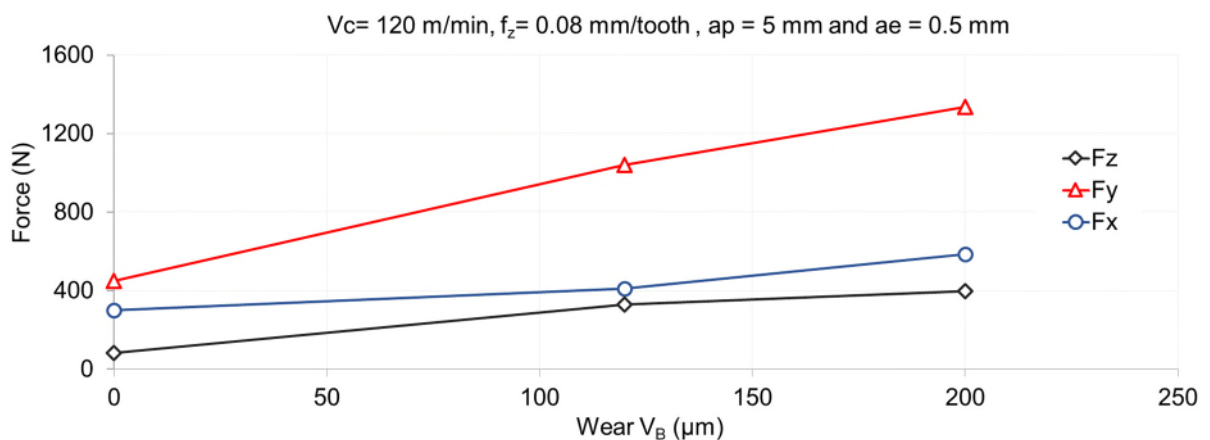


Figure 52. Milling forces curves under different tool wear for Ti-48Al-2Mn-2Nb [142].

Cutting environment causes different variations in cutting forces behavior [80]. An increase in lubricant flow pressure, from 6 bar to 300 bar, causes an increase in tangential force, reduction in radial force, and does not cause a significant impact on axial force (Figure 53). This behavior is the result of lubricant action on the cutting edge of the tool, which decreases the thermal effect on the ductility of TiAl.

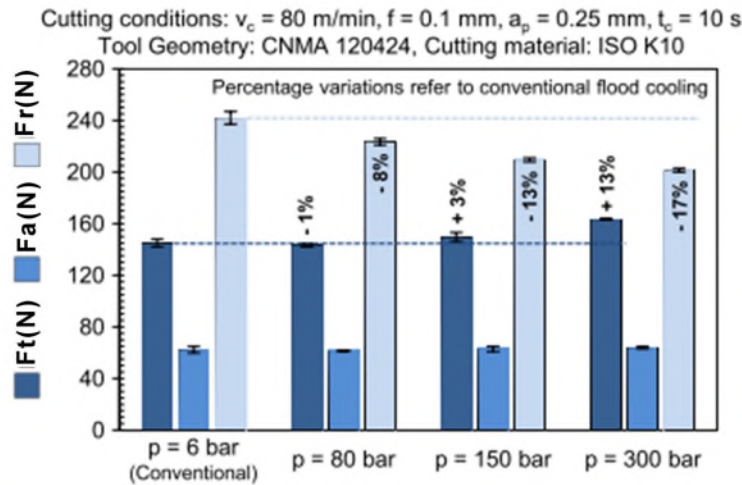


Figure 53. Cutting forces components at different lubricoolant supply pressure [80].

About this tendency, the main disadvantage of the increase in tangential forces is the concentration of the mechanical load in a reduced contact zone, which increases the risk of breaking the cutting edge (Figure 54).

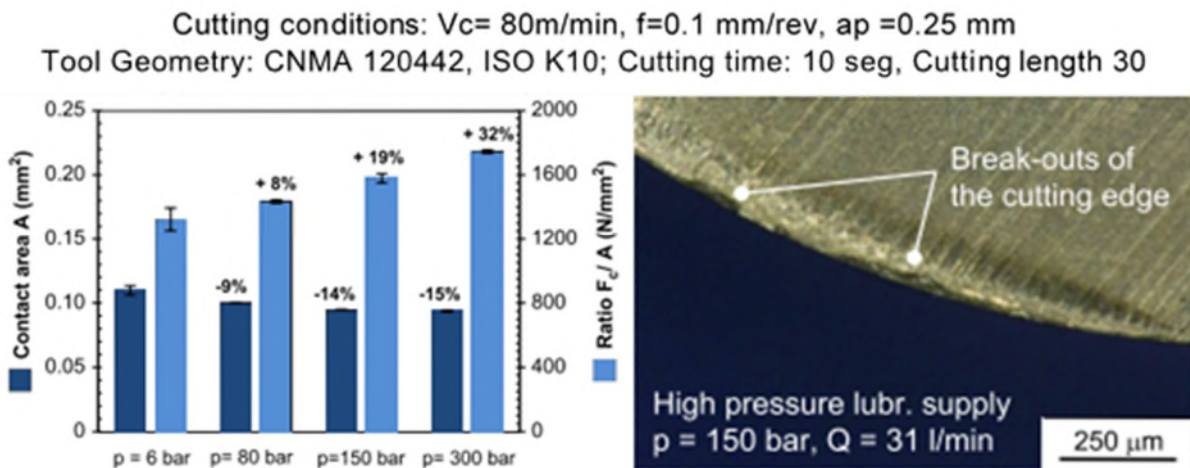


Figure 54. The ratio of cutting forces to tool/chip contact area at different lubricoolant pressure, and break-outs on the tool cutting edge (adapted from [80]).

Uhlmann et al. [73], studied the influence of the temperature in the chip formation of TiAl and observed an increase in cutting forces from 2000 N to 4500 N when the temperature in the material varies from 20°C (RT) to 700°C (BDTT). In addition, cutting forces profile

show a sawtooth contour at RT and 400°C (Figure 55.a and Figure 55.b), which is explained by the formation of the characteristic segmented chip of TiAl. In contrast, above the BDTT temperature a continuous profile (Figure 55.c), caused by the temperature effect, induces softening of the material and the formation of continuous chips [73].

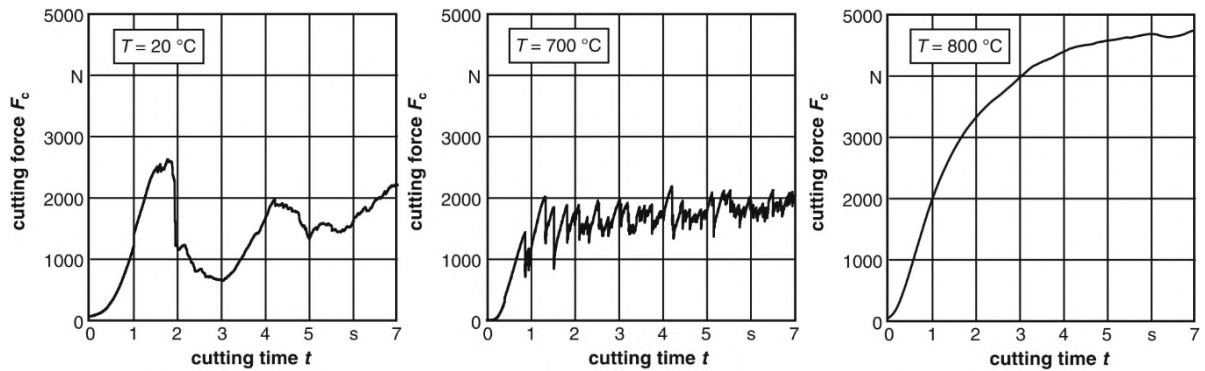


Figure 55. Cutting force at different workpiece temperatures in Ti-45Al-5Nb-0.2B-0.2C (TNBV5) alloy (adapted from [73]).

This study also reports a significant increase in specific cutting force (K_c), from 1366 N/mm² at RT to 4110 N/mm² (245%) at the brittle-ductile transition temperature, where chip formation from segmented to continuous begins (Figure 56). It concludes that heating the workpiece from 300°C already leads to a significant improvement in surface integrity.

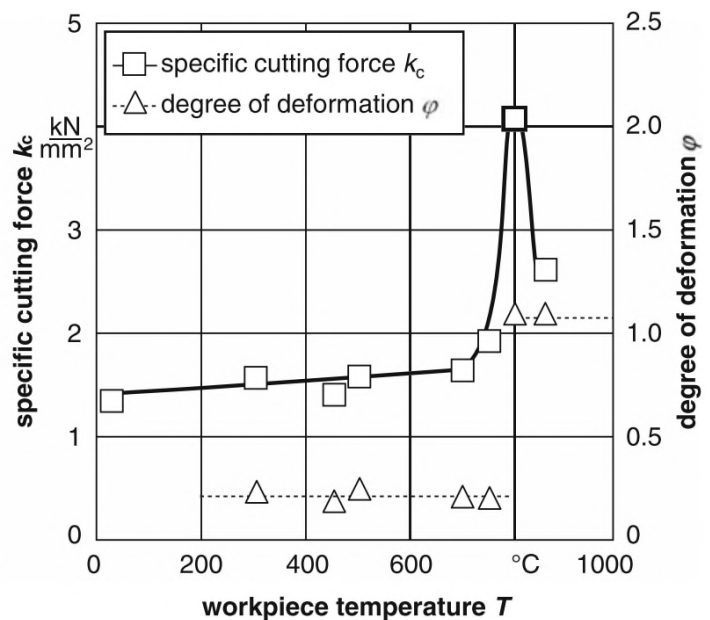
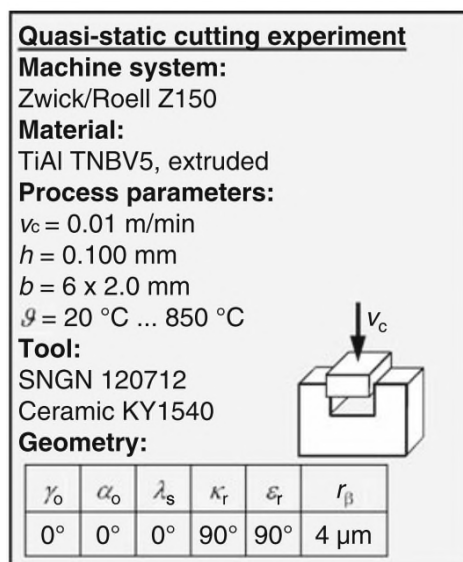


Figure 56. Specific cutting force as a function of the workpiece temperature of the TNBV5 alloy (adapted from [73]).

In general, experimental results show that the energy used to machine TiAl is ~5 times greater than that of conventional Ti alloys [68, 126, 127]. Depending on machining

parameters, tool condition and cutting process, cutting forces can vary from 50 to 300 N [44, 79, 126, 127].

Overall, cutting depth, tool wear, feed rate, and tool geometry are the most important input parameters for cutting forces. The effect of cutting speed, cutting environment and temperature, among other parameters, can also affect cutting forces, but to a lesser extent [24, 80, 129, 163]. For the machinability of TiAl, cutting force data can provide relevant information to understand the behavior of these alloys.

2.4.3. Summary

In terms of cutting tools, the machining of TiAl affects mainly the service lifetime of the tool. The study of machinability from the perspective of tools includes topics such as wear mechanisms, materials, geometries, service lifetime and cutting environments, which are some of the main aspects that allow for widening the knowledge of this research field.

The information available on machining parameters, such as cutting speed, feed rate, cutting depth, tool features, cutting environment, among others, are still scarce and limited. Therefore, to achieve machined components with excellent functional properties and with acceptable productivity rates, cutting parameters and tools must be carefully studied and optimized for each machining process and TiAl type.

Reported cutting forces in TiAl machining are significantly higher than those of other titanium alloys. In addition, the behavior of these forces varies according to the microstructure type, tool type, and process, making it even more challenging to define a trend about the behavior of this material.

Appendix A-2 presents a summary with the principal works about the cutting parameters for the TiAl machining.

Chapter 3 : Experimental Design

This chapter details the experimental program used in the analysis of the machinability of the intermetallic titanium aluminide Ti-48Al-2Nb-0.7Cr-0.3Si in the milling of surfaces with round insert tools. In addition, the design of the research plan created to carry out this study is outlined, aspects such as the evaluation criteria, the definition of the effect caused by the different factors involved in the milling process and the experimental procedure are described.

3.1. Experimental Approach

Machinability studies are generally carried out based on data obtained from experience in the production of workpieces or studies performed in specialized laboratories. This information seeks to determine the combination of machining parameters (factors) that provide parts with proper quality levels and an acceptable tool useful life in common operating conditions [64, 105, 118, 164–166].

Before establishing an experimental methodology, it is essential to understand that machinability is not an exclusive property of the material, it is a property of a machining system operating under a set of conditions [66]. For the study of the machinability in the flat surface milling in TiAl, there is no detailed experimental procedure to evaluate this property. Therefore, it was necessary to design an experimental methodology to assess the machinability of this alloy for milling with round inserts.

This methodology was designed so that it can be used in future experiments with cutting tools of different geometries and materials. The proposed experimental design was divided into four stages as observed in Figure 57.

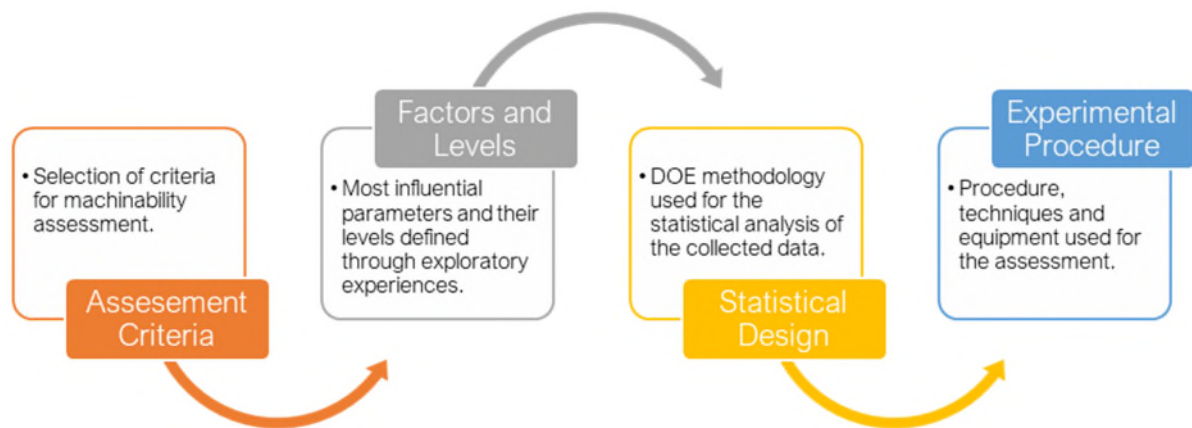


Figure 57. Phases of the proposed experimental plan.

The goal of this research is to analyze the machinability of an alloy γ -TiAl (Ti-48Al-2Nb-0.7Cr-0.3Si) in the milling of a flat surface with round inserts. For the accomplishment of this purpose, a set of experimental tests was planned which allowed assessing the mechanical characteristics of the workpiece, the texture of the machined surface, the metallurgical alterations of the surface, the variation of the cutting forces and the chip formation.

The tests were conducted under a range of machining parameters (factors) at different levels previously studied through a series of exploratory experiences. These tests allowed to meet the objectives outlined in Section 1.4 of this research.

3.2. Assessment criteria

The machinability of a material can be assessed by several evaluation criteria (Figure 58). However, performing all these experiments would require an extensive amount of testing, time and resources. So, five criteria were used in the present work, which are highlighted. These techniques were selected considering the characteristics of the milling process and the methods used by other researchers in the analysis of the machining of other TiAl.



Figure 58. The most commonly used criteria for assessing machinability [64, 66].

The following sections describe the criteria, and the objective applied for this research.

3.2.1. Material properties

The machinability is directly related to the physical, chemical and mechanical properties of the workpieces material [65]. In the case of titanium aluminides, several studies [59, 97, 126, 129] have shown that features such as chemical composition, hardness, ductility, yield strength, tensile strength, thermal conductivity and microstructure have a significant influence on its machinability.

As a result of the bibliographic review of chapter 2, it was determined that among the different γ -TiAl used in industrial applications, the primary interest is in those that have a content of 48 at% Al. This is due to properties such as low density, high melting point,

excellent oxidation and corrosion resistance, and mainly higher ductility at room temperature [32, 63, 167].

This type of alloy is used mostly in components for advanced applications in automotive and aeronautical engines. In the automotive area, its main field of application is the manufacture of turbocharger wheels and exhaust valves [31, 38, 47], while in the aerospace industry it is used in the production of low-pressure turbine blades [10, 38].

In our case, the objective was to identify some of the properties of this γ -TiAl alloy. This evaluation criterion provides essential information, which will allow correlating the machinability of alloys with a similar percentage of Al and microstructure.

3.2.2. Surface Integrity

Titanium aluminides are characterized by having a high susceptibility to metallurgical damage caused by machining operations. The main reported disadvantages are microhardening of the surface, lamellar deformation and poor surface topographic quality. Considering the application fields of TiAl, the poor surface integrity caused by machining operations is one of the main significant drawbacks that has prevented its diffusion in other industrial areas.

Against this background, this research focuses on the analysis of surface integrity as the primary criterion for evaluating the machinability of this alloy. The study of the characteristics of the machined surfaces uses several factors for the analysis of surface integrity (SI). According to Astakhov [119], the basic set of data for the evaluation of the SI includes the following parameters:

1. Roughness
2. Surface hardness
3. Surface defects
4. Microstructural changes
5. Microhardness
6. Subsurface damage

The proposed experimental design evaluated these parameters, and they were grouped into two studies, which are the evaluation of surface texture and surface properties. This

information was analyzed according to the characteristics of the tool and the cutting parameters.

The surface texture was evaluated by measuring the arithmetic mean of the roughness (Ra) and the surface topography. In addition to this, a characterization of the surface defects in all machined parts was made.

For the case of surface properties, the evaluation consisted in determining the characteristics of the subsurface hardened layer (surface hardness, depth of the hardness layer, peak hardness value and its thickness) and the evaluation of the lamellar deformation.

The objective of these evaluations was to define the machinability of this alloy from the perspective of the quality of the surface and to find the range of suitable cutting parameters for each of the analyzed inserts.

3.2.3. Cutting Forces

The measurement of cutting forces is one of the most used methodologies in the study of the machinability of materials. This procedure is mainly used to evaluate the effect of the operational parameters during the machining process. The main advantage of this methodology is the reduced number of tests required for the analysis of the cutting process.

The titanium aluminides are characterized by high cutting forces, which according to several authors [79, 80, 127, 163] are altered by the wear of the tool and the cutting parameters. In general, low cutting forces represent better machinability, mainly because it implies less wear of the tool, of the machine, and greater dimensional accuracy of the workpiece.

In the present research, the analysis of the cutting forces was used to study the effect of cutting-edge geometry, insert materials and the variation of the cutting parameters.

3.2.4. Chip Formation

Metallurgical and geometrical characteristics of the chips represent the behavior and performance of a cutting process. Due to this, the study of chip formation during machining operations has proved to be a useful technique as a method for evaluating

machinability. This approach usually is used to analyze the interaction between the cutting edge of the tool and the workpiece, however, it is important to note that the mechanism of chip formation is also associated with the properties of the material, the wear of the cutting tool and the stability of the process [168–170].

The limited ability of these alloys to deform plastically, produces tiny chips similar to needles, which makes the use of this analysis technique very challenging. However, there are several theories [24, 73, 125] that apply this methodology. This analysis avoids carrying out destructive tests on the workpieces, simplifying the machinability analysis.

In this research, this evaluation method was used to study the effect of the geometry of the cutting edge on the process of chip formation. For the study of machinability, this assessment complements the analysis of the relationship between cutting edge geometry, cutting forces and surface integrity.

3.3. Factors and levels

The purpose of this section was to determine the most important parameters that are involved in the milling of a TiAl alloy with round inserts. The initial evaluation of the possible factors and levels to be investigated was made based on a set of analyzes and exploratory experiments based on the studies presented in chapter 2.

The literature review showed that the central sets of factors that affect the surface integrity in γ -TiAl are the characteristics of the work material [56, 171], tool properties [24, 108] and cutting parameters [69, 97, 130].

Based on the aforementioned the exploratory testing stage was structured under a sequence of iterative steps that allowed defining the factors and levels to be studied in the following stages.

These experiments consisted in face milling simple specimens of the analyzed material at a cutting time of 1 min, using parameters proposed in several research works in milling operations with flat and ball end-mill tools. The evaluation parameters of the exploratory tests were the wear of the tool and the surfaces roughness Ra.

The studied factors in the exploratory experiments are presented in Table 7

Table 7. Factors and level analyzed in the program of the exploratory experiment.

N°	Type	Factor	Levels	Ref.
1	Workpiece	Surface conditions	Casting / EDWM / Abrasive wet cutting + grinding	[10, 33, 62, 119, 172]
2		ISO classification	S10 (GC1010) / S15 (GC1030) / S25 (S30T) / S30 (GC1040) / S35 (S40T)	[24, 98, 108, 124, 131, 173]
3		Coating	PVD-TiAlN / PVD-TiAlN+TiN / CVD-TiCN + Al ₂ O ₃ +TiN	
4		Cutting Tool	Cutter geometry	
5		Cutting edge geometry	Sharp Edge / T-land Edge	[46, 89, 178, 179]
6		Tool Holder	HSK / Collet Chuck / Hydraulic	[65, 66]
7		Teeth number	Single / 4	[180, 181]
8	Cutting Parameters	Cutting Speed (m/min)	20 / 45 / 70 / 110 / 150 / 300	[23, 68, 69, 98, 127]
9		Chip Thickness (hex)	0.05 / 0.08	
10		Axial depth of cut (mm)	0.5 / 1	
11		Engagement (%)	30 / 60 / 100	
12		Cutting Environment	Dry / Wet / High-Pressure 70 bar	

As a result of the exploratory experiences, it was observed that considering an analysis that covers all the levels and factors presented in Table 7 would consume a considerable amount of time and resources, so for this study only the factors that were detected as the most influential were considered. All other factors were kept constant, and their values were determined based on the results of the exploratory tests and information obtained from the literature review. In the following sections, the selected factors and the levels established in this research are presented.

3.3.1. Workpiece material factors

The present work studies a commercial γ -TiAl alloy (Ti-48Al-2Nb-0.7Cr-0.3Si), cast cylindrical ingots of 55 mm diameter and 310 mm in length, produced via triple vacuum arc melting (VAR) in metallic molds by the Gfe Metalle and Materialien GmbH of Germany (Figure 59).



Figure 59. Cast cylindrical ingots of Ti-48Al-2Nb-0.7 Cr-0.3Si obtained via VAR.

Due to the large dimensions of the ingots, the samples for machining tests were obtained by a cutting process. In order to carry out this procedure, two cutting methods (Abrasive wet cutting and EDWM) were tested.

The first cutting experiment was conducted with abrasive cutting discs, which proved to be ineffective due to the low accuracy and the high consumption of discs and cutting time. The samples obtained by this process showed not homogeneous surfaces, for which an additional grinding process was required to achieve an adequate surface.

As a result of this cutting and grinding process, it was determined that this sequence of operations causes lamellar deformation in the microstructure of the sample at a depth of up to $\sim 25 \mu\text{m}$, as observed in Figure 60.a. This deformation is related to phenomena such as hardening and residual stresses on the surface as discussed in chapter 2 [139].

The following cutting process carried out was the cut by EDWM. The experimental trial was conducted using machining parameters recommended by Aust and Niemann [98]. As in the previous case, a high consumption of cutting material (brass wire) was shown. For this process cutting time was considerably shorter than in the first one, besides it was not necessary to carry out additional finishing operations and the cuts presented greater accuracy.

The major drawback observed was a white layer effect on the cutting surface (Figure 60.b), caused by the characteristic high-temperature gradient of this process [182]. However, the observed layer was tiny ($\sim 5 \mu\text{m}$), heterogeneous and less deep than the axial depth of the cut.

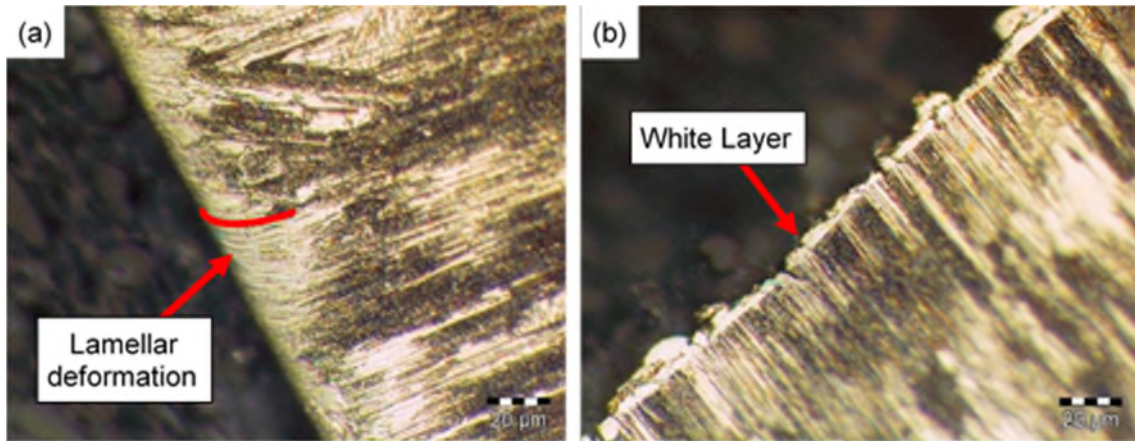


Figure 60. Micrograph of Ti-48Al-2Nb-0.7Cr-0.3Si after; (a) abrasive wet cutting process, and (b) EDWM process.

As a result of these experiences, it was defined that the process that produces minor alterations in the surface of the material and consequently fewer disturbances in the machining tests would be cutting by EDWM. For this reason, this factor was selected for the preparation of all the samples required in this work.

3.3.2. Cutting tools factors

The first step in choosing a cutting tool is to define its essential characteristics. This selection is determined by factors such as operation type (finishing or roughing), machine features, work material clamping, tool holder system, cutter geometry, workpiece material, among others. For this study, several scientific articles were analyzed, and some exploratory tests were carried out to investigate characteristics such as the geometry and number of teeth.

Because of this study, an indexable profiling milling cutter with round insert (Figure 61) was chosen. This selection was made due to the versatility that it has for milling profiles and flat surfaces using the same type of insert.

Relatively to the number of teeth, experimental tests were carried out using the single insert methodology, due to the run-out presented by the use of several inserts in indexable milling cutters [180], as well as the high experimental costs involved in the use of several cutting inserts.



Figure 61. Round insert face milling cutter.

For the selection of the specific characteristics of the milling cutter, several recommendations from the cutting tools manufacturers [166, 178, 183] and technical literature [65, 66] about tool selection were followed.

Table 8 presents the criteria used to determine the specifications of the cutting tool.

Table 8. Milling cutter specifications.

Indexable Milling Cutter			
Tool characteristic	Value	Selection Criteria	Ref.
Diameter	35 mm	Small tool diameters usually require high rotation frequencies, and for measurement of cutting forces, this condition means a higher data acquisition frequency.	[162, 184]
Axial rake angle	Positive	Double positive cutters reduce the cutting pressure, consume less power, create less heat, reduce deflection, and result in less strain on the machine bearings, ways, and spindle. This geometry is suitable for finish milling.	[64, 179]
Radial rake angle	Positive		
Tool Holder	HSK 63A	The HSK provides simultaneous taper and face spindle contact that gives a higher stiffness, radial and axial positioning accuracy and repeatability.	[66]
Cutting tool Clamping	Capto C3	The Capto system provides self-centering and self-aligning properties and high torque stiffness, it transmits torque through the taper shank avoiding the presence of balancing problems.	[65, 166]
Coolant system	Internal high pressure	The internal coolant system is used to assist chip removal, to control the heat at the cutting edge and reduce tool wear. High-pressure coolant applied through the spindle/tools shows better results than external supply and low pressure.	[80, 158]

The following set of defined factors were the characteristics of the cutting inserts. The first characteristic to be established was the material. In the case of the present work, it was decided to use tungsten carbide inserts (WC) recommended for the machining of heat-

resistant alloys (ISO Classification). This decision was made because milling of γ -TiAl with these materials proved to perform better than PCBN and PCD, which have several disadvantages due to the discontinuous cutting process [44, 107, 131].

To define the material inserts, the main factors to consider are their composition and coating type. Before this selection, exploratory tests were carried out with various kinds of different commercial tools, with five kinds of materials and three coatings (Table 7). The selection criteria was the wear resistance against a range of cutting parameters recommended by several scientific works (Table 9) [24, 69, 140, 142].

Table 9. Cutting parameters used in the exploratory test.

Test	Vc	hex	ap (mm)	ae (%)	Environment	Cutting Time	Ref
1	70	0.05	0.5	100	HP 70 bar	1 min	[69]
2	110	0.05	0.5	100	HP 70 bar	1 min	[140]
3	150	0.05	0.5	100	HP 70 bar	1 min	[142]
4	300	0.05	0.5	100	HP 70 bar	1 min	[24]

Vc= Cutting Speed, hex = chip thickness, ap=axial depth of cut, ae= radial depth of cut

In addition to the different composition of the insert material and their coating, two geometries of rectified cutting edges, designated as XL and XM, were tried. These geometries are recommended for finishing operations in titanium and stainless-steel alloys.

The XL geometry (T-land edge) has a sharp cutting edge with a rake angle of 5° and a rake land angle of 15° . The tool supplier states that this geometry reduces cutting forces, vibration and tolerates high cutting speeds. The XM (Sharp edge) geometry has a rake angle of 0° , giving a higher cutting edge sharpness, which allows faster cutting feeds [166]. Figure 62 presents the geometries used in this work.

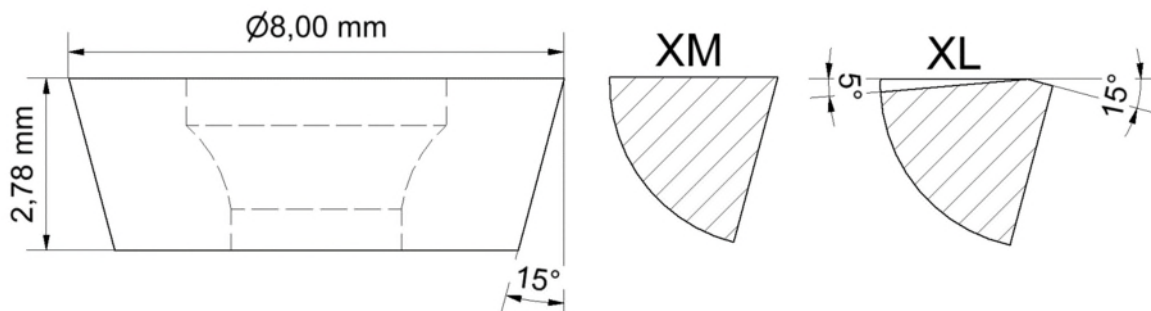


Figure 62. Cutting insert and edge geometries.

The geometry of the cutting edge has been defined by several authors [159, 185–187] as a crucial factor in the cutting process of the material, as well as in the surface integrity of the machined parts. For this reason, two geometries were proposed as an analysis factor.

After the exploratory tests, the best performing inserts were selected and identified according to the ISO standard of the workpieces and their cutting-edge geometry. All used inserts are of tungsten carbide coated with a $\sim 2.5 \mu\text{m}$ layer of TiAlN deposited through PVD (Physical Vapor Deposition). Only one type of coating was selected to control the number of variables.

The composition of each insert material varied mainly in its cobalt content and grain size. All tools were supplied by Sandvik Coromant (Sweden). Next, an analysis of the composition and grain size of the material is presented, as well as the manufacturer's description of the grade.

S10 is an insert material with a cobalt content of 7% and submicron grain size less than $1 \mu\text{m}$. This composition gives the insert higher resistance to plastic deformation, thermal cracking and other types of wear. This material is used in machining operations at high cutting speeds, but under stable machining conditions and without vibrations. Figure 63 shows the microstructure and composition of this material.

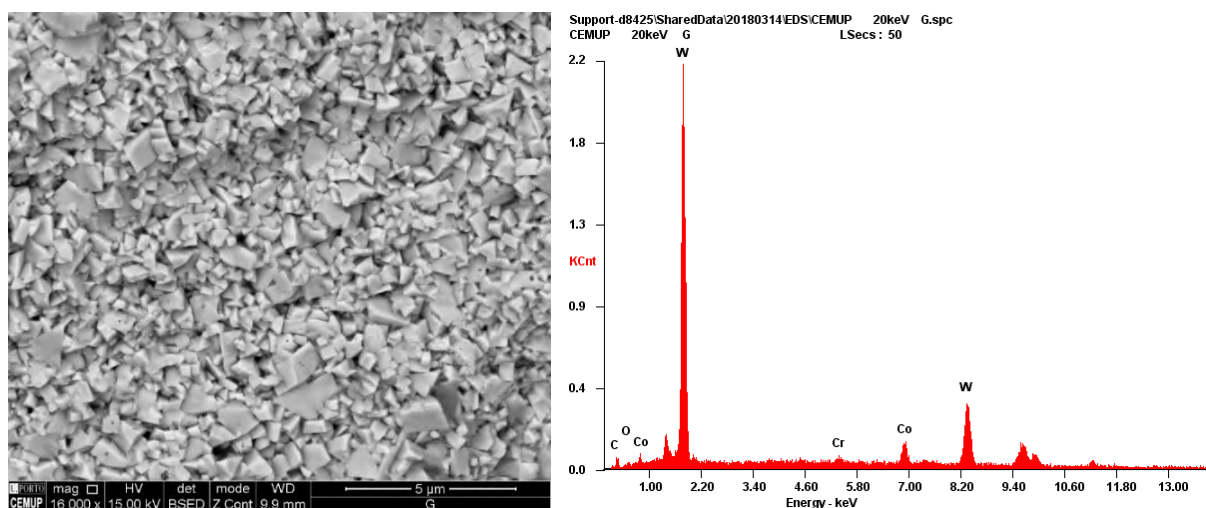


Figure 63. Cutting insert material S10, (a) SEM micrograph in BSED mode, and (b) EDS analysis.

S25 is a material with a cobalt content higher than that of S10 (11.2%) with fine grains of $\sim 1 \mu\text{m}$. It is an optimized material for the machining of titanium alloys. These inserts preserve sharp cutting edges with excellent fatigue resistance and micro chipping at high

cutting speeds. Figure 64 shows the microstructure and composition of this material [178, 188].

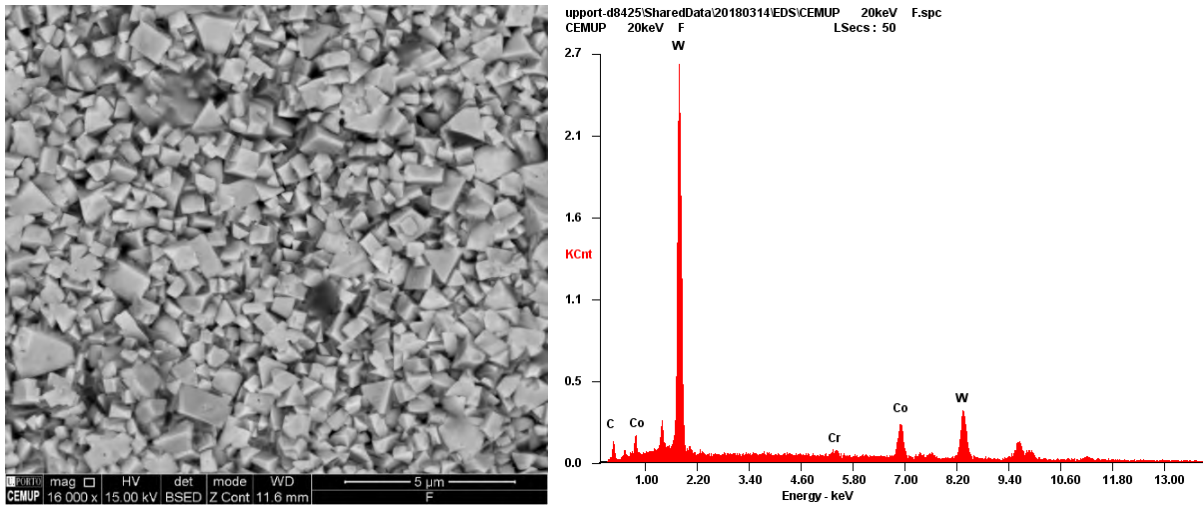


Figure 64. Cutting insert material S25, (a) SEM micrograph in BSED mode, and (b) EDS analysis.

S30 is a material with a cobalt content of 13.5% and a fine grain size of $\sim 1 \mu\text{m}$, used in unstable machining conditions with low feeds and cutting speeds to cut materials such as austenitic stainless steels, duplex steels, and heat resistant materials [178, 188]. This type of material is not commercially used for the manufacture of circular geometry inserts and was specially prepared for this research work. Figure 65 shows the microstructure and composition of the material.

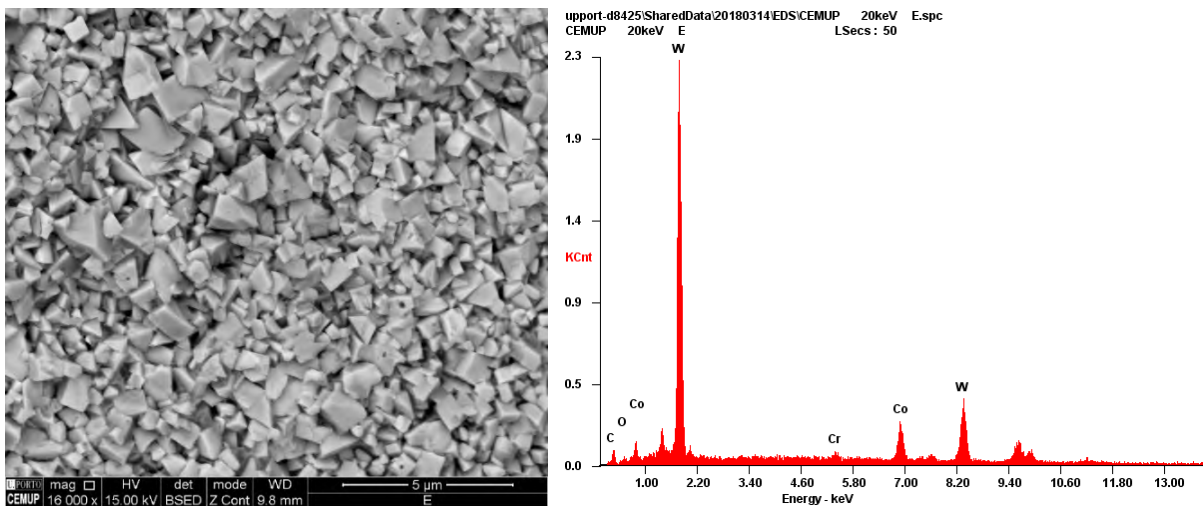


Figure 65. Cutting insert material S30, (a) SEM micrograph in BSED mode, and (b) EDS analysis.

Table 10 presents the designations and main specifications of the six type of inserts.

Table 10. Cutting insert specifications (Tool geometry and material).

Designation	S10-XL	S10-XM	S25-XL	S25-XM	S30-XL	S30-XM
Material Characteristics						
Cobalt content (%)	7	7	11.2	11.2	13.5	13.5
Hardness (HV)	~1900	~1900	~1650	~1650	~1550	~1550
Coating	PVD - TiAlN					
Coating thickness	~2.5 μm					
Geometry Characteristics						
Rake angle	5°	0°	5°	0°	5°	0°
Rake land angle	15°	0°	15°	0°	15°	0°
Clearance angle	15°					
Insert diameter (mm)	8					
Nose radii (mm)	4					
Insert thickness (mm)	2.78					

The selected factors and their respective levels are presented in Table 11.

Table 11. Factors and selected levels in exploratory tests for cutting tools.

N°	Factor	Levels
1	ISO classification	S10 / S25 / S30
2	Coating	PVD-TiAlN
3	Cutter geometry	Profile milling
4	Cutting edge geometry	Flat, T-land edge
5	Tool holder	HSK
6	Teeth number	single

It is essential to note that unlike most cutting inserts used in milling, these inserts can also be used in spherical surface turning operations. This capacity was used in this work to carry out an analysis of the chip formation process.

3.3.3. Cutting parameters

The main cutting parameters that influence all the machining processes are cutting speed (V_c), feed per tooth (f_z), axial (a_p) and radial (a_e) depth of cut. The proper selection of these values affects both the quality of the machined surfaces, as well as the useful life of the cutting tools. These parameters are selected according to the kind of material, the type of operation, the geometry and the material of the tool.

In general for milling γ -TiAl, the information of cutting parameters for cutting tools with round tip radii is limited [23]. However, several authors mention [23, 82, 159, 163] that in terms of surface integrity, the use of tools with large pointed radius is advantageous. Due to this lack of information, it was decided to conduct a set of initial experiments using the parameters proposed in several research works [23, 24, 69, 79, 97, 140, 142], as well as those recommended for the machining of Ti-based alloys by the tool manufacturer.

The first objective in this stage of experimentation was to define the essential aspects of the effect that the geometry of the inserts has on the cutting parameters. In milling with round insert tools, V_c and f_z are parameters that vary along the cutting edge.

The V_c varies according to the effective cutting diameter (D_{cap}), which depends on the axial depth of cut (Figure 66). Due to these aspects, the rotation frequencies of the tools were calculated according to the D_{cap} , to ensure the real cutting speed in the cutting area.

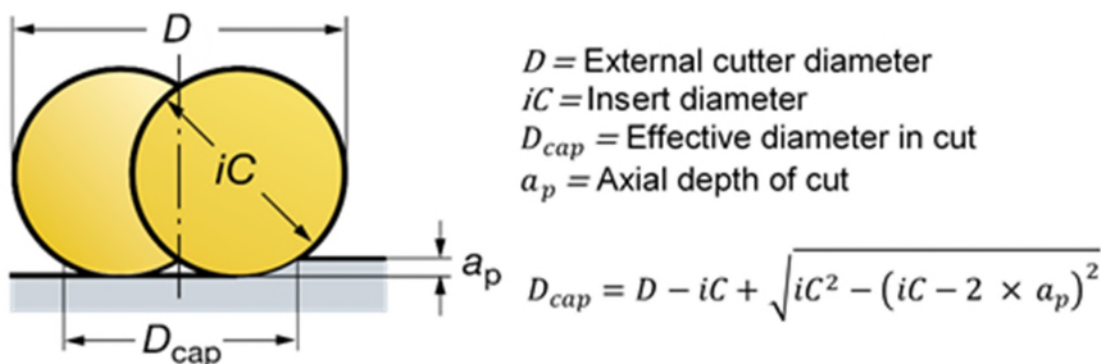


Figure 66. Effective diameter in cut for round cutter insert, and calculation formula [178].

For the case of f_z , this parameter depends on the chip thickness (h_{ex}). It is due to the effect of the axial depth of cut (Figure 67). Therefore, the width of the chip was selected as an evaluation factor, and the value of f_z was obtained as a function of this parameter.

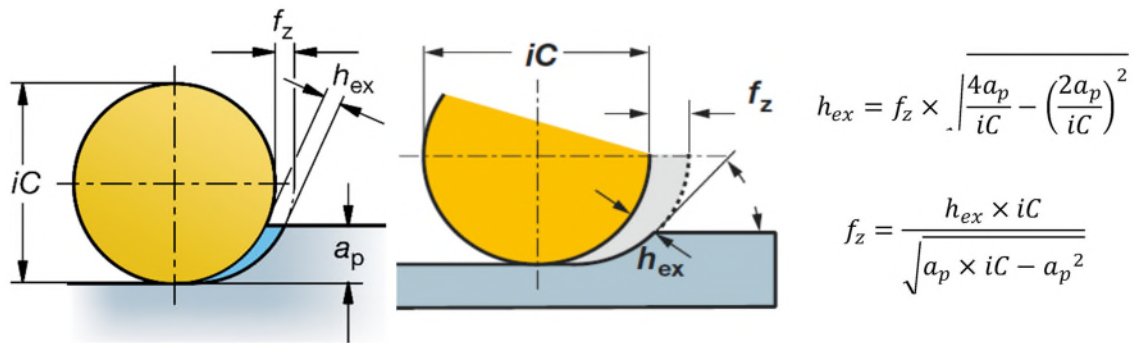


Figure 67. Chip thinning effect on round inserts [178].

The evaluation for the selection of the range of cutting parameters was carried out by measuring the wear of the cutting edge (no higher than 100 μm) and surface roughness (less than or equal to 0.4 μm) in a cutting time of 1 minute. The performance of each kind of insert varied according to the characteristics of its materials and cutting-edge geometry.

As a result of these exploratory experiences, it was determined that for this geometry, the combination of $V_c = 110$ m/min, $a_p = 0.5$ mm and $h_{ex} = 0.05$ mm with full engagement, could be the maximum working limit in this group of inserts. These rates were selected due to the rapid wear (leading to the catastrophic loss of the cutting-edge after the first contact with the material) that the tool presented over this range of cutting parameters.

Although the depth of radial or engagement (a_e), showed to be influential in the exploratory tests, it was also observed that the axial depth and thickness of the chips are even more influential in the cutting process, also due to the shape of the samples makes it difficult to vary this parameter.

Concerning the cutting environment, all the exploratory experiences carried out in dry, ended with the deformation and in some cases, with the fracture of the cutting edge, for which the use of a cutting fluid turned out to be indispensable.

The use of external low-pressure lubrication proved to improve the performance of the tool; however, it did not show notable improvement. The use of internal high-pressure lubrication presented a considerable improvement for the useful life of the tool, which was also confirmed in the studies carried out by Klocke et al. [80].

Factors and levels of cut parameters selected to perform this study are presented in Table 12.

Table 12. Factors and levels selected in exploratory tests for cutting parameters.

Factor	Levels
Cutting Speed (m/min)	20 / 45 / 70 / 110
Axial depth of cut (mm)	0.3 / 0.5
Chip Thickness (h_{ex})	0.02 / 0.03 / 0.04 / 0.05
Engagement (%)	100%
Cutting Environment	Internal High-Pressure 70 bar

3.4. Statistical Design

The machinability assessment is commonly obtained through tests and statistically designed iterative experiments. This methodology is known as Design of Experiments (DOE) and can be done through three levels of experimentation; full factorial, fractional or partial [189]. The complete factorial experimentation provides a comprehensive view of all possible effects of the experimental factors and their interactions. However, the scale of tests may be too extensive and expensive for scientific research. Consequently, the conduction of fractional factorial experiments, such as the Taguchi methodology, has been widely used in machinability assessment processes, especially in difficult-to-machine materials such as TiAl [97, 147, 164, 190].

The Taguchi methodology is commonly used for its orthogonal array design, which provides a considerable reduction of time and resources necessary for the evaluation of the effect caused by each of the factors involved in a process. In the case of milling, several authors have demonstrated the effectiveness of this technique for the evaluation and optimization of flat surfaces [118, 160, 177, 191].

One of the objectives of this work is to understand the effect of machining parameters on the material through various evaluation criteria. In the case of surface integrity and cutting forces assessment, these were evaluated using the Taguchi DOE methodology using different factors and levels selected in the exploratory tests.

The experimentation was conducted in two stages. The first one comprised an individual study for each insert in a series of standard cutting parameters for all inserts, and the second reached an extended experimental analysis phase, only for the insert that presented the best performance at high cutting speeds. The two stages were designed to identify the

effect of the cutting parameters and inserts characteristics on the machined surface. Figure 68 shows a diagram that allows visualizing the experiences conducted in this work

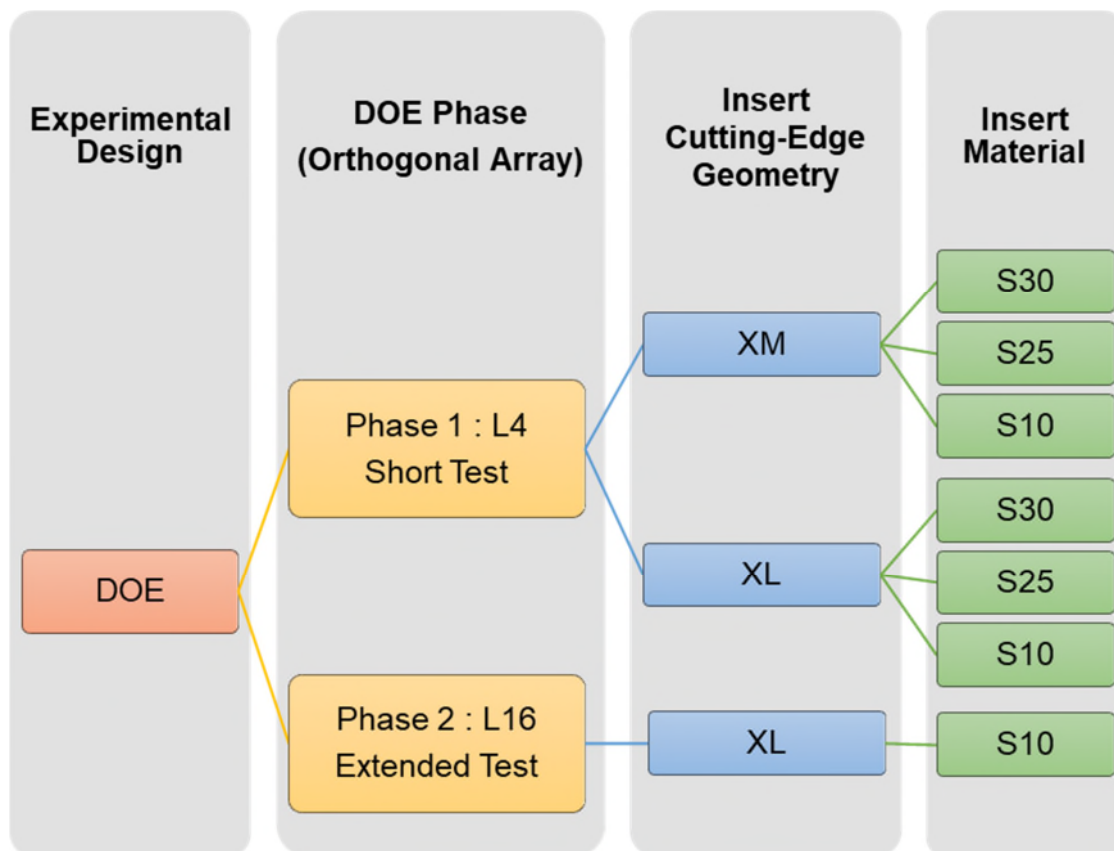


Figure 68. Chart of work stages.

The first phase of tests used an L4 fractional orthogonal array with 3 factors at 2 levels each, which was performed individually for each insert. The objective of this stage was to understand the effect that the geometry of the cutting edge and the tool material have on the cutting surface. Besides, the DOE configuration was designed to allow the integration of new tools in the machinability analysis for later studies. This methodology would allow comparing new results with the information obtained in this work.

The levels of the evaluation factors selected in this stage were those values in which all the tools presented a similar performance in the exploratory experiences. Due to the type of arrays, it was not possible to assess the interaction between factors. The experiment sequence was carried out randomly. Each trial was replicated three times, and a new cutting insert was used for each experience. This procedure intended to minimize the possibilities of systematic error during the measurement of machinability results. Table 13 shows the factors, their levels and the orthogonal array.

Table 13. L4 orthogonal array used in the first phase of the experimental work.

Taguchi Orthogonal Array L4			
TEST	Cutting Speed (m/min)	Axial Depth (mm)	h_{ex} (mm)
Trial 1	70	0.3	0.03
Trial 2	70	0.5	0.04
Trial 3	45	0.3	0.04
Trial 4	45	0.5	0.03

The second phase consisted of a set of tests carried out using an orthogonal Taguchi L16 array. This array was modified to study 2 factors at 4 levels and 1 factor at 2 levels. This phase was aimed at understanding the effect of the cutting tool at high and low cutting speeds on the machined surface of TiAl. In addition, this experience allows to better identify the impact of the variation of the speed and thickness of the chip. Table 14 shows the orthogonal array used in this phase.

Table 14. L16 orthogonal array for the first phase of the experimental work.

Taguchi Orthogonal Array L4			
TEST	Cutting Speed (m/min)	Axial Depth (mm)	Hex (mm)
Trial 1	20	0.02	0.3
Trial 2	20	0.03	0.3
Trial 3	20	0.04	0.5
Trial 4	20	0.05	0.5
Trial 5	45	0.02	0.3
Trial 6	45	0.03	0.3
Trial 7	45	0.04	0.5
Trial 8	45	0.05	0.5
Trial 9	70	0.02	0.5
Trial 10	70	0.03	0.5
Trial 11	70	0.04	0.3
Trial 12	70	0.05	0.3
Trial 13	110	0.02	0.5
Trial 14	110	0.03	0.5
Trial 15	110	0.04	0.3
Trial 16	110	0.05	0.3

As in the first phase, it was not possible to evaluate the interactions between factors with the array used. The tests were conducted randomly and replicated three times using a new cutting edge for each experience. The number of milling tests performed was 120 trials, 72 in the first phase (DOE L4) and 48 in the second phase. In this case, the maximum levels obtained in the exploratory experiences were used.

To define a robust adjustment of the factors and to avoid the interference caused by the noise factors in the statistical analysis of the results, the S/N ratio "the lower, the better" was defined, due to the type of assessment criteria used in this work.

3.5. Experimental Procedure

The effectiveness of the robust experimental design is determined largely by the validity of its results. The adequate definition of the experimental procedure in this investigation allowed establishing a starting point for future experiences in the evaluation of the machinability of this alloy with other tools.

This section describes the equipment, techniques, and procedures used in the experimental tests and the acquisition of the data required for the assessment criteria selected in this experimental design.

Regarding milling tests, all trials were conducted in a DECKEL-MAHO DMU 60 eVo linear (Germany) vertical machining center with 25 kW of power, with a maximum spindle speed of 18,000 rpm and 5 axes (3 linear axes and 2 rotary axes) (Figure 69.a). This machine is considered a robust equipment commonly used in the industry for medium-sized machine components weighing up to 400 kg.

This equipment has a Renishaw palpation system with the accuracy of up to 0.001 mm (Figure 69.b), and a BLUM laser tool device with accuracy up to 0.001 mm (Figure 69.c). These systems were used for the centering of the piece and measurement of the cutting tool, respectively.

The milling experiments were carried out under high-pressure lubrication environment with an AVILUB METACOOOL BFH (MAFICETI-Portugal) water-miscible cutting fluid at a concentration of 6%. The cutting fluid was supplied through an internal system of high pressure at 70 bar with a flow rate of 26 l/min applied on the face of the cutting insert (Figure 69.d).

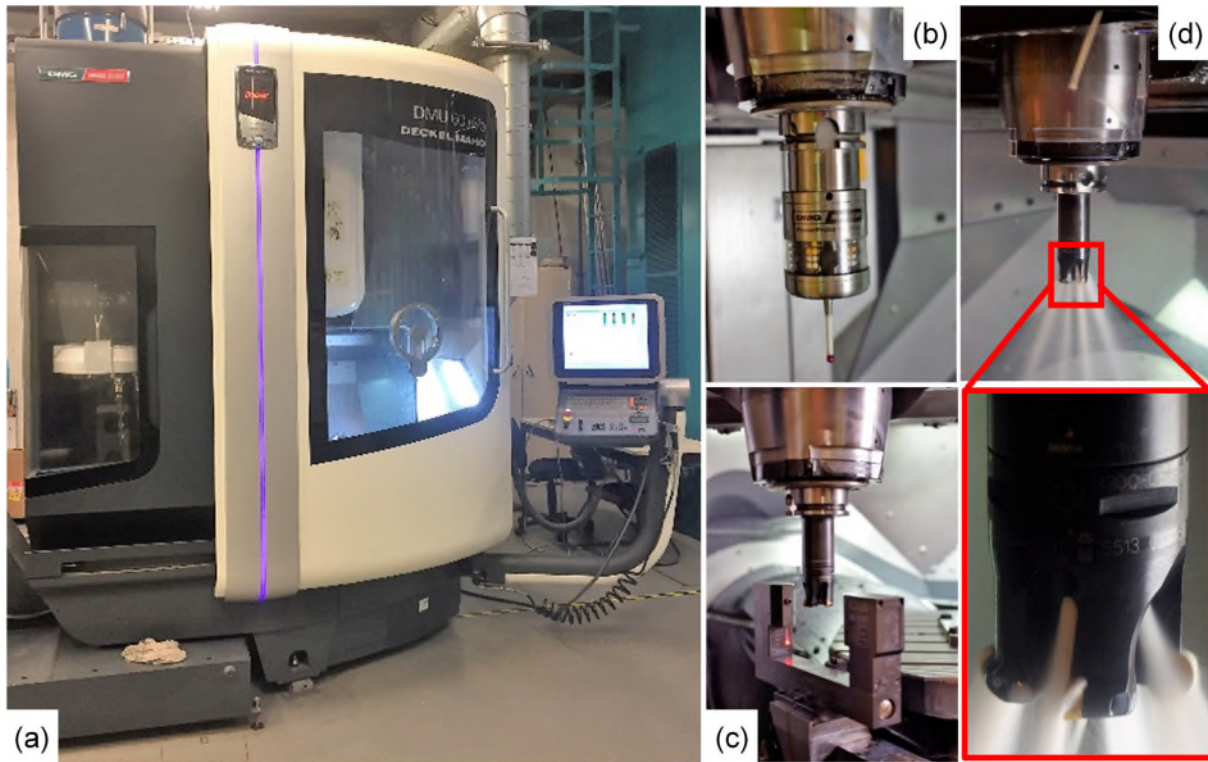


Figure 69. (a) DECKEL-MAHO DMU 60 eVo linear machining centre used for milling tests, (b) Renishaw touch probe device for workpiece measurement, (c) BLUM laser measuring system, and (d) high-pressure internal lubrication system.

The samples used in the milling tests are cylindrical pieces of 55 mm diameter and 15 mm thickness (Figure 70.a), cut from ingots of Ti-48Al-2Nb-0.7Cr-0.3Si using an EDWM process (MITSUBISHI DWC 90SZ). These samples were fixed by employing a four-wheel self-centering mandrel; the tightening binary was 50 Nm.

Additionally, the horizontality of each sample's surface was analyzed through the palpation system of the machine. This procedure was carried out to decrease the variation of the a_p along the surface. The compensation of this variation was made through rotary movements of the machine. The maximum variation allowed was $\pm 5\%$ of a_p .

The procedure for milling the surface corresponded to one transversely run of the cutting tool in each sample (Figure 70.b). This originated a channel of 30 mm wide by 0.3 and 0.5 mm deep, respectively. Each test was performed with a new cutting insert, to avoid the influence of cutting-edge wear.

The trajectory of the cutting tool made a roll-in-the-cut input until reaching 100% a_e ; this programming was carried out to reduce the vibration and the possibility of breaking the cutting edge of the tool.

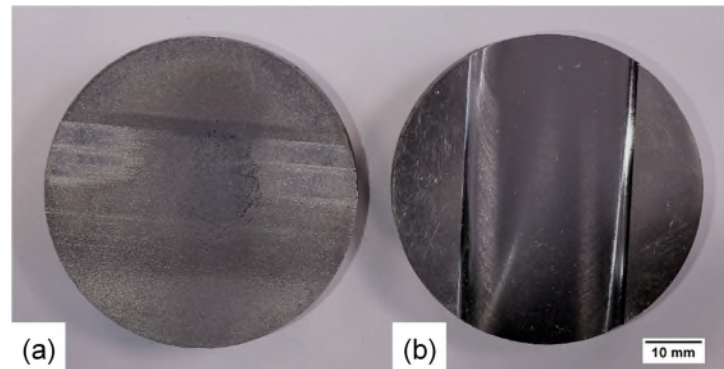


Figure 70. Samples of Ti-48Al-2Nb-0.7Cr-0.3Si; (a) before, and (b) after milling operation.

3.5.1. Workpiece material characterization

Metallographic and mechanical studies were conducted for the characterization of the work material. All sample cuts for material characterization tests and surface integrity analysis were performed on an EDM machine MITSUBISHI DWC 90SZ (Germany) (Figure 71). This equipment has a 50 A anti-electrolysis power supply and a Mitsubishi CNC control that coordinates independent movements between X, Y and Z-axes. The samples were cut with brass wire of 0.25 mm diameter, with positive polarity of the electrode and immersed in a dielectric fluid of demineralized and deionized water.



Figure 71. Wire EDM Machine MITSUBISHI DWC 90SZ.

The samples for the metallographic studies were mechanically polished using a STRUERS Planopol-3 semi-automatic polishing machine (Denmark) (Figure 72.a) with sandpaper grit numbers 80, 320, 600, 1000, 1200 and a cloth with 0.03 μm alumina with a solution of hydrogen peroxide (H_2O_2) at 150 rpm. For analysis of the microstructure, the polished samples were chemically etched with a Kroll reagent (1 ml of hydrofluoric acid, 3 ml of nitric acid and 500 ml of water) for 10 seconds. The metallographic analysis of all the

samples was performed using an OLYMPUS PMG 3 optical microscope with up to 1000 X magnification (Figure 72.c).

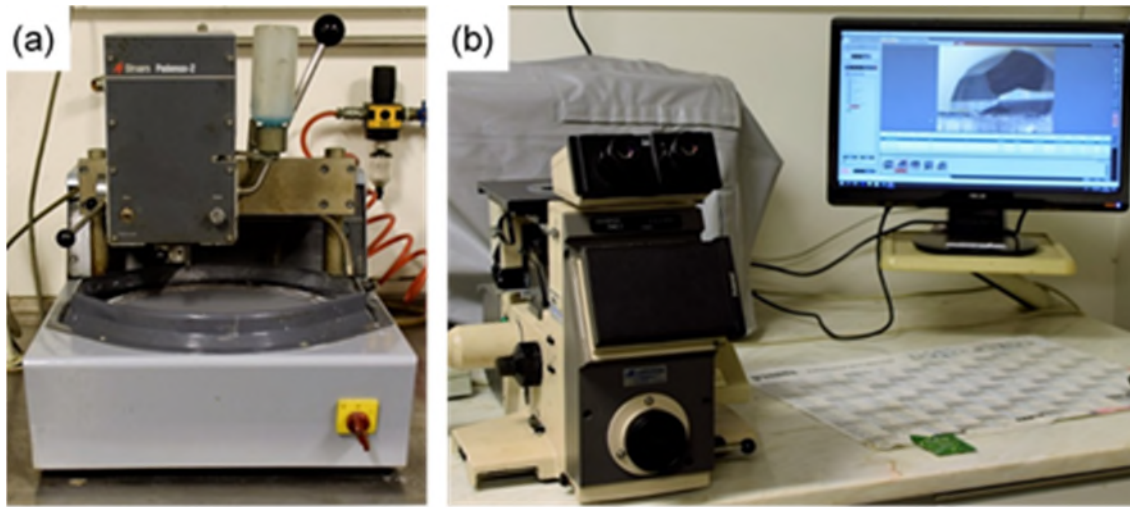


Figure 72. (a) STRUERS Planopol-3 automatic grinder polishing machine, (b) Olympus PMG 3 optical microscope.

For the determination of the mechanical properties, six specimens were prepared from an ingot according to EN-10002-1 (Figure 73). The tests were carried out at room temperature, at a deformation speed of 2 mm/min in an MTS 810 machine (Figure 74.a) with a load cell of 150 kN. The deformation of the samples was measured using an MTS 634.25F-24 extensometer with a gauge length of 50 mm (Figure 74.b).

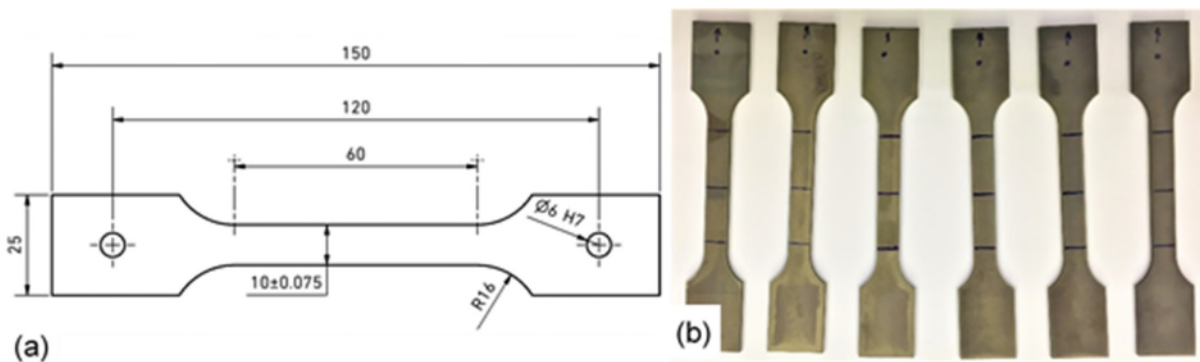


Figure 73. Tensile test specimen geometry; (a) dimension, and (b) cut samples.

The hardness of the base material was measured directly in the transversal and longitudinal samples cut in different sections of the material, using a MATSUZAWA MXT70 (Figure 74.c) microdurometer, using a Vickers penetrator (HV) with loads of 100 and 25 g for surface hardness and subsurface profile of hardness, respectively. The indentation time was 20 seconds in all cases.

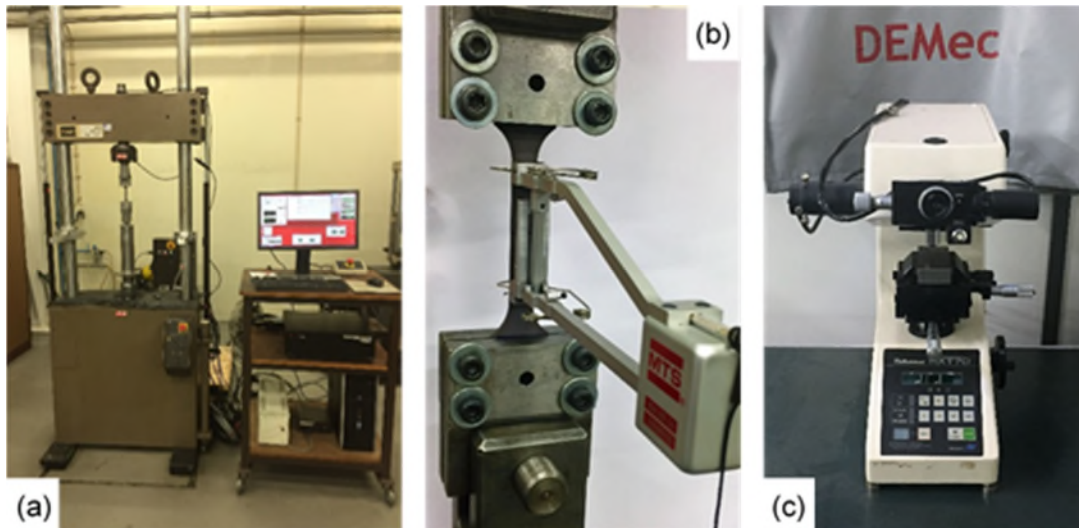


Figure 74. (a) MTS 810 material testing system, (b) MTS 634.25F-24 mechanical extensometer, and (c) Microhardness tester MATSUZAWA MXT70

3.5.2. Surface integrity

The surface integrity was evaluated by studying the texture and mechanical properties of the surface and subsurface. These criteria provide a set of essential data for the assessment of the surfaces and the understanding of the machinability of the material. In published literature about TiAl machining [97, 126, 140, 192], surface integrity information is one of the main criteria evaluated.

3.5.2.1. Surface texture

The texture of the machined surface was assessed quantitatively and qualitatively. The quantitative evaluation was carried out by measuring the arithmetic mean of the surface roughness profile (Ra) using a HOMMELWERKE LV-50 roughness tester (Germany) (Figure 75.a) with a resolution of 0.05 μm , a probe angle of 90 $^\circ$ and a tip radius of 5 nm. The measurements were made in the direction of advance of the cutting tool, following the ISO 4287 standard. This measurer was set at 5 mm traverse length and 0.5 cut-off value in three different sectors spaced 130 mm apart (Figure 75.c).

Additionally, the 3D surface roughness (Sa) was analyzed using a BRUKER NPlex (USA) digital microscope (Figure 75.b), with a standard 10x lens, a vertical resolution <0.1 nm and an optical resolution of 0.33 μm , in a measurement area of 250 μm x 250 μm . The evaluation was carried out in the same sector for all the milled samples. The measuring zones within this section are spaced 6 mm apart (Figure 75.c).

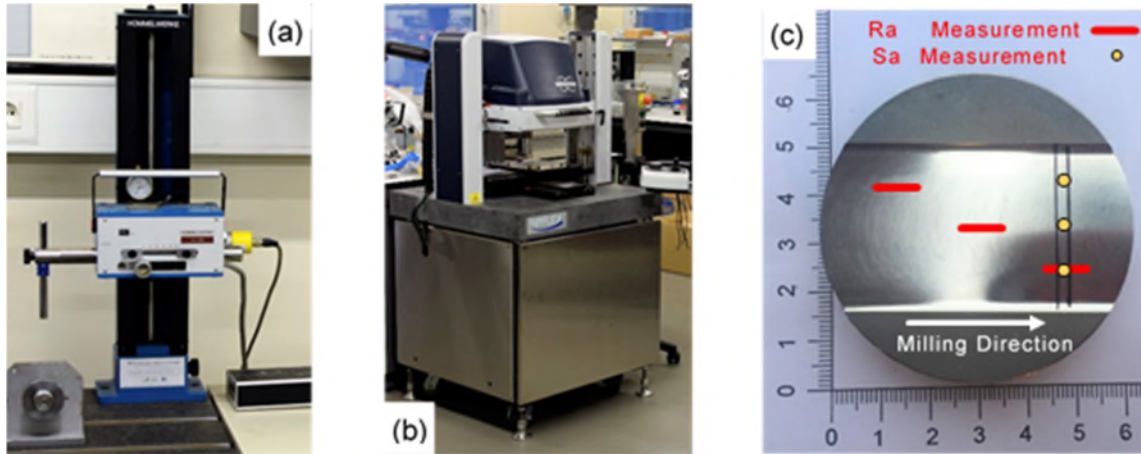


Figure 75. (a) HOMMELWERKE LV-50 surface measurer system, (b) BRUKER NPLEX 3D digital microscope, and (c) Layout of the workpiece surface sections where roughness was determined.

The qualitative evaluation consisted of the analysis of the surface topography; this assessment allowed detecting and classifying the defects and faults caused in the machined surfaces. This study was conducted using an OLYMPUS PMG 3 optical microscope with a magnification of up to 500 X.

3.5.2.2. Surface Properties Analysis

The evaluation of the surface mechanical properties was carried out through the measurement of the surface hardness (Figure 76), the definition of the micro-hardening profile, the depth of lamellar deformation and the residual stresses of the machined surface.

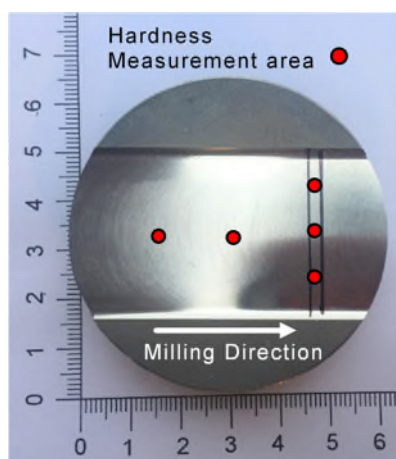


Figure 76. The layout of the workpiece surface sections where hardness was determined.

To perform the analysis, a sample of each machining test was randomly selected from all the trials carried out, that is, a total of 4 samples per insert for phase 1 (DOE L4 orthogonal array) and 16 samples for the phase 2 (DOE L16 orthogonal array).

All samples were cut by EDWM (using the same equipment and parameters for the metallographic samples) in two sections of 18 x 15 x 4 mm (Figure 77). The cut sections were hot mounted with epoxy resin (EpoVit Buehler), to be mechanically polished and chemically etched following the same procedure for material characterization.

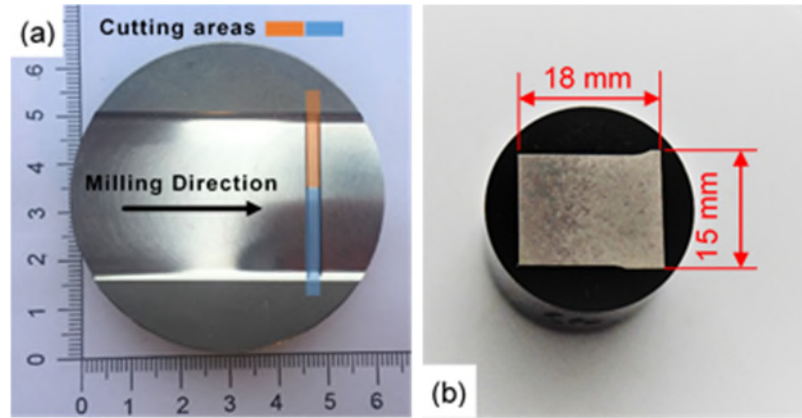


Figure 77. (a) Layout of the workpiece sections used for the surface metallurgy analysis, and (b) dimensions of cutted sample mounted on epoxy hot resin.

The micro hardening profile was measured with a MATSUZAWA MXT70 (Figure 74.c), microdurometer, using a Vickers scale (HV) with a 25 g load and an indentation time of 20 seconds. The indentation was made in three different regions of each sample following the pattern presented in Figure 78.

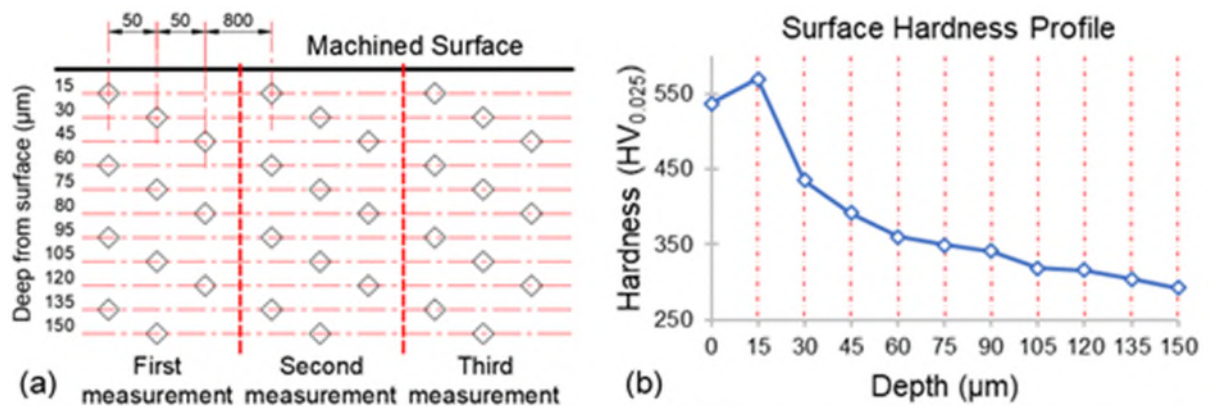


Figure 78. Microhardness measuring template and example of surface roughness depth profile.

In the case of lamellar deformation, the measurement was performed on images captured by an OLYMPUS PMG 3 optical microscope with a magnification of 500 X and using a LEICA MC170 HD camera equipped with the LEICA APPLICATION SUITE measurement software. The deflection was measured from the cutting surface to the deflection point (Figure 79) in three different regions.

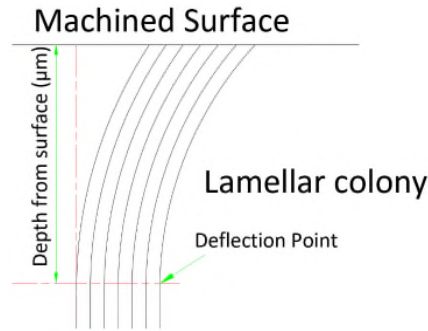


Figure 79. Lamellar deformation measuring template

3.5.3. Cutting Forces

Cutting forces were measured using a KISTLER 9272 4-component electric dynamometer connected to a KISTLER 5070A 8-channel amplifier (Swiss). The signals of the cutting forces generated during the milling were transmitted to an Advantech USB 4750A data acquisition card (Taiwan) in which they were processed and digitized at a sampling frequency of 800 Hz.

The signals were acquired and observed using a personal computer with DAQNavi Data logger software. Subsequently, the conversion and analysis of the acquired data were made in Microsoft Excel version 365 ProPlus. Figure 80 shows the equipment to measure the cutting forces.

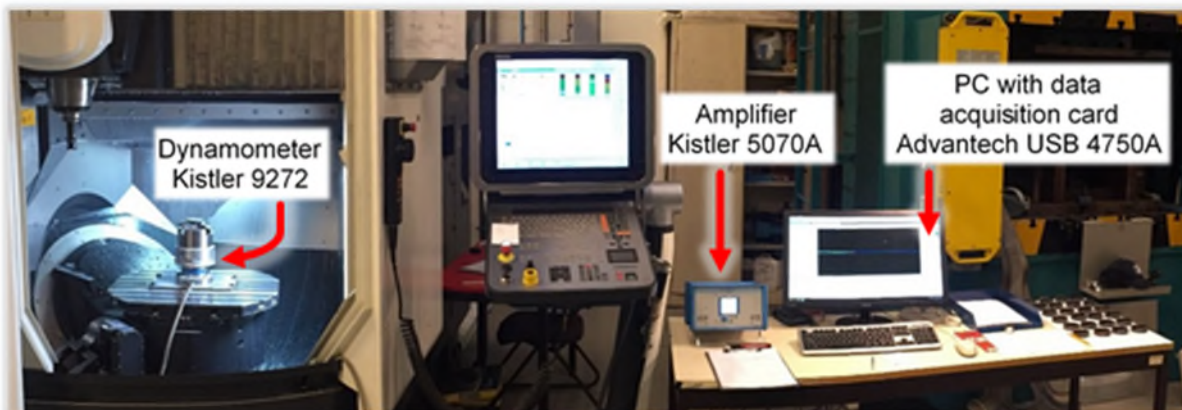


Figure 80. Experimental set-up for cutting force measurement in milling operations.

The workpiece was fixed by a 4-jaws self-centering chuck, which was coupled to the dynamometer by means of assembly system designed for this work. The dynamometer was mounted on a concentrically fixed metal plate, which in turn was centered on the machine table. This system allowed the secure clamping and interchangeability of the

workpieces, guaranteeing the repeatability of the tests and the symmetry between the sample surface and the machining plane.

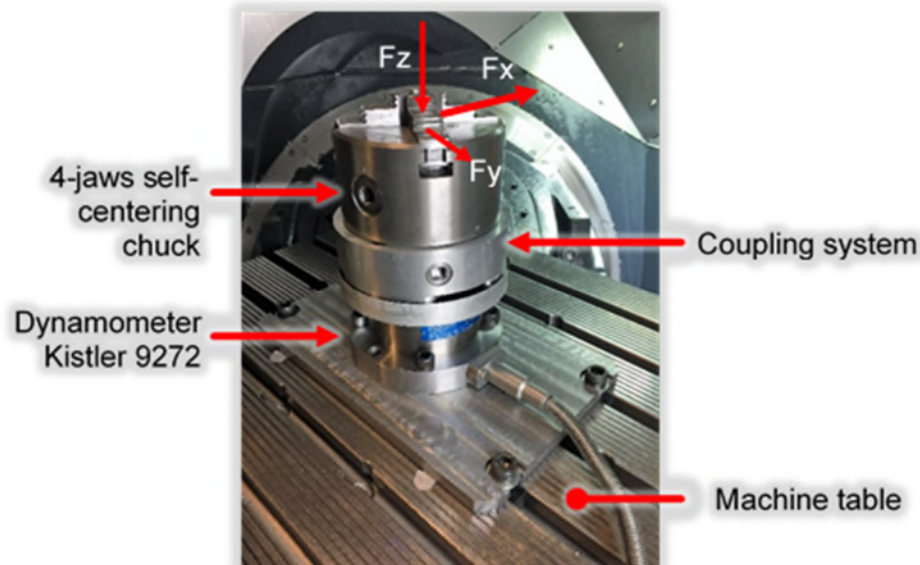


Figure 81. Dynamometer set-up for cutting force measurement in milling operations.

3.5.4. Chip Formation

The study of the chip formation was carried out with bulk γ -TiAl alloy through the image analysis of the cutting process acquired with a high-speed camera and the measurement of cutting forces in a conventional turning process.

The cut parameters were varied considering the analysis of the results presented in phase 1, and with the inserts that demonstrated the best performance. The experimental DOE is represented in Table 15.

Table 15. Experimental array for the chip formation.

Experimental Array				
TEST	Cutting Speed (m/min)	Rotation Frequency (rpm)	Depth of cut (mm)	Feed (mm/rev)
Trial 1	38	224	0.3	0.14
Trial 2	53	315	0.3	0.14
Trial 3	38	224	0.5	0.14
Trial 4	53	315	0.5	0.14

The equipment selected was a conventional mechanical lathe FFI (Figure 82.a) of 10 kW of power, with a maximum spindle speed of 2500 rpm and a minimum automatic feed of

0.14 mm/rev, due to the greater accessibility and space available for the installation of the recording equipment. The cutting inserts were mounted on a specific commercial support for this type of insert, which is used in the turning of cylindrical surfaces (Figure 82.b). All the turning experiments were conducted with new pads for each test and were performed in dry conditions.

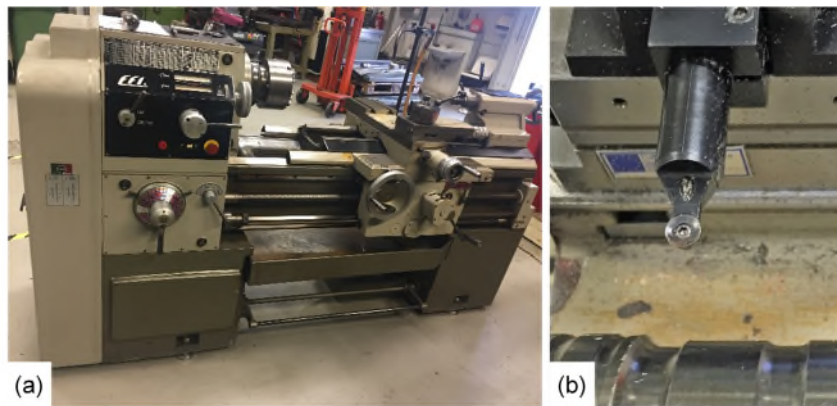


Figure 82. (a) Conventional lathe machine FFI, and (b) experimental setup for analyses of the chip formation.

The process was registered with a high-speed camera FASTCAM SA3 model 120K (Figure 83.a), with an acquisition speed of 5000 frames per second (fps) and 720 x 480 pixels resolution. The cutting forces were measured using a 3-component piezoelectric dynamometer KISTLER 9257B (Swiss) connected to an 8-channel KISTLER 5070A amplifier (Swiss). The signals of the cutting forces generated during turning were processed using the same procedure adopted for milling. The data conversion and analysis were made in Microsoft Excel version 365 ProPlus. Figure 83.b shows the experimental configuration for measuring the cutting forces.

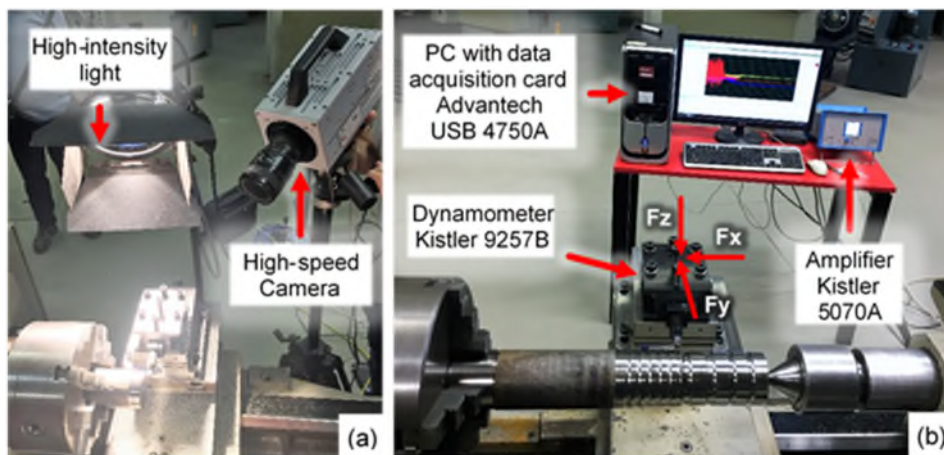


Figure 83. Experimental set-up for; (a) high-speed recording of chip formation, and (b) cutting force measurement.

3.6. Discussion

The description and analysis of the experimental design process presented in this section aim to provide the necessary information to understand the approach from which the study of the machinability of this γ -TiAl alloy was addressed.

Through the proposed experimental design, the main aspects involved in the machinability of this material were analyzed. The most relevant criteria were the study of the superficial integrity and the cutting forces, which were complemented with the analysis of the chip formation and the material characterization. This set of criteria was selected considering the existing information about the machinability of these alloys, in addition to the need to present new knowledge that contributes to the study of the machining of these materials.

For the study of surface integrity and cutting forces the use of the L4 configuration allows preliminary experimental testing with other materials and edge geometries facilitating initial performance conclusions prior to more advanced analysis. Therefore, this examination would help as a point of reference for future studies that are carried out using the same experimental plan.

Chapter 4 : Results and Discussions

This chapter presents the information obtained in the experimental program proposed in chapter 3 for the study of the machinability of this TiAl alloy. It also discusses the results obtained for each evaluation criterion and presents an analysis of the cutting-insert characteristics and cutting parameters effect on cutting forces, surface integrity and chip formation.

4.1. Material Characterization

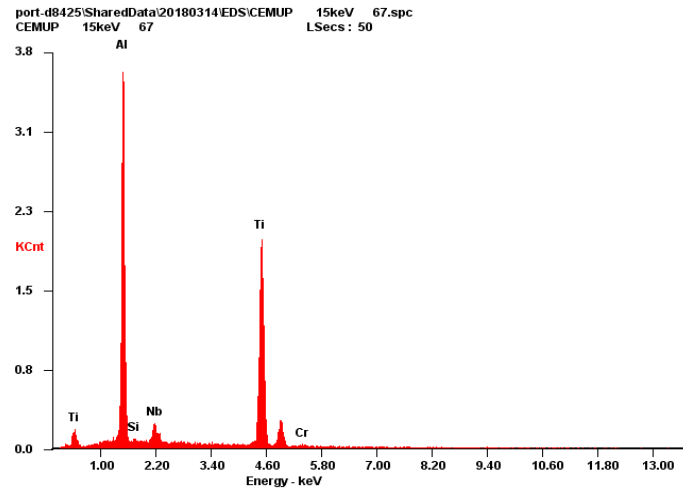
In general, the mechanical properties of a material are the main factor that directly or indirectly defines its machinability. Due to this reason, the first evaluation criteria performed in this study was the type of TiAl to be used. The main objective of this criterion was to observe the morphological characteristics and some of the main mechanical properties that are used as a reference for the study of the TiAl machinability. These results, together with the studies of cutting forces and surface integrity, will define the range of cutting parameters most suitable for machining this specific alloy with round WC inserts.

The alloy studied in this work was invented by Daido Steel Corporation (Japan) for the casting of turbine wheels for turbochargers in commercial vehicles such as the Mitsubishi Lancer since 1998.

The ingots used in this work were bought by the Institute for Science and Innovation in Mechanical and Industrial Engineering (INEGI-Portugal) from the Gfe Metalle y Materialien GmbH (Germany) for the development of investment casting of turbocharger turbine wheels for automotive applications (2012-2014) and later for this work. At the time of the acquisition of this alloy (2012) this material was the only one commercially available for complex foundry applications at reasonable prices, and in minimum quantities (100 kg).

Considering that the material was obtained through a casting process, the first step was the confirmation of its chemical composition, the inspection of the quality of the ingots and the identification of surface defects that could negatively influence the cutting process.

The chemical composition was determined in three different samples of the base material, by quantitative microanalysis using a Scanning Electron Microscopy with Energy Dispersive Spectroscopy (SEM/EDS). The results obtained are observed and detailed in Figure 84.



Element in wt%	Ti	Al	Nb	Cr	Si	Fe	N	O
Gfe specification	Balance	32.90 to 34.10	4.50 to 5.10	0.80 to 1.20	0.10 to 0.30	0.08 max.	0.015 max	0.10 max
Gfe analysis	60.20	33.55	4.89	1.07	0.19	0.027	0.001	0.045
SEM/EDS analysis	60.63	32.70	5.37	1.03	0.21	-----	-----	-----

Figure 84. Chemical composition of raw material (wt%).

All the ingots (310 mm length) were inspected and the surface defects identified. The primary surface defects found were flow marks and scars, which were observed on the base and cylindrical surfaces (Figure 85.a and b respectively). The major fault identified was the shrinkage cavity on the feeding face (Figure 85.c), with 70 to 90 mm depth. To avoid this defect and ensure the homogeneity of the samples, the machining tests were only performed on samples obtained from a central region (110 mm to 290 mm).

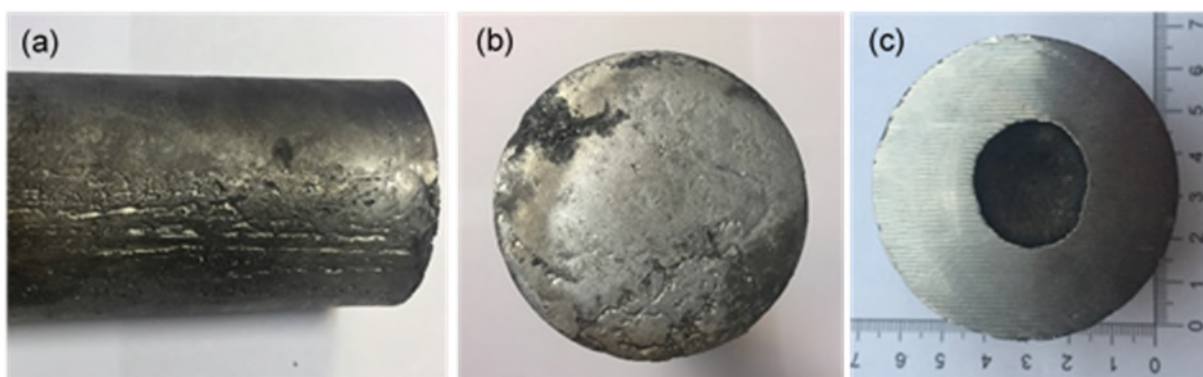


Figure 85. Casting defects in ingots of Ti-48Al-2Nb-0.7Cr-0.3Si; a) scar, b) flow marks, and c) shrinkage cavity.

The internal inspection revealed homogeneous surfaces with density values between 3.92 and 3.97 g/cm³ (Archimedes technique). However, in several of the transverse and longitudinal samples, pores of up to 20 μm (Figure 86.a) were detected, and an average

porosity of ~ 50 pores/mm² was determined. These porosities were detected mainly in the center of the ingots (Figure 86.b).

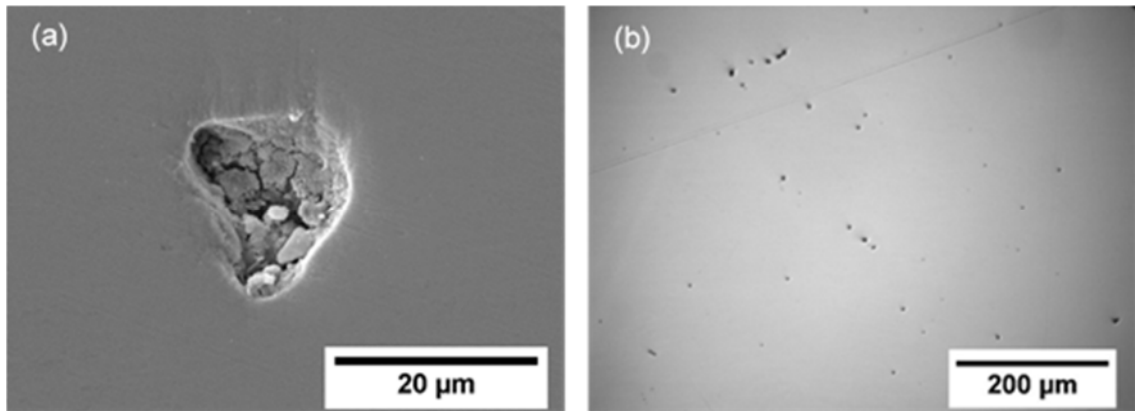


Figure 86. (a) SEM image of a pore, and (b) optical microscope image of the cross-section in the central region of the Ti-48Al-2Nb-0.7Cr-0.3Si ingot.

4.1.1. Metallographic analysis

The microstructure of the material presented variations in the orientation of the lamellar colonies in both the longitudinal and radial directions. In the cross-section, it was observed that the columnar growth is oriented in the radial direction to the center of the bar (Figure 87.a), with colonies size variation in the center of the ingot. The longitudinal section shows a radial columnar growth identified in the outer part that is changing until it is almost axial near the center (Figure 87.b). This phenomenon has been identified by other researchers as an effect of the temperature gradient during solidification [2, 193, 194].

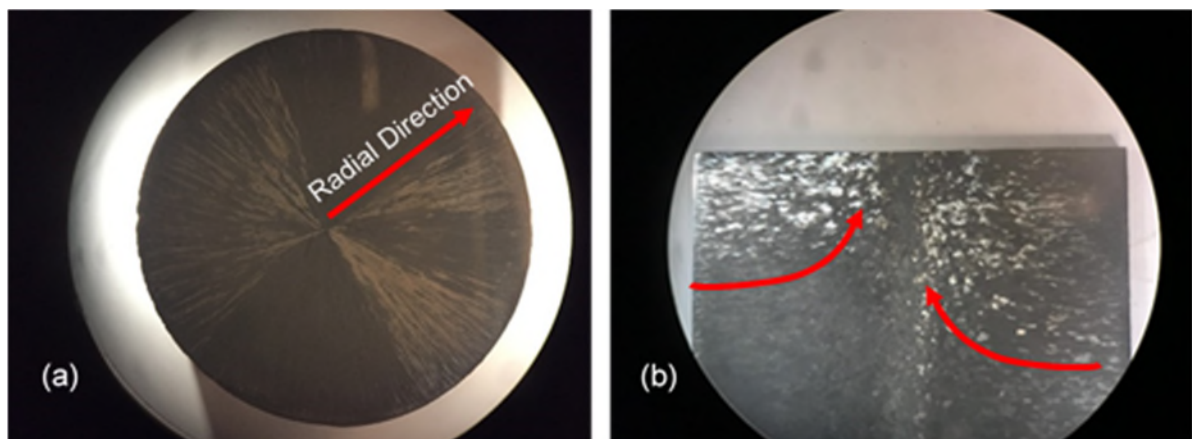


Figure 87. (a) Transversal, and (b) longitudinal samples of the Ti-48Al-2Nb-0.7Cr-0.3Si ingot. The microstructure observed in Figure 88 reveals the presence of γ (TiAl) grains the darkest phase, α_2 (Ti₃Al) the lighter phase, and α_2/γ colonies.

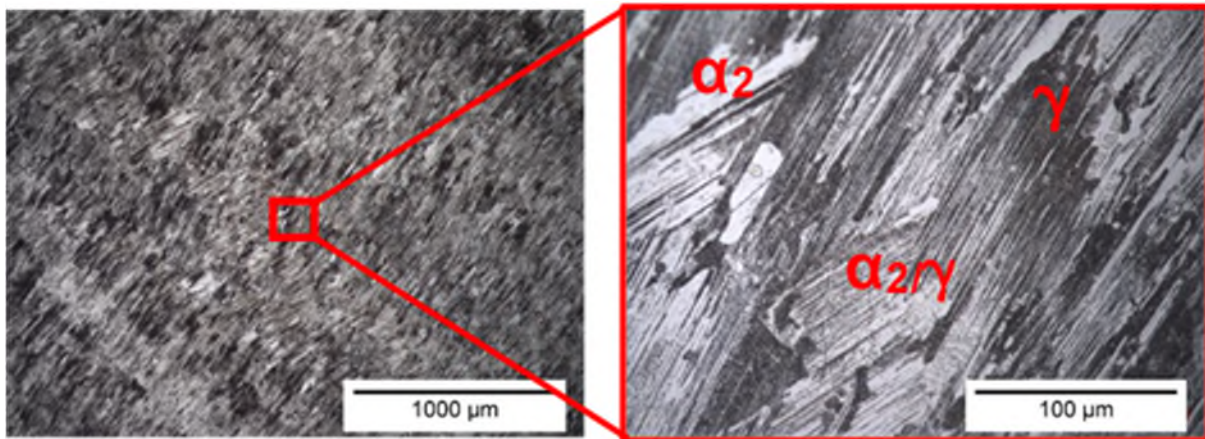


Figure 88. Microstructure of the Ti-48Al-2Nb-0.7Cr-0.3Si.

The material has a duplex microstructure, composed of large lamellar colonies with sizes between 300 and 400 μm , and small globular grains (between 5-30 μm) of γ and α_2 embedded within the eutectoid lamellar structure (Figure 88), which is in agreement with the one found by other authors [22, 52, 63, 195]. The different regions were measured through the method of segments intersection.

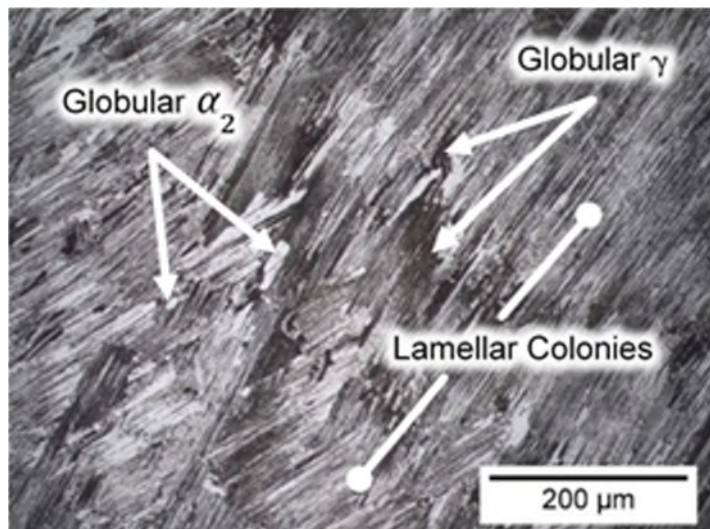


Figure 89. Micrograph of Ti-48Al-2Nb-0.7Cr-0.3Si showing γ -TiAl and α_2 -Ti₃Al phases segregated at lamellar colonies.

From the images obtained by optical microscopy of three different ingot samples and by a morphological contrast processing, it was defined that the volume percentage of the α_2 and γ phases within lamellar colonies are approximately 55% and 45% respectively (Figure 90).

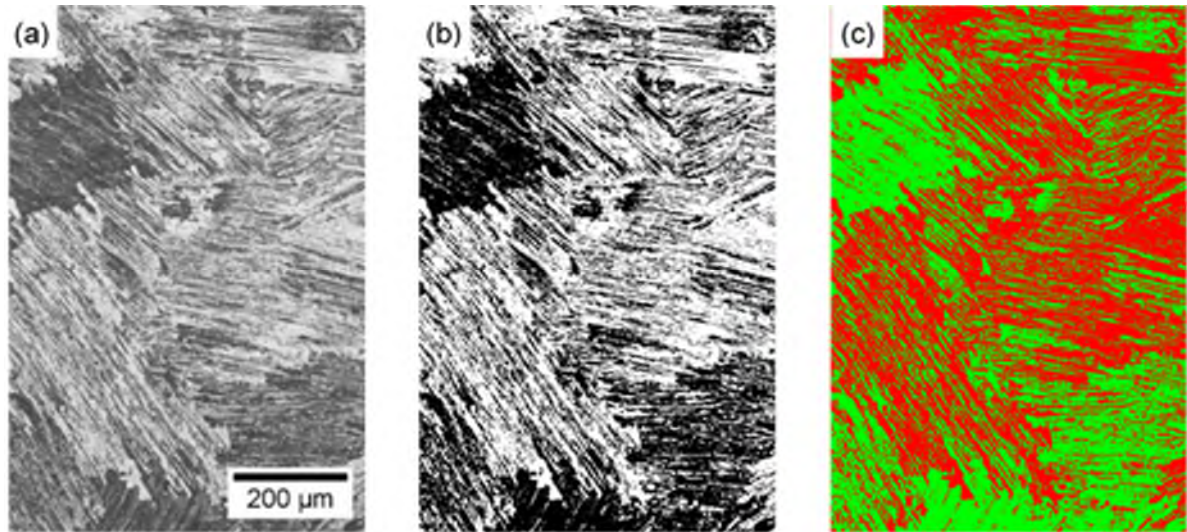


Figure 90. Morphological contrast of Ti-48Al-2Nb-0.7Cr-0.3Si microstructure; (a) optical microscope image, (b) segmented regions image of α_2 (white) and γ (black) phases, and (c) phase map distribution of α_2 (red) and γ (green) phases in eutectoid lamellar colonies.

4.1.2. Mechanical Tests

Regarding the tensile tests, the results revealed that the variation of the ultimate tensile strength and the yield strength among samples is less than 5% (Figure 91), which shows the raw material homogeneity. Moreover, it was observed that the ductility of this material varied between 1.3 and 2.3 % (Figure 92), observing that the highest deformation capacity was presented in the section between the center of the ingot and the outer area (samples 3 and 4), this variation would be given by the variation of the size of the laminar colonies, nevertheless the values observed are within the range stipulated for this type of alloys. Table 16 summarizes the values obtained.

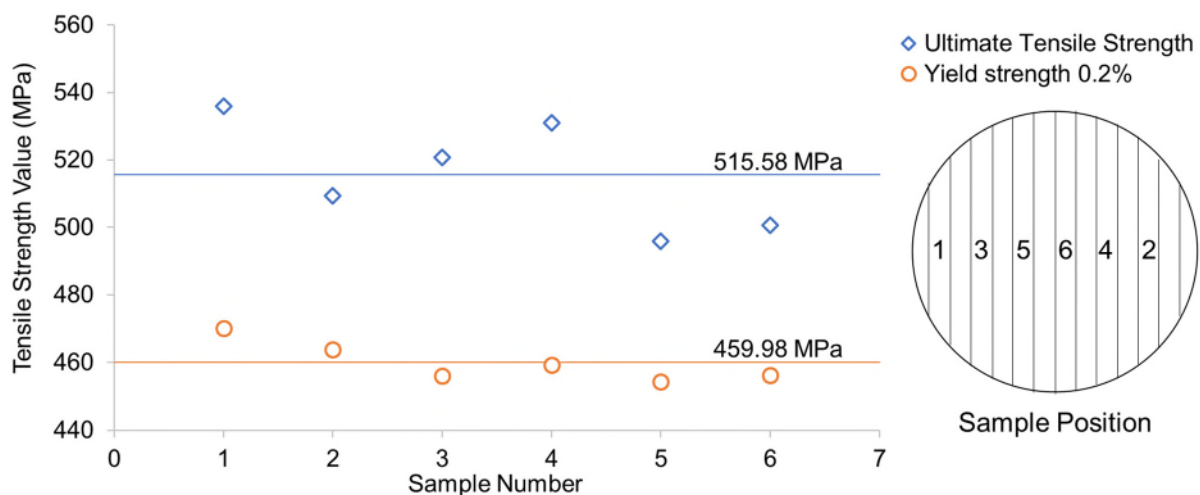


Figure 91. Tensile strength of Ti-48Al-2Nb-0.7Cr-0.3Si.

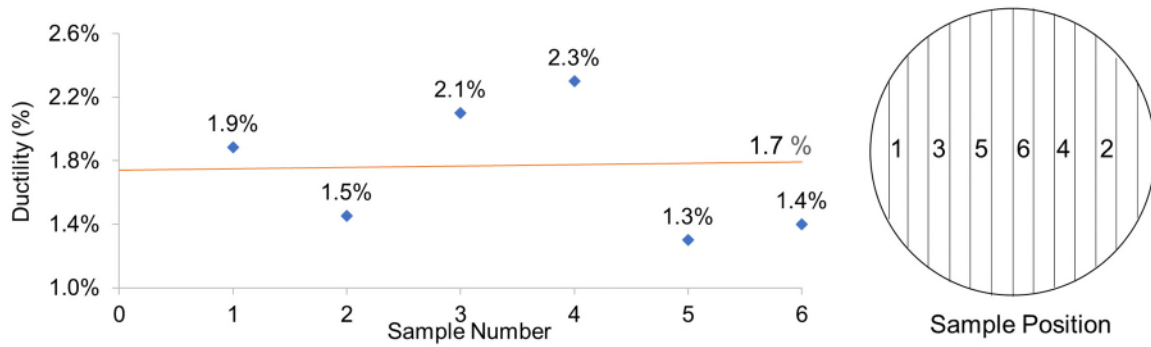


Figure 92. Ductility of Ti-48Al-2Nb-0.7Cr-0.3Si.

Five measurements were made along the cross-section of the samples to determine its hardness. The results obtained showed variations from the periphery to the nucleus, along the columnar orientation of the lamellar colonies to a depth of ~7.5mm. From this depth, the material did not show considerable variations, as observed in Figure 93. The average internal hardness of the material is 286 HV_{0.025}.

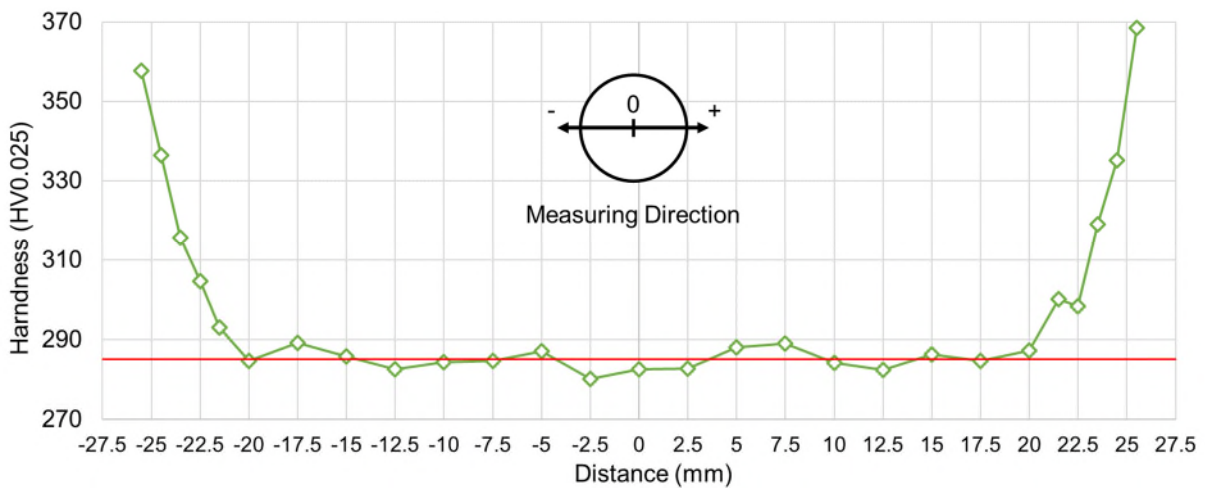


Figure 93. Radial hardness profile distribution across ingot.

4.1.3. Summary

The alloy has a duplex/near-lamellar microstructure, with large lamellar structure colonies randomly oriented and small α_2 and γ globular grains heterogeneously distributed. This type of structure is characterized by having greater resistance to traction and longer life to fatigue [32, 61–63].

The lamellar colonies have sizes of ~400 μm and a higher amount of the α_2 phase. According to Appel et al. [2], this higher content of the α_2 phase mainly affects the ductility of the material. However, the ductility is ~1.7%, which is similar to that of alloys such as Ti-48Al-2Cr-2Nb or Ti-47.4Al-2.6Cr [22, 196]. The material presented an average

value of 286 HV_{0.025} in almost all its diameter, exhibiting only an increase of up to 50 HV in the surface layer. The tensile and hardness tests showed homogeneity in the mechanical properties of the material. The summary of the main properties is presented in table 16.

Table 16. Mechanical properties of Ti-48Al-2Nb-0.7Cr-0.3Si.

Mechanical Properties	Values
Density (g/cm³)	3.95
Hardness (HV0.025)	286
Young Modulus at RT (GPa)	166
Ultimate tensile strength (MPa)	516
Yield strength (0.2 % offset) (MPa)	460
Ductility (%)	1.7

4.2. Cutting Forces

The study of cutting forces is one of the main criteria used to evaluate the machinability of a material. This procedure allows to monitor and record the effect that the different parameters cause during the machining process. In the case of the present research, this methodology was selected for the evaluation of the cutting inserts performance to the variation of the cutting parameters. To perform this analysis a DOE L4 configuration was used, while for the ANOVA study of the impact level of the cutting parameters, a Taguchi L16 DOE with an S10-XL insert was applied (see section 3.2).

The acquisition of the cutting forces was carried out in all the milling samples. The obtained graphs (Figure 94.a) contemplate the three forces measured; F_x , F_y and, F_z . In general terms, all the results indicate that the component (F_z) can be up to $\sim 1.7x$ greater than the F_x and F_y forces, due to . Considering this factor and in order to facilitate the Taguchi analysis, the resulting cutting force (F_R) was calculated by combining the three forces, measured using equation 1:

$$F_R = \sqrt{F_x^2 + F_y^2 + F_z^2} \quad (1)$$

Each of the values F_R is based on the average of three measurements of forces taken from the area where the measurements of surface integrity characteristics were carried out (Figure 94). In addition, it is important to note that, to avoid the effect of cutting-edge wear on the data collection, new inserts were used in all trials.

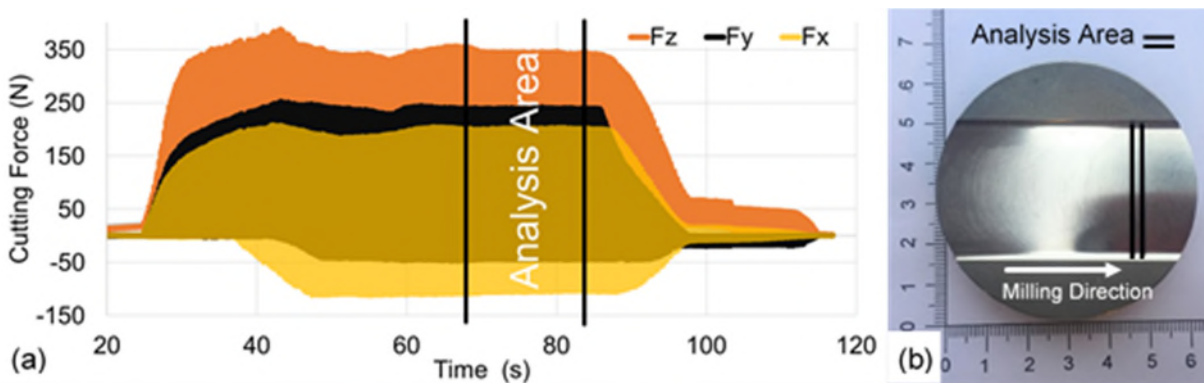


Figure 94. (a) Cutting forces profile when machining with a S10-XL insert at $V_c=70$ m/min, $a_p=0.5$ mm and $hex=0.04$ mm, and (b) Layout of the workpiece sections where surface integrity was determined.

In general, F_R is ~ 390 N, while the highest recorded force was 1523 N (S30-XM) and the lowest was 257 N (S10-XL). Considering that the inserts analyzed have the same geometry and the machining parameters were kept constant, this wide variation of F_R suggests that the effect caused by the variation of the characteristics of the inserts and cutting parameters is significant. For a better understanding of these effects, the following sections present the results observed for each of these factors

4.2.1. Effect of tool characteristics on cutting forces

In general, the results indicate that inserts with a high content of cobalt and small WC grains reduce the cutting forces. However, this analysis also showed that the cutting tools effect on the machinability of these alloys varies according to the range of cutting parameters.

Figure 95 presents the results of the F_R force variation according to the characteristics of the inserts. As expected, the highest value F_R corresponds to the material with lower hardness, which indicates that these inserts have a greater wear for the range of the cut parameters experienced.

This behavior was demonstrated by the S30-XM and S30-XL inserts (Figure 96) when tested at $V_c=70$ m/min, $a_p=0.5$ mm and $h_{ex}=0.04$ mm. However, the S25 inserts that have only a hardness 100 HV greater than the S30 exhibit, in the case of the XM geometry, F_R values similar to S10-XL inserts which are 350HV harder than the S30.

This disparity in the behavior of the materials could be related mainly to the difference in the grain size of the inserts. Similar results have been reported by other authors [24, 44] in the milling of TiAl.

For the cutting-edge geometry, Figure 95.b shows that the T-land (XL) geometry present a cutting force of $\sim 24\%$ less than the Sharp edge (XM). This behavior is related to the reinforced cutting edge that characterizes the inserts with a negative face rake angle [66].

The XL edge is revealed as an advantage due to the low ductility of the material. However, as seen in Figure 95.c, this geometry does not always exhibit the same behavior in all the inserts, which allows to understand that the effect caused by the geometry of the edge would vary depending on the range of parameters.

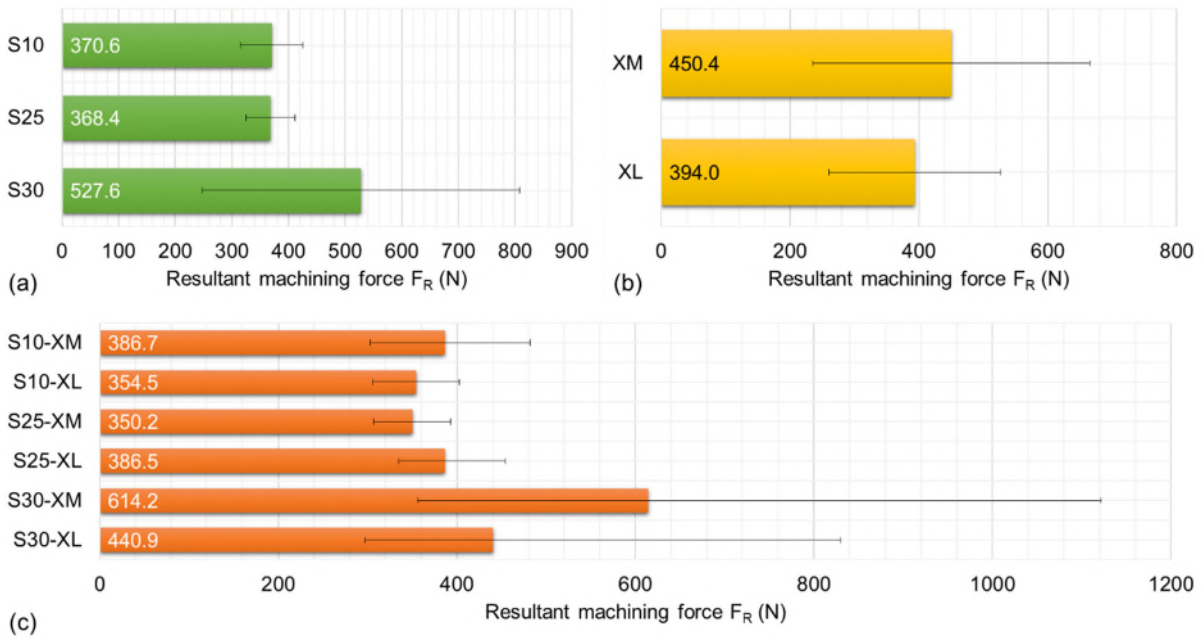


Figure 95. Resultant machining force F_R by; a) material, b) edge insert geometry, and c) cutting insert.

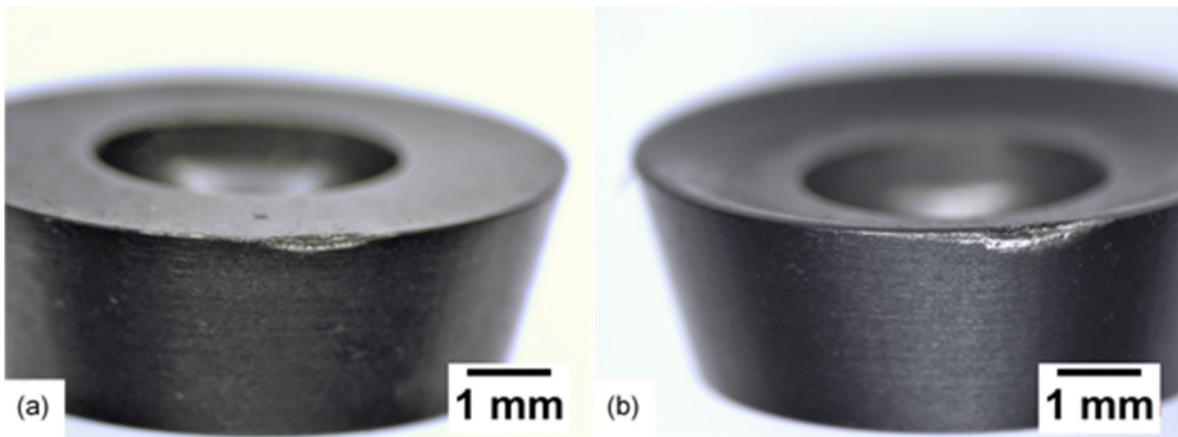


Figure 96. Tool wear of; (a) S30-XM, and (b) S30-XL inserts after milling Ti-48Al-2Nb-0.7Cr-0.3Si at $V_c=70$ m/min, $a_p=0.5$ mm and $h_{ex}=0.04$ mm (Trial 4).

4.2.2. Effect of cutting parameters on cutting forces

Figure 97 shows the impact of V_c in F_R for all inserts. The results indicate that the change of the cutting speed in a range between 45 and 70 m/min causes a slight increase in the resultant force for the inserts S10 and S25, while in the case of the S30 is between 77 and 122%, according to the geometry type of the edge.

These effects indicate that the inserts with materials of greater toughness and lower hardness are more sensitive to the variation of the V_c , and that for the case of the S30 inserts, their optimum working speed would be below 70 m/min.

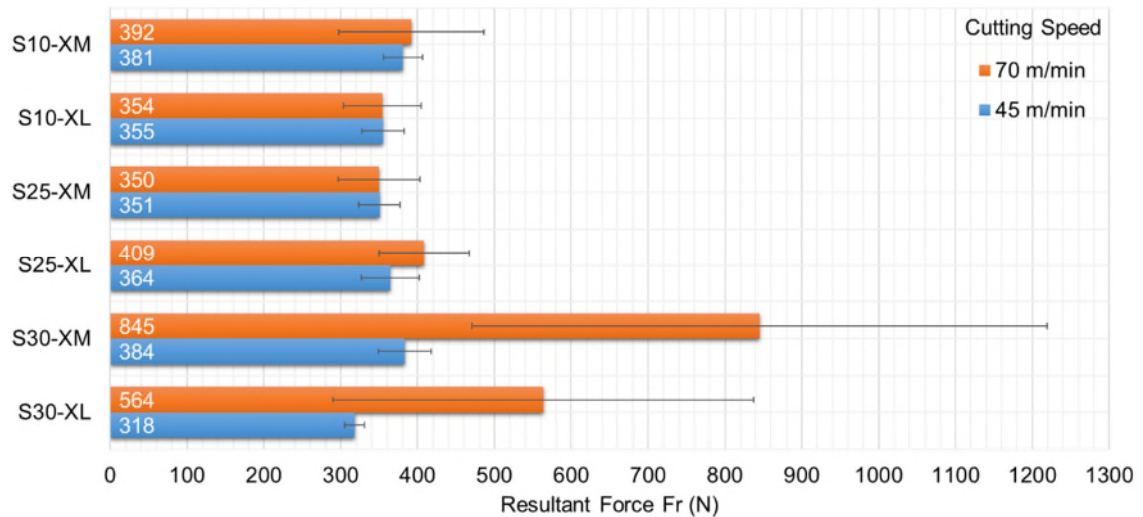


Figure 97. Effect of cutting speed (V_c) on resultant machining force (F_R).

The F_R variation for a_p (depth of cut) and h_{ex} (chip thickness) is presented in Figure 98. As it was expected, an increase of a_p and h_{ex} raises F_R . This trend proved to be more evident for the case of a_p (Figure 98.a), mainly because of the effect it has on the amount of material removed. As in the V_c , the inserts with S30 material showed greater sensitivity to the changes on the cutting parameters.

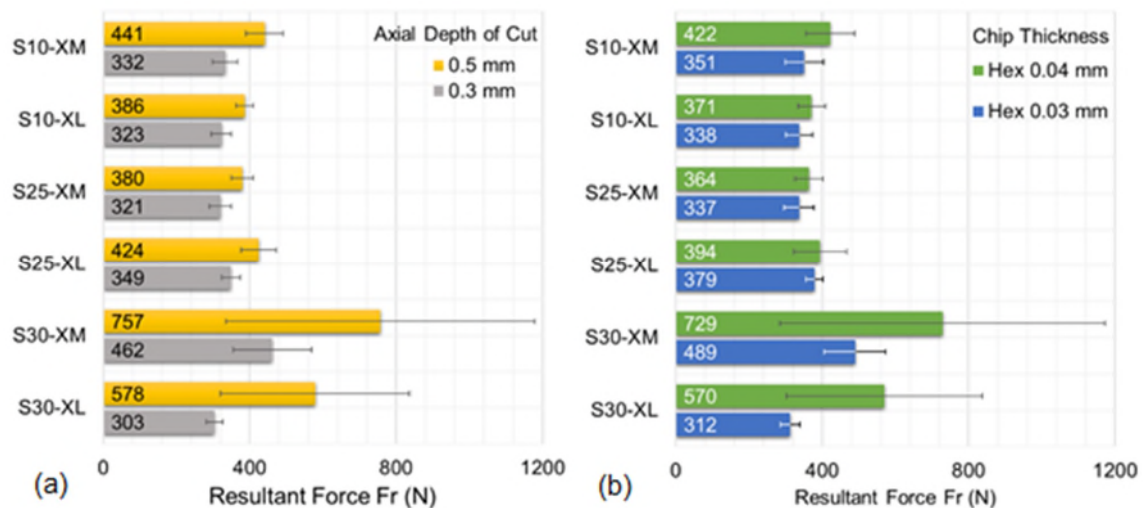


Figure 98. Effect of; (a) depth of cut (a_p), and (b) chip thickness (h_{ex}) in resultant machining force (F_R).

In general, the results show that in all the inserts, the variation of the cutting parameters caused the same response in F_R , although with different intensity. This variation clearly indicates the influence of the cutting tool material's properties and the edge geometry.

The main effect plots-means for force F_R , showed in Figure 99, presents the values obtained in the second phase of experimentation with insert S10-XL. This graph shows

that the average value of the F_R is 400N and that the range of measured forces is between ~300 to 550 N. The results obtained with this insert are lower than those reported by Vargas Pérez et al. [24] in the milling of γ -TiAl with round inserts using a similar range of cutting parameters.

The graph shows that V_c is the most influential factor on the cutting forces, and that the highest growth peak occurs in the range of 70 to 110 m/min. Therefore, in a smaller range, the effect of the V_c could be less significant, as was registered in phase 1 (Figure 97).

On the other hand, from the perspective of the h_{ex} and the a_p , it is evident that these factors modify the results of the F_R forces. However, their level of contribution is possibly higher in a V_c range between 20 and 70 m/min, as also shown by other researchers [44, 67, 127].

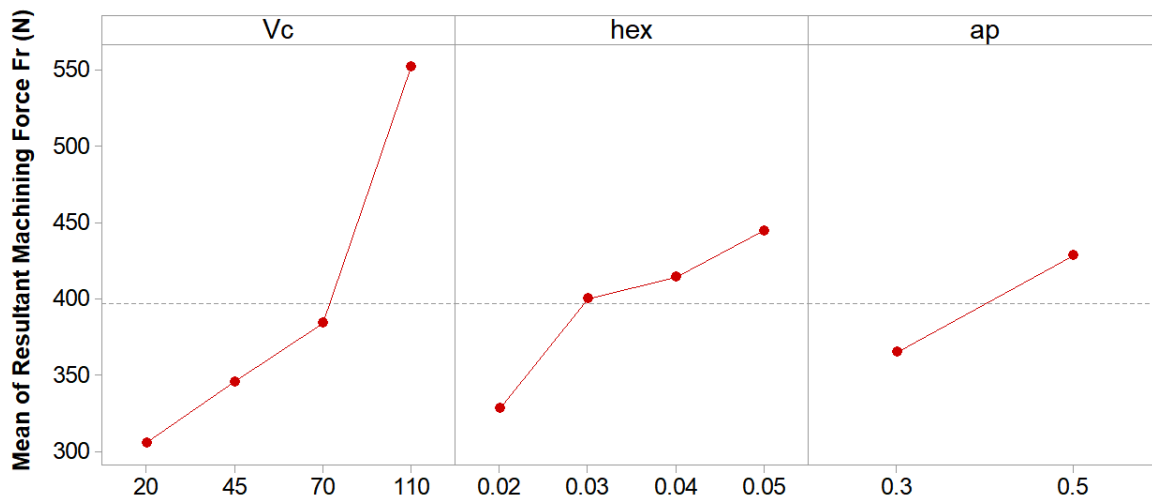


Figure 99. Main effect plot – means for resultant machining force F_R (N).

ANOVA analysis for the F_R force is presented in Table 17. This statistical analysis identified that all the factors have a significant effect on the average value of the F_R . It is not a surprise to observe that the V_c presents a PCR (Percentage Contribution Ratio) more significant than that of h_{ex} and a_p . This effect was mainly due to the variation that the F_R force presented when V_c increases from 70 to 110 m/min (see Figure 99). This information contributes to the definition of the upper limit of the cutting speed for this insert.

The PCR of the residual error of 13% is mainly influenced by the interactions between factors, pressure variations in the cooling system and difficulty to control the cutting conditions.

Table 17. ANOVA table for resultant force F_R .

Source	DF	Adj SS	Adj MS	F-Value	PCR (%)
Vc	3	421753.16	140584.39	80.51	66.43%
h_{ex}	3	87422.71	29140.90	16.69	13.11%
a_p	1	47991.68	47991.68	27.48	7.38%
Error	40	69845.13	1746.13		13.09%
Total	47	627012.68			

4.3. Assessment of surface integrity

The evaluation of the surface integrity is the main criterion used in this work to determine the effects of the cutting tool characteristics and machining parameters have on the machined surfaces.

The evaluated surface parameters were the surface roughness, the hardened layer, the lamellar deformation, and the residual stresses. Each of these features were analyzed in two phases. The first phase was oriented towards the study of the geometry effect and the composition of the cutting inserts material, for which a DOE L4 was used for each of the inserts (section 3.2) and the second one observed the influence of V_c , h_{ex} and a_p , in each insert. In addition, an ANOVA analysis was performed, using the Taguchi DOE L16 methodology, for the insert that presented the best performance in the first stage. The results obtained are presented following the same sequence.

In general, the results of surface integrity were encouraging, with a significant proportion of tests that presented values of average roughness of around 0.240 μm , a maximum surface layer thickness of 150 μm , with a hardness increase below 125%.

However, the use of different cutting inserts and process parameters produced considerable variations in some cases. Consequently, without further statistical analysis, it is difficult to conclude the effect of round cutting inserts on the machinability of this alloy.

4.3.1. Surface Roughness and surface topography

The arithmetic mean roughness (Ra) in a machining component is the first index that indicates the quality and integrity of its surface. In general, a low Ra is synonymous of a

surface with few alterations and a good subsurface state. The Ra results obtained are in a range between 0.09 and 0.270 μm , which prove to be similar and in some cases even better than those reported by other authors [24, 59, 68, 81, 127, 157] in milling γ -TiAl (Table 18). It is essential to point out that due to the scarce information about milling these alloys with inserts of round geometry, the comparison was made with other tools geometry, machining times and cutting parameters.

Table 18. Surface Roughness in the machining of γ -TiAl.

Reference	Tool	Best result of Ra (μm)	Mean result of Ra (μm)
Kolahdouz et al. [68]	End-mill	0.13	0.31
Beranoagirre et al. [157]	End-mill	0.31	0.45
Priarone et al. [81]	End-mill	0.19	0.25
Settineri et al. [59]	Toroidal end-mill	0.42	0.50
Hood et al. [127]	Ball nose end-mill	0.10	0.60
Vargas Perez et al. [24]	Round insert mill cutter	0.18	0.50
Present research	Round insert mill cutter	0.10	0.17

4.3.1.1. Effect of tool characteristics on surface finish

Figure 100.a presents the average Ra of milled samples for each cutting insert. These results allow a global view of their behavior and compare them according to their composition. In this analysis, it is possible to identify that inserts with a cobalt content of 7% and fine WC grains (S10) produce surfaces with lower Ra than inserts with higher cobalt content (Figure 100.a). It is important to note that this phenomenon has also been reported by Vargas Pérez et al. [24] in the milling of γ -TiAl.

From the perspective of the cutting edge, the results exhibited in Figure 100.b show that the Sharp edge (XM) geometry can produce surfaces with lower roughness than the T-land edge (XL). The variation shown between the geometry of the edges (~14%) is smaller than that which occurs between the types of insert materials (~23%).

It can be concluded that the combination between the geometry of the cutting edge and the chemical composition of the insert material interferes in the performance of each insert. Figure 100.c presents the Ra for each insert. The ones with a XM geometry allow surfaces smoother than the XL geometry and behave similarly in materials S25 and S30.

However, this behavior is the opposite one, when considering S10 inserts, where the XL geometry achieved the best roughness results.

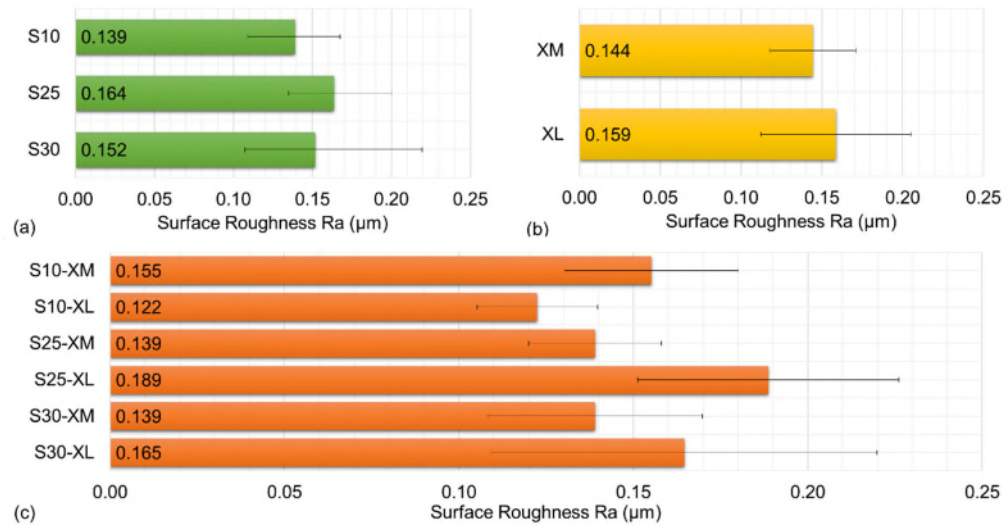


Figure 100. Arithmetical mean roughness Ra by; a) tool material, b) edge insert geometry, and c) cutting insert.

Additionally, it is essential to consider that the cutting parameters directly influence the roughness of the surfaces and that the results may vary according to the range of cutting parameters.

4.3.1.2. Effect of cutting parameters on surface finish

In general, the main cutting parameters that influences the roughness of the machined surfaces is the cutting speed. In this study, it was observed that in most cases higher V_c improves Ra, as seen in Figure 101. This behavior has already been reported by several authors [69, 97, 114] in other γ -TiAl. However, in this research, it is observed that in the case of the S10-XM inserts this behavior was not similar to what was expected, since higher V_c increased the Ra by 20%, while in the other cases Ra was reduced up to 70%, as is the case of insert S30-XL.

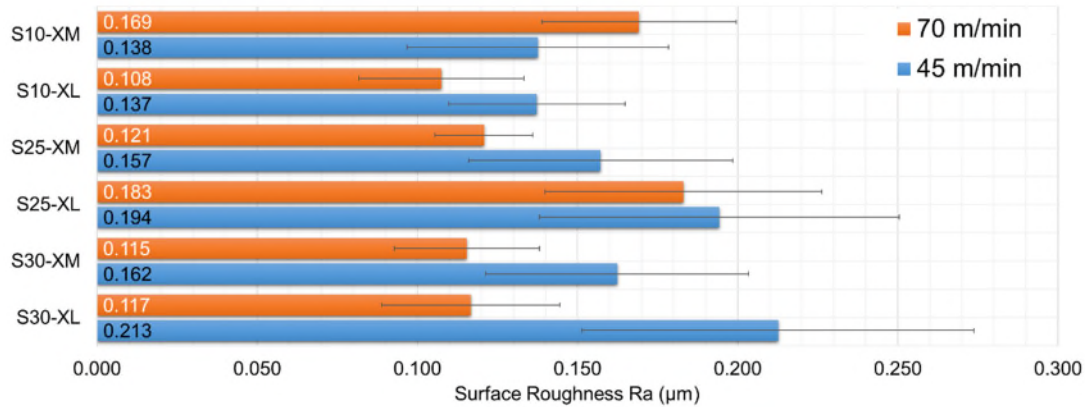


Figure 101. Effect of cutting speed (V_c) in arithmetical mean roughness Ra.

In the machining the usual tendency is that lower axial depth of cut (a_p) promotes better surface finishing [66, 140, 163]. However, the results obtained do not always show this behavior. As one can see in Figure 102, an a_p increase during milling with round inserts caused a reduction of the Ra for 5 of the 6 inserts. Nevertheless, the S30-XL insert shows an opposite behavior, which is attributed to the wear that this insert showed in the execution of the test with higher V_c and a_p (Trial 4).

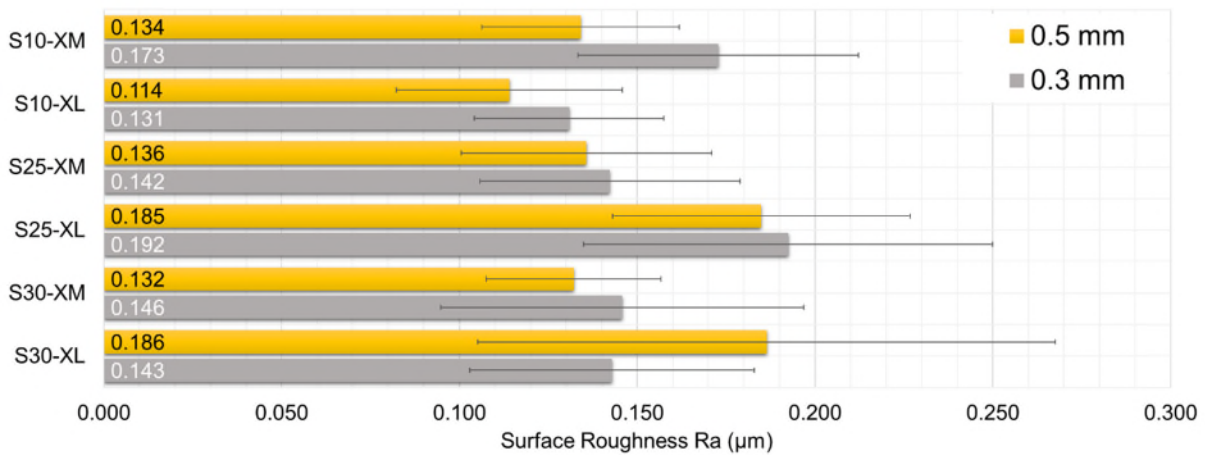


Figure 102. Effect of depth of cut (a_p) in arithmetical mean roughness Ra.

The next factor examined was the chip thickness (h_{ex}), which is related by the feed rate (f_z) of the cutting tool, and consequently to the value of Ra. In general, the results analyzed indicate that this alloy shows a high sensitivity of the Ra to the variation of the h_{ex} . As one can see in Figure 103, raising the h_{ex} 0.01 mm enhance Ra between 7 and 48%. The only exception was the insert S30-XL, which presented an opposite behavior. This tendency, as in the case of a_p , is attributed mainly to the tool cutting edge wear presented in trial 4.

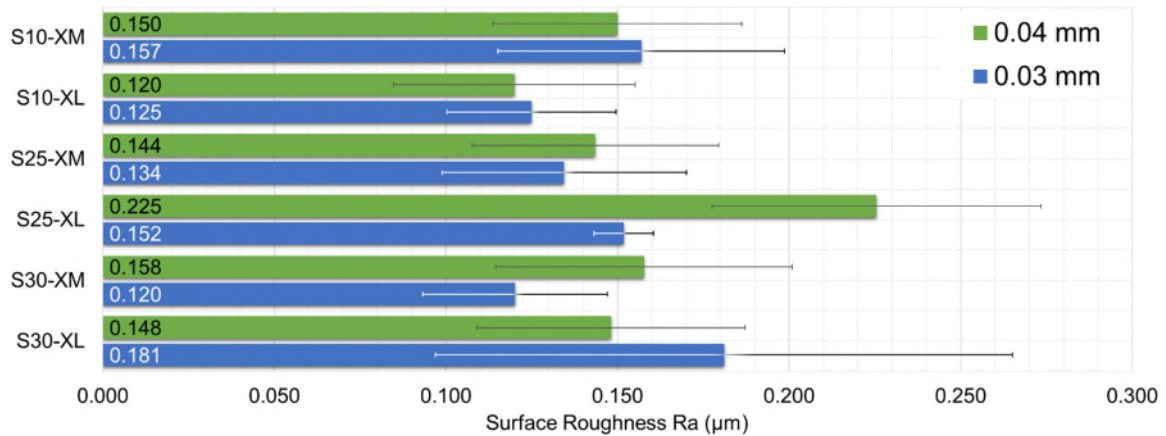


Figure 103. Effect of chip thickness (h_{ex}) in arithmetical mean roughness Ra.

The analysis of the effect of the cutting parameters on the Ra show that in general, the inserts have a similar response to the variation of the cutting parameters, although at different levels. However, the exceptions demonstrated by the S10-XM and S30XL inserts suggest the high sensitivity of this alloy to the variation of the cutting parameters.

The evaluation of the effect of each cut parameters on the surface integrity, was further studied by ANOVA analysis. The second phase of tests was executed with inserts S10-XL, because they presented the best results during the first phase of trials.

Figure 104 shows a graph composed by the effect of the cut parameters on the mean of the roughness Ra. As in the previous analysis, the increase of the h_{ex} is the most influential factor since it induces rapid Ra growth. However, it is important to note that in the interval between 0.02 and 0.04 mm the slope of growth is lower.

In the case of the V_c , it was perceived that for 45 to 70 m/min the behavior is similar to the first phase, which makes it constant. However, to reach a smoother surface, the reduction of the cutting speed to 20 m/min is presented as the best option. Contrary to the behavior reported by other authors [69, 97, 142], a higher speed (110 m/min) does not seem advisable. From the perspective of the a_p , as in the previous analysis, 0.5 mm generates the best roughness, confirming the trend of this insert.

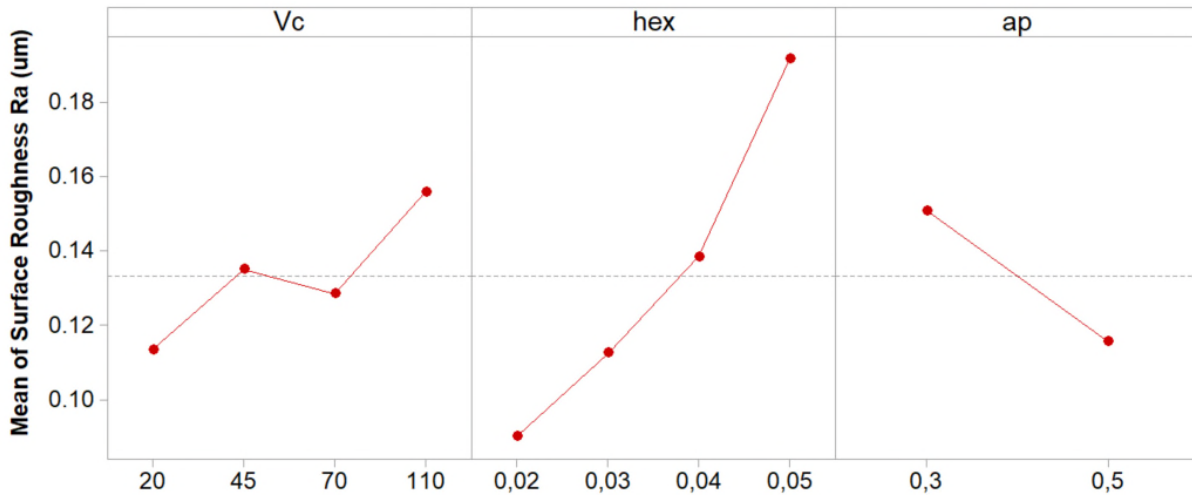


Figure 104. Main effect plot – means for arithmetical mean roughness Ra (μm) for S10-XL inserts.

The ANOVA analysis is presented in Table 19. All the cutting parameters have a certain level of influence. The h_{ex} is the most influential factor for Ra, followed by a_p and V_c . The level of error presented is 37.68%, which could be considered relatively high. However, this error degree is related to the manufacturing conditions of the inserts, the control of parameters in the work environment, the possible measurement errors and the fact that the interactions between the factors were omitted.

Table 19. ANOVA table for the arithmetic means roughness Ra.

Source	DF	Adj SS	Adj MS	F-Value	PCR (%)
Vc	3	0.0112	0.0037	3.33	5.60 %
hex	3	0.0688	0.0229	20.45	46.78 %
ap	1	0.0150	0.0150	13.41	9.95 %
Error	40	0.0449	0.0011		37.68 %
Total	47	0.1400			

4.3.1.3. Surface topography

The poor topographic quality of the surfaces in the TiAl is one of the biggest problems during machining, since the low ductility at RT commonly causes several defects that are extremely problematic and that modify the surface roughness. The evaluation of the quality of the surfaces was conducted in all the samples obtained (first and second phase). The observed damages consisted mainly of surface cracks, cavities, tearing and smearing material scattered in different surfaces areas.

Appendix A-3 presents an example of the surfaces obtained in each test. In general, the affected areas did not show any evident tendency between their location and the machining process, since in the same sample areas with a large number of defects and others with a limited level of damage were found. Figure 105 shows two zones of a machined sample obtained in the second phase of machining.

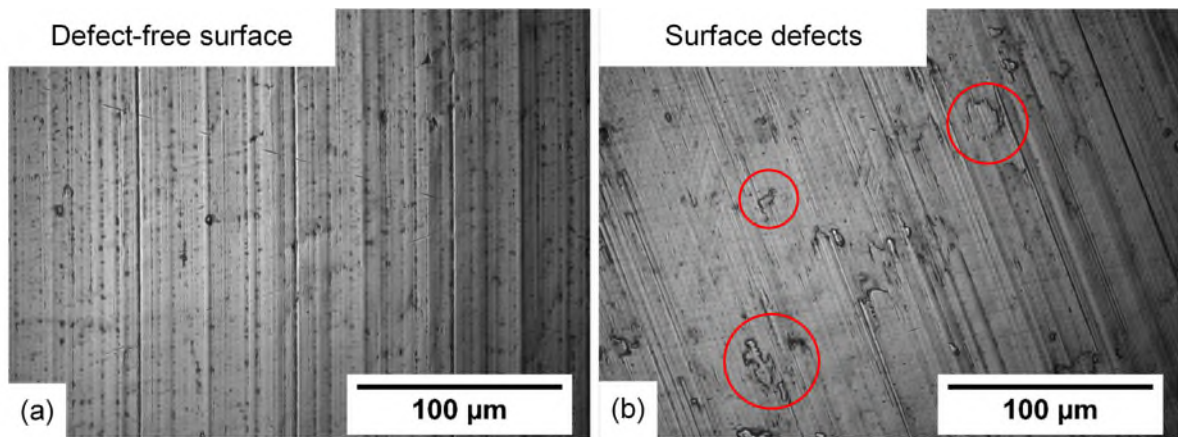


Figure 105. Machined surfaces with S10-XL at $V_c = 110$ m/min, $a_p = 0.5$ mm, $h_{ex} = 0.04$ mm; (a) defect-free area, and (b) region with defects.

From the perspective of the cutting parameters, it was observed that the surfaces are mainly affected by the increase of h_{ex} and a_p (Figure 104), while for V_c it was observed that an increase of this parameter decreases the number of defects, producing smoother surfaces. This behavior would be associated with the increase of temperature caused by the V_c variation, raising the ductility of the material in the cutting zone. However, in the case of an $a_p = 0.5$ mm, this tendency is opposite, affecting the surface quality.

This demonstrates that the increase in temperature and cutting forces affects surface quality. This behavior was constant in all inserts. As can be seen in the images in Appendix A-3, the inserts with the lower surface defects were the S10-XL and the S25-XM.

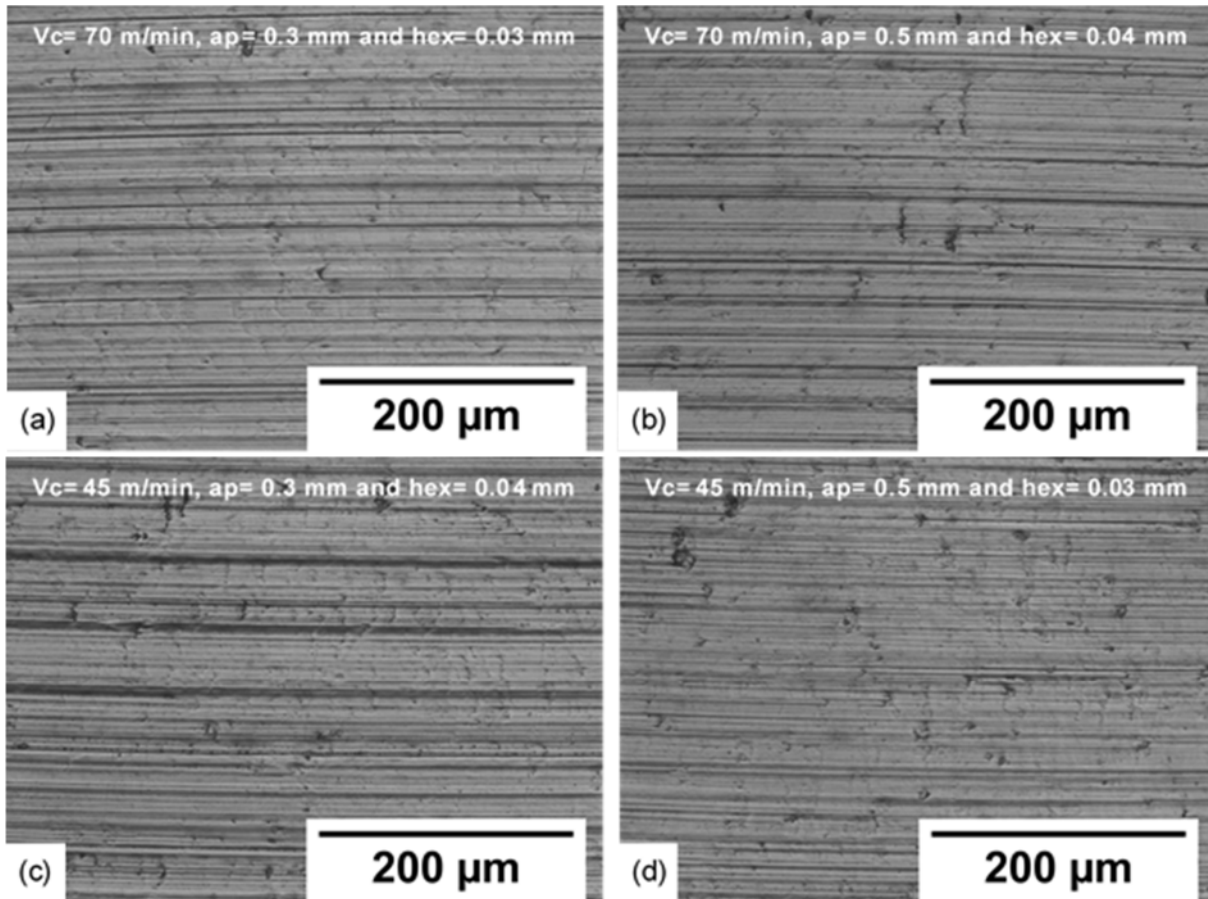


Figure 106. Machined surfaces with S10-XL inserts at; (a) $V_c= 70$ m/min, $a_p= 0.3$ mm and $h_{ex}=0.03$ mm, (b) $V_c= 70$ m/min, $a_p= 0.5$ mm and $h_{ex}= 0.04$ mm, (c) $V_c= 45$ m/min, $a_p= 0.3$ mm and $h_{ex}= 0.04$ mm, and (d) $V_c= 45$ m/min, $a_p= 0.5$ mm and $h_{ex}= 0.03$ mm.

To perform a more detailed analysis of the surfaces, a 3D topographic survey of several defects was developed, to determine the depth and size of the damage. Figure 107.a shows a milled region with an insert S30-XM after the fracture of its cutting edge. The tendency to smear material (Figure 107.b) was the most common defect detected in all the surfaces, mainly in those that were machined with an a_p of 0.5 mm. It was also observed that these are always oriented perpendicular to the feed marks. Similar behaviors have been reported by several researchers [69, 82, 163] in the machining of other TiAl.

On the other hand, the formation of cavities and surface tearing is a behavior characteristic of materials with low ductility, which was more evident in the face of a worn cutting edge. The cavities and cracks were found mainly on surfaces with worse finishing.

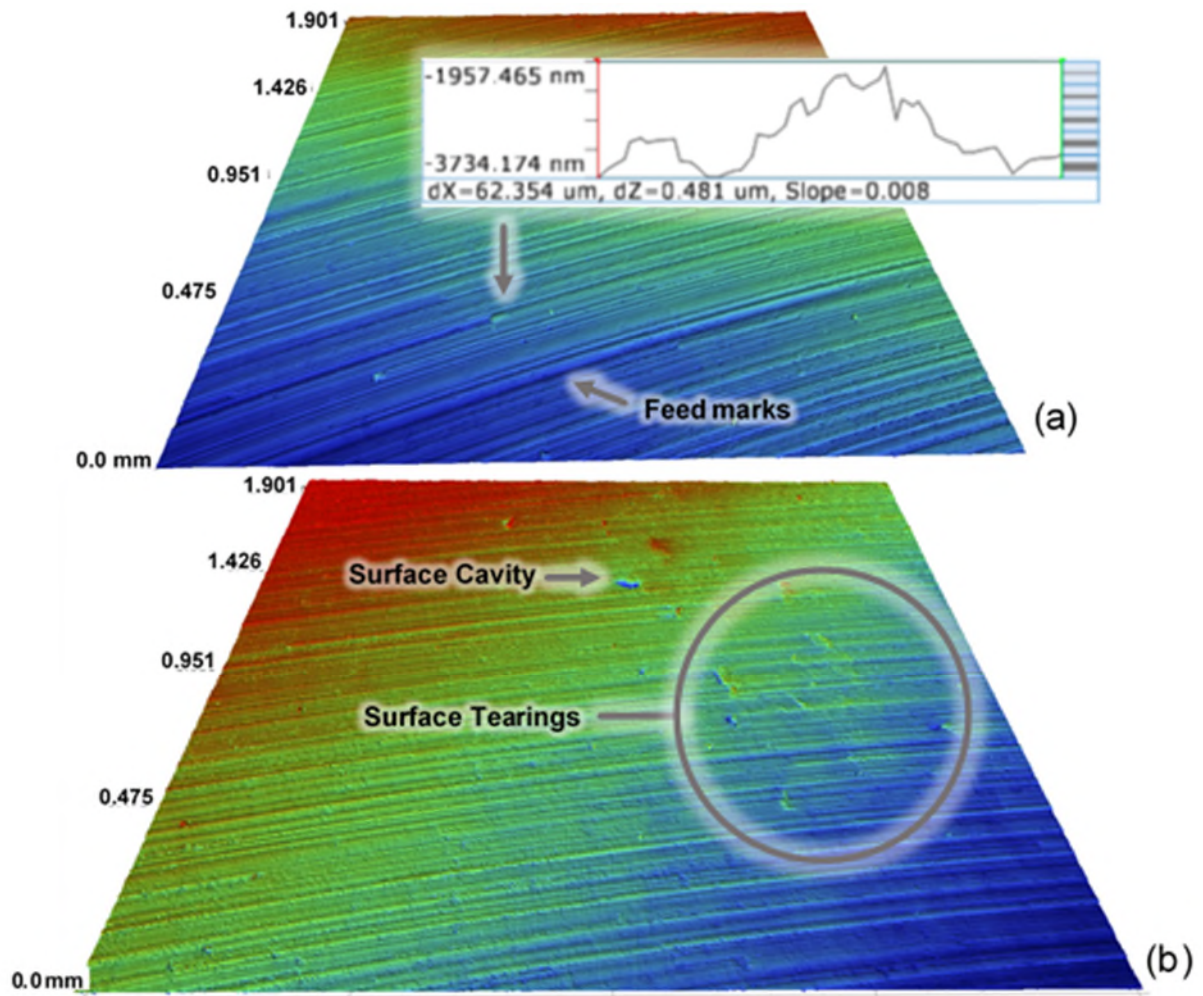


Figure 107. Topographies of the machined surfaces; (a) Cutting insert S30-XM: $V_c = 45 \text{ m/min}$, $a_p = 0.5 \text{ mm}$ and $hex = 0.03 \text{ mm}$, and (b) Cutting insert S30-XM: $V_c = 70 \text{ m/min}$, $a_p=0.5 \text{ mm}$ and $hex = 0.04 \text{ mm}$.

In general, all surfaces exhibited cavities and surface cracks, which were no larger than $\sim 30 \mu\text{m}$. Figure 108 presents several examples of defects found in the same sample. The type and quantity of defects varied, which made it challenging to define a trend that relates this behavior to the parameters of machining or tool type. However, inserts S10-XL and S30-XL were those that on average showed a slight decrease in percentage of defects on their surfaces.

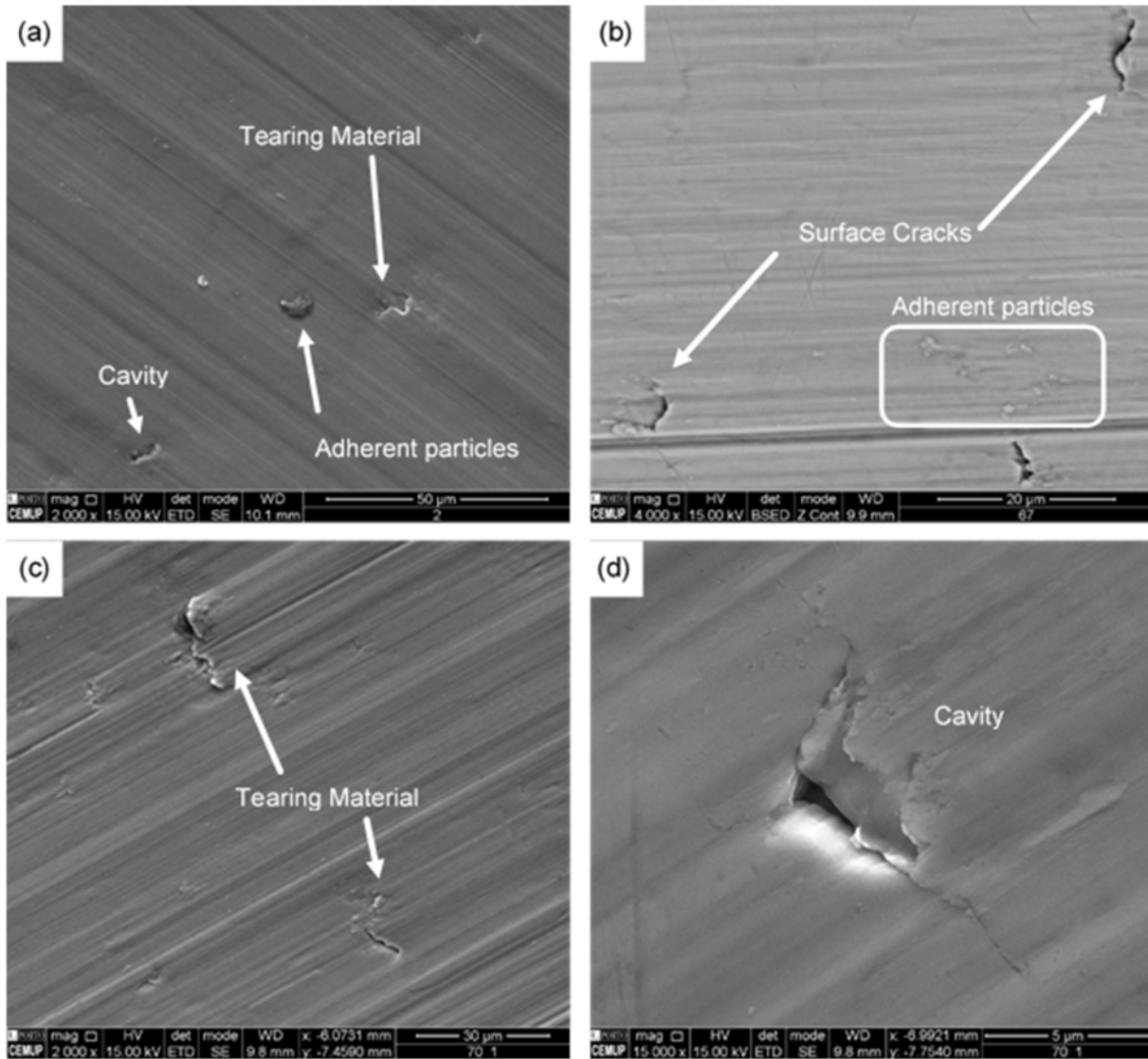


Figure 108. Surface defects on machined surface of different samples; (a) S10-XL at $V_c=110$ m/min, $a_p=0.5$, $hex=0.04$, (b) S25-XM at $V_c=70$ m/min, $a_p=0.3$, $hex=0.03$, (c) and (d) S30-XL at $V_c=70$ m/min, $a_p=0.3$, $hex=0.03$.

4.3.2. Hardened surface layer

One of the main effects caused by machining operations in γ -TiAl is the creation of a hardened surface layer (work hardening). The study of this layer intends to analyze the surface hardness and the subsurface microhardness profile. This is influenced by the characteristics of the tools and machining parameters [69, 80, 197]. A hardened surface layer contributes to accelerate the wear of the cutting tools.

4.3.2.1. Surface hardness

For the study of surface hardness, measurements were made in several sectors of all the milled samples (procedure described in section 3.5.2.2). The results obtained show that in general, the average surface hardness obtained with the round inserts is of $\sim 530\text{HV}_{0.025}$. This value is considerably lower than the one presented by Vargas Pérez [24] ($\sim 800\text{HV}$) in the milling of a Ti-47Al-2Nb-2Mn (at%) + 0.8 TiB₂ alloy with inserts of round geometry.

4.3.2.1.1. Effect of tool characteristics on surface hardness

The analysis of the surface hardness increases as a function of the chemical composition of the inserts (Figure 109.a) shows that the S25 material causes harder surfaces, however, the variation between the materials is only $\sim 6\%$.

From the perspective of the cutting edge, the XL type geometry produces a smaller increase than XM geometry. In a more detailed way, Figure 109.c shows the tendency of XL geometry to promote less surface hardening. Additionally, this graphic also shows that S30 XL and S10-XL tools stand out as the ones causing less surface hardening.

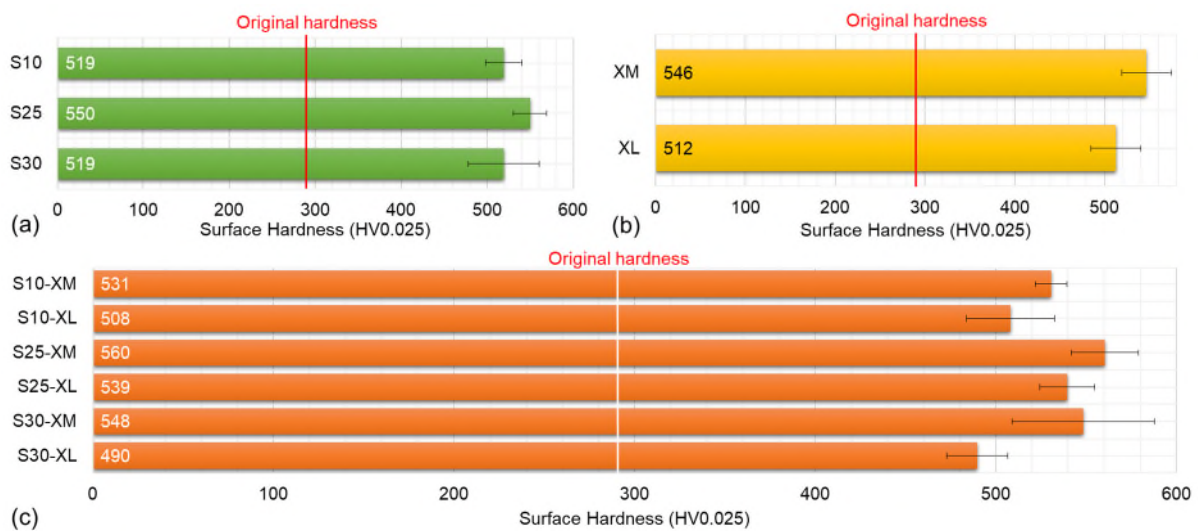


Figure 109. Average surface hardness by; (a) cutting tool materials, (b) edge insert geometry, and (c) cutting insert.

In general, in the milling of this TiAl alloy, the geometry of the cutting edge and the type of material of a round insert has an influence on the surface hardened layer, considering a specific range of cutting parameters.

4.3.2.1.2. Effect of cutting parameters on surface finish

To complement the study of the round inserts impact in the surface hardening, an analysis of the effect of V_c , a_p and h_{ex} on this phenomenon was carried out. It is important to note that the published work carried out in milling these alloys with round inserts [23, 24] does not present information about this topic.

As it is displayed in Figure 110 for V_c , the tendency is an increase in surface hardness (initial surface hardness: 285.7 HV_{0.025}) with V_c . For a 55% increase in V_c , a hardness variation around 5% is obtained. Other researchers [142, 163] claimed similar behavior. However, their works used cutting tools with geometries of nose radius considerably smaller ($R_n = 0.8$ mm), which could mean that the nose radius do not contribute to the effect of V_c on the surface hardening.

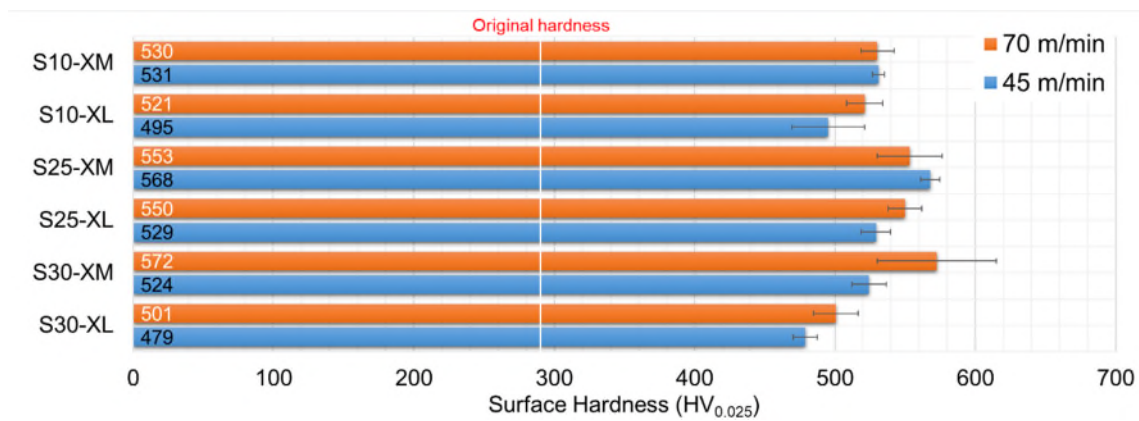


Figure 110. Effect of cutting speed (V_c) on the average surface hardness.

On the other hand, the surface hardening effect derived from the a_p is ~4%, however depends on the edge geometry, as observed in Figure 111. The negative angle of the cutting edge contributes to the reduction of the hardening effect.

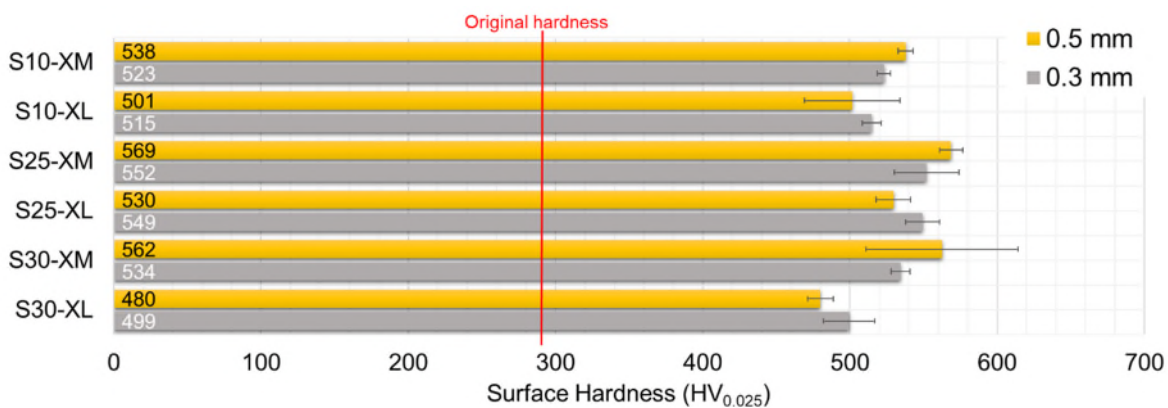


Figure 111. Effect of axial depth of cut (a_p) on the average surface hardness.

For the h_{ex} (Figure 112) it seems that it does not have a specific tendency. However, it is possible to extract that in general rising the h_{ex} increases the surface hardness. It is important to note that in tools such as S10-XL, S25-XM, and S30-XM this increase can even affect the hardness values more considerably than in the case of the other cutting parameters.

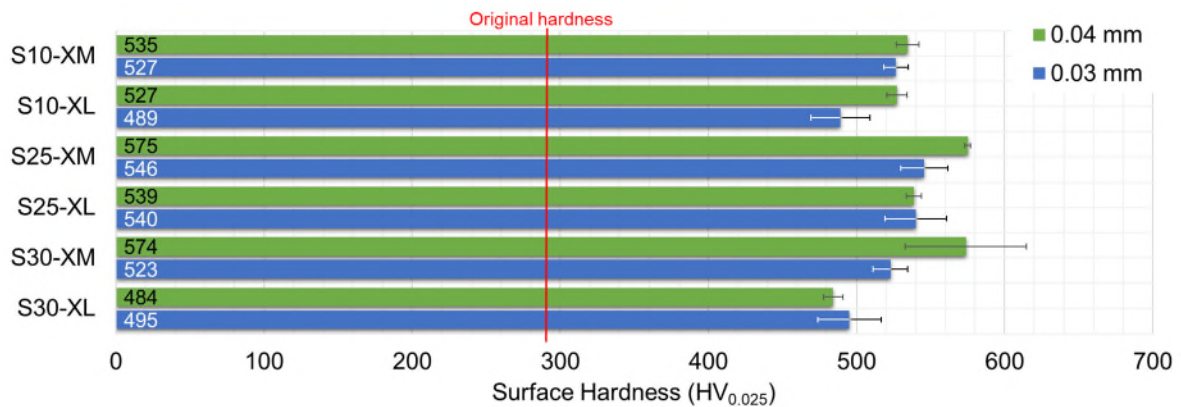


Figure 112. Effect of chip thickness (a_p) in the average of the Surface hardness.

In general, the results obtained show that the surface hardening caused by milling with round inserts is mainly affected by the cutting parameters. However, it was observed that this variation is correlated in the same way with the geometry of the cutting edge.

The graph of the effect of the cutting parameters on the average surface hardening for inserts S10-XL is represented in Figure 113. It is confirmed that the increase in the deformation velocity, by varying the V_c and the h_{ex} , contributes to a hardened surface layer. This tendency is more evident for the case where the V_c is in the range of 20 to 45 m/min, while in the case of the h_{ex} , the increase is more evident from 0.02 to 0.03 mm. Therefore, to achieve parts with low surface hardening values, a V_c of 20 m/min, a h_{ex} of 0.02 mm and an a_p of 0.5 mm should be used.

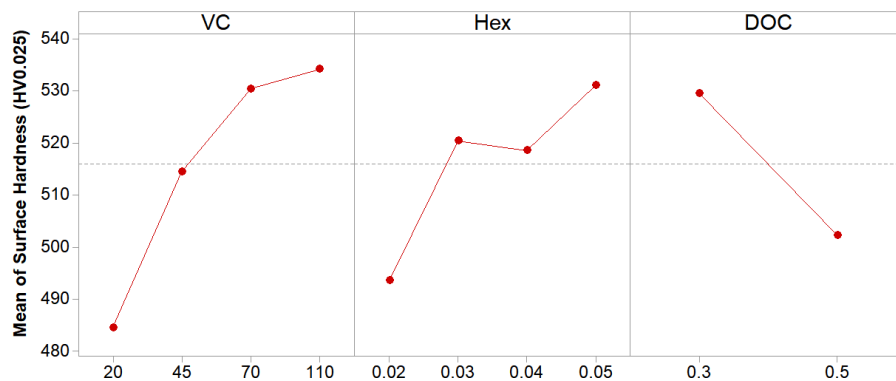


Figure 113. Main Effects Plot – means for surface roughness (HV_{0.025}).

The ANOVA analysis performed for surface hardening (Table 20) showed that all cutting parameters are representative. The percentage contribution ratio (PCR) values indicate that the V_c is the most influential factor followed by the a_p and the h_{ex} . This result proves the relationship between the speed of deformation and the surface hardening. Furthermore, as in the case of the Ra, it is observed that the level of error is 35%, which is related to the omission of the interactions between the factors, the possible measurement errors due to the scale used and the control of the conditions of the work environment.

Table 20. ANOVA table for the arithmetic means surface hardness.

Source	DF	Adj SS	Adj MS	F-Value	PCR (%)
Vc	3	18415.29	6138.43	15.86	33.27%
hex	3	9061.92	3020.31	7.81	15.23%
ap	1	8900.85	8899.85	23.00	16.42%
Error	40	15479.78	386.97		35.07%
Total	47	51855.84			

4.3.2.2. Microhardness Profile

Studies about the surface hardened layer of TiAl [24, 68, 69, 132] are mainly oriented to the observation of the effect of tool type, wear of the cutting edges and the lubrication systems (Figure 114). However, the information about the effect of the cutting parameters on this phenomenon is scarce. Considering this particular, the present analysis focuses on identifying the impact of the cutting parameters and tools design on this layer.

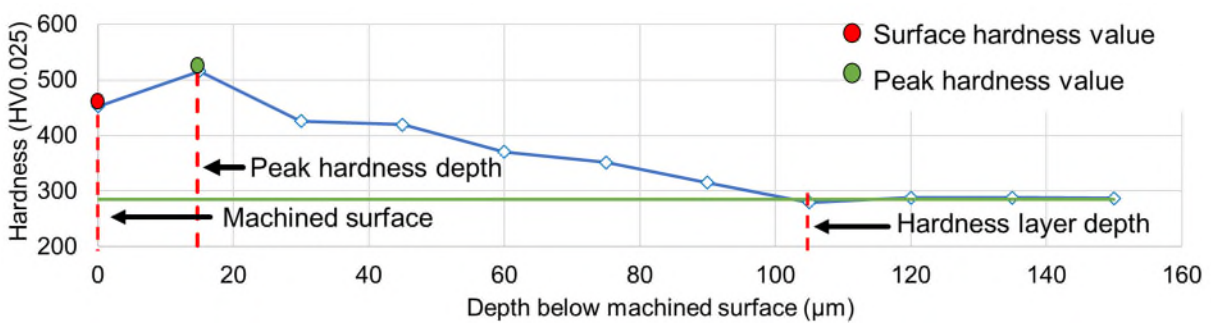


Figure 114. Hardness profile as a function of the depth below the machined surface.

4.3.2.2.1. Effect of tool characteristics on microhardness profile

The thickness of the hardened layer is a parameter that allows estimating the level of alteration suffered by the surface after the cutting process. This value is obtained from the graphic of the hardening profile. Figure 115 presents an example of the microhardness profile of four samples machined using the configuration of cutting parameters proposed

by DOE L4 (section 3.2) with inserts S25-XL (Appendix A-4 presents the individual and combined profiles for all the inserts, and the values of all the tests are presented in Appendix A-5).

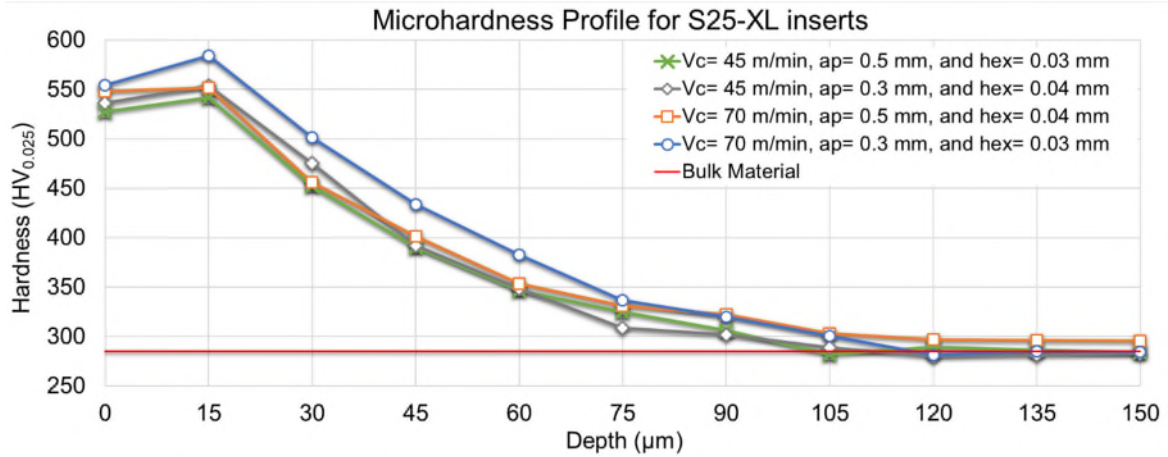


Figure 115. Hardness profiles for S25-XL insert.

The results obtained indicated that the maximum hardness layer depth (HLD) measured was 150 μm (S30-XM Trial 3), and the maximum peak hardness value (PHV) was 624 $\text{HV}_{0.025}$ (S30-XM Trial 3). However, these maximum values were $\sim 30\%$ lower than those reported by Vargas Pérez [24] ($\text{PHV} = \sim 800 \text{ HV}_{0.025}$ and $\text{HLD} = 200 \mu\text{m}$) when milling a $\gamma\text{-TiAl}$ alloy ($\text{Ti-47Al-2Nb-2Mn (at\%)} + 0.8 \text{ TiB}_2$) with round inserts at $V_c = 20 \text{ m/min}$, $h_{ex} = 0.056 \text{ mm}$, $a_p = 1 \text{ mm}$ and $a_e = 60\%$.

Besides, the results also showed that the maximum difference between the surface hardness and the PHV was 9.2%, This variation was lower than the one demonstrated by ball nose end mills and flat end mills, which have shown differences of up to 14% [127] and 18% [142] respectively.

As expected in the case of the edge geometry and the insert materials composition, the behavior followed a pattern similar to that presented in surface hardening. However, it is interesting to note that in general, the edge geometry XL tends to show a better performance than the XM, as detected in the individual analysis by inserts of Figure 116.

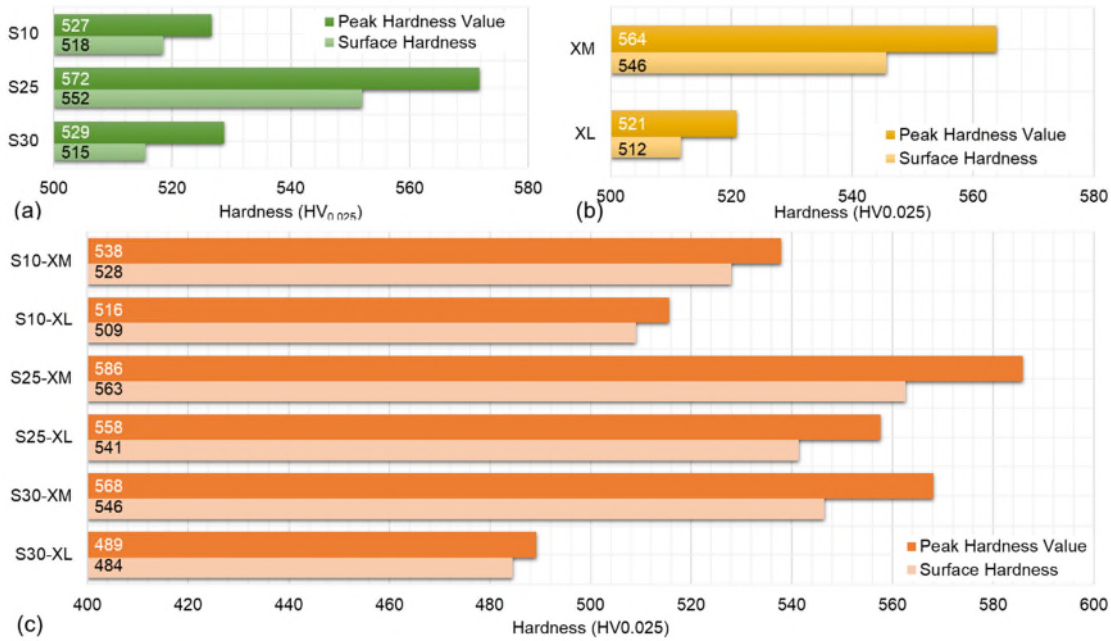


Figure 116. Difference between surface hardness and peak hardness sorted by; (a) material type, (b) edge insert geometry, and (c) cutting insert.

On the other hand, as seen in Appendix A-5, the depth of the PHV was located at a maximum distance of $\sim 15\mu\text{m}$. It is important to note that none of the samples obtained with any insert or set of parameters presented a value outside this range. This behavior, together with the low variation between the surface hardness and the PHV, is a clear indication that the use of round geometry inserts in the milling of this material presents a low level of changes in the creation of the surface hardened layer.

4.3.2.2.2. Effect of cutting parameters on microhardness profile

For the interpretation of the effect of the cutting parameters on the characteristics of the surface hardened layer, it was decided to use the difference between the PHV and the surface hardness (Δ Hardness) and the thickness of the hardened layer as the main analysis variables. It is important to define that the Δ Hardness is related to the microstructural changes that occur in the subsurface hardened layer.

In the case of the Δ Hardness analysis (Figure 117), the high variability of the results for each insert present it very complex to define a general behavior trend. This variability demonstrates high sensitivity of the hardened layer to the variation of the cutting parameters. However, in the case of the cutting speed, it was observed that the increase in V_c from 45 to 70 m/min causes the Δ Hardness to decrease, which means that an increase in V_c causes the depth of the PHV being located closer to the machined surface.

In the case of the a_p and the h_{ex} , it can be observed that the sensitivity of the response of the material causes a particular behavior for each insert. This behavior reduces the possibility of carrying out a general analysis and shows that the study of the effect of the cutting parameters on the surface hardened layer must be carried out individually for each insert.

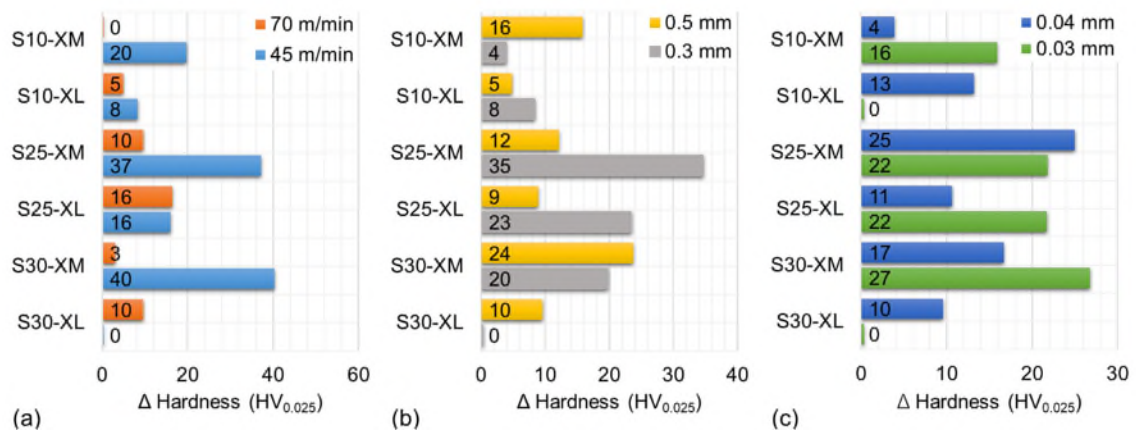


Figure 117. Effect of; (a) cutting speed (V_c), (b) axial depth of cut (a_p), and (c) chip thickness (h_{ex}), in the average values of the difference between surface hardness and peak hardness (Δ Hardness).

The results obtained in the study of the HLD (Figure 118) showed that an increase of the V_c and the h_{ex} tends to reduce the thickness of the hardened layer. For the a_p , this behavior is different for each insert, which indicates that the effect of the parameters, in this case, would be related to the type of material. In the same way, when observing Figure 118, it is noted that there are variations of the HLD between the kinds of insert materials. This behavior denotes that in the case of the depth of the hardened layer, the material of the tool is a representative factor.

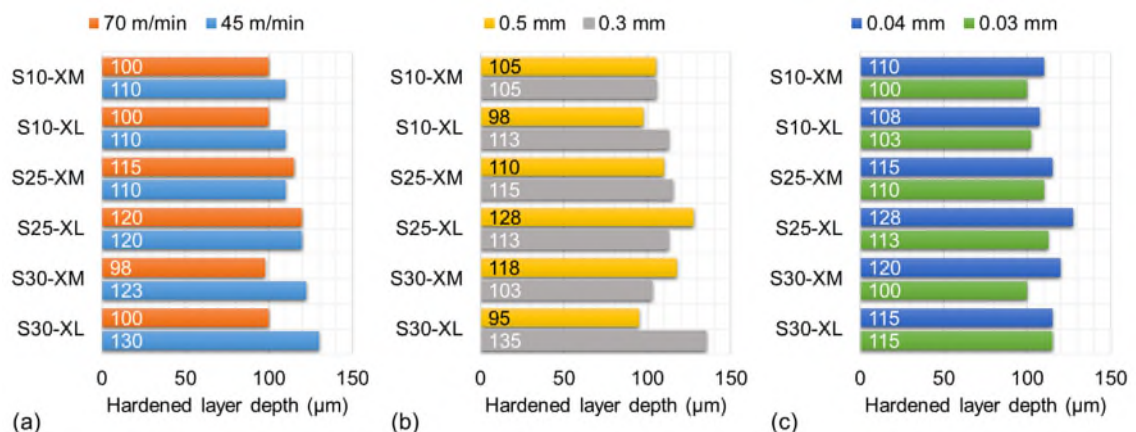


Figure 118. Effect of; (a) cutting speed (V_c), (b) axial depth of cut (a_p), and (c) chip thickness (h_{ex}) in the average hardened layer depth.

For a better understanding about the effect of the cutting parameters on the Δ Hardness, an extensive study was performed with the insert S10-XL. The obtained results present, in a more precise way, the effect of the V_c , a_p and h_{ex} variation on the Δ Hardness. For this kind of insert, Figure 119 shows that for a range of V_c between 20 and 70 m/min, surface hardness and PHV tend to increase. However, the difference between these hardness experiences a slight decrease. While for a V_c of 110 m/min the Δ Hardness is considerably lower. This behavior raises the hypothesis that milling with high V_c , reduces the difference between the two hardnesses, and consequently the microstructural changes on the subsurface layer could also be diminished.

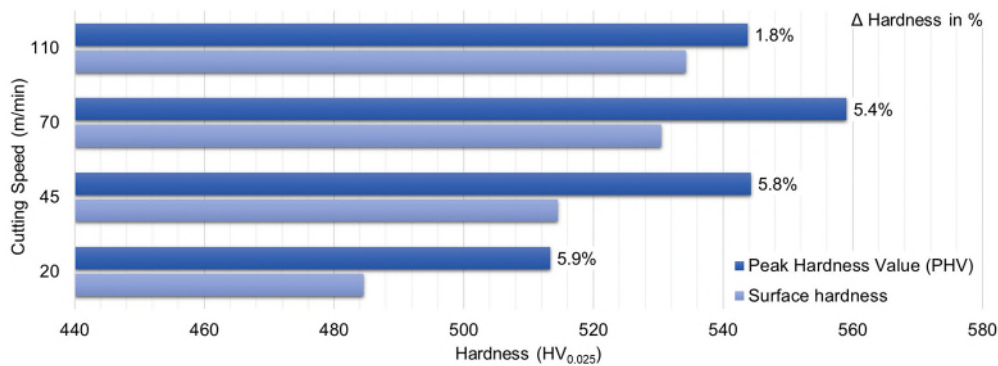


Figure 119. Effect of cutting speed (V_c) in the peak hardness value and surface hardness.

As seen in Figure 120, the increase of the a_p , affects the values of the surface hardness and PHV. Despite this fact, the difference between harnesses is considerably increased. This behavior determines that the affected area of the subsurface layer would be possible greater.

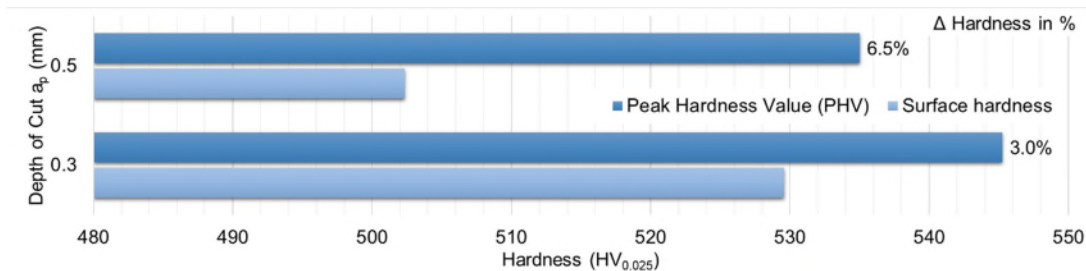


Figure 120. Effect of the axial depth of cut (a_p) in the peak hardness value and surface hardness.

For h_{ex} , as seen in Figure 121, results show that the values of the surface hardness and PHV increase with h_{ex} , while the difference between harnesses tend to decreases. These facts mean that the increase of the h_{ex} causes a zone of minor structural variation, but with higher values of surface hardness and PHV.

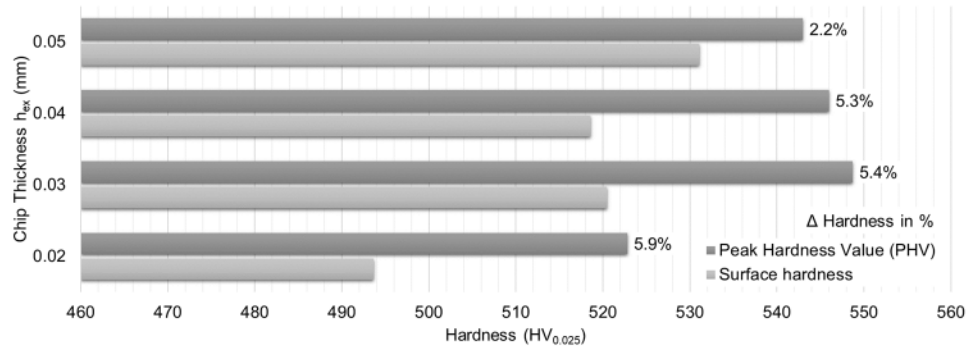


Figure 121. Impact of the chip thickness (h_{ex}) in the peak hardness value and surface hardness.

In general, the results about the behavior of the parameters of cut determine that the increase of the displacement (controlled by the h_{ex}) and rotation of the cutting tool (controlled by the V_c), together with an a_p of 0.3 mm, create a zone of higher surface hardness and PHV values. Contrary to this behavior an a_p of 0.5 mm causes lower hardening rates.

4.3.3. Lamellar deformation

Because the cut of the material simultaneously deforms the surface and subsurface layer, the lamellar deformation is a phenomenon that is associated with the surface hardening, as well as with the residual stresses of the machined surfaces.

In this work, the depth measurement of the deformed layer was made in the same samples used for the profile of the hardened layer. The results presented are the average of six measurements made in different sectors of the same sample. In general, the values of the depth of the deformed layer (DDL) were not easy to define, mainly due to the depth variation relatively to the orientation of the lamellar colonies, as seen in Figure 122.a.

Another drawback for the measurement was the areas with a lamellar structure with a more significant presence of the γ phase (Figure 122.b), which present higher DDL values. To reduce the level of error in the measurement of this phenomenon, the areas with lamellar colonies with an orientation between 45° and 80° were selected.

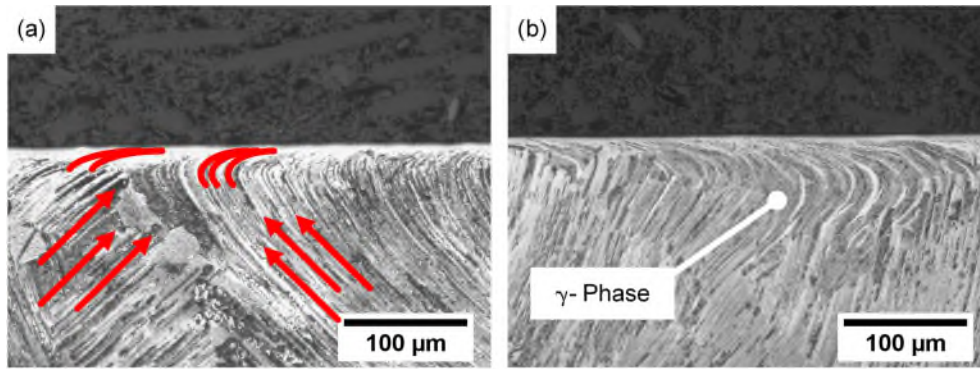


Figure 122. Deformed lamellar layer in accordance with; (a) lamellar orientation, and (b) γ -phase content.

In general, the DDL proved not to exceed 70 μm in depth in the selected areas. From the perspective of the tool material, it was observed that the inserts with a material of higher toughness (S30) and with negative cutting edges (XL), were those with less lamellar deformation. This tendency was very similar to that presented by the hardening of the surface, as observed in Figure 123.

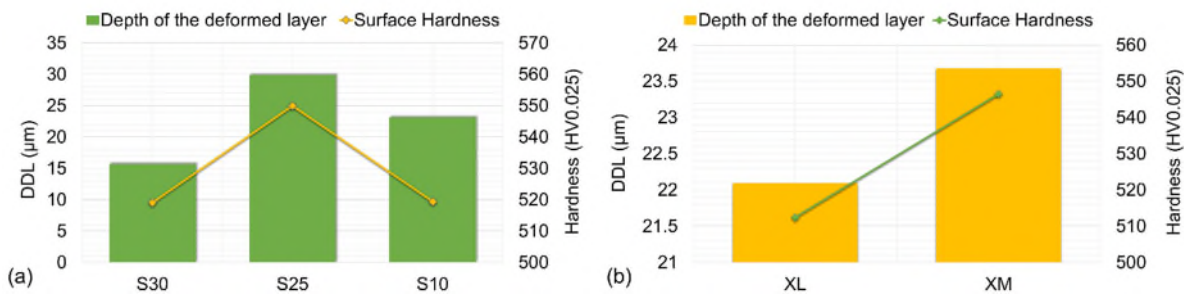


Figure 123. Average of the depth of the deformed layer vs. surface hardness by; (a) material, and (b) edge insert geometry.

Concerning the effect of the cutting parameters on the lamellar deformation, it was possible to observe that for the harder inserts (S10 and S25), a similar behavior for V_c and h_{ex} was identified, as seen in Figure 124. In the same way, it can be observed that the lower hardness (S30) inserts exhibited a completely opposite performance, with the lowest DDL values for all the tests and for all the cutting parameters. This behavior emphasizes that a material with greater toughness affects the milled surfaces to a lesser extent, and even in some cases, it causes almost no lamellar deformation levels.

Figure 124.a and c show that in the harder tool materials, an increase in V_c and h_{ex} can be beneficial, because it decreases the lamellar deformation, possibly due to the temperature increase in the cut zone and speed of chip removal. In the case of a_p (Figure 124.b) the

values varied according to the type of insert, so it is very difficult to define a specific trend.

However, the results obtained from the samples of the second test phases (Figure 125), show that low ranges of V_c and h_{ex} can produce surfaces with less surface damage, which corroborates the results obtained for surface hardening. In the case of V_c it is important to note that an increase up to 120m/min causes surfaces with high DDL values, while the behavior between 45 and 70 m/min is similar to the first stage. This tendency allows understanding that, this type of alloys are very sensitive to the variation of this parameter. For h_{ex} and a_p , as expected, they showed that the increase in the amount of material removed and the removal speed the deformation was greater (Figure 125.b y c).

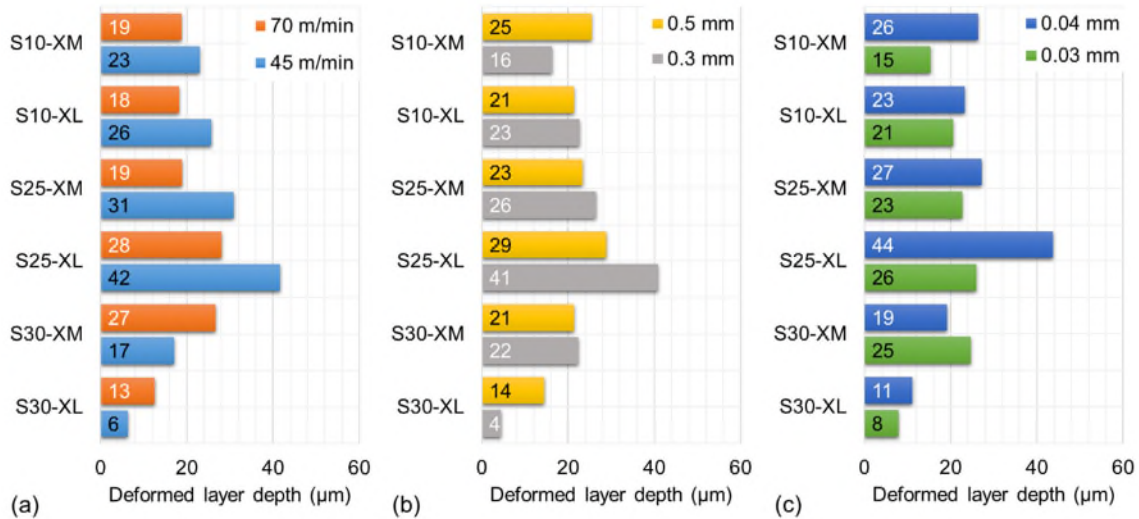


Figure 124. Effect of; (a) cutting speed (V_c), (b) axial depth of cut (a_p), and (c) chip thickness (h_{ex}) in the depth of the deformed layer (DDL).

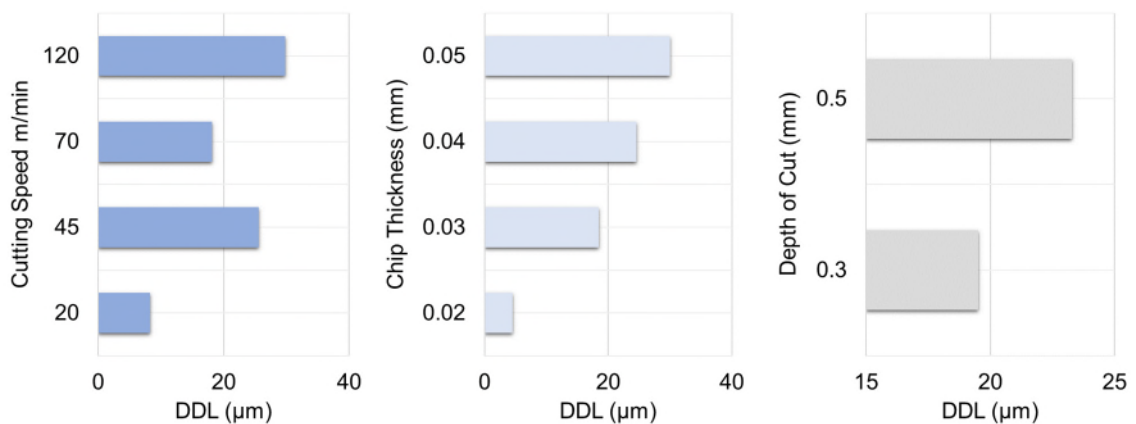


Figure 125. Effect of; (a) cutting speed (V_c), (b) axial depth of cut (a_p), and (c) chip thickness (h_{ex}) in the depth of the deformed layer (DDL) for S10-XL insert.

4.4. Chip Formation

The study of chip formation is a technique commonly used to evaluate the machinability of a material. This criterion identifies the characteristics of the chips and associates them with the properties of the material, the cutting parameters, the properties of the tools, the stability of the process among other factors involved in the machining process [119].

Considering that TiAl are difficult to machine, the study of chip formation is not an easy task in this material, mainly due to its low ductility and anisotropic microstructure. The theories formulated for the analysis of the chips in metallic alloys, are not applicable in this class of intermetallic materials. However, there are some works [24, 73, 108] that have begun to address this issue.

In the case of this evaluation criterion, the experimental phase was conducted using a range of cutoff parameters based on the analysis of the results presented in sections 4.2 and 4.3. Inserts S10-XL and S25-XM were selected to carry out the tests, as they generally show better performance. The experimental design used in this phase is described in section 3.3.4 (Table 21).

Table 21. Experimental array used in the experimental work for the chip formation.

Experimental Array				
TEST	Cutting Speed (Vc) (m/min)	Rotation Frequency (rpm)	Depth of cut (ap) (mm)	Feed (f) (mm/rev)
Trial 1	38	224	0.3	0.14
Trial 2	53	315	0.3	0.14
Trial 3	38	224	0.5	0.14
Trial 4	53	315	0.5	0.14

The study of chip formation was also performed through high-speed recording technique. This process has been used by several researchers because it allows to observe the dynamics of chip formation during the cutting operation [168, 198, 199]. The experimental phase was carried out in a conventional turning process. This process was selected mainly due to the simplicity of analysis, visualization of the chip formation and installation of the equipment. Additionally, the analysis of the cutting forces was carried out to complement the study.

4.4.1. Results from high-speed recording

Figure 126 presents the sequence of images recorded in the cutting process using inserts S10-XL and S25-XM (completely new) at a V_c of 50 m/min, feed of 0.14 mm/rev and an a_p of 0.3 mm. The high-speed photographs acquired with the insert S25-XM showed that in an initial phase, the chips tend to form a well-defined curl up along the rake face of the insert. However, the low ductility of this alloy limits the process of the formation and quickly leads to breakage, forming several thin chips known as needle-type chips (this can be better visualized on the frame of the S10-XL). This type of chips has been observed by several researchers [24, 71, 80, 98] in other machining processes, which suggests that the type of machining does not determine the type of chips.

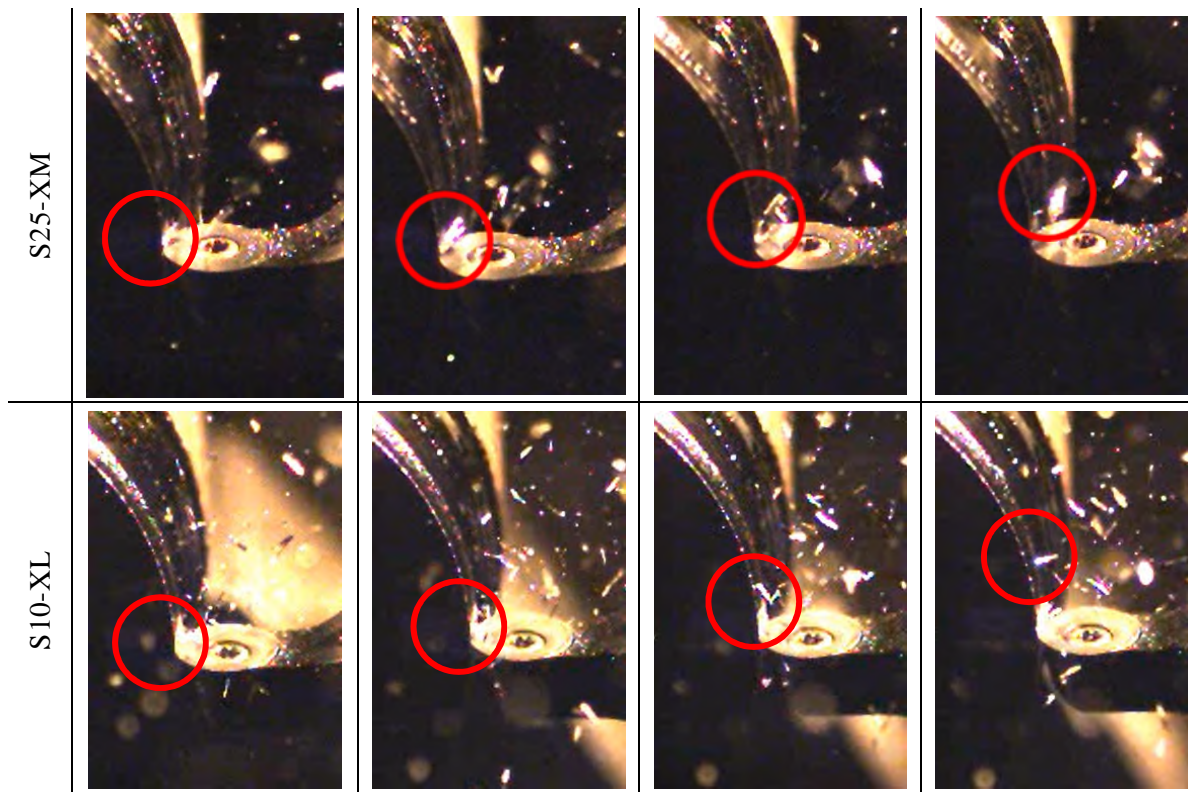


Figure 126. Frames from video sequences during chip formation in the trial 1 for: (a) S10-XL and (b) S25-XM inserts.

Figure 127 shows the typical geometry of the chips obtained. In the magnified image, one can see in detail the free surface of the chip, in which the array of plates that make up the chip is perceptible. This distribution shows the formation of the thin plates slightly linked together and cracks propagation along the chip thickness. Figure 128 shows a cross section of the chip where the formation of the individual plates is observed, demonstrating that the brittle fracture is the main mechanism that controls the process of chip formation.

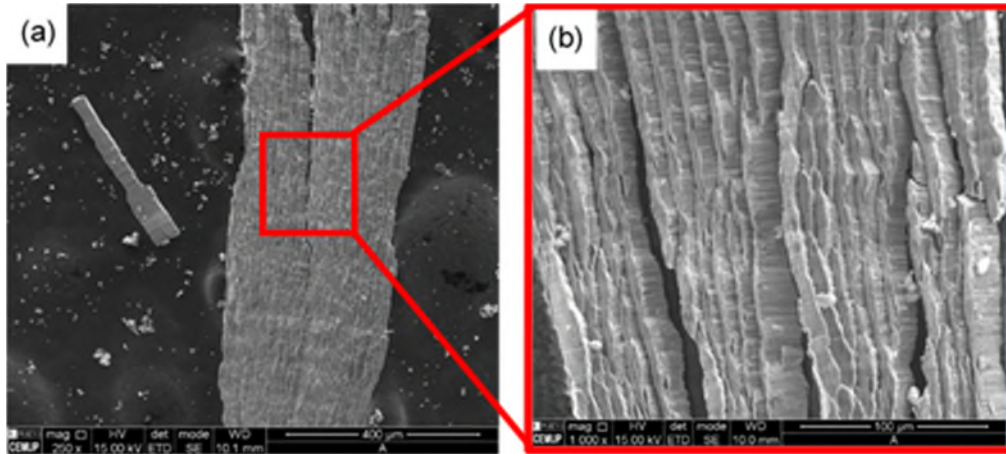


Figure 127. SEM images of; (a) chip obtained with S25-XM at $V_c=38$ m/min, $a_p=0.3$ and $f=0.14$ mm/rev, and (b) magnification of the upper side of the chip.

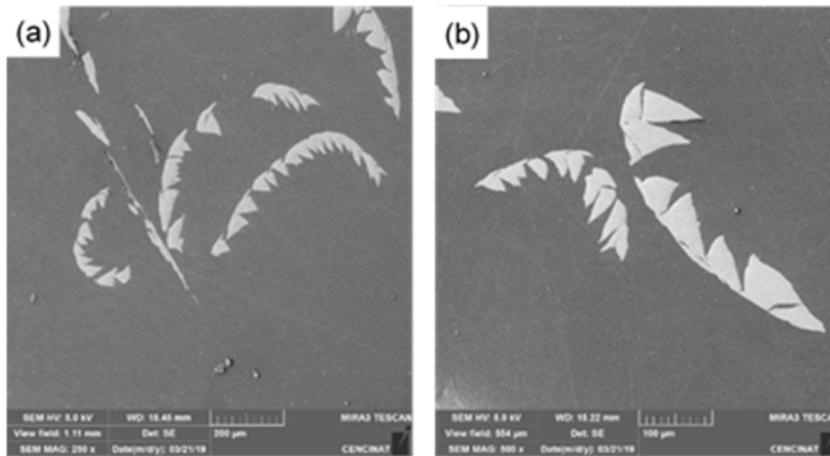


Figure 128. Optical microscopy image of the cross-section of a Ti-48Al-2Nb-0.7Cr-0.3Si chip obtained when cutting with S25-XM at: (a) $V_c=38$ m/min, $a_p=0.3$ mm, and $f=0.14$ mm/rev, and (b) $V_c=53$ m/min, $a_p=0.5$ mm, and $f=0.14$ mm/rev.

As shown in Figure 129, in general, all the experimental tests conducted showed small segmented chips with sharp edges. However, it is also important to register that there is a variation in the average size of these chips, depending on the test parameters.

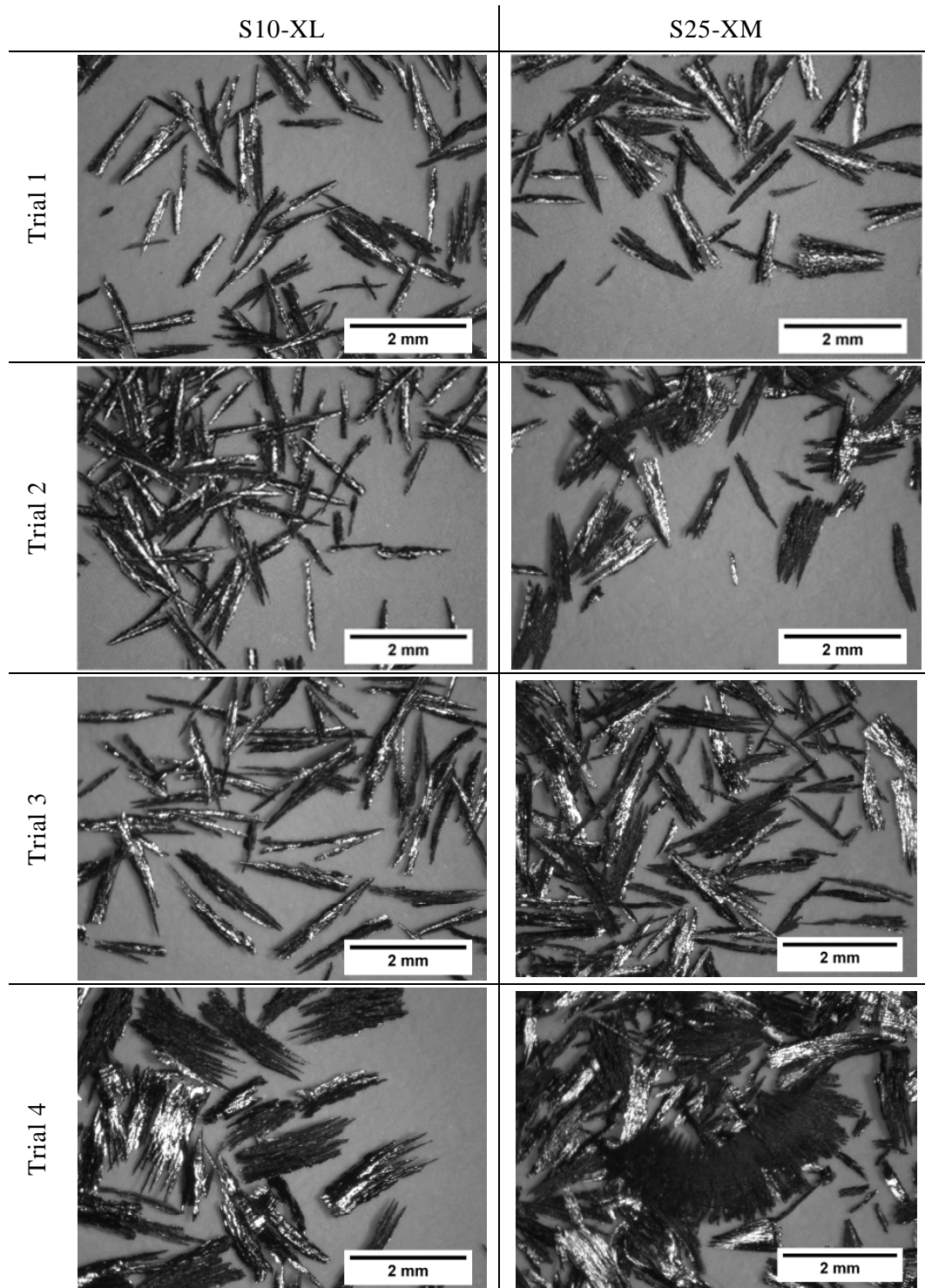


Figure 129. Optical microscopy images of chips obtained from experimental trials.

4.4.1.1. Effect of tool characteristics on chip formation

The insert with T-Land (XL) edge modified the shape of the chip due to the negative angle rake. In general, inserts S10-XL formed chips considerably shorter and more disintegrated than the ones created with S25-XM geometry. This behavior is caused by the anticipated fracture suffered by the individual plates due to the negative angle of the cutting-edge T-

Land. This mechanism of chip formation contributes to the reduction of the temperature at the cutting edge due to the decrease in the sliding of the plates on the rake face [24].

4.4.1.2. Effect of cutting parameters on chip formation

Figure 129 allows identifying that the chips of the tests with V_c of 53 m/min (2 and 4) are higher than those of V_c of 38 m/min (1 and 3). This figure also shows that the sliding surface of the larger chips is softer and more regular. This phenomenon reveals an increase in the ductility of the material, which was caused by the rise in temperature in the cutting zone created by the increase in V_c .

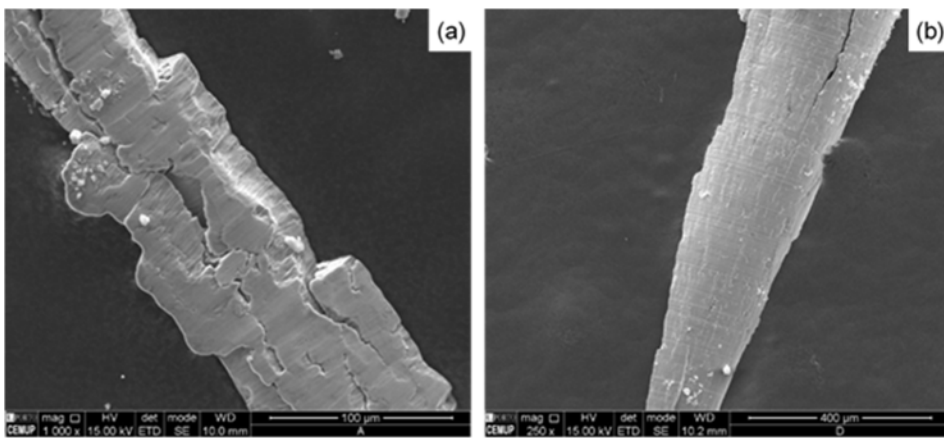


Figure 130. Sliding surface of chips cut with S10-XL inserts in experiments; (a) 1, and (b) 2.

4.4.2. Cutting forces

Figure 131 shows the profiles of the cutting forces versus the machining time of the most particular tests of this experimental phase (Appendix A-6 shows the individual profile of each trial). The results obtained showed that, in general, the dominant forces in all the tests were the tangential (F_t) and radial (F_r) forces. It was also observed that these forces were the most sensitive to the variations presented in the cutting process. As seen in Figure 131.a and c, the variation of the V_c reduces the amplitude of the F_r and F_t forces. This effect is related to the increase in the ductility of the material caused by the increase in V_c . As expected, the rise of the a_p caused an increase in the magnitude and amplitude of the F_r and F_t forces (Figure 131 a and b). In addition, it was also observed that the main sign of wear of the cutting edge was the increase of the F_r (Figure 131.d). For better visualization, the overlap zones of the F_t force were plotted partially transparent (gray color).

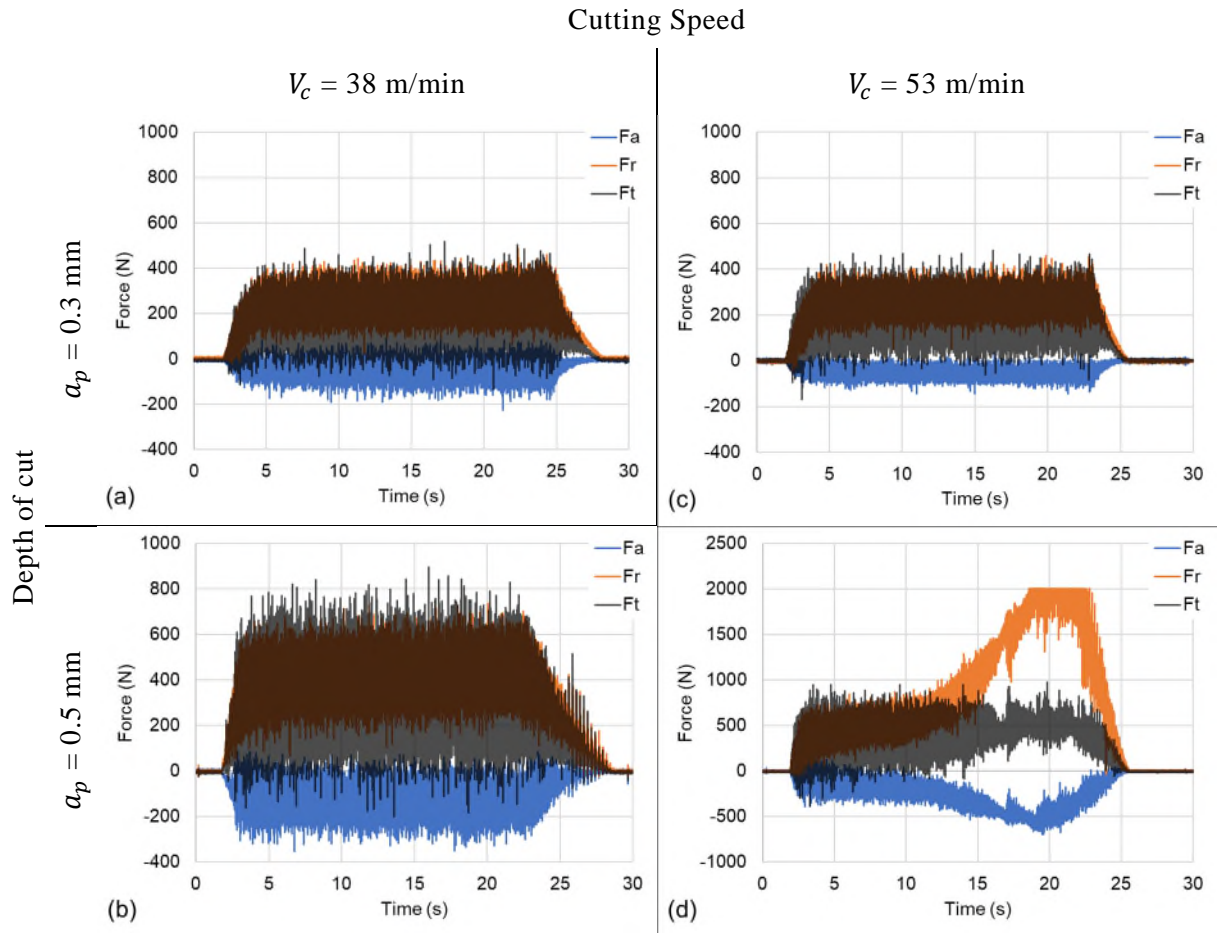


Figure 131. Cutting forces profiles for S10-XL insert at: (a) $V_c=38$ m/min, $a_p=0.3$ mm, (b) $V_c=38$ m/min, $a_p=0.5$ mm, (c) $V_c=53$ m/min, $a_p=0.3$ mm, and (d) $V_c=38$ m/min, $a_p=0.3$ mm.

From the perspective of the cutting tools, as shown in the Appendix A-6, the results presented by these two inserts, in the range of $V_c=38$ m/min, were very similar, so it was not possible to identify a clear trend to distinguish the effect of the geometry or the type of tool material in this cutting condition. However, for $V_c=53$ m/min, the performance of the inserts was different. The S25-XM inserts proved to have a high sensitivity to the increase in V_c . Figure 132 shows the performance of these inserts in the tests conducted with $V_c=53$ m/min. In Figure 132.a, the behavior of the F_r is related to the wear of the tool cutting edge. Considering that the increase in the cutting speed increases the temperature in the cutting area, this would probably be the main reason for the type of wear presented by this tool [66].

Similarly, Figure 132.b shows that the cutting forces suffer a constant increase until reaching the moment where the cutting-edge fractures. This indicates that the increase of the V_c and the a_p causes immediate wear on the cutting edge of the insert, revealing the

inability of this insert to withstand constant cutting forces higher than 500N. This type of failure would be related to the lower structural strength of the sharp geometry of the cutting edge and the lower hardness of the material S25 [65, 66].

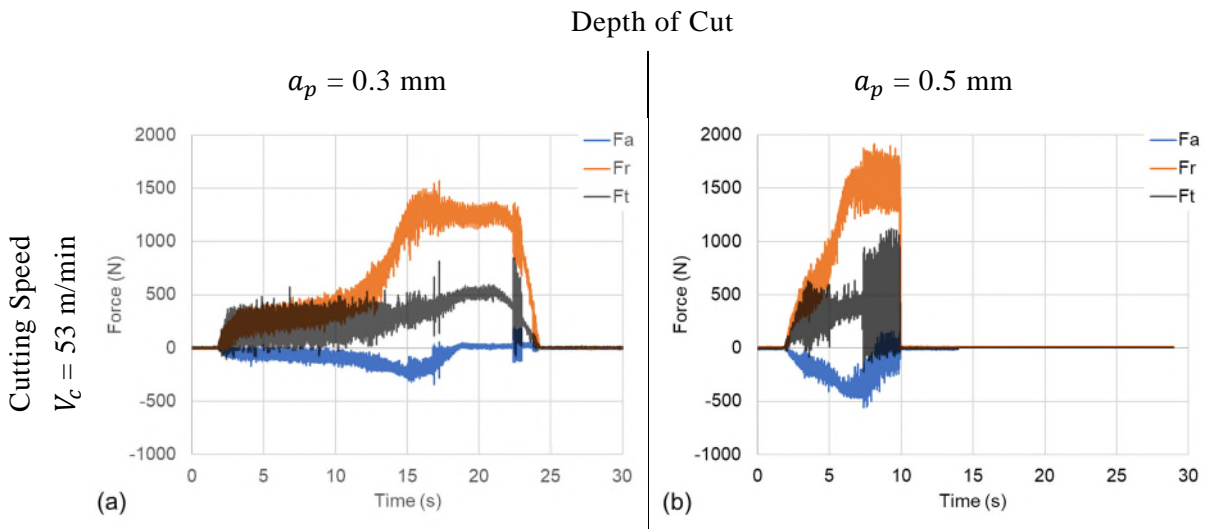


Figure 132. Cutting forces profiles for S25-XM insert at $V_c = 53$ m/min, (a) $a_p = 0.3$ mm, and (b) $a_p = 0.5$ mm

On the other hand, the S10-XL inserts presented a better performance before the increase of the V_c . However, due to the increase in V_c for 53 m/min and the a_p up to 0.5 mm, these inserts showed wear on the cutting edge after cutting. The failure mechanism demonstrated in this range of parameters was a progressive wear of the cutting edge, possibly caused by the increase in temperature.

Chapter 5 : Conclusions and future work

This chapter presents the main conclusions about the machinability study of Ti-48Al-2Nb-0.7Cr-0.3Si alloy. The conclusions presented in this chapter are mainly oriented to answer the questions initially raised and to reach the goals proposed in chapter 1

Additionally, this section shows the contributions of this work to the study of the machinability of TiAl and proposes, from the author's perspective, some alternatives for future work that could contribute to the development of this research area.

5.1. General Conclusions

The main objective of this thesis was to systematically study the machinability problems of γ -TiAl. Therefore, this research presents a detailed characterization of the milling process of an alloy of Ti-48Al-2Nb-0.7Cr-0.3Si concerning surface roughness, subsurface hardening, cutting forces and mechanism of chip formation.

This section summarizes the main conclusions, highlighting the most important contributions.

a. Literature review

In order to understand the machinability of TiAl, around 180 articles about the production of components in this type of alloys were analyzed. Only 48 articles (from 1992 to the present) were experimental case studies that provide information about the cutting process.

From the perspective of the machinability assessment, these works are mainly focused on turning, milling and grinding operations. The most applied criteria for the evaluation of the machining parameters effect on the machinability are the tool life tests, tool wear rates and the measurement of cutting forces. In addition, these studies analyze the most influential factors and the main problems that arise in machining.

However, currently the published results on these alloys do not provide enough information to define a set of suitable cutting parameters, as well as the relationship that the cutting parameters and the characteristics of the tools have on the integrity of the surfaces obtained.

Consequently, this framework reveals that there is a limited amount of information about the study of the machinability of TiAl, and that several issues need a deeper study.

b. Experimental Design

One of the main problems observed in the experimental study cases review was the difficulty of comparing results, due to the great variety of the characteristics of the tools and machining parameters. This circumstance is obviously limiting, because although the experimental procedure and the evaluated factors are known, it is not

possible to establish a machinability reference that allows the selection of useful tools and operational parameters for the machining of these alloys.

Because of this drawback, the present research defined and proposed an experimental design of its own, through the application of several machinability assessment criteria, in order to define the characteristics of the tools and the range of cutting parameters, providing parts with good quality level.

The proposed methodology was also designed to be used in future experiences with other types of cutting tools, in different materials and geometries for this type of alloys. And so that their results are also comparable with the trends presented in this work.

The suggested method consists of two stages, the first one that briefly evaluates the performance of each insert in a range of parameters and cutting conditions defined with nominal values, and a second phase that defines the range of effective cutting parameters for the cutting tool. These phases were executed and analyzed following a Taguchi DOE L4, with three factors at two levels for phase 1, and a Taguchi DOE L16 mixed of three factors of which two are at four levels and one at two levels.

The execution and analysis of the first experimental stage provided significant information to define the performance of an insert and the degree of machinability that it could be achieved, from the point of view of the obtained surface and the cutting forces present in the process. In addition, this stage proved to work as a filter, to define the feasibility of using the insert or as a reference for the selection of the levels of analysis for the second stage of the study.

Likewise, this experimental design proved to be simple, low consumption cutting inserts, with a limited number of trials and easy interpretation of results. However, it was observed that the effectiveness of this technique is subject to two important factors.

The first one is the preparation of the surface of the samples, which must be obtained by cutting through an EDWM process, to avoid significant changes in the subsurface layer. The second factor is the horizontality of the surface, which must be controlled prior to machining, in order to avoid variations in the depth of cut greater than 10% of

the parallelism, due to the effect that the depth of cut has in the machining of these tools.

In addition, this experimental model was mainly designed to assess the machinability from the perspective of the integrity of the surface, which is not suitable for the execution of techniques for evaluation of wear or life time of the cutting tool, due to the short machining path that this performs.

c. Parametric Study

The experimental design evaluated the effect of the characteristics of the tools and the cutting parameters on the machinability of this alloy. The range of selected cutting parameters also proved to be adequate to study the response of the material to milling with round cutting inserts.

In general, the results of the analysis of the first stage revealed that the cutting speed and the chip thickness are the most influential parameters in the cutting forces and surface hardening. While the depth of cut has a minor effect on these parameters, it was revealed as an influencing factor. These trends were confirmed in the ANOVA analysis conducted in the second experimental phase.

In relation to surface finishing, as expected, the increase in the chip thickness caused an increase in the values of Ra. However, this effect was diminished due to the increase in Vc (up to 70 m/min), which caused an increase in temperature in the cutting zone that improved the ductility of the material.

On the other hand, the effect of the tool geometry was also analyzed, together with the evaluation of the cutting parameters. In general, a negative geometry in the cutting edge presents a better performance and presumably a longer useful life. In the same way, the composition of the insert materials was evaluated, and it was observed that insert materials with greater hardness manage to work under more demanding cutting conditions. However, inserts with lower hardness induce fewer effects on the subsurface integrity of the samples.

It is important to note that in the case of the characteristics of the cutting tools, it was more difficult to define trends about any of the two factors, since the results showed that these two characteristics are related.

d. Chip Formation

Considering the cutting parameters, mechanisms of chip formation that implies fracture of the material were observed. The information obtained by high-speed frames showed that the low ductility of this alloy limits the process of chip formation and quickly leads to breakage, forming several thin chips known as needle-type chips.

In general, all the conducted experimental tests presented small segmented chips with presence of sharp edges. However, it was possible to appreciate that there is a variation in the average size of the chips, according to the edge type of the cutting insert and the cutting speed.

The insert with negative rake angle formed considerably shorter and more disintegrated chips. This behavior is caused by the anticipated fracture suffered by the individual plates due to the negative angle of the cutting edge. The analyzed results about the cutting speed showed that the increase of the cutting speed causes an increase in the ductility of the material and reduces the cutting forces.

e. Machinability

Although it was known from the beginning of this work that this type of alloys have low machinability, the evaluation criteria used allowed to define more specifically the machinability of Ti-48Al-2Nb-0.7Cr-0.3Si for milling with round inserts. Despite of this, it was not possible to determine a machinability index, mainly because there is no nominal alloy that allows to compare the results and define a level of machinability for this material. This circumstance forced the need to define a point of study for the machinability analysis for this machining system (material, tool and process).

The obtained results showed that, from the perspective of the surface integrity, some difficulties of machinability of these alloys could be reduced by the use of round inserts. As observed in the Chapter 4, surface roughness results obtained with this type of inserts can produce softer surfaces (Table 18), with scarce defects and less hard and deep surface hardened layer, than those presented by other types of tools.

Likewise, the effect of the geometry of the T-Land edge (XL) allows diminishing the effects of the poor machinability of this alloy, which allows to conclude that inserts of negative geometry, could be a viable solution for the milling process. In the case of the cutting parameters, it was observed that the effect of these in the evaluation of the

machinability is representative. In addition, it was detected that the characteristics of the cutting inserts can cause severe variations in the assessment results.

The analysis of the cutting forces showed that for this type of inserts, the limit at which they start rapid wear is ~500 N. This tendency was observed in both the turning and milling tests.

This material has a machinability similar to that of other TiAl such as Ti-48Al-2Cr-2Nb, although relatively to surface hardness and roughness, the alloy Ti-48Al-2Nb-0.7Cr-0.3Si, proved to be more machinable.

5.2. Answer to the Research Questions

In this section, the main conclusions reached during the development of this research are gathered to answer the questions that originated this research work (section 1.3).

1. What is the procedure that must be followed to evaluate the machinability of a TiAl alloy for milling with toroidal cutting tools of round interchangeable inserts?

To answer this first question and support it, it was necessary to carry out an extensive bibliographical study related to the machining of titanium aluminides, which is presented in chapter 2.

As a result of this analysis, it was found that there are no works that execute standardized tests. In general, the investigations explore different criteria and conduct diverse experimental procedures to evaluate the machinability, based on the specific needs of each research.

In addition, these criteria are applied from different perspectives, using a wide range of cutting parameters, mainly the cutting speed, the feed and the radial and axial cut depths. This makes the results of these assessments to have considerable differences between them, and even in some cases they are not disclosed due to confidentiality terms, making it even more difficult to define an adequate study procedure for new research projects.

One can conclude that there is no established procedure to evaluate the machinability for any type of machining operation in this type of alloys. However, the lack of a

defined procedure that can be replicated to assess this property, limits the possibility of comparing the results between the studies developed and future research, forcing, as in the case of this work, to start a study from the beginning.

However, before the need to establish a procedure to evaluate the machinability of this alloy in the milling with tools of round inserts, a method was developed to define the machinability of this alloy. This procedure is based on the analysis of the bibliographic compilation in chapter 2. Considering these results, it was observed that the most adequate procedure to evaluate the machinability consists of several criteria, which are presented in Table 22.

These criteria have a recommended sequence, which is based on obtaining results that can be easily compared with the ones obtained by this and other research. In addition, the proposed procedure uses two phases of analysis that allow the development of an experimental stage of 12 initial tests (Taguchi DOE L4) that gives a perception of the behavior of the cutting insert before executing a more extensive experimental stage (section 3.4).

The factors of analysis (characteristics of the tools and cutting parameters) and their respective levels were defined considering the parameters and ranges that, in the study of Chapter 2, were observed to be the most representative. A broad description of the selection process is detailed in section 3.3.

The results obtained from this procedure for the evaluation of the machinability are mainly oriented to answer two of the main questions that are formulated at the beginning of any machining work with cutting inserts that are:

Which material and edge geometry of the cutting insert should be selected? and

Which range of cutting parameters can be used?

In the case of this research, the generic question about the selection of the characteristics of the cutting insert is complemented with the need to obtain a good surface quality. This is because for TiAl the biggest drawback is obtaining acceptable levels of surface integrity.

Table 22. Procedure for Assessing Machinability

Execution Sequence	Procedure	Description
1	General Specimens Preparation	EDWM cutting of specimens for mechanical tensile tests, microstructural and for milling tests
2	Material Properties Assessment	Evaluation of mechanical properties and characterization of the workpiece material
3	First phase of testing	Execution of milling test for each cutting insert using DOE Taguchi L4
4	Cutting Force Assessment	Measurement of cutting forces during the first stage of tests
5	Surface finish Assessment	Measurement of surface roughness, defects control, topographic survey of machined surfaces
6	Machined Specimens Preparation	Selection and cutting of specimens for micro-hardening tests by EDWM
7	Surface Integrity Assessment	Measurement of surface hardness and definition of microhardness profile
8	Analysis of cutting insert performance	Analysis of the results, and selection of the insert and cutting parameters for evaluation of chip formation and second evaluation phase
9	Turning Specimens Preparation	Preparation of material for machining tests turning of specimen with low cutting parameters
10	Chip formation Assessment	Observation of the chip formation process with selected inserts using recommended cutting parameters first stage analysis
11	Cutting Force	Measurement of cutting forces during the turning process
12	Analysis of cutting insert performance	Analysis of the results, definition of the performance of the inserts, and selection of the tool for the second evaluation phase
13	Second test stage	of milling test for each cutting insert using DOE Taguchi L16
14	Cutting Force	Measurement of cutting forces during the second stage of milling tests
15	Surface finish	Measurement of Surface Roughness, defects control, topographic survey of machined surfaces
16	Machined Specimens Preparation	Selection and cutting of specimens for micro-hardening tests by EDWM
17	Surface Integrity	Measurement of surface hardness and definition of microhardness profile
18	Analysis of cutting insert performance	Analysis of the results, definition of the performance of the insert.

2. What type of round cutting inserts are best suited for finishing operations when milling a Ti-48Al-2Nb-0,7Cr-0,3Si alloy?

Contrary to what was expected at the beginning of this research, defining a simple answer to this question was very complicated, due to the variation that the results presented as a function of the combination between edge geometry and insert material.

The first step in answering this question is to define the concept of surface quality in TiAl. As studied in chapter 2, surface integrity and cutting forces are the main analyzed factors.

Regarding surface integrity, several studies propose that a surface with good properties for this type of alloy should have an average surface roughness value R_a of $0.4 \mu\text{m}$ and a surface hardened layer that is as thin and as hard as possible. While from the perspective of cutting forces keeping low values benefits the service life of the cutting edges.

In general terms, from the perspective of the composition, it was observed that, although the compositions with lower content of cobalt and smaller WC grains presented a greater resistance and durability to wear, they were not always the best solution in terms of surface integrity. It was also evident that in most cases, the best geometry of the cutting edge was the T-Land (XL), which would be related to the greater resistance of the cutting edge provided by the negative geometry of the tip of the edge.

For a better definition of the answer, it is necessary to present the conclusions of the analysis of the most influential criteria.

a. Cutting Forces

The inserts that presented lower cutting forces were the S10-XL and the S25-XM, because its greater hardness provides better resistance to the cutting edge to the effect of the abrasive wear caused by these alloys. However, it was expected that XL geometry would cause greater forces due to its negative rake face angle, this performance was only observed on the S25 material.

This allows concluding that in the case of milling with round inserts, the presence of a negative angle in combination with a harder material would tend to extend the insert

life time. However, it is important to note that this behavior is strongly linked to the range of cutting parameters used, since as it could be observed in the measurement of the cutting forces both in milling and turning, the behavior of the inserts S10-XL and S25-XM is similar to V_c below 45 m/min.

b. Surface Integrity

Surface integrity is undoubtedly the most important parameter to evaluate in the machining of TiAl, mainly due to the field of application of these alloys.

In the case of roughness, it is important to note that all the inserts managed to reach average values below 0.2 μm , which comparatively with other research works are promising values. However, it is important to consider that the machining distance was relatively short. The S10-XL insert had the lowest roughness value (Figure 133.a), which would be related to the hardness of the insert material and the negative rake angle of the cutting edge. This better performance could be caused by the increase in the cutting temperature, which raises the ductility of the material. This phenomenon would not occur in the same way in materials S25 and S30 due to the lower hardness of these inserts.

In the case of the surface hardened layer, the observed results in the Figure 133.b showed that an insert with less hardness, such as S30, causes a lower hardness increase, and that the geometry of the negative edge (XL) is the one which causes lower hardness. This could be related with the temperature enhancement as an effect of the negative rake face angle. This phenomenon is directly related to the lower lamellar deformation that this geometry presents.

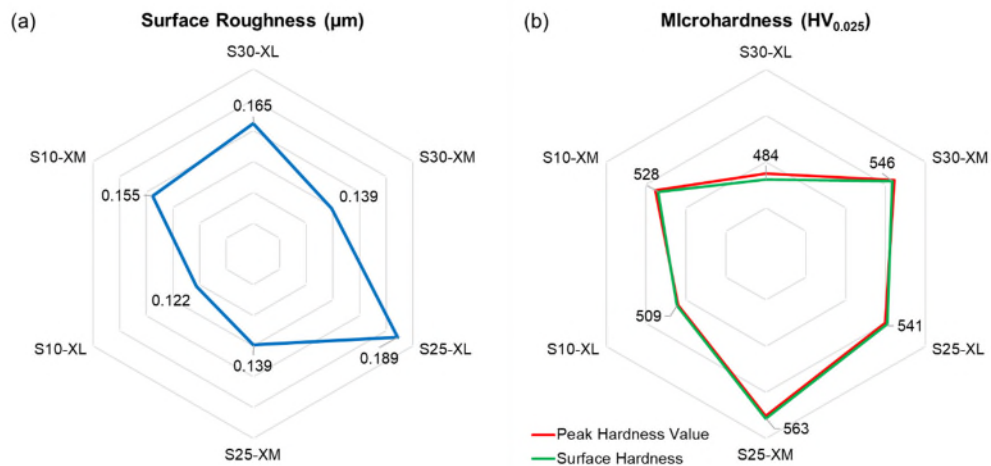


Figure 133. Radar graph: (a) surfaces roughness, and (b) surface microhardness and peak value of microhardness profile.

The overall conclusion from the perspective of surface integrity is that the inserts that caused the least changes in the surface topography (roughness) were the S10-XL and S25-XM, while in the case of the sub-surface alterations were the S30-XL and the S10-XL.

As mentioned at the beginning, the answer to this question does not have a simple or unique solution, due to the insert's performance. It was defined to present the three inserts with better performance and define their capabilities.

The insert that in general terms showed the best performance was the S10-XL, which mainly stands out for getting surfaces with less roughness, which are related to the greater wear resistance of its cutting edge, although this causes greater subsurface alterations.

A second alternative to this insert would be the S25-XM, which, according to the analysis of the cutting forces, would have a wear resistance similar to S10-XL. In the same way, it showed a tendency to produce surfaces with good roughness values, although with high surface and subsurface hardening values. The main drawback presented by this insert was in the turning tests, where it showed that its wear resistance is lower than the S10-XL.

A final option that exhibited good roughness values and surface and subsurface hardening was the S30-XL insert. This tool exhibited a good performance in the machining of this alloy. Its main drawback being its high sensitivity to the variation of the cutting speed, which limits productivity.

3. What range of cutting parameters should be used in finishing operations when milling a Ti-48Al-2Nb-0,7Cr-0,3Si alloy with interchangeable round insert tools?

Before answering this question, it must be understood that a range of cutting parameters can be specified, only after defining the cutting insert to be used and the required integrity requirements. In the case of this work, the inserts and requirements were considered as a solution to the second question.

The answer to this question was addressed from two different perspectives. The first one defines a specific range for each insert proposed, and the second determines a common range for all the inserts that were presented as viable. The answer is presented

according to each of the inserts considered and from the perspective of the conducted experimental design.

a. S10-XL

As far as this insert is concerned, a more extensive investigation was carried out than with the other inserts. This was due to the performance shown in the machining of the trials of the first phase of experimentation. The conducted tests allowed to analyze in more detail the effect of the cutting parameters and to define a range of suitable parameters. The results of the ANOVA analysis (Table 23) show that for the subsurface integrity and cutting forces, the most significant factors were the chip thickness and the cutting speed. Due to this, these will be the factors that most influence the selection of the range of cutting parameters.

Table 23. Percentage contribution ratio (PCR) of cutting parameters in evaluation criteria.

Source	Resultant Force PCR (%)	Roughness Ra PCR (%)	Surface Hardness PCR (%)
Vc	66.43%	5.60 %	33.27%
hex	13.11%	46.78 %	15.23%
ap	7.38%	9.95 %	16.42%
Error	13.09%	37.68 %	35.07%

As seen in Figure 134, the ideal cutting parameter range in terms of surface integrity and cutting forces is a V_c of 20 m/min, a h_{ex} of 0.02 mm and an a_p of 0.5 mm. This promotes low roughness surfaces, surface hardness and low loads on the cutting edge, which would result in a longer lifetime of the inserts.

However, this cut condition, although it would achieve parts with good quality, the productivity would be limited to a Material Removal Rate (MRR) of 131.5 mm³/min. Considering that, the round geometry of the insert has been shown to produce surfaces with low Ra and less than 0.2 μm, and surface hardness variation that does not exceed 10%. The nominal range for this insert would be a Vc of 70 m/min, hex between 0.03 and 0.04 mm and ap of 0.5 mm, which would have an MRR between 690 and 920 mm³/min, which is a level of productivity 7 times greater with an adequate surface integrity.

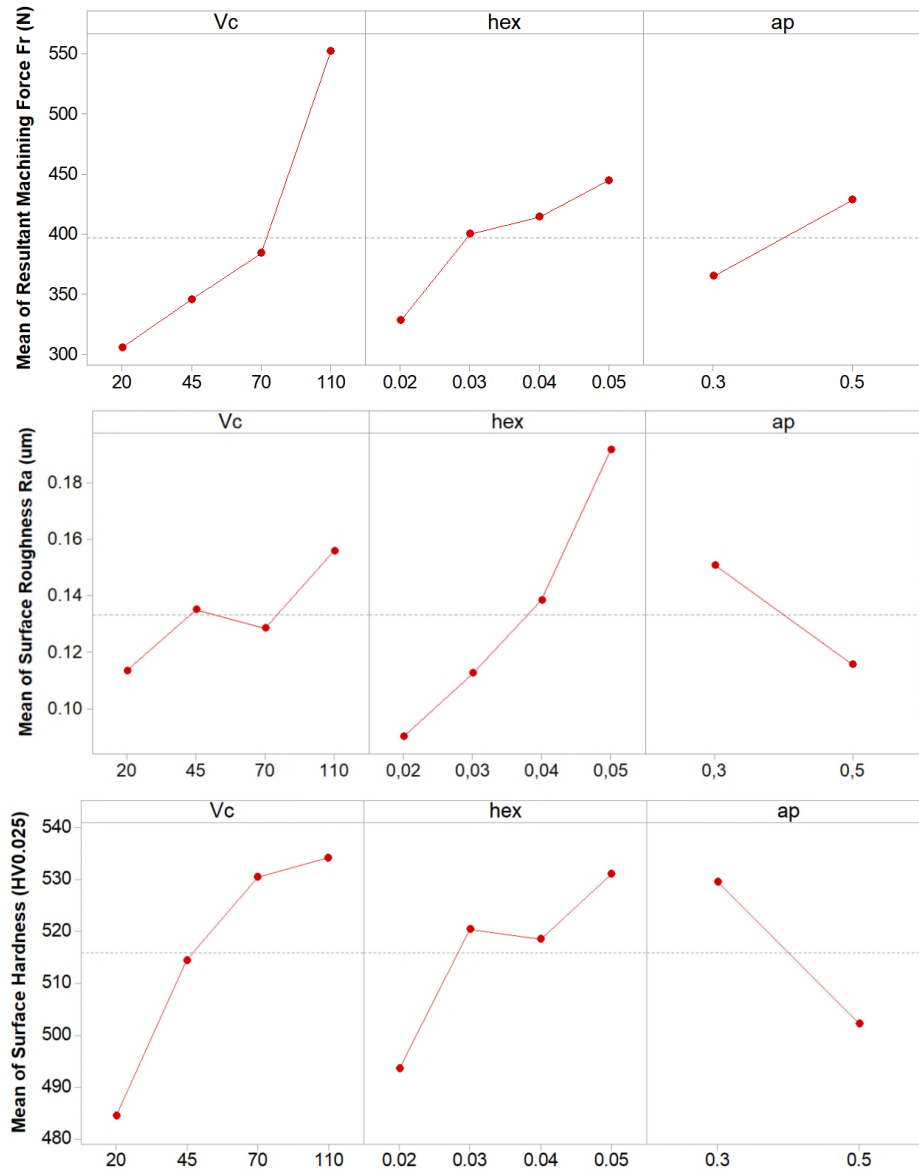


Figure 134. Main effects plot-means for; (a) resultant machining forces Fr, (b) surface roughness Ra, and (c) Surface hardness.

b. S25-XM

The range of defined cutting parameters for the S25-XM inserts are nominal values derived from the information obtained in the first phase of tests. As seen in Figure 135, the alteration of the cutting parameters mainly affects the resulting cutting force and surface roughness. Considering these effects, it is defined that the suitable working range would be $V_c = 70$ m/min, $h_{ex} = 0.03$ mm and $a_p = 0.3$ mm.

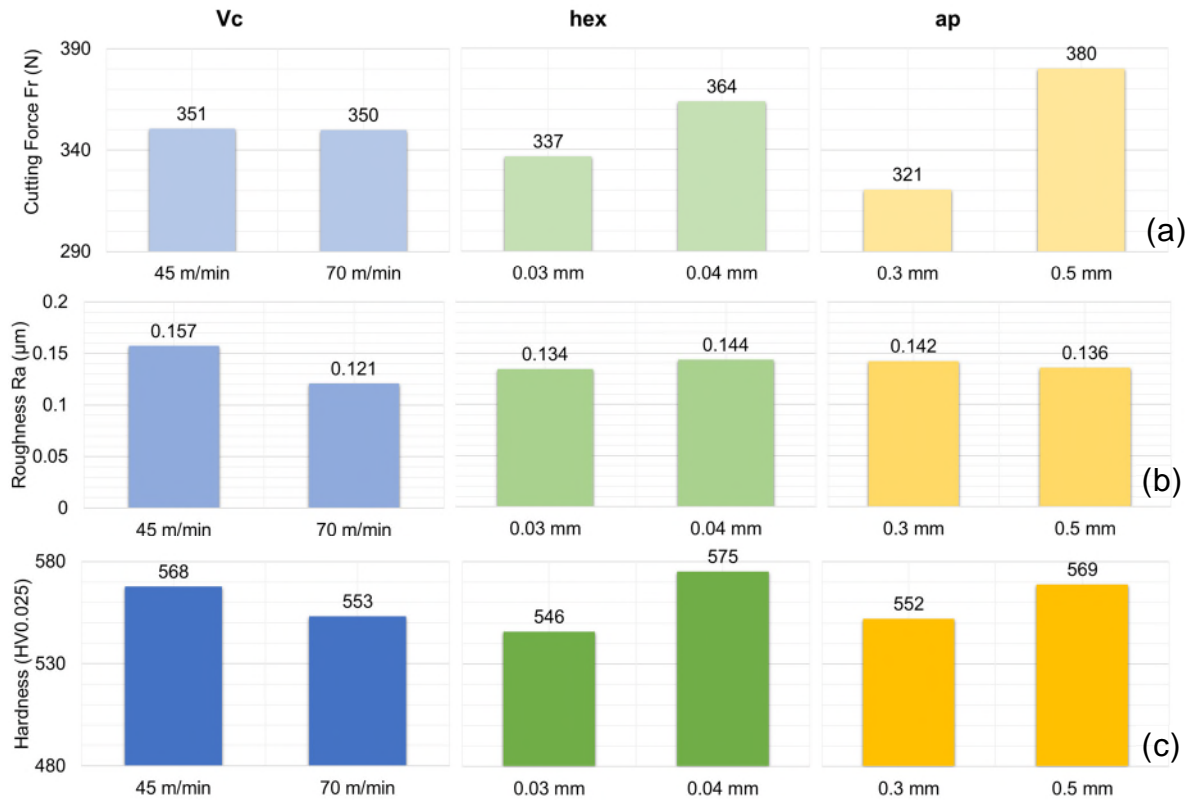


Figure 135. Effect of cutting speed, chip thickness and axial depth of cut with an S25-XM cutting insert on the; (a) Cutting force Fr, (b) Surface roughness Ra, and (c) Surface hardness.

c. S30-XL

As seen in Figure 136, the S30-XL inserts proved to be very sensitive to the increase in the cutting parameters, mainly affecting the cutting forces, which leads to rapid wear of the cutting edge and consequent deterioration of the machined surface. However, as seen in Figure 136.b and Figure 136.c, these ranges are also capable of producing surfaces with good integrity levels. Considering that a short life time is a factor that would significantly limit the performance of the cutting tool, it was defined that the appropriate configuration for this type of insert would be $V_c = 45$ m/min, $h_{ex} = 0.03$ mm and $a_p = 0.3$ mm.

In general terms, a chip thickness between 0.03 and 0.04 mm, a cutting depth of 0.3 mm and a cutting speed of 70 m/min are a range of nominal cutting parameters to produce surfaces with suitable finishing when milling with round inserts. However, it is important to define that these parameters are reference values, which can be affected by the size of the insert.

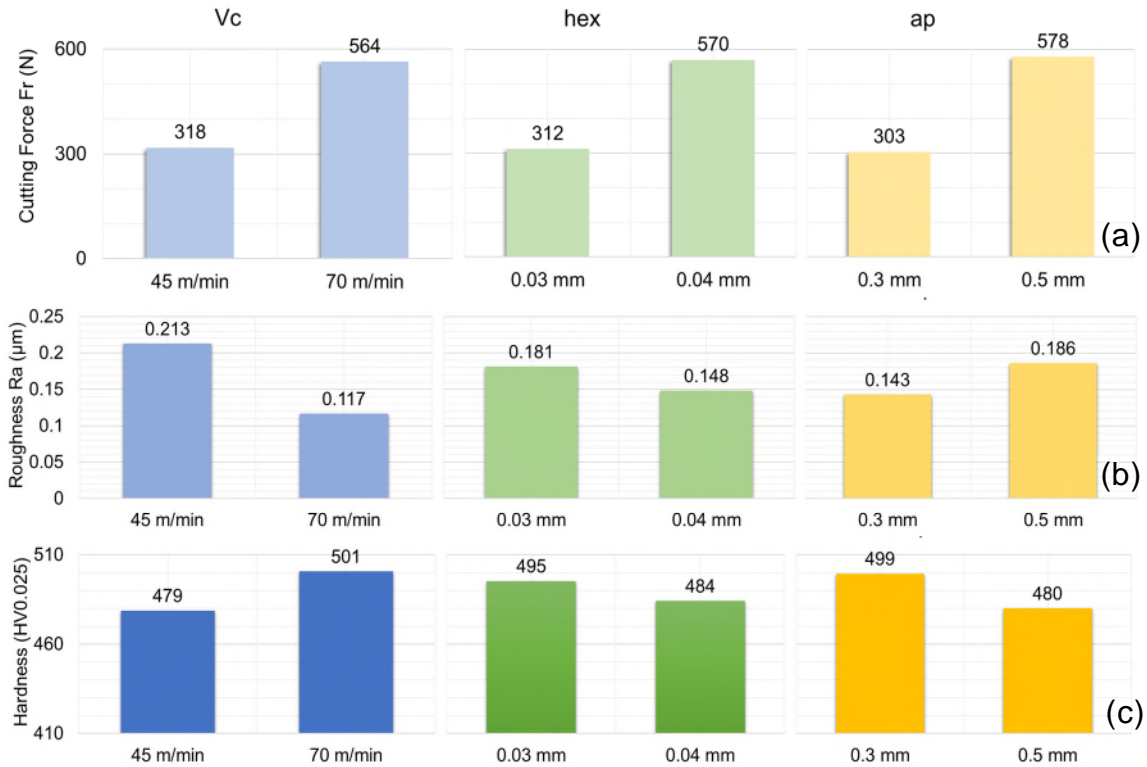


Figure 136. Effect of cutting speed, chip thickness and axial depth of cut with a S25-XM cutting insert on the; (a) Cutting force Fr, (b) Surface roughness Ra, and (c) Surface hardness.

5.3. Major Contributions

The present research work was conducted in order to achieve a deeper vision of the machinability of TiAl, mainly in the milling of surfaces with round inserts. In this thesis the following aspects have been successfully addressed.

- An experimental program has been established that involves several criteria of evaluation of the machinability that allow selecting a cutting tool and defining the adequate range of work in function of the surface integrity required for a Ti-48Al-2Nb-0.7Cr-0.3Si alloy.
- The effect of the cutting parameters and the characteristics of the round inserts on the cutting forces, surface roughness Ra and characteristics of the surface hardened layer in the milling of this alloy have been determined.
- A machinability study of a Ti-48Al-2Nb-0.7Cr-0.3Si alloy is presented for the first time using five evaluation criteria.

- It has been demonstrated that round interchangeable inserts cutting tools have great potential to achieve finished surfaces that meet some of the standards required by the aeronautical sector.

Due to this, the information obtained from this research would have an importance for the academic fields and the industries involved in machining TiAl.

5.4. Future Work

The doctoral thesis presented here aims to open different paths for future work related to this area of research, some of which could probably be done in the following areas:

Evaluation of the machinability of the Ti-48Al-2Nb-0.7Cr-0.3Si alloy with samples subjected to thermal treatments of HIP (Hot Isostatic Pressuring).

Study the machinability of a Ti-48Al-2Nb-0.7Cr-0.3Si alloy during the machining of sculpted surfaces with toroidal tools of interchangeable inserts.

Application of the machinability assessment methodology in a Ti-48Al-2Cr-2Nb alloy, to define the performance of the cutting tools, as well as the effect of their characteristics and definition of cutting parameters.

Application of the machinability evaluation methodology in the same alloy (Ti-48Al-2Nb-0.7Cr-0.3Si) with interchangeable inserts cutting tools with different geometries.

Use of different materials of more advanced cutting tools such as ceramic materials and CBN (Cubic Boron Nitride).

5.5. Publications

S. Castellanos and J. L. Alves, “A Review of Milling of Gamma Titanium Aluminides,” *U.Porto J. Eng.*, vol. 3, no. 2, pp. 1–9, Mar. 2018.

S. Castellanos, A. Cavaleiro, A. de Jesus, R. Neto, and J. L. Alves, “Machinability of titanium aluminides: A review,” *Proc. Inst. Mech. Eng. Part L J. Mater. Des. Appl.*, p. 146442071880938, Nov. 2018.

S. D. Castellanos, J. Lino Alves, R. Neto, and A. Cavaleiro, “The Effect of Machining on Surface Integrity of Gamma Titanium Aluminides Using Different Cemented Carbide Tools,” Springer, Cham, 2019, pp. 363–384.

S. D. Castellanos, J. L. Alves, and R. J. Neto, “A comparative study of manufacturing processes of complex surface parts in Titanium Ti6Al4V,” *Ciência Tecnol. dos Mater.*, vol. 29, no. 2, pp. 73–78, May 2017.

L. Amaral, R. Quinta, T. E. Silva, R. M. Soares, S. D. Castellanos, and A. M. de Jesus, “Effect of lead on the machinability of brass alloys using polycrystalline diamond cutting tools,” *J. Strain Anal. Eng. Des.*, vol. 53, no. 8, pp. 602–615, Nov. 2018.

K. Castro, L. J. Segura, S. D. Castellanos, and J. L. Alves, “Optimization of Geometric Quality in a 5 Axis Machining of Curved Surfaces in a EN-AW-7075 Alloy by Taguchi Method,” Springer, Cham, 2017, pp. 347–360.

References

- [1] F.H. Froes, *Titanium : Physical Metallurgy, Processing, and Applications*, 1st ed. Ohio: ASM International.
- [2] F. Appel, J. D. Paul, and M. Oehring, *Gamma Titanium Aluminide Alloys Science and Technology*. Weinheim: Wiley-VCH, 2011.
- [3] E. A. Loria, “Quo vadis gamma titanium aluminide,” vol. 9, pp. 997–1001, 2001.
- [4] MTU Aero Engines AG Corporate Communications and Public Affairs, “Titanium aluminide - MTU Aero Engines develops new turbine blade material,” 2017. [Online]. Available: http://www.mtu.de/fileadmin/EN/7_News_Media/1_Press/3_Press_kits/Paris_Air_Show_2017/Backgrounder/Titanaluminid_en.2017.final.docx. [Accessed: 12-Jun-2018].
- [5] E. O. Ezugwu, J. Bonney, and Y. Yamane, “An overview of the machinability of aeroengine alloys,” *J. Mater. Process. Technol.*, vol. 134, no. 2, pp. 233–253, 2003.
- [6] F. Appel, H. Clemens, and F. D. Fischer, “Modeling concepts for intermetallic titanium aluminides,” *Prog. Mater. Sci.*, vol. 81, pp. 55–124, 2016.
- [7] M. Allen and V. Güther, “Production of TiAl alloys,” in *Titanium Europe 2018 Sevilla Conference Proceeding*, 2018.
- [8] B. P. Bewlay, S. Nag, A. Suzuki, and M. J. Weimer, “TiAl alloys in commercial aircraft engines,” *Mater. High Temp.*, vol. 33, no. 4–5, pp. 549–559, 2016.
- [9] H. Clemens and S. Mayer, “Design, processing, microstructure, properties, and applications of advanced intermetallic TiAl alloys,” *Adv. Eng. Mater.*, vol. 15, no. 4, pp. 191–215, 2013.
- [10] H. Clemens and S. Mayer, “Intermetallic titanium aluminides in aerospace applications – processing , microstructure and properties,” *Mater. High Temp.*, vol. 33, no. 4–5, pp. 560–570, 2016.
- [11] M. Allen, V. Güther, and G. Metalle, “Production of TiAl alloys,” in *TITANIUM EUROPE 2018 CONFERENCE PROCEEDINGS*, 2018, p. 26.
- [12] M. Pike, “Titanium Demand and Trends in the Commercial Aero Engine Market,” in *TITANIUM EUROPE 2018 - SEVILLE CONFERENCE PROCEEDINGS*, 2018, p. 21.
- [13] K. J. Cain, “Industrial Titanium Demand Forecast,” in *Titanium Europe 2018 Sevilla Conference Proceeding*, 2018.
- [14] F. Appel, M. Oehring, and J. D. H. Paul, “Physical Metallurgy and Performance of the TNB and γ -Md Alloys,” Y.-W. Kim, W. Smarsly, J. Lin, D. Dimiduk, and F. Appel, Eds. New Jersey: Wiley, 2014, pp. 9–20.
- [15] CORDIS European Commision, “MMTech New aerospace advanced cost effective materials and rapid manufacturing technologies,” 2017. [Online]. Available: https://cordis.europa.eu/result/rcn/196469_en.html. [Accessed: 25-Jun-2017].

References

- [16] CORDIS European Commission, “DATACAST- Development of a low cost Advanced gamma Titanium Aluminide Casting Technology.” [Online]. Available: https://cordis.europa.eu/result/rcn/178111_en.html. [Accessed: 25-Jun-2017].
- [17] CORDIS European Commission, “LIVALVES Report Summary High efficient production of TiAl valve blanks,” *Light weight valves for high efficient engines (LIVALVES)*, 2005. [Online]. Available: https://cordis.europa.eu/project/rcn/52097_en.html. [Accessed: 09-Jan-2018].
- [18] N. E. Prasad and R. J. H. Wanhill, *Aerospace Materials and Material Technologies*, vol. 1. Singapore: Springer Science+Business Media, 2017.
- [19] A. Lasalmonie, “Intermetallics: Why is it so difficult to introduce them in gas turbine engines?,” *Intermetallics*, vol. 14, pp. 1123–1129, 2006.
- [20] M. Mathes, “Four approaches for TiAl LPT-Blade production Four approaches for TiAl LPT-Blade production 1 LPT-Blade 4 approaches,” in *TITANIUM EUROPE 2018 - SEVILLE CONFERENCE PROCEEDINGS*, 2018, p. 25.
- [21] S. D. Castellanos, J. L. Alves, and R. J. Neto, “A comparative study of manufacturing processes of complex surface parts in Titanium Ti6Al4V,” *Cienc. e Tecnol. dos Mater.*, vol. 29, no. 2, pp. 73–78, 2017.
- [22] F. Appel and R. Wagner, “Intermetallics: Titanium Aluminides,” in *Encyclopedia of Materials: Science and Technology*, Elsevier, 2001, pp. 4246–4264.
- [23] G. Radkowski and J. Sep, “Surface Quality of a Milled Gamma Titanium Aluminide for Aeronautical Applications,” *Manag. Prod. Eng. Rev.*, vol. 5, no. 2, pp. 60–65, 2014.
- [24] R. G. Vargas Pérez, “Wear mechanisms of WC inserts in face milling of gamma titanium aluminides,” *Wear*, vol. 259, no. 7–12, pp. 1160–1167, 2005.
- [25] G. Lütjering and J. C. Williams, *Titanium*, Second. Berlin: Springer, 2007.
- [26] C. Leyens and M. Peters, *Titanium and Titanium Alloys. Fundamentals and Applications*, 1st ed. we: Wiley-VCH, 2003.
- [27] D. M. Dimiduk, “Gamma titanium aluminide alloys—an assessment within the competition of aerospace structural materials,” *Mater. Sci. Eng. A*, vol. 263, no. 2, pp. 281–288, 1999.
- [28] S. C. Deevi and W. J. Zhang, “Intermetallics: Applications,” in *Encyclopedia of Materials: Science and Technology*, Elsevier, 2001, pp. 4165–4173.
- [29] X. Wu, “Review of alloy and process development of TiAl alloys,” *Intermetallics*, vol. 14, no. 10–11, pp. 1114–1122, 2006.
- [30] P. Janschek, “Wrought TiAl Blades,” in *Materials Today: Proceedings*, 2015, vol. 2, pp. S92–S97.
- [31] K. Gebauer, “Performance, tolerance and cost of TiAl passenger car valves,” *Intermetallics*, vol. 14, no. 4, pp. 355–360, 2006.
- [32] T. Noda, “Application of cast gamma TiAl for automobiles,” *Intermetallics*, vol. 6, no. 7–8, pp. 709–713, 1998.

-
- [33] S. Biamino, B. Klöden, T. Weißgärber, B. Kieback, and U. Ackelid, “Properties of a TiAl Turbocharger Wheel Produced by Electron Beam Melting,” in *DDMC 2014 Fraunhofer Direct Digital Manufacturing Conference*, p. 4.
- [34] C. Cui, B. Hu, L. Zhao, and S. Liu, “Titanium alloy production technology, market prospects and industry development,” *Mater. Des.*, vol. 32, no. 3, pp. 1684–1691, 2011.
- [35] H. Clemens and S. Mayer, “Development Status , Applications and Perspectives of Advanced Intermetallic Titanium Aluminides,” *Mater. Sci. Forum*, vol. 786, pp. 15–20, 2014.
- [36] Y. Chen, Y. Chen, F. Kong, and S. Xiao, “Fabrication and processing of gamma titanium aluminides — a review,” vol. 642, pp. 1281–1287, 2010.
- [37] International Titanium Association, “Titanium — The Infinite Choice,” *Int. Titan. Assoc. Educ. Comm.*, p. 24, 2011.
- [38] J. Lapin, “TiAl-based alloys: present status and future perspectives,” in *METAL 2009*, 2009, pp. 1–12.
- [39] H. Clemens and W. Smarsly, “Light-Weight Intermetallic Titanium Aluminides – Status of Research and Development,” *Adv. Mater. Res.*, vol. 278, pp. 551–556, 2011.
- [40] S. L. Draper *et al.*, “Development and evaluation of TiAl sheet structures for hypersonic applications,” *Mater. Sci. Eng. A*, vol. 464, no. 1–2, pp. 330–342, 2007.
- [41] H. Clemens and H. Kestler, “Processing and Applications of Intermetallic γ -TiAl-Based Alloys,” *Adv. Eng. Mater.*, vol. 2, no. 9, pp. 551–570, 2000.
- [42] G. Baudana *et al.*, “Titanium aluminides for aerospace and automotive applications processed by Electron Beam Melting: Contribution of Politecnico di Torino,” *Met. Powder Rep.*, vol. 71, no. 3, pp. 193–199, 2016.
- [43] Helmholtz-Zentrum Geesthacht Zentrum für Material- und Küstenforschung, “ γ -TiAl alloys,” *Institute of Material Research*, 2017. .
- [44] K. Weinert, S. Bergmann, and C. Kempmann, “Machining sequence to manufacture a γ -TiAl-conrod for application in combustion engines,” *Adv. Eng. Mater.*, vol. 8, no. 1–2, pp. 41–47, 2006.
- [45] M. Bünck, T. Stoyanov, J. Schievenbusch, H. Michels, and A. Gußfeld, “Titanium Aluminide Casting Technology Development,” *JOM*, vol. 69, no. 12, pp. 2565–2570, Dec. 2017.
- [46] M. J. Donachie, *Titanium: A Technical Guide*, 2nd ed. Ohio: ASM International, 2000.
- [47] K. Kothari, R. Radhakrishnan, and N. M. Wereley, “Advances in gamma titanium aluminides and their manufacturing techniques,” *Prog. Aerosp. Sci.*, vol. 55, pp. 1–16, 2012.
- [48] R. Boyer, G. Welsch, and E. W. Collings, *Materials Properties Handbook: Titanium Alloys*, First. Materials Park: ASM International, 1994.
- [49] E. P. George, M. Yamaguchi, K. S. Kumar, and C. T. Liu, “Ordered Intermetallics,”
-

References

- Annu. Rev. Mater. Sci.*, vol. 24, no. 1, pp. 409–451, 1994.
- [50] Y.-W. Kim, W. Smarsly, J. Lin, D. M. Dimiduk, and F. Appel, *Gamma Titanium Aluminide Alloys 2014*, 1st ed. New Jersey: Wiley, 2014.
- [51] C. Mccullough, J. J. Valencia, C. G. Levi, and R. Mehrabian, “Phase Equilibria and Solidification in TiAl alloys,” *Acta Metall.*, vol. 37, no. 5, pp. 1321–1336, 1989.
- [52] A. K. Gogia, “High-temperature titanium alloys,” *Def. Sci. J.*, vol. 55, no. 2, pp. 149–173, 2005.
- [53] W. E. Voice, M. Henderson, E. F. J. Shelton, and X. Wu, “Gamma titanium aluminide, TNB,” *Intermetallics*, vol. 13, no. 9, pp. 959–964, Sep. 2005.
- [54] A. P. Mouritz, *Introduction to aerospace materials*, 1st ed. Cambridge: Woodhead Publishing, 2012.
- [55] J. H. Westbrook and R. L. Fleischer, *Structural applications of intermetallic compounds*, 1st ed. West Sussex: Wiley, 2000.
- [56] S. L. Semiatin, V. Seetharaman, and I. Weiss, “Hot workability of titanium and titanium aluminide alloys—an overview,” *Mater. Sci. Eng. A*, vol. 243, pp. 1–24, 1998.
- [57] E. A. Loria, “Gamma titanium aluminides as prospective structural materials,” vol. 8, pp. 1339–1345, 2000.
- [58] F. Appel, P. Heaton, and M. Oehring, *Nanomaterials for the Life Sciences Intermetallic Compounds Oxide Scale Behavior in High Temperature Metal Processing*. 2011.
- [59] L. Settineri, P. C. Priarone, M. Arft, D. Lung, and T. Stoyanov, “An evaluative approach to correlate machinability, microstructures, and material properties of gamma titanium aluminides,” *CIRP Ann. - Manuf. Technol.*, vol. 63, no. 1, pp. 57–60, 2014.
- [60] J. G. Wang and T. G. Nieh, “Creep of a beta phase-containing TiAl alloy,” *Intermetallics*, vol. 8, no. 7, pp. 737–748, 2000.
- [61] G. Baudana *et al.*, “Ti-48Al-2Nb-2Cr-0.3Si Titanium aluminide for automotive applications processed by Electron Beam Melting,” 2016.
- [62] G. Baudana *et al.*, “Electron Beam Melting of Ti-48Al-2Nb-0.7Cr-0.3Si: Feasibility investigation,” *Intermetallics*, vol. 73, pp. 43–49, 2016.
- [63] Y. Koyanagi, “Development of new Gamma TiAl for turbocharger application Daido Steel Co.” 2008.
- [64] ASM International, *ASM Handbook: Machining*, 9th ed. Ohio: ASM International, 1989.
- [65] W. Grzesik, *Advanced Machining Processes of Metallic Materials*, 2nd ed. Amsterdam: Elsevier, 2016.
- [66] D. A. Stephenson and J. S. Agapiou, *Metal Cutting Theory and Practice*, 3rd ed. Boca Raton: Taylor & Francis Group, 2016.
- [67] A. R. C. Sharman, D. K. Aspinwall, R. C. Dewes, and P. Bowen, “Workpiece

- surface integrity considerations when finish turning gamma titanium aluminide,” *Wear*, vol. 249, no. 5–6, pp. 473–481, 2001.
- [68] S. Kolahdouz, M. Hadi, B. Arezoo, and S. Zamani, “Investigation of Surface Integrity in High Speed Milling of Gamma Titanium Aluminide under Dry and Minimum Quantity Lubricant Conditions,” *Procedia CIRP*, vol. 26, pp. 367–372, 2015.
- [69] A. L. Mantle and D. K. Aspinwall, “Surface integrity of a high speed milled gamma titanium aluminide,” *J. Mater. Process. Technol.*, vol. 118, no. 1–3, pp. 143–150, 2001.
- [70] A. R. C. Sharman, D. K. Aspinwall, R. C. Dewes, D. Clifton, and P. Bowen, “The effects of machined workpiece surface integrity on the fatigue life of γ -titanium aluminide,” *Int. J. Mach. Tools Manuf.*, vol. 41, no. 11, pp. 1681–1685, 2001.
- [71] A. L. Mantle and D. K. Aspinwall, “Surface integrity and fatigue life of turned gamma titanium aluminide,” *J. Mater. Process. Technol.*, vol. 72, no. 3, pp. 413–420, 1997.
- [72] E. Uhlmann and S. Herter, “Studies on conventional cutting of intermetallic nickel and titanium aluminides,” *Proc. Inst. Mech. Eng. Part B J. Eng. Manuf.*, vol. 220, no. 9, pp. 1391–1398, 2006.
- [73] E. Uhlmann, S. Herter, R. Gerstenberger, and M. Roeder, “Quasi-static chip formation of intermetallic titanium aluminides,” *Prod. Eng.*, vol. 3, no. 3, pp. 261–270, 2009.
- [74] S. Sun, M. Brandt, and M. S. Dargusch, “Characteristics of cutting forces and chip formation in machining of titanium alloys,” *Int. J. Mach. Tools Manuf.*, vol. 49, no. 7–8, pp. 561–568, 2009.
- [75] A. Beranoagirre and L. N. López de Lacalle, “Grinding of gamma TiAl intermetallic alloys,” *Procedia Eng.*, vol. 63, pp. 489–498, 2013.
- [76] N. T. Mathew and L. Vijayaraghavan, “Environmentally friendly drilling of intermetallic titanium aluminide at different aspect ratio,” *J. Clean. Prod.*, vol. 141, pp. 439–452, 2017.
- [77] M. E. Merchant, “Mechanics of the metal cutting process. I. Orthogonal cutting and a type 2 chip,” *J. Appl. Phys.*, vol. 16, no. 5, pp. 267–275, 1945.
- [78] E. Uhlmann and S. Herter, “Studies on conventional cutting of intermetallic nickel and titanium aluminides,” *Proc. Inst. Mech. Eng. Part B J. Eng. Manuf.*, vol. 220, no. 9, pp. 1391–1398, Sep. 2006.
- [79] A. L. Mantle and D. K. Aspinwall, “Cutting Force Evaluation when High Speed End Milling a Gamma Titanium Aluminide Intermetallic Alloy,” in *Intermetallics and Superalloys*, D. G. Morris, S. Naka, and P. Caron, Eds. Weinheim: WILEY-VCH Verlag GmbH, 2000, pp. 209–215.
- [80] F. Klocke, L. Settineri, D. Lung, P. C. Priarone, and M. Arft, “High performance cutting of gamma titanium aluminides: Influence of lubricoolant strategy on tool wear and surface integrity,” *Wear*, vol. 302, no. 1–2, pp. 1136–1144, 2013.
- [81] P. C. Priarone, S. Rizzuti, G. Rotella, and L. Settineri, “Tool wear and surface

- quality in milling of a gamma-TiAl intermetallic,” *Int. J. Adv. Manuf. Technol.*, vol. 61, no. 1–4, pp. 25–33, 2012.
- [82] P. C. Priarone, M. Robiglio, L. Settineri, and V. Tebaldo, “Milling and Turning of Titanium Aluminides by Using Minimum Quantity Lubrication,” *Procedia CIRP*, vol. 24, no. Mic, pp. 62–67, 2014.
- [83] R. Ivester, E. Whinton, J. Hershman, and K. Chou, “Analysis of Orthogonal Cutting Experiments Using Diamond-Coated Tools with Force and Temperature Measurements.”
- [84] D. K. Aspinwall, A. L. Mantle, W. K. Chan, R. Hood, and S. L. Soo, “Cutting temperatures when ball nose end milling γ -TiAl intermetallic alloys,” *CIRP Ann. - Manuf. Technol.*, vol. 62, no. 1, pp. 75–78, 2013.
- [85] L. Zhu, X. Chen, and B. Viehweger, “Experimental study on deep hole drilling gamma titanium aluminide,” *Key Eng. Mater.*, vol. 455, pp. 293–296, 2011.
- [86] N. Khanna and J. P. Davim, “Design-of-experiments application in machining titanium alloys for aerospace structural components,” *Meas. J. Int. Meas. Confed.*, vol. 61, pp. 280–290, 2015.
- [87] J. Lindemann, M. Glavatskikh, and C. Leyens, “Surface Effects on the Mechanical Properties of Gamma Titanium Aluminides,” *Mater. Sci. Forum*, vol. 706, pp. 1071–1076, 2012.
- [88] V. M. Imayev, R. M. Imayev, and G. A. Salishchev, “On two stages of brittle-to-ductile transition in TiAl intermetallic,” *Intermetallics*, vol. 8, no. 1, pp. 1–6, 2000.
- [89] P. J. Arrazola, A. Garay, L. M. Iriarte, M. Armendia, S. Marya, and F. Le Maître, “Machinability of titanium alloys (Ti6Al4V and Ti555.3),” *J. Mater. Process. Technol.*, vol. 209, no. 5, pp. 2223–2230, 2009.
- [90] E. O. Ezugwu and Z. M. Wang, “Titanium alloys and their machinability,” *J. Mater. Process. Technol.*, vol. 68, no. 3, pp. 262–274, 1997.
- [91] A. K. Eriki, K. P. Rao, and K. C. Varaprasad, “Machinability Improvement in Turning of Titanium Alloy (gr2) Using Cubic Boron Nitride (cBN) Cutting Tool,” *Appl. Mech. Mater.*, vol. 564, pp. 507–512, 2014.
- [92] S. I. Jaffery and P. T. Mativenga, “Assessment of the machinability of Ti-6Al-4V alloy using the wear map approach,” *Int. J. Adv. Manuf. Technol.*, vol. 40, no. 7–8, pp. 687–696, 2009.
- [93] C. Ohkubo, I. Watanabe, J. P. Ford, H. Nakajima, T. Hosoi, and T. Okabe, “The machinability of cast titanium and Ti-6Al-4V,” *Biomaterials*, vol. 21, no. 4, pp. 421–428, 2000.
- [94] C. R. Dandekar, Y. C. Shin, and J. Barnes, “Machinability improvement of titanium alloy (Ti-6Al-4V) via LAM and hybrid machining,” *Int. J. Mach. Tools Manuf.*, vol. 50, no. 2, pp. 174–182, 2010.
- [95] M. H. Ali, M. N. M. Ansari, B. A. Khidhir, B. Mohamed, and A. A. Oshkour, “Simulation machining of titanium alloy (Ti-6Al-4V) based on the finite element modeling,” *J. Brazilian Soc. Mech. Sci. Eng.*, vol. 36, no. 2, pp. 315–324, 2014.
- [96] S. J. Trail and P. Bowen, “Effects of stress concentrations on the fatigue life of a

- gamma-based titanium aluminide,” *Mater. Sci. Eng. A*, vol. 192–193, pp. 427–434, 1995.
- [97] D. K. Aspinwall, R. C. Dewes, and A. L. Mantle, “The Machining of γ -TiAl Intermetallic Alloys,” *CIRP Ann. - Manuf. Technol.*, vol. 54, no. 1, pp. 99–104, 2005.
- [98] E. Aust and H.-R. Niemann, “Machining of γ -TiAl,” *Adv. Eng. Mater.*, vol. 1, no. 1, pp. 53–57, 1999.
- [99] A. Beranoagirre, D. Olvera, L. N. López De Lacalle, and G. Urbicain, “Drilling of intermetallic alloys gamma tial,” in *AIP Conference Proceedings INTERNATIONAL CONFERENCE ON ADVANCES IN MATERIALS AND PROCESSING TECHNOLOGIES (AMPT2010)*, 2011, vol. 1315, pp. 1023–1028.
- [100] J. F. Kahles, M. Field, D. Eylon, and F. H. Froes, “Machinability and Machining of Titanium Alloys: A Review,” in *Machining of Titanium Alloys*, vol. 1, J. P. Davim, Ed. Berlin: Springer-Verlag Berlin Heidelberg, 2014, pp. 1–30.
- [101] M. Hashish, “AWJ Milling of Gamma Titanium Aluminide,” *J. Manuf. Sci. Eng.*, vol. 132, no. 4, p. 041005, 2010.
- [102] X. Yang and C. R. Liu, “Machining Titanium and Its Alloys,” *Mach. Sci. Technol. An Int. J.*, vol. 3, no. 1, pp. 107–139, 1999.
- [103] J. P. Davim, *Machining of Titanium Alloys*, 1st ed. Berlin: Springer-Verlag Berlin Heidelberg, 2014.
- [104] A. A. Dawood, “A Study on the Sustainable Machining of Titanium Alloy,” Western Kentucky University, 2016.
- [105] F. C. Campbell, *Manufacturing Technology for Aerospace Structural Materials*, First. London: Elsevier Science, 2006.
- [106] A. Pramanik and G. Littlefair, “Machining of Titanium Alloy (Ti-6Al-4V)—Theory to Application,” *Mach. Sci. Technol.*, vol. 19, no. February 2015, pp. 1–49, 2015.
- [107] H. Zhang, M. L. H. Wise, and D. K. Aspinwall, “The Machining of TiAl-Based Intermetallics,” in *Proceedings of the Thirtieth International MATADOR Conference*, 1993, pp. 111–118.
- [108] P. C. Priarone, S. Rizzuti, L. Settineri, and G. Vergnano, “Effects of cutting angle, edge preparation, and nano-structured coating on milling performance of a gamma titanium aluminide,” *J. Mater. Process. Technol.*, vol. 212, no. 12, pp. 2619–2628, 2012.
- [109] A. R. Zareena and S. C. Veldhuis, “Tool wear mechanisms and tool life enhancement in ultra-precision machining of titanium,” *J. Mater. Process. Technol.*, vol. 212, no. 3, pp. 560–570, 2012.
- [110] K. Liu, X. P. Li, and S. Y. Liang, “The mechanism of ductile chip formation in cutting of brittle materials,” *Int. J. Adv. Manuf. Technol.*, vol. 33, no. 9–10, pp. 875–884, 2007.
- [111] R. Hood, F. Lechner, D. K. Aspinwall, and W. Voice, “Creep feed grinding of gamma titanium aluminide and burn resistant titanium alloys using SiC abrasive,”

- Int. J. Mach. Tools Manuf.*, vol. 47, no. 9, pp. 1486–1492, 2007.
- [112] S. . Bentley, N. . Goh, and D. K. Aspinwall, “Reciprocating surface grinding of a gamma titanium aluminide intermetallic alloy,” *J. Mater. Process. Technol.*, vol. 118, no. 1–3, pp. 22–28, Dec. 2001.
- [113] D. Ulutan and T. Ozel, “Machining induced surface integrity in titanium and nickel alloys: A review,” *Int. J. Mach. Tools Manuf.*, vol. 51, no. 3, pp. 250–280, 2011.
- [114] S. A. Bentley, A. L. Mantle, and D. K. Aspinwall, “Effect of machining on the fatigue strength of a gamma titanium aluminide intermetallic alloy,” *Intermetallics*, vol. 7, no. 8, pp. 967–969, 1999.
- [115] S. J. Balsone, J. M. Larsen, D. C. Maxwell, and J. Wayne Jones, “Effects of microstructure and temperature on fatigue crack growth in the TiAl alloy Ti-46.5Al-3Nb-2Cr-0.2W,” *Mater. Sci. Eng. A*, vol. 192–193, no. PART 1, pp. 457–464, Feb. 1995.
- [116] F. Appel, U. Sparka, and R. Wagner, “Work hardening and recovery of gamma base titanium aluminides,” *Intermetallics*, vol. 7, no. 3, pp. 325–334, 1999.
- [117] B. Griffiths, *Manufacturing Surface Technology*. London: Penton Press, 2001.
- [118] I. S. Jawahir *et al.*, “Surface integrity in material removal processes: Recent advances,” *CIRP Ann. - Manuf. Technol.*, vol. 60, pp. 603–626, 2011.
- [119] V. P. Astakhov, “Surface Integrity -- Definition and Importance in Functional Performance,” in *Surface Integrity in Machining*, J. P. Davim, Ed. London: Springer London, 2010, pp. 1–35.
- [120] Y. B. Guo, W. Li, and I. S. Jawahir, “Surface integrity characterization and prediction in machining of hardened and difficult-to-machine alloys: A state-of-art research review and analysis,” *Mach. Sci. Technol.*, vol. 13, no. 4, pp. 437–470, 2009.
- [121] D. Novovic, R. C. Dewes, D. K. Aspinwall, W. Voice, and P. Bowen, “The effect of machined topography and integrity on fatigue life,” *Int. J. Mach. Tools Manuf.*, vol. 44, no. 2–3, pp. 125–134, 2004.
- [122] L. Kandra *et al.*, “Statistical Analysis of Cutting Force, Temperature and Power of FEM Modeling when Machining Titanium Alloy,” *Appl. Mech. Mater.*, vol. 693, pp. 358–363, 2014.
- [123] D. Cui, D. Zhang, B. Wu, and M. Luo, “An investigation of tool temperature in end milling considering the flank wear effect,” *Int. J. Mech. Sci.*, vol. 131–132, no. July, pp. 613–624, 2017.
- [124] P. C. Priarone, F. Klocke, M. G. Faga, D. Lung, and L. Settineri, “Tool life and surface integrity when turning titanium aluminides with PCD tools under conventional wet cutting and cryogenic cooling,” *Int. J. Adv. Manuf. Technol.*, vol. 85, no. 1–4, pp. 807–816, 2016.
- [125] F. Klocke, D. Lung, M. Arft, P. C. Priarone, and L. Settineri, “On high-speed turning of a third-generation gamma titanium aluminide,” *Int. J. Adv. Manuf. Technol.*, vol. 65, no. 1–4, pp. 155–163, 2013.
- [126] A. Beranoagirre, D. Olvera, and L. N. Lopez De Lacalle, “Milling of gamma

- titanium-aluminum alloys,” *Int. J. Adv. Manuf. Technol.*, vol. 62, no. 1–4, pp. 83–88, 2012.
- [127] R. Hood, D. K. Aspinwall, C. Sage, and W. Voice, “High speed ball nose end milling of γ -TiAl alloys,” *Intermetallics*, vol. 32, pp. 284–291, 2013.
- [128] M. T. Nithin, “Drilling of titanium aluminide at different aspect ratio under dry and wet conditions,” *J. Manuf. Process.*, vol. 24, pp. 256–269, 2016.
- [129] V. Tebaldo and M. G. Faga, “Influence of the heat treatment on the microstructure and machinability of titanium aluminides produced by electron beam melting,” *J. Mater. Process. Technol.*, vol. 244, pp. 289–303, 2017.
- [130] R. Hood, D. K. Aspinwall, S. L. Soo, A. L. Mantle, and D. Novovic, “Workpiece surface integrity when slot milling Gamma TiAl intermetallic alloy,” *CIRP Ann. - Manuf. Technol.*, vol. 63, no. 1, pp. 53–56, 2014.
- [131] A. R. C. Sharman, D. K. Aspinwall, R. C. Dewes, and P. Bowen, “Tool Life When Turning Gamma Titanium Aluminide Using Carbide with PCD tools with Reduced Depths of Cut and High Pressure Cutting Fluid,” in *Proc. of the XXVIII NAMRC*, 2000, no. 01, p. 6.
- [132] A. Ginting and M. Nouari, “Surface integrity of dry machined titanium alloys,” *Int. J. Mach. Tools Manuf.*, vol. 49, no. 3–4, pp. 325–332, Mar. 2009.
- [133] C. H. Che-Haron and A. Jawaid, “The effect of machining on surface integrity of titanium alloy Ti–6%Al–4%V,” *J. Mater. Process. Technol.*, vol. 166, no. 2, pp. 188–192, 2005.
- [134] C. M. Lee, W. S. Woo, D. H. Kim, W. J. Oh, and N. S. Oh, “Laser-assisted hybrid processes: A review,” *Int. J. Precis. Eng. Manuf.*, vol. 17, no. 2, pp. 257–267, 2016.
- [135] M. J. Bermingham, W. M. Sim, D. Kent, S. Gardiner, and M. S. Dargusch, “Tool life and wear mechanisms in laser assisted milling Ti-6Al-4V,” *Wear*, vol. 322–323, pp. 151–163, 2015.
- [136] C. Brecher, C.-J. Rosen, and M. Emonts, “Laser-assisted Milling of Advanced Materials,” 2010.
- [137] J. . Kruzic, J. . Campbell, and R. . Ritchie, “On the fatigue behavior of γ -based titanium aluminides: role of small cracks,” *Acta Mater.*, vol. 47, no. 3, pp. 801–816, Feb. 1999.
- [138] P. Crawforth, B. Wynne, S. Turner, and M. Jackson, “Subsurface deformation during precision turning of a near-alpha titanium alloy,” *Scr. Mater.*, vol. 67, no. 10, pp. 842–845, Nov. 2012.
- [139] W. Grzesik, B. Kruszynski, and A. Ruszaj, “Surface Integrity of Machined Surfaces,” in *Surface Integrity in Machining*, J. P. Davim, Ed. London: Springer London, 2010, pp. 143–179.
- [140] R. Hood, “The Machinability of a Gamma Titanium Aluminide Intermetallic,” 2010. [Online]. Available: http://etheses.bham.ac.uk/1380/1/Hood_10_PhD.pdf. [Accessed: 01-Aug-2016].
- [141] G. D. Revankar, R. Shetty, S. S. Rao, and V. N. Gaitonde, “Analysis of surface roughness and hardness in titanium alloy machining with polycrystalline diamond

- tool under different lubricating modes,” *Mater. Res.*, vol. 17, no. 4, pp. 1010–1022, 2014.
- [142] Y. F. Ge, Y. C. Fu, and J. H. Xu, “Experimental Study on High Speed Milling of γ -TiAl Alloy,” *Key Eng. Mater.*, vol. 339, pp. 6–10, 2007.
- [143] T. Goswami, “Fatigue crack growth behavior of Ti–6Al–4V alloy forging,” *Mater. Des.*, vol. 24, no. 6, pp. 423–433, 2003.
- [144] M. Girinon, V. Robin, E. Jourden, F. Valiorgue, J. Rech, and E. Feulvarch, “A Method to Characterize Residual Stresses Induced by Machining,” in *Proceedings of the ASME 2016 Pressure Vessels and Piping Conference*, 2016, pp. 1–6.
- [145] P. J. Withers, M. Turski, L. Edwards, P. J. Bouchard, and D. J. Buttle, “Recent advances in residual stress measurement,” *Int. J. Press. Vessel. Pip.*, vol. 85, no. 3, pp. 118–127, 2008.
- [146] F. Klocke, C. Zeppenfeld, and Z. Nachmani, “Advanced grinding of titanium aluminides,” *Int. J. Manuf. Technol. Manag.*, vol. 12, no. 1/2/3, pp. 60–71, 2007.
- [147] R. Zitoune, V. Krishnaraj, and J. P. Davim, Eds., *Machining of Titanium Alloys and Composites for Aerospace Applications*, First. Durnten-Zurich: Trans Tech Publications, 2013.
- [148] E. Uhlmann, G. Frommeyer, S. Herter, S. Knippscheer, and J. M. Lischka, “Studies on the conventional machining of TiAl based Alloys,” in *Ti-2003 Science and Technology 10th World Conference on Titanium*, 2003, pp. 2239–2300.
- [149] M. Rahman, Z.-G. Wang, and Y.-S. Wong, “A Review on High-Speed Machining of Titanium Alloys *,” *JSME Int. J.*, vol. 49, no. 1, pp. 11–20, 2006.
- [150] N. T. Mathew and L. Vijayaraghavan, “High-Throughput Dry Drilling of Titanium Aluminide,” *Mater. Manuf. Process.*, vol. 32, no. August, pp. 199–208, 2017.
- [151] M. Rahman, Z.-G. Wang, and Y.-S. Wong, “A review on High-Speed machining of Titanium Alloys,” *JSME Int. J.*, vol. 49, no. 1, pp. 11–20, 2006.
- [152] J. García, V. Collado Ciprés, A. Blomqvist, and B. Kaplan, “Cemented carbide microstructures: a review,” *Int. J. Refract. Met. Hard Mater.*, vol. 80, pp. 40–68, Apr. 2019.
- [153] F. Klocke, *Manufacturing Processes 1*. Berlin, Heidelberg: Springer Berlin Heidelberg, 2011.
- [154] A. Jawaid, C. H. Che-Haron, and A. Abdullah, “Tool wear characteristics in turning of titanium alloy Ti-6246,” *J. Mater. Process. Technol.*, vol. 92–93, pp. 329–334, 1999.
- [155] S. Pervaiz, A. Rashid, I. Deiab, and M. Nicolescu, “Influence of Tool Materials on Machinability of Titanium- and Nickel-Based Alloys : A Review,” *Mater. Manuf. Process.*, vol. 29, no. 04 March 2014, pp. 219–252, 2014.
- [156] P. C. Priarone, S. Rizzuti, G. Rotella, and L. Settineri, “Technological and Environmental Aspects in Milling of γ -TiAl,” *Adv. Mater. Res.*, vol. 223, pp. 340–349, 2011.
- [157] A. Beranoagirre and L. N. López de Lacalle, “Optimising the milling of titanium

- aluminide alloys,” *Int. J. Mechatronics Manuf. Syst.*, vol. 3, no. 5/6, p. 425, 2010.
- [158] D. Finkeldei and F. Bleicher, “Investigation of Coolants in Machining of Titanium Aluminides,” in *Proceedings of the 26th DAAAM International Symposium*, 2016, pp. 825–833.
- [159] R. Meyer, J. Köhler, and B. Denkena, “Influence of the tool corner radius on the tool wear and process forces during hard turning,” *Int. J. Adv. Manuf. Technol.*, vol. 58, no. 9–12, pp. 933–940, 2012.
- [160] S. Ramesh, L. Karunamoorthy, and K. Palanikumar, “Fuzzy Modeling and Analysis of Machining Parameters,” pp. 439–447, 2008.
- [161] R. Dubovska, J. Majerik, and I. Baska, “Experimental Measurement of Cutting Forces in the Turning Technology,” in *DAAAM International Scientific Book 2012*, B. Katalinic, Ed. Viena: DAAAM International, 2012, pp. 255–266.
- [162] M. Milfelner, F. Cus, and J. Balic, “An overview of data acquisition system for cutting force measuring and optimization in milling,” vol. 165, pp. 1281–1288, 2005.
- [163] C. Yao, J. Lin, D. Wu, and J. Ren, “Surface integrity and fatigue behavior when turning γ -TiAl alloy with optimized PVD-coated carbide inserts,” *Chinese J. Aeronaut.*, vol. 31, no. 4, pp. 826–836, 2018.
- [164] T. S. Graham, *Cutting Tool Technology*, 1st ed., vol. 33. London: Springer-Verlag London, 2008.
- [165] A. Y. C. Nee, *Handbook of Manufacturing Engineering and Technology*, 1st ed. London: Springer-Verlag London, 2015.
- [166] Sandvik Coromant, *Modern Metal Cutting*, 1st ed. New Jersey: Sandvik Coromant, 1996.
- [167] T. Tetsui and S. Ono, “Endurance and composition and microstructure effects on endurance of TiAl used in turbochargers,” *Intermetallics*, vol. 7, no. 6, pp. 689–697, Jun. 1999.
- [168] G. Sutter, “Chip geometries during high-speed machining for orthogonal cutting conditions,” *Int. J. Mach. Tools Manuf.*, vol. 45, no. 6, pp. 719–726, 2005.
- [169] L. Ning, S. C. Veldhuis, and K. Yamamoto, “Investigation of wear behavior and chip formation for cutting tools with nano-multilayered TiAlCrN/NbN PVD coating,” *Int. J. Mach. Tools Manuf.*, vol. 48, no. 6, pp. 656–665, 2008.
- [170] A. Hosseini and H. Kishawy, “Cutting Tools Materials and Tool Wear,” in *Machining of Titanium Alloys*, J. P. Davim, Ed. Berlin: Springer-Verlag Berlin Heidelberg, 2014, pp. 31–56.
- [171] P. . Kobryn and S. . Semiatin, “Microstructure and texture evolution during solidification processing of Ti–6Al–4V,” *J. Mater. Process. Technol.*, vol. 135, no. 2–3, pp. 330–339, 2003.
- [172] B. Song, S. Dong, B. Zhang, H. Liao, and C. Coddet, “Effects of processing parameters on microstructure and mechanical property of selective laser melted Ti6Al4V,” *Mater. Des.*, vol. 35, pp. 120–125, 2012.

References

- [173] B. Pazhanivel, T. P. Kumar, and G. Sozhan, “Machinability and scratch wear resistance of carbon-coated WC inserts,” *Mater. Sci. Eng. B Solid-State Mater. Adv. Technol.*, vol. 193, no. C, pp. 146–152, 2015.
- [174] S. P. Radzevich, *Generation of Surfaces Kinematic Geometry of Surface Machining*, 1st ed. Boca Raton: Taylor & Francis, 2014.
- [175] S. P. Radzevich, *CAD/CAM of Sculptured Surfaces on Multi-Axis NC Machine: The DG/K-Based Approach*, 1st ed. Michigan: Morgan & Claypool All, 2008.
- [176] M. Gdula, J. Burek, Ł. Żyłka, and P. Turek, “Analysis of Accuracy of the Shape of Sculptured Surfaces in Simultaneous Five-Axis Machining of Parts Made from Difficult to Machine Materials Used in Aviation Technology,” *Arch. Mech. Technol. Autom.*, vol. 34, no. 4, pp. 11–24, 2014.
- [177] J. P. Davim, *Machining of Complex Sculptured Surfaces*, 1st ed. London: Springer, 2012.
- [178] Sandvik Coromant, *Superaleaciones termorresistentes (HRSA)*, 1st ed. Madrid: Sandvik Coromant Iberica, 2010.
- [179] V. P. Astakhov, *Geometry of Single-point Turning Tools and Drills*, 1st ed. London: Springer-Verlag London, 2010.
- [180] S. Jayaram, S. G. Kapoor, and R. E. Devor, “Estimation of the specific cutting pressures for mechanistic cutting force models,” *Int. J. Mach. Tools Manuf.*, vol. 41, no. 2, pp. 265–281, 2001.
- [181] S. S. Park, “High frequency bandwidth cutting force measurements in milling using the spindle integrated force sensor system,” The University of British Columbia, 2003.
- [182] A. Haşçalık, U. Çaydaş, A. Haşçalık, and U. Çaydaş, “Electrical discharge machining of titanium alloy (Ti-6Al-4V),” *Appl. Surf. Sci.*, vol. 253, no. 22, pp. 9007–9016, 2007.
- [183] Kennametal, “Titanium Machining Guide,” 2011.
- [184] H. Li and Y. Chen, “Machining Process Monitoring,” in *Handbook of Manufacturing Engineering and Technology*, 1st ed., A. Y. C. Nee, Ed. London: Springer-Verlag London, 2014, pp. 1–33.
- [185] J. A. Ghani *et al.*, “Failure mode analysis of carbide cutting tools used for machining titanium alloy,” *Ceram. Int.*, vol. 39, no. 4, pp. 4449–4456, 2013.
- [186] R. Iyer, P. Koshy, and E. Ng, “Helical milling: An enabling technology for hard machining precision holes in AISI D2 tool steel,” *Int. J. Mach. Tools Manuf.*, vol. 47, no. 2, pp. 205–210, 2007.
- [187] V. Nayyar *et al.*, “An Experimental Investigation of the Influence of Cutting-Edge Geometry on the Machinability of Compacted Graphite Iron,” vol. 3, no. March, pp. 1–13, 2013.
- [188] Sandvik Coromant, *Fresado – técnicas de aplicación*, 1st ed. Madrid: Sandvik, 2007.
- [189] R. K. Roy, *A Primer on The Taguchi Method*, 2nd ed. Michigan: Society of

-
- Manufacturing Engineers, 2010.
- [190] I. S. Conference, “Application of Taguchi method for determining optimum surface.pdf,” no. November, 2014.
- [191] F. Wang, Y. Liu, Y. Zhang, Z. Tang, R. Ji, and C. Zheng, “Compound machining of titanium alloy by super high speed EDM milling and arc machining,” *J. Mater. Process. Technol.*, vol. 214, no. 3, pp. 531–538, 2014.
- [192] A. Beranoagirre and L. N. López de Lacalle, “Grinding of gamma TiAl intermetallic alloys,” in *Procedia Engineering*, 2013, vol. 63, pp. 489–498.
- [193] W. M. Yin, V. Lupinc, and L. Battezzati, “Microstructure study of a γ -TiAl based alloy containing W and Si,” *Mater. Sci. Eng. A*, vol. 239–240, no. 1–2, pp. 713–721, 1997.
- [194] M. N. Mathabathe, S. Govender, A. S. Bolokang, R. J. Mostert, and C. W. Siyasiya, “Phase transformation and microstructural control of the α -solidifying γ -Ti-45Al-2Nb-0.7Cr-0.3Si intermetallic alloy,” *J. Alloys Compd.*, vol. 757, pp. 8–15, 2018.
- [195] G. Basile *et al.*, “Characterization of an Additive Manufactured TiAl Alloy-Steel Joint Produced by Electron Beam Welding,” *Materials (Basel)*, vol. 11, no. 1, pp. 1–9, 2018.
- [196] F. Appel, J. D. H. Paul, and M. Oehring, *Gamma Titanium Aluminide Alloys: Science and Technology*. Weinheim, Germany: Wiley-VCH Verlag GmbH & Co. KGaA, 2011.
- [197] T. Furusawa, H. Hino, S. Tsuji, S. Koroyasu, and A. Ichikawa, “Generation of defects due to machining of TiAl intermetallic compound and their effects on mechanical strength,” *J. Manuf. Sci. Eng. Trans. ASME*, vol. 126, no. 3, pp. 506–514, 2004.
- [198] J. Pujana, P. J. Arrazola, and J. A. Villar, “In-process high-speed photography applied to orthogonal turning,” *J. Mater. Process. Technol.*, vol. 202, no. 1–3, pp. 475–485, 2008.
- [199] G. List *et al.*, “Wear behaviour of cemented carbide tools in dry machining of aluminium alloy,” *Wear*, vol. 259, no. 7–12, pp. 1177–1189, 2005.

Appendices

Appendix A-1. Summary of surface integrity studies on machining TiAl alloys.

Research Study	Chemical Composition	Machining Process	Cutting Speed (m/min)	Feed	DOC (mm)	Environment	Conclusions
The machining of TiAl-based intermetallic [107].	Ti-48Al-2Nb-2Mn	Turning	20 - 40	0.13, 0.25 mm/rev	1	Dry	Tool life can be improved by using negative rake angle but with lower surface finish, fine grain straight grade carbide tools with positive rake angle is the most suitable for Ti-48Al-2Nb-2Mn. In terms of roughness, the best combination of cutting parameters is Vc=30m/min, f=0.13mm/rev and DOC= 1mm.
Machining sequence to manufacture a γ -TiAl conrod for application in combustion engines [44].	Ti-46Al-0.5Mo-0.8Cu-0.2Si	Milling	30 - 70	0.1 - 1 mm/tooth	0.5	HP 20 bar	Best surface quality and tool wear can be obtained with cutting speeds between Vc =30 m/min and 50 m/min and a feed between fz = 0.01 mm and 0.25 mm using emulsion as lubricant. In boring fine-grained WC achieved best results. Low feed rate is able to produce good surface quality.
		Drilling	10 – 70	0.2 - 1.8	---	HP 80 bar and 100 bar	
		Boring	60, 90, 120	0.04 - 0.14 mm/rev	2	HP 20 bar	
Technological and environmental aspect in milling TiAl [156].	Ti-(32-33.5) Al-(4.5-5.1) Nb-(2.2-2.6) Cr	Milling	35, 50, 71	0.06,0.08, 0.10 mm/tooth	0.3	Dry and MQL	Total roughness Rt and the mean roughness Ra present the same clear trend vs. the cutting speed and the feed per tooth. Rt and Ra decrease as the cutting speed increases and the feed per tooth decreases.
Milling of Gamma Titanium aluminum alloys [126].	Ti-45Al-(5-10) Nb-(0,2-0,4) C TNB	Milling	50,60,70	0.04, 0.05, 0.06 mm/tooth	1	Wet	Surface finishing is directly influenced by material toughness and the nature of chip formation. Roughness in MoCuSi extruded alloy are slightly higher than those for TNB. Increasing the cutting speed in 16% results in a better surface finish in MoCuSi material, but not in the TNB alloys.
	Ti-(43-46) Al-(1-2) Mo - (0,2) Si-Cu MoCuSi						
High performance cutting of γ -TiAl: Influence of lubricoolant strategy on tool wear and surface integrity [80].	Ti-45Al-2Mn-2Nb+0.8 vol% TiB2XD	Turning	80	0,1 mm/rev	0.25	Cryogenic, Conv, HP and MQL	Cryogenic cooling is the most promising lubrication strategy, providing potentially enormous benefits in terms of tool wear reduction and consequent surface quality improvement.
High speed ball nose end milling of TiAl alloys [127].	Ti-45Al-8Nb-0,2C	Milling	160/250	0,06 mm/tooth	0,25	Dry	Fracture/pullout was observed on every milled surface that was assessed. The size of the fracture/ pullout varied from a few microns to millimeters, with higher cutting speeds and tool flank wear levels causing increased damage.
On high-speed turning of third generation gamma titanium aluminide [125].	Ti-45Al-8Nb-0.2C-0.2B at% TNBV3	Turning	60-100	0.05, 0.1, 0.2 mm/rev	0.1-0.4	MQL, Dry and Cryogenic	The use of MQL allowed to obtain smooth surfaces (Ra<0,4 μ m) and almost without cracks, although the useful life of the tool was extremely short, especially with the chosen process parameters. Cryogenic cooling successfully counteracted the thermal load at the cutting edges, providing potentially enormous benefits in terms of surface integrity.

Research Study	Chemical Composition	Machining Process	Cutting Speed (m/min)	Feed	DOC (mm)	Environment	Conclusions
Workpiece surface integrity when slot milling γ -TiAl intermetallic alloy [130].	Ti-45Al-2Mn-2Nb+0.8 vol% TiB2XD	Milling	55	0.01 mm/tooth	0.1	Wet	Slot surfaces show redeposited/adhered and smeared workpiece material. Brittle fracture of the slot edges was restricted to <10 mm with sporadic top burr formation. The residual stress parallel to the feed was 10% higher (more compressive) than that measured perpendicular to the feed direction. Workpiece surface roughness (Ra) measurements showed a range in values from 0.8 to 1.2 μm . Slots machined from solid showed the worst surface integrity of all the features machined.
Milling and turning of TiAl using minimum quantity lubrication [82].	Ti-48Al-2Nb-2Cr	Milling	25, 50, 100	0.08 mm/tooth	0.3	Wet and MQL	Mean Roughness (Ra) and the maximum roughness profile height (Rt) decrease with the increase of cutting speed. The adoption of wet cutting conditions results in a benefit in term of area roughness parameters Sa and Sz. MQL allows to obtain the best surface quality results, with a noticeable decrease of roughness, by approximately 30 % in comparison to dry machining.
		Turning	25 - 50	0.1 - 0.3 mm/rev	0.3 - 0.7		
Investigation of surface integrity in HSM Milling of γ -TiAl under dry and MQL conditions [68].	Ti-48Al-2Nb-2Cr-1B	Milling	300, 600	0,005 mm/tooth	0,1	Dry and MQL	The best Ra value was obtained using a $V_c= 600\text{m/min}$. Axial depth of cut and cutting speed have the most important effects on the surface roughness
Tool life and surface integrity when turning TiAl with PCD tools under conventional wet and cryogenic cooling [124].	Ti-43.5Al-4Nb-1Mo-0.1B (TNM)	Turning	80	0.1 mm/rev	0.25	Wet and Cryogenic	The average values of the roughness indices were lower than 0.4 and 3 μm for Ra and Rz respectively. For PCD tools, Ra was 0.28 μm and Rz was 1.8 μm . For CBN tools, Ra was 0.24 μm and Rz was 1.5 μm . For PCD cryogenic-assisted cutting, a significant increase in tool life was achieved, up to $TL\approx 30$ min
Influence of the heat treatment on the microstructure and machinability of TiAl produced by electron beam melting [129].	Ti-48Al-2Nb-2Cr	Turning	20, 35	0.07, 0.15, 0.25 mm/rev	0.5	Dry	Heat-treated material (HT-M) showed higher machinability than untreated material (UT-M) in dry turning operations. For both materials the surface roughness was less than 0.4 μm . A further reduction in ductility was detected as a result of the hardened layer (1015.40 ± 61 HV) below the surface. Surface analysis showed small surface cracks with an average depth of less than 10 μm . The cutting conditions used in this work allow minimum surface damage to be obtained.

Appendix A-2. Summary of machining parameters studies on TiAl alloys.

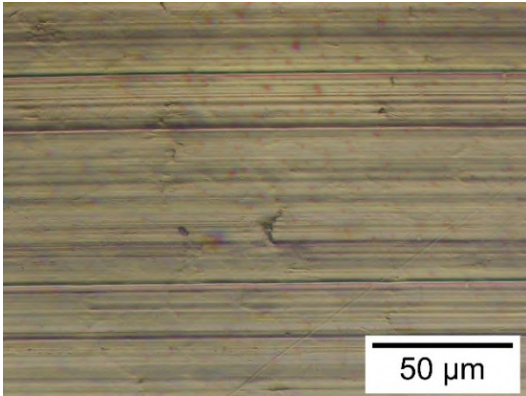
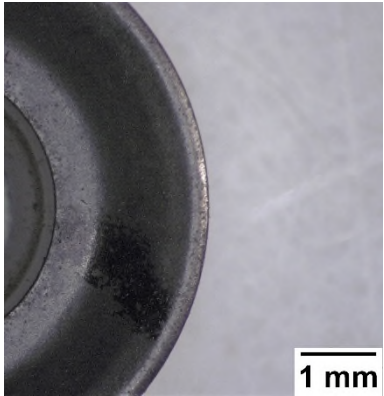
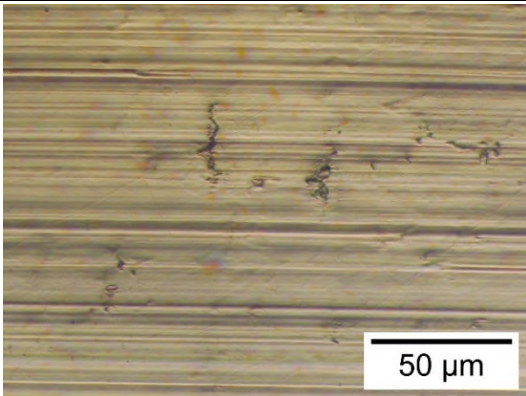
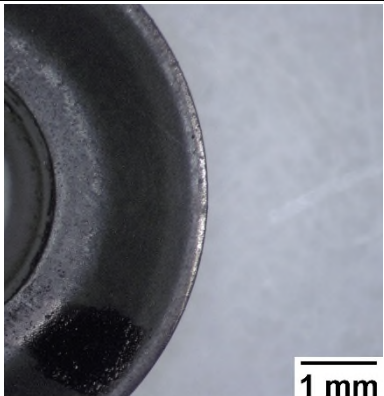
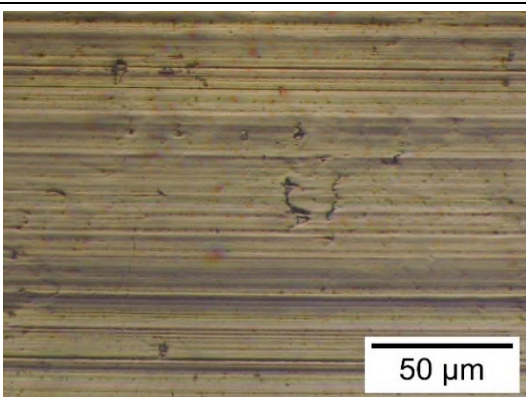
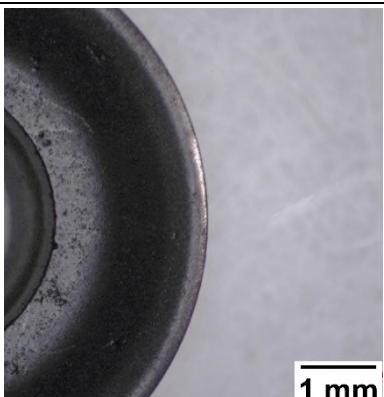
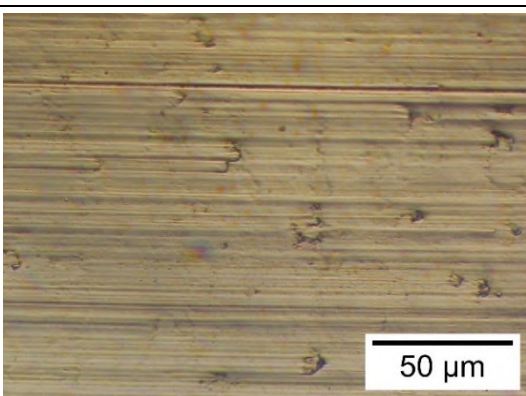
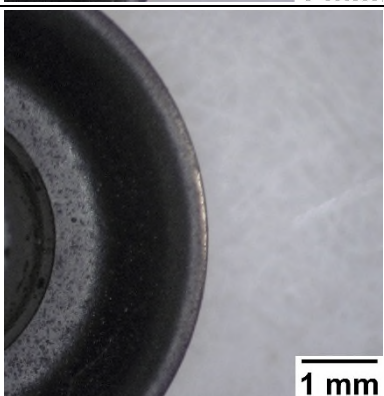
Research Study	Chemical Composition	Machining Process	Tool Material	Cutting Speed (m/min)	Feed	DOC (mm)	Environment	Conclusions
The machining of TiAl-based intermetallic [107].	Ti-48Al-2Nb-2Mn	Turning	WC and PCBN 98	20, 40	0.13, 0.25 mm/rev	1	Dry	Fine grained, straight grade carbide tools with positive rake are suggested as being the most suitable for machining TiAl-based intermetallic. Plain, mixed and whisker reinforced alumina-based ceramics and PCBN tools containing titanium compounds are not suitable for machining titanium based intermetallic.
Cutting force evaluation when High Speed Milling TiAl [79].	Ti-45Al-2Mn-2Nb+0.8 vol% TiB ₂ XD	Milling	WC	50, 70, 120, 135, 240, 345	0.12 mm/tooth	0.2	Dry	Cutting forces increased with increasing tool wear. Milling with a worn TiAl coated tool (0.3 mm flank wear), forces were found to increase by a factor of 10 compared to a new tool. This gave an increase in tool push-off of up to 31% of the programmed depth of cut.
Workpiece surface integrity considerations when finish turning γ -TiAl [67].	Ti-45Al-2Mn-2Nb+0.8 vol% TiB ₂ XD	Turning	WC ISO K10	25, 40	0.05 mm/rev	0.05-0.1	HP 65 bar and HP 20 bar	The use of high-pressure cutting fluid supply has been shown to reduce cutting force by preventing seizure of chips on the rake face, reducing friction and altering the chip contact length and shear plane angle. When turning, TiAl radial force was larger than the feed force. The low value of feed force was a function of the very small chip contact area and limited chip flow across the rake face seen with this material.
Studies on the conventional machining of TiAl-based alloys [72].	Ti-46.8Al-1Mo-0.2 Si	Turning	WC ISO K10	10, 60	0.05 mm/rev	0.5	Dry	Homogeneous structure material causes lower cutting forces, higher surfaces qualities and tool lives. The uncoated cemented carbide tools reached the limit of their productivity at a cutting speed of 60 m/min. The nominal cutting forces rise linearly with increasing feed.
Wear mechanisms of WC inserts in face milling of γ -TiAl [24].	Ti-47Al-2Mn-2Nb+0.8 vol% TiB ₂	Milling	WC ISO K10, K20 and K35	20, 50, 80, 100, 300, 400	0.5, 0.1 mm/tooth	1	Wet	Cutting forces increased with an increase in both cutting speed and feed. The increase seemed more influenced by cutting speed, indicating a strain rate sensitivity of these alloys. The cutting force signal exhibited a dynamic component having a high frequency because of the type of chip formed in the cutting process. Insert geometries having large radius and sharp cutting edges proved advantageous in the machining of γ -TiAl alloys.
Experimental study on high speed milling of γ -TiAl alloy [142].	Ti-48Al-2Nb-2Cr	Milling	WC	120, 240	0.08 mm/tooth	5	Dry	The milling forces increased slightly with increasing cutting speed but increased rapidly with the elevated flank wear value. Force increases in all three components with the increase of cutting speed in a range of 30-50N. This might be due to the high temperature and high tool wear rate at a high cutting speed.
Technological and environmental aspect in milling γ -TiAl [156].	Ti-48Al-2Nb-2Cr	Milling	WC ISO K30 and K40	35,50,71	0.06, 0.08, 0.10 mm/tooth	0.3	Dry and MQL	The decreasing of the tool life is especially severe moving from 35 m/min to 50 m/min, while it is almost flat between 50 m/min and 71 m/min. At the same time, tool life decreases at increasing the feed per tooth, and this decrease is quicker in the range included between 0.06 mm/tooth and 0.08 mm/tooth.

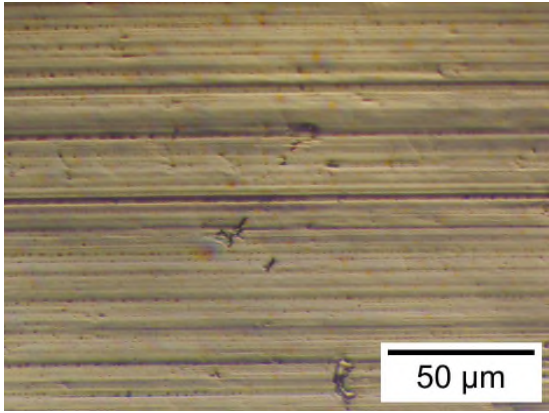
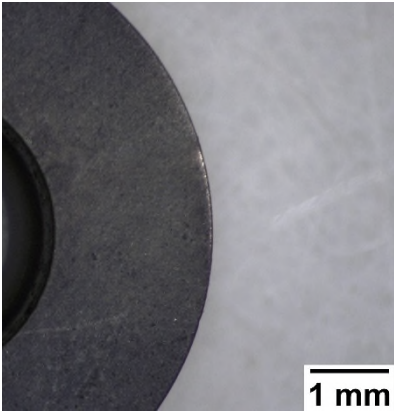
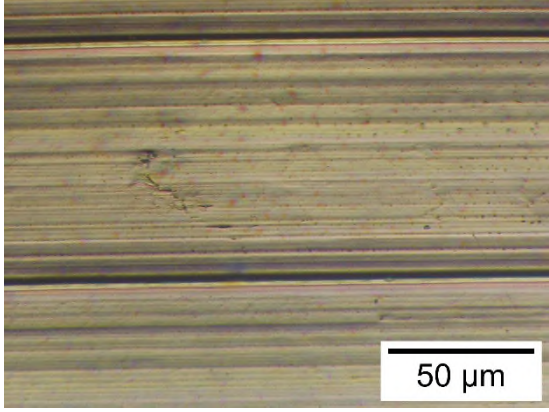
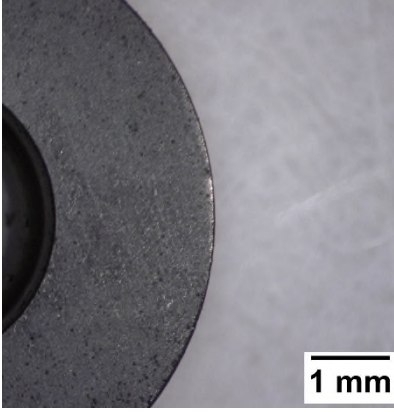
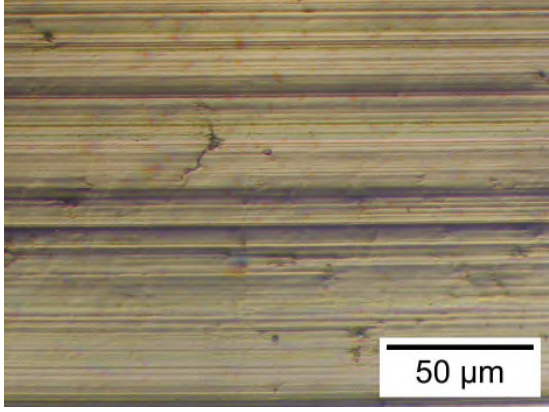
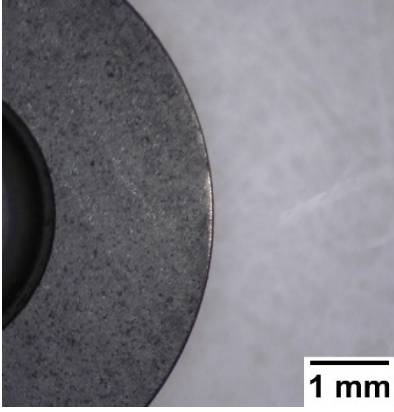
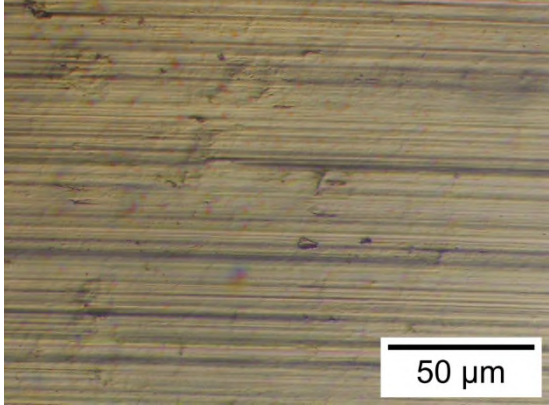
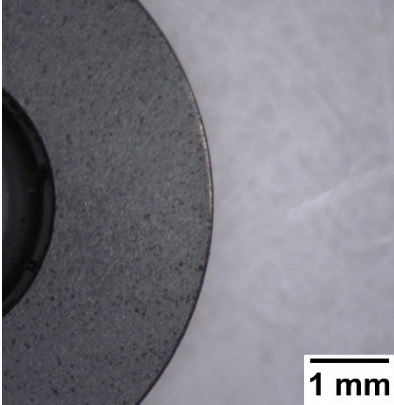
Research Study	Chemical Composition	Machining Process	Tool Material	Cutting Speed (m/min)	Feed	DOC (mm)	Environment	Conclusions
Milling of γ -TiAl alloys [126].	Ti-(44-45) Al-(5-10) Nb-(0.2-0.4) C TNB	Milling	WC	50,60,70	0.04, 0.05, 0.06 mm/tooth	1	Wet	Cutting speed reduces tool life significantly. For the TNB alloy, considering the cutting speed of 50 m/min as reference point, a 20% increase reduced tool life by 25%, and a 40% increase reduced tool life by 45%. The effect of feed per tooth was less significant; an increase of 20% reduced tool life by approximately 19%. The results showed that the most difficult-to-cut material is the TNB alloy followed by the MoCuSi alloy in its ingot form.
	Ti-(43-46) Al-(1-2) Mo-(0.2) Si-Cu MoCuSi							
Optimizing the turning of γ -TiAl alloys [157]	Ti (43-45) Al-(5-8) Nb-Mo-(0-0.4) B-C TNM	Turning	WC	40, 50, 60	0.05, 0.1, 0.15 mm/rev	0.5, 1, 1.5, 2		For the TNB alloy, from cutting speed of 40 m/min as reference point, a 25% increase reduces the tool 75% the tool life, a 50% increase reduces the tool life in 95%. The cutting speed is the main factor on the durability of the turning tools. The alloy brittleness is a problem to be considered, in TNB and TNM material.
High performance cutting of γ -TiAl alloys: Influence of lubricoolant strategy on tool wear and surface integrity [80].	Ti-45Al-2Mn-2Nb+0.8vol% TiB2XD	Turning	WC	80	0,1 mm/rev	0.25	MQL, Wet 6 bar, HP 80, 150, and 300 bar, Cryogenic	Cutting forces increase rapidly as a result of tool wear, and this observation can already be pointed out in the first seconds of machining time. Cryogenic cooling with liquid nitrogen was identified as a promising way to lower tool wear and furthermore to limit surface and sub-surface defects. Cryogenic machining with liquid nitrogen cooling decreases VB max up to 61% in comparison with conventional lubrication. Remarkable results can already be obtained by using 80 bar, whereby VB max is reduced by 29%.
High speed ball nose end milling of TiAl alloys [127].	Ti-45Al-8Nb-0,2C Ti-45Al-2Mn-2Nb+0.8vol% TiB2XD	Milling	WC	160/250	0,06 mm/tooth	0,25	Dry	An increase in cutting force was measured with increasing flank wear because of the increased contact and rubbing between the flank face and the workpiece. Initial wear consisted of uniform flank wear which progressed to non-uniform flank wear at the central point of the wear scar. Stair-formed face wear was also evident on the rake face. At higher cutting speeds of 250-340 m/min, wear progression is extremely fast once a flank wear of 200 μ m had been reached.
On high-speed turning of third generation γ -TiAl alloys [125]	Ti-45Al-8Nb-0.2C-0.2B TNBV3	Turning	WC ISO K10, K20	60, 100	0.05, 0.2 mm/rev	0.1, 0.4	MQL, Dry and Cryogenic LN2	The main drawback regarding this machining strategy is that the increased thermal impact to the cutting edges of the tools results in stronger tool wear. Cutting forces increase rapidly because of tool wear, this is more evident in absence of a lubricoolant. The results show that effective cutting in dry conditions is not practicable. In addition, with MQL lubrication, the tool life is extremely short, especially with the chosen process. Cryogenic cooling could be successfully applied to counteract the huge thermal load on the cutting edges.

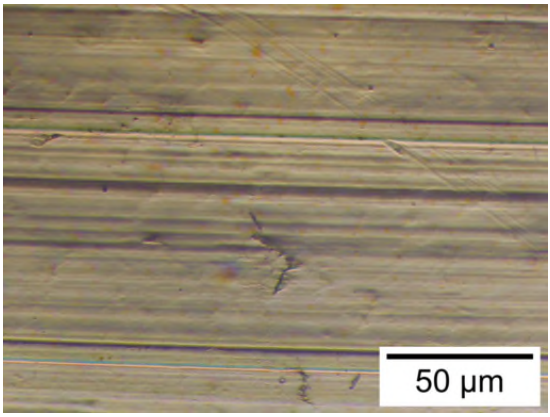
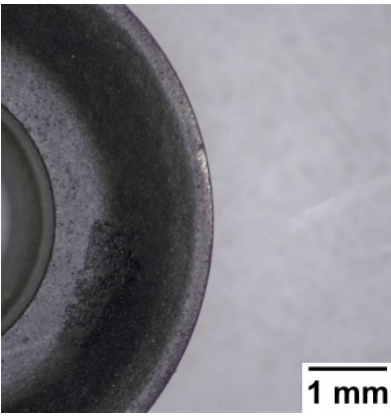
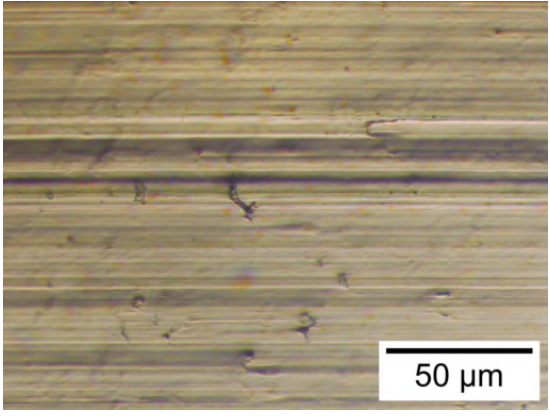
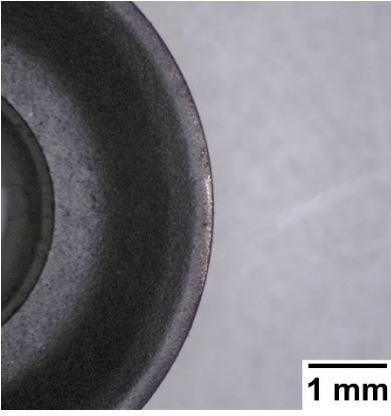
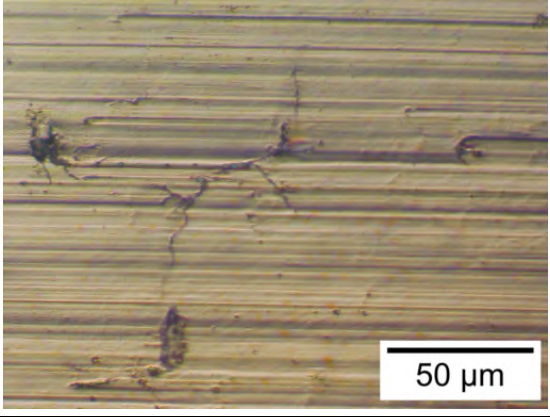
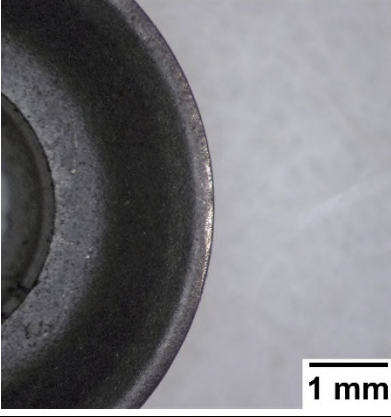
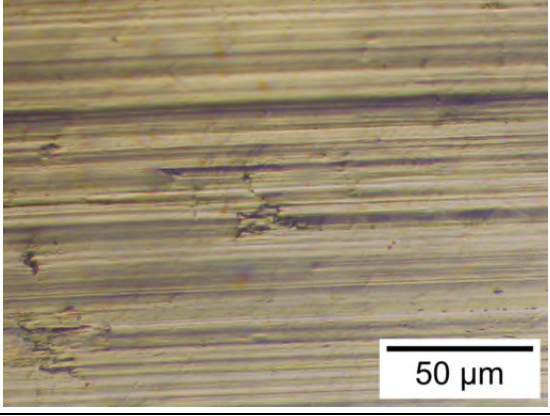
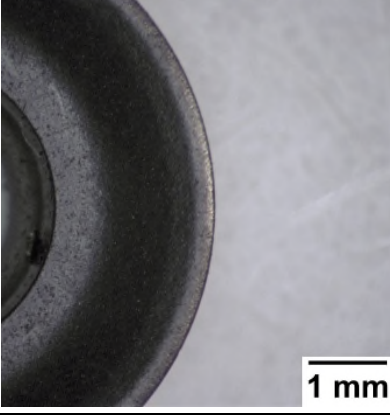
Research Study	Chemical Composition	Machining Process	Tool Material	Cutting Speed (m/min)	Feed	DOC (mm)	Environment	Conclusions
On high-speed turning of third generation γ -TiAl alloys [125]	Ti-45Al-8Nb-0.2C-0.2B TNBV3	Turning	WC ISO K10, K20	60, 100	0.05, 0.2 mm/rev	0.1, 0.4	MQL, Dry and Cryogenic LN2	The main drawback regarding this machining strategy is that the increased thermal impact to the cutting edges of the tools results in stronger tool wear. Cutting forces increase rapidly because of tool wear, this is more evident in absence of a lubricoolant. The results show that effective cutting in dry conditions is not practicable. In addition, with MQL lubrication, the tool life is extremely short, especially with the chosen process. Cryogenic cooling could be successfully applied to counteract the huge thermal load on the cutting edges.
An evaluative approach to correlate machinability, microstructures, and material properties of γ -TiAl [59].	Ti-48Al-2Nb-2Cr Ti-45Al-2Mn-2Nb+0.8vol% TiB ₂ XD Ti-43.5Al-4Nb-1Mo-0.1B (TNM)	Milling	WC ISO K10	90	0.1 mm/tooth	0.3	Wet 6 bar	The tool wear mechanism is mainly abrasive, and wear consisted of almost uniform flank wear. Chipping and micro-chipping of the cutting edges was also detected, and adhesion of material on the worn areas was noticed. Under the same cutting conditions, uncoated carbide tools are proved suitable to get a stable turning process for Ti-48-2-2 alloy. The Ti-45Al-2Nb-2Mn + 0.8 vol% TiB ₂ XD is confirmed to be the most difficult-to-cut alloy. As far as the effect of process parameters is concerned, further investigations confirmed that tool life increases when decreasing cutting speed, feed, and depth of cut, according to literature.
Milling and turning of TiAl by using minimum quantity lubrication [82].	Ti-48Al-2Nb-2Cr	Milling Turning	WC	25, 50, 100 25 - 50	0.08 mm/tooth 0.1-0.3 mm/rev	0.3 0.3-0.7	Wet and MQL	The wear evolution is quite fast in absence of lubricoolant supply, because of the lack of lubrication and cooling effects. tool wear increases with the increase of cutting speed, feed, and depth of cut. Moreover, for the same process parameters, process performance considerably improves by using round cutting insert. Larger corner radius of the main cutting edge leads to the increase of tool life, and to the decrease of cutting forces.
Drilling of TiAl at different aspect ratio under dry and wet conditions [128].	Ti-48Al-2Nb-2Cr	Drilling	Tungsten - Carbide	72	0.01 mm/rev	---	Dry and Wet	The high temperature generated during the dry drilling was the major cause for the adhesion of chip particles to the tool. Due to the low thermal conductivity of TiAl, the temperature in the cutting-edge area can easily reach very high values and in such a high pressure and temperature, the surface hardness of the work material will rapidly lessen, then quickly build and expand the adhesion process. This mechanism decreases the sharpness of the cutting edge and develops conditions, which stimulate the adhesion of the work material on the cutting tool as a BUE.

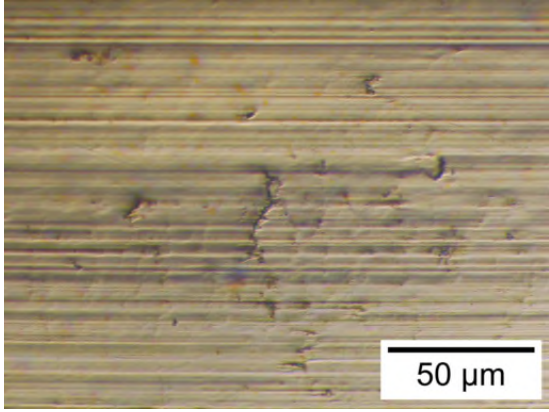
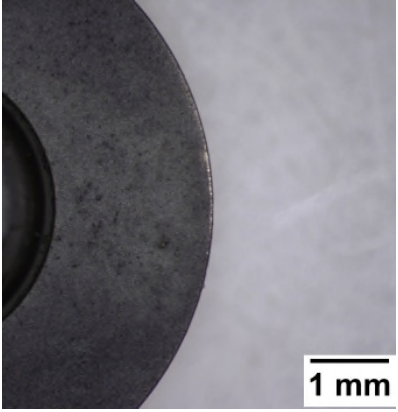
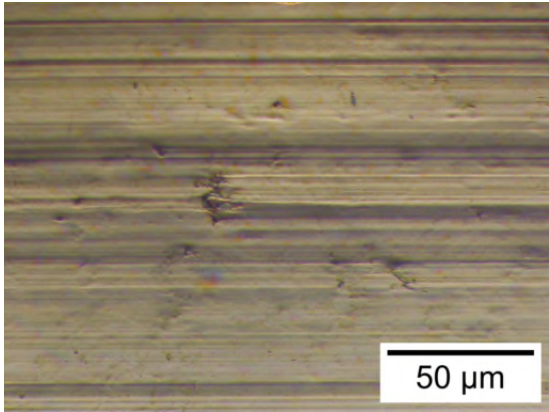
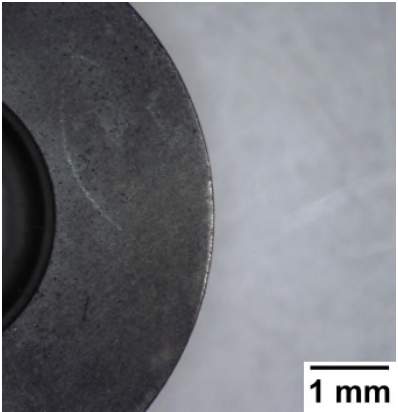
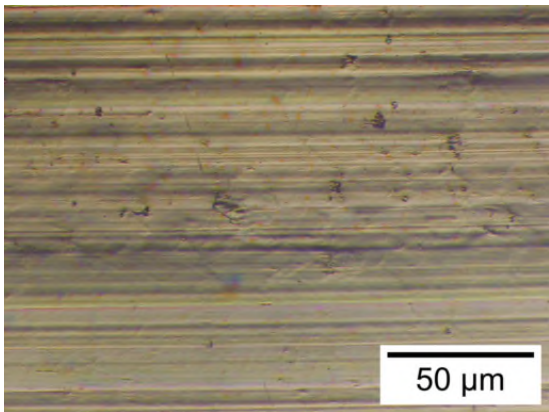
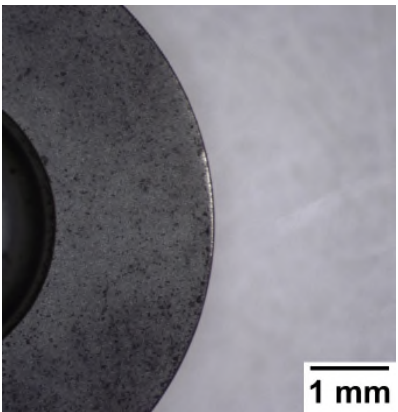
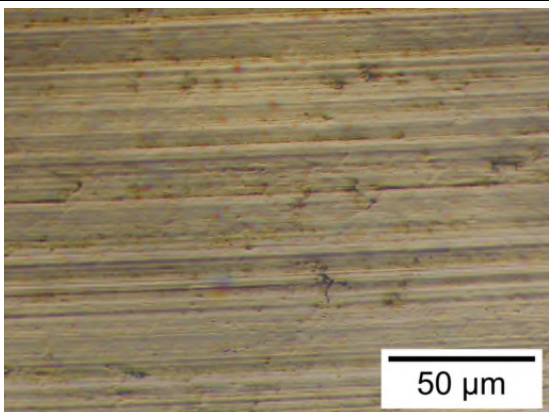
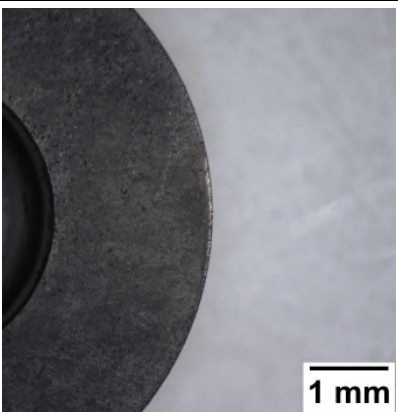
Research Study	Chemical Composition	Machining Process	Tool Material	Cutting Speed (m/min)	Feed	DOC (mm)	Environment	Conclusions
Tool life and surface integrity when turning TiAl with different tools under conventional wet cutting and cryogenic cooling [124].	Ti-43.5Al-4Nb-1Mo-0.1B (TNM)	Turning	WC ISO K10 PCD and CBN	80	0.1 mm/rev	0.25	Wet 6 bar, and Cryogenic	Experimental results proved that tool failure was suddenly reached when using coated carbide and low-content CBN inserts. Thermal conductivity and resistance against abrasive wear increase with CBN content and grain size. Tool life of approximately 2 min was achieved with uncoated carbide tools. Inserts with 92 % CBN content lead to a more stable process, with average tool life of 7.2 min, and PCD tool is superior to all the other materials, with an increase in tool life up to TL≈14 min. CBN and PCD tools are suitable to withstand the heat and pressure developed during material removal without compromising surface integrity, because of their ability to retain a sharp cutting edge for longer cutting time.
Influence of the heat treatment on the microstructure and machinability of titanium aluminides produced by electron beam melting [129]	Ti-48Al-2Nb-2Cr	Turning	WC	20, 35, material B 20	0.07, 0.15, 0.25	0.5	Dry	The influence of the cutting temperature as major factor that induce built up edge (BUE) formation. The cutting forces are in direct correlation with the flank wear of the cutting edge and increase when the tool loses its cutting properties. The large radius of the round insert, in fact, is useful to obtain a lower wear of the cutting edge, but at the same time, tends to increase the extent of the radial force.

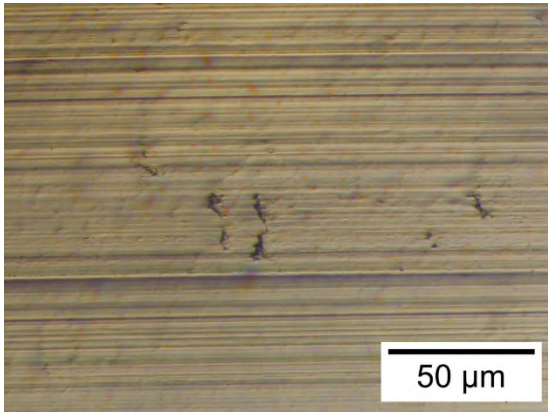
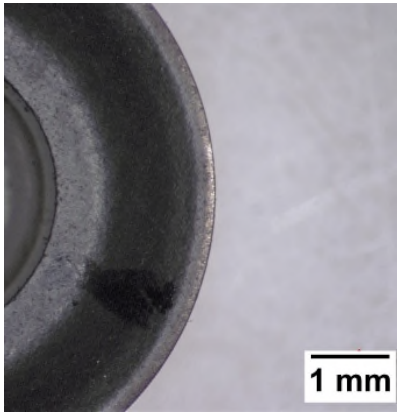
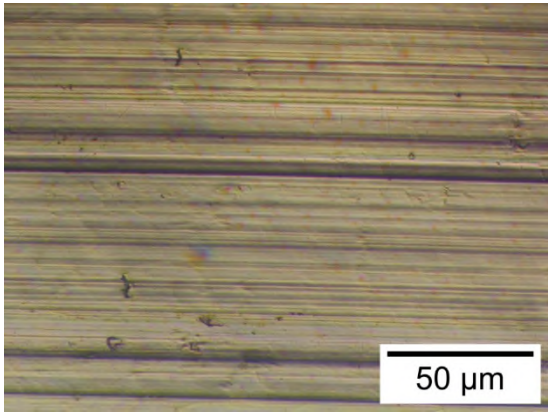
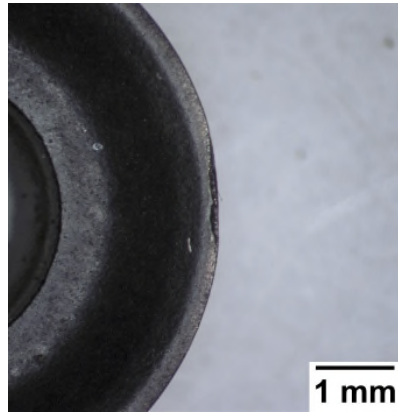
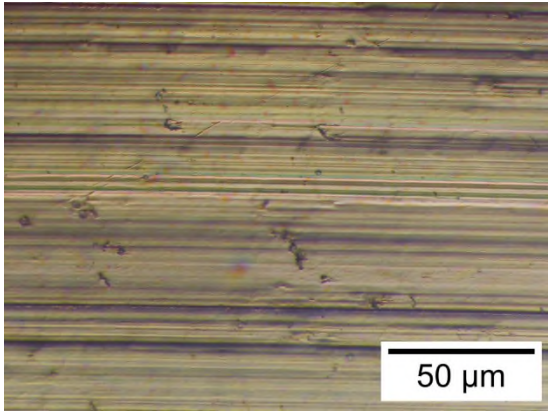
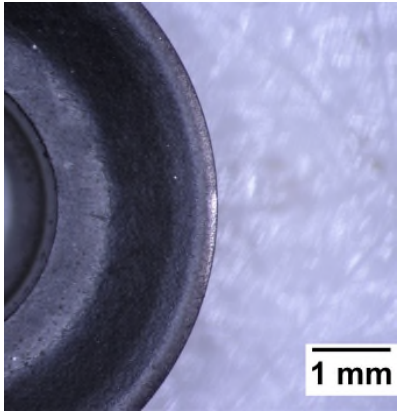
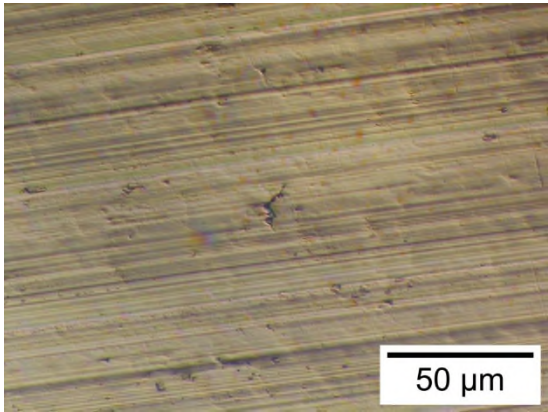
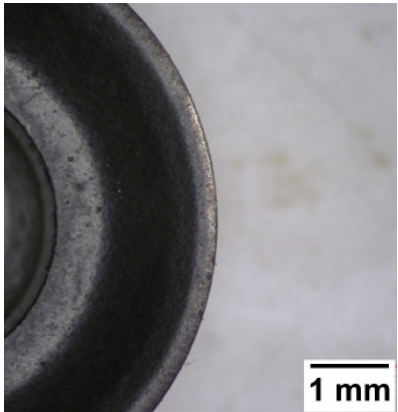
Appendix A-3. Observations of machined surfaces and cutting-edge condition, by insert.

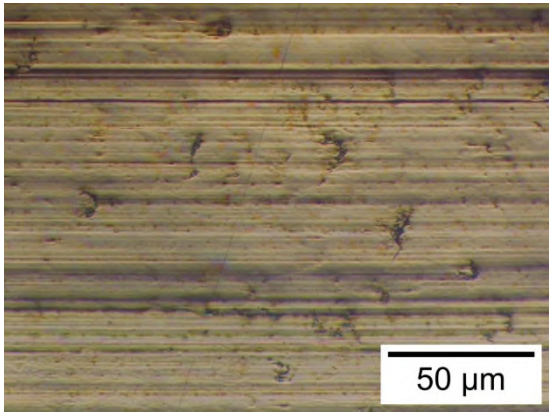
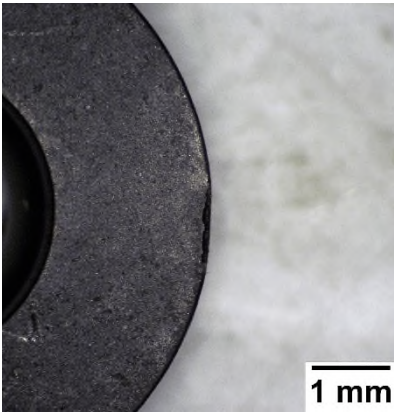
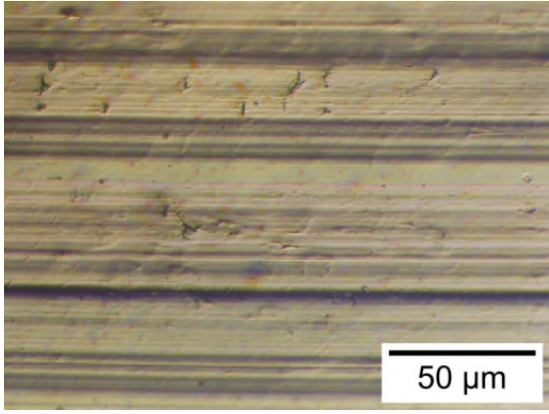
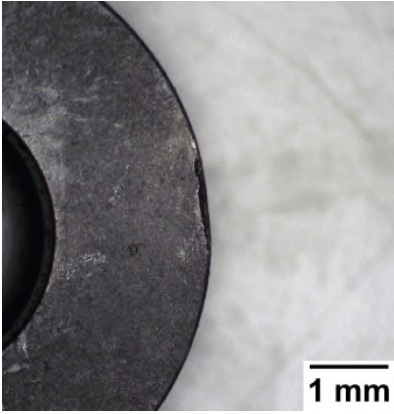
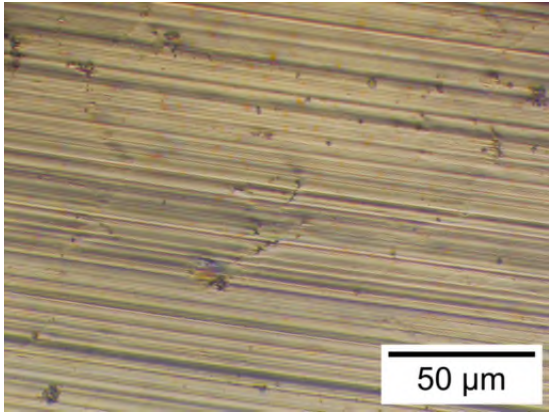
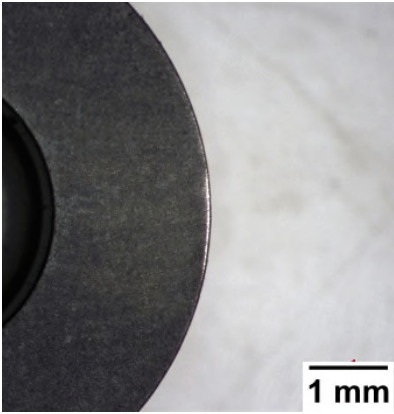
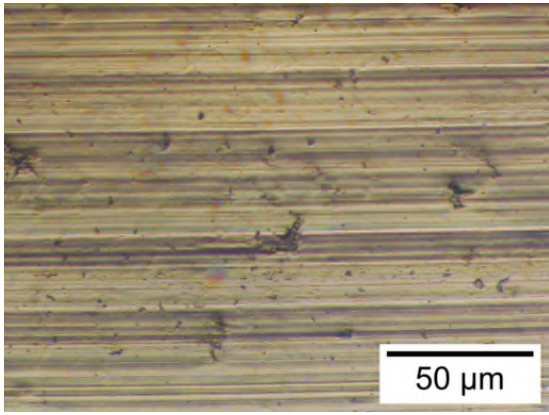
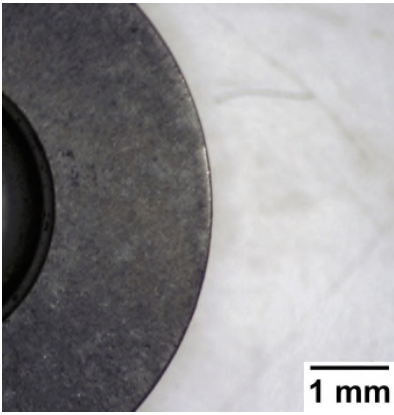
Cutting Parameters	S10-XL	
	Machined Surface	Insert
$v_c = 70 \text{ m/min}$ $a_p = 0,3 \text{ mm}$ $h_{ex} = 0,03 \text{ mm}$		
$v_c = 70 \text{ m/min}$ $a_p = 0,5 \text{ mm}$ $h_{ex} = 0,04 \text{ mm}$		
$v_c = 45 \text{ m/min}$ $a_p = 0,3 \text{ mm}$ $h_{ex} = 0,04 \text{ mm}$		
$v_c = 45 \text{ m/min}$ $a_p = 0,5 \text{ mm}$ $h_{ex} = 0,03 \text{ mm}$		

Cutting Parameters	S10-XM	
	Machined Surface	Insert
$v_c = 70 \text{ m/min}$ $a_p = 0,3 \text{ mm}$ $h_{ex} = 0,03 \text{ mm}$		
$v_c = 70 \text{ m/min}$ $a_p = 0,5 \text{ mm}$ $h_{ex} = 0,04 \text{ mm}$		
$v_c = 45 \text{ m/min}$ $a_p = 0,3 \text{ mm}$ $h_{ex} = 0,04 \text{ mm}$		
$v_c = 45 \text{ m/min}$ $a_p = 0,5 \text{ mm}$ $h_{ex} = 0,03 \text{ mm}$		

Cutting Parameters	S25-XL	
	Machined Surface	Insert
$v_c = 70 \text{ m/min}$ $a_p = 0,3 \text{ mm}$ $h_{ex} = 0,03 \text{ mm}$		
$v_c = 70 \text{ m/min}$ $a_p = 0,5 \text{ mm}$ $h_{ex} = 0,04 \text{ mm}$		
$v_c = 45 \text{ m/min}$ $a_p = 0,3 \text{ mm}$ $h_{ex} = 0,04 \text{ mm}$		
$v_c = 45 \text{ m/min}$ $a_p = 0,5 \text{ mm}$ $h_{ex} = 0,03 \text{ mm}$		

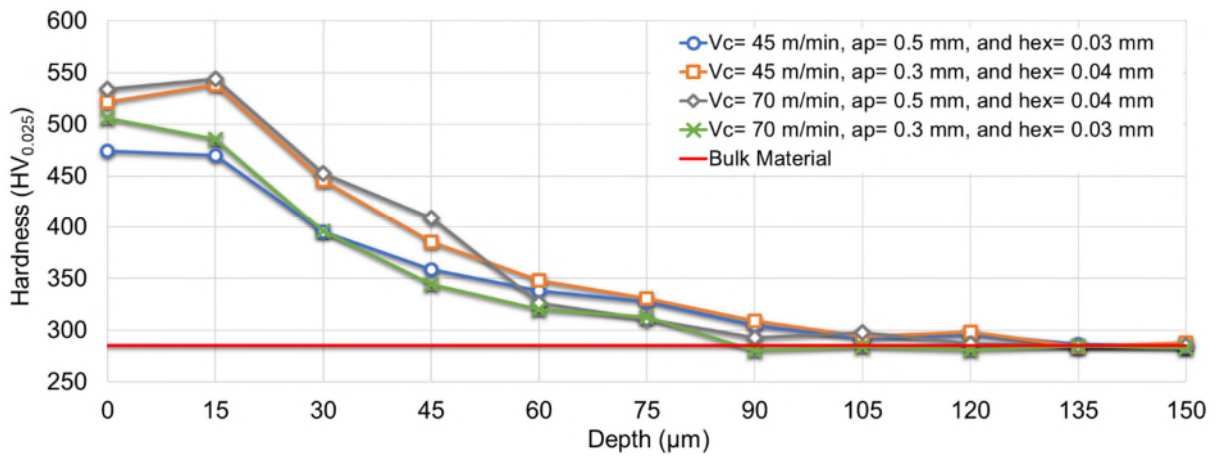
Cutting Parameters	S25-XM	
	Machined Surface	Insert
$v_c = 70 \text{ m/min}$ $a_p = 0,3 \text{ mm}$ $h_{ex} = 0,03 \text{ mm}$		
$v_c = 70 \text{ m/min}$ $a_p = 0,5 \text{ mm}$ $h_{ex} = 0,04 \text{ mm}$		
$v_c = 45 \text{ m/min}$ $a_p = 0,3 \text{ mm}$ $h_{ex} = 0,04 \text{ mm}$		
$v_c = 45 \text{ m/min}$ $a_p = 0,5 \text{ mm}$ $h_{ex} = 0,03 \text{ mm}$		

Cutting Parameters	S30-XL	
	Machined Surface	Insert
$v_c = 70 \text{ m/min}$ $a_p = 0,3 \text{ mm}$ $h_{ex} = 0,03 \text{ mm}$		
$v_c = 70 \text{ m/min}$ $a_p = 0,5 \text{ mm}$ $h_{ex} = 0,04 \text{ mm}$		
$v_c = 45 \text{ m/min}$ $a_p = 0,3 \text{ mm}$ $h_{ex} = 0,04 \text{ mm}$		
$v_c = 45 \text{ m/min}$ $a_p = 0,5 \text{ mm}$ $h_{ex} = 0,03 \text{ mm}$		

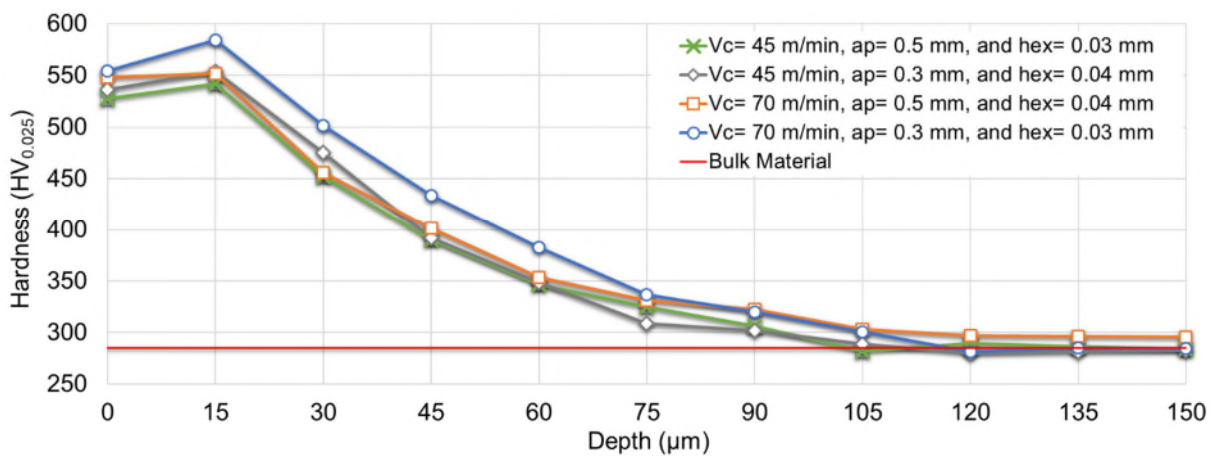
Cutting Parameters	S30-XM	
	Machined Surface	Insert
$v_c = 70 \text{ m/min}$ $a_p = 0,3 \text{ mm}$ $h_{ex} = 0,03 \text{ mm}$		
$v_c = 70 \text{ m/min}$ $a_p = 0,5 \text{ mm}$ $h_{ex} = 0,04 \text{ mm}$		
$v_c = 45 \text{ m/min}$ $a_p = 0,3 \text{ mm}$ $h_{ex} = 0,04 \text{ mm}$		
$v_c = 45 \text{ m/min}$ $a_p = 0,5 \text{ mm}$ $h_{ex} = 0,03 \text{ mm}$		

Appendix A-4. Microhardness profile by inserts.

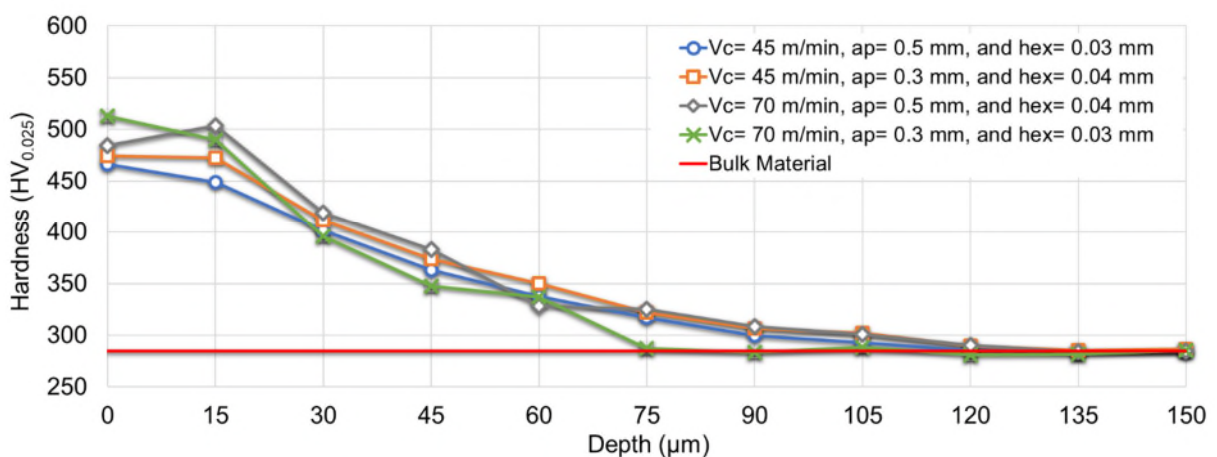
Microhardness profile for S10-XL inserts



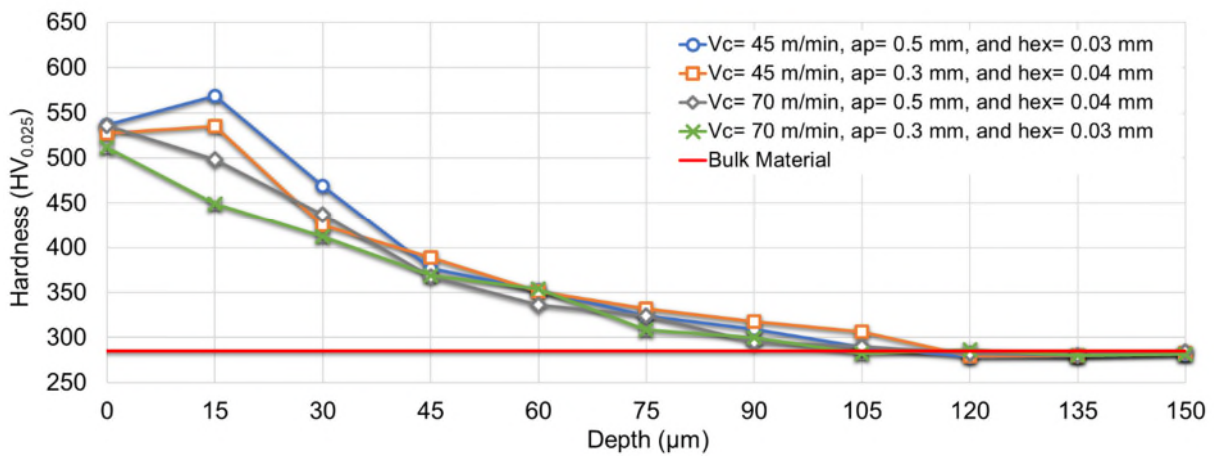
Microhardness Profile for S25-XL inserts



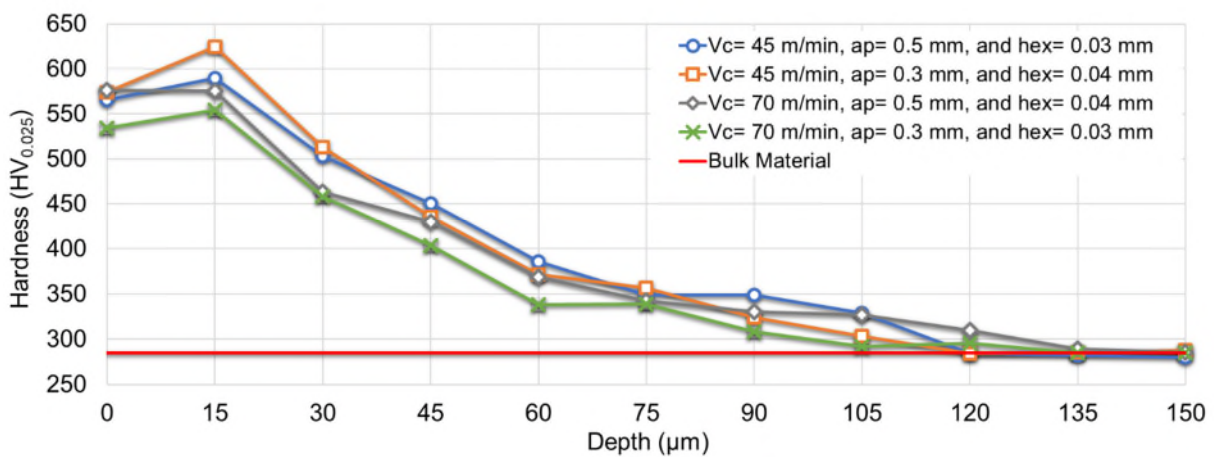
Microhardness Profile for S30-XL inserts



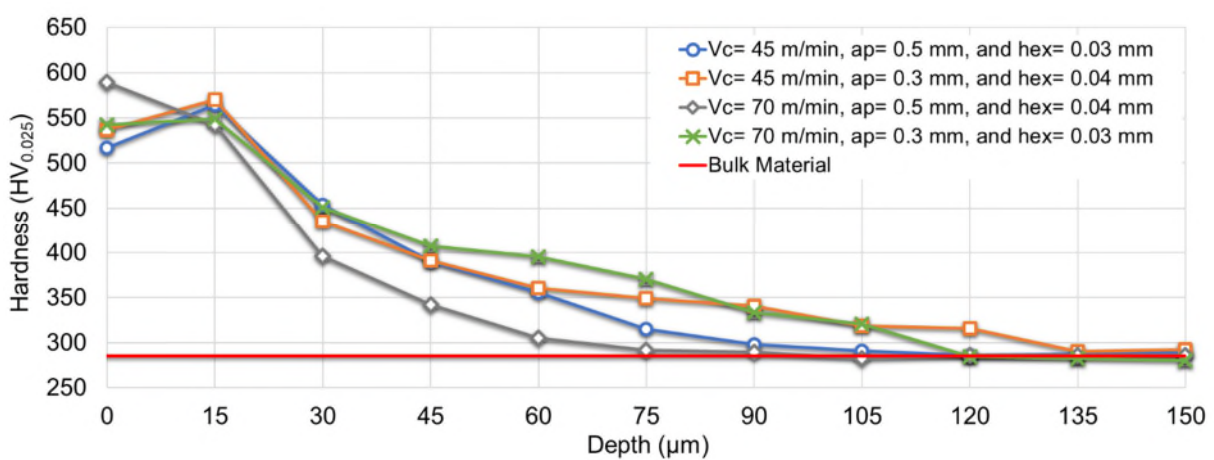
Microhardness Profile for S10-XM inserts



Microhardness Profile for S25-XM inserts



Microhardness Profile for S30-XM inserts



Appendix A-5. Surface hardened layer data, by insert

Insert	Trial	Surface Hardness (HV0.025)	Peak Hardness (HV0.025)	Maximum hardness depth (um)	Peak hardness depth (um)
S10-XM	1	512	512	105	0
S10-XM	2	536	536	95	0
S10-XM	3	527	535	120	15
S10-XM	4	537	568	100	15
S10-XL	1	506	506	95	0
S10-XL	2	534	544	105	15
S10-XL	3	521	538	115	15
S10-XL	4	474	474	105	0
S25-XM	1	535	554	105	15
S25-XM	2	576	576	135	0
S25-XM	3	574	624	120	15
S25-XM	4	566	590	120	15
S25-XL	1	554	584	115	15
S25-XL	2	548	552	115	15
S25-XL	3	536	554	115	15
S25-XL	4	528	542	105	15
S30-XM	1	543	549	120	15
S30-XM	2	589	589	80	0
S30-XM	3	537	570	150	15
S30-XM	4	517	564	110	15
S30-XL	1	513	513	80	0
S30-XL	2	484	503	115	15
S30-XL	3	475	475	125	0
S30-XL	4	466	466	120	0
	Aver	528	542	111	9.4
	Max	589	624	150	15
	Min	466	466	80	0

Appendix A-6. Cutting forces profiles for S10-XL and S25-XM inserts in turning operations.

